Physical Gels based on Charge-Driven Co-Assembly

Marc Lemmers

Thesis committee

Thesis supervisor
Prof. dr. M.A. Cohen Stuart
Professor of Physical Chemistry and Colloid Science
Wageningen University

Thesis co-supervisor
Dr. ir. J. van der Gucht
Assistant professor at the Laboratory of Physical Chemistry and Colloid Science
Wageningen University

Other members

Prof. dr. M. Scheffer	Wageningen University
Prof. dr. C. Tsitsilianis	University of Patras, Greece
Prof. dr. M.A.J. Michels	Technical University Eindhoven
Dr. R.H. Tromp	NIZO food research B.V., Ede

This research was conducted under the auspices of Graduate School VLAG.

Physical Gels based on Charge-Driven Co-Assembly

Marc Lemmers

Thesis

submitted in fulfilment of the requirements for the degree of doctor
at Wageningen University
by the authority of the Rector Magnificus
Prof. dr. M.J. Kropff,
in the presence of the
Thesis Committee appointed by the Academic Board
to be defended in public
on Friday the 10th of February 2012
at 4 p.m. in the Aula.

Marc Lemmers
Physical Gels based on Charge-Driven Co-Assembly
188 pages

Thesis Wageningen University, Wageningen, The Netherlands (2012)
With references, with summaries in Dutch and English

ISBN: 978-94-6173-118-0

Aan al mijn docenten
Bedankt voor jullie tijd, geduld, aandacht en kennis

Voor mijn ouders
van wie ik zoveel heb geleerd
maar bovenal
hoe van je gezin te houden

This research forms part of the research program of the
Dutch Polymer Institute (DPI)
Technology Area Coating Technology
DPI project #657

Contents

Chapter 1

General Introduction

In this Chapter we will give an introduction to the other Chapters of this Thesis. The aim of this General Introduction is to get the reader acquainted with concepts and terms that are central for the understanding of the motivation for the research described in the other Chapters. It starts at undergraduate level and becomes gradually more technical as we approach the motivation and definition of this PhD project. We also discuss the synthetic routes that we use to obtain our starting material. We end with an outline and brief discussion of the other Chapters in this Thesis.

1

1.1 Physical gels

Gels are an important part of everyday life. Hair gel, ketchup, contact lenses, deserts such as bavarois, the liquid inside your eye-ball and water-based paints can all be considered as gelled substances.[1,2] All of these substances contain a lot of water (up to 99.9%!), yet they behave very much unlike water. This difference in behaviour is caused by the incorporation of relatively small amounts of molecules capable of 'capturing' the water. Doing so, the flow of water is restricted and the material will show the typical gel-like behaviour: not really solid, not really fluid.

Molecules that are very effective in restricting the flow of solvents, such as water, are *polymers*. Polymers are extremely long molecules compared to the size of a solvent molecule. Because of their length (up to hundreds of nanometers) polymers can easily interact with each other, even when a relatively small number of polymers is dissolved. These interactions can be chemical in nature or physical in nature.

By chemical interactions, or reactions, two polymer chains can become connected to each other by a covalent bond. A covalent bond is so strong that it can be considered to be irreversible, *i.e.* the two connected chains will never ever disconnect again. Now imagine that we have a large number of polymers in solution, and that they all chemically react with each other. This would lead to a three-dimensional *network* of polymer chains, which are all connected to each other, see figure 1.1. Such a network greatly impedes the flow of the solvent, and therefore we obtain a gel. Since the network in the solvent is of chemical origin, such a gel is called a chemical gel, or a hydrogel in case the solvent is water. Examples of hydrogels are contact lenses and superabsorbers such as the polymers used in diapers.[1]

The interactions between polymer molecules can also be of physical origin. Perhaps the most basic of all physical interactions originates from the fact that two polymer chains cannot be at the same spatial position at the same time. This is not so much of a problem if the polymer chains hardly meet each other. However, as soon as the polymer solution becomes more concentrated, this interaction results in a three dimensional network of entangled polymer chains, in which the movement of the polymer chains becomes restricted. There are many other types of physical interactions that can lead to such a situation, *e.g.* hydrophobic interactions, hydrogen bonding and electrostatic interactions. Again, the solvent is trapped in a three dimensional network, leading to gel-like properties. Since in this case the network originates from physical interactions between the polymers, the gel is referred to as a *physical gel*.

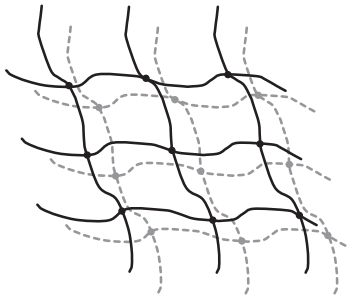

Figure 1.1: Schematic representation of a three-dimensional network of polymer chains. The chains are attached to each other at the cross-links, or nodes, which greatly limits the individual movement of the polymer chains. As a result we obtain a gel.

The difference between chemical gels and physical gels is the origin of the points where the polymers connect, which form the *nodes* in the network. Physical interactions are generally much weaker than chemical bonds. Physical nodes are therefore reversible, meaning that they can be formed, but also broken again. If the breaking of physical nodes requires an energy on the order of kT, the thermal energy, then nodes are broken and reformed frequently. The network in a physical gel is therefore also referred to as a *transient network*, because the nodes of the network exist only for a certain amount of time.

The difference between a chemical gel and a physical gel might seem small: irreversible versus reversible nodes. It has, however, major consequences for the mechanical properties of both types of gels. It determines whether the gel is a solid or a liquid. Chemical gels are visco-elastic solids, meaning that they can be deformed by a force, but these gels will always return to their initial shape when the force is taken away. This is because all the molecules that comprise the network can be stretched to a certain extent, but they will relax back to their original state once the stretching force is released. If deformed too much, these gels will fracture, break, fall apart and remain separated.

Physical gels are visco-elastic liquids. The reversible nature of the nodes in the network enables physical gels to flow, and adapt their shape to the environmental conditions. Physical gels also have the property that separate drops of gel can recombine again to form one single piece. In other words, physical gels are self-healing. Physical gels have these particular properties, because the nodes in the network can be broken, allowing the network to adopt a different shape, or to make new nodes at the interface between two separate pieces of gel.

The attractive force that keeps the nodes together determines also how much

energy is needed to disassemble a node. This energy is related to the *relaxation time* of the gel. If the required energy to disassemble a node is low, then the lifetime of the node will be short, hence the relaxation time will be low. In this case the gel can easily adapt its shape to external forces, meaning it has little resistance to flow and the gel will have a low *viscosity*. On the contrary, if the energy needed to break-up a node is high, then the relaxation time will be high and the gel will have a high internal friction to flow, meaning a high viscosity. In this view, a chemical gel can be considered as a physical gel with an infinitely large relaxation time, leading to an infinitely large viscosity.

There are many examples of physical gels in real products, ranging from personal care products and food products [1,2] to ballistics gel [3] and gelled water-bombs. [4] One important class of products in which transient networks play a key role are water-based coating formulations, or water-based paints. For environmental and health reasons, paint formulations are moving from being solvent-based to being water-based. [5] Although we are all very familiar with paints and their flow behaviour, paint is not as easy a product as it might seem. To end up with a high quality coating, a paint should behave differently in the different stages of application. A paint should be easy to stir, so components can mix well. It should stick to the brush without dripping too much. It should be easy to apply to a surface, without using too much force. It should stick to the wall without flowing down due to gravity. Yet, it should flow a little, to get rid of the brush marks. It is actually quite complicated to make a product that complies to all these specific behaviours. For physical and chemical reasons it is even more difficult to make such a product with water as the main component, compared to the 'old-fashioned' solvent-based formulations.

1.2 Classical associative thickeners

To acquire the desired flow properties in water-based coating formulations, manufacturers turn their paint into a relatively weak physical gel. The weak physical gel should prevent 'sagging' of the paint once applied on a vertical surface. To turn the coating into a weak physical gel, manufacturers add special polymers called *associative thickeners* to the formulation. [6] These are polymers with 'sticky' ends, and are also called 'telechelic' polymers, originating from the two Greek words *tele*, meaning 'remote', and *chele*, meaning 'claw'. [7] A more general name for such a polymer is *triblock copolymer*, because it consists of three 'blocks' and out of more than one type, hence 'copolymer'. A schematic drawing of such a polymer is given

Figure 1.2: Schematic drawing of a telechelic triblock copolymer.

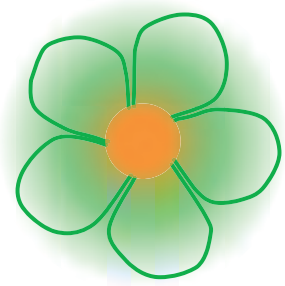

Figure 1.3: Schematic drawing of a flowerlike micelle. The core of the micelle consists of the hydrophobic tails of the telechelic polymers, while the corona consists of looped hydrophilic polymer.

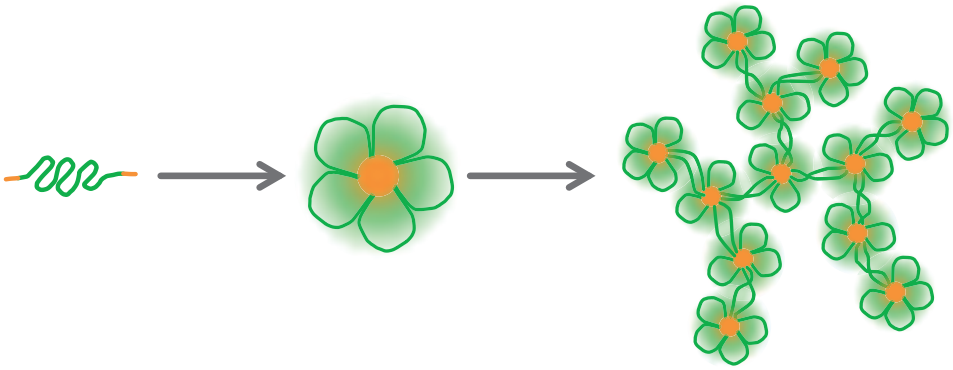

Figure 1.4: Schematic drawing of what happens in an aqueous solution of associative thickeners upon an increase in concentration. Single polymers are present in solution at very low concentration (left), flowerlike micelles are present in solution at intermediate concentration (middle) and a transient network of interconnected micelles is present in a concentrated solution (right).

in figure 1.2. Contrary to the middle-block of the polymer, which is 'hydrophilic', the ends do not like to be surrounded by water molecules. These parts are 'hydrophobic', and prefer to stick together. Dissolving these associative thickeners in water results in the spontaneous self-assembly of the hydrophobic tails and the formation of so-called *flowerlike micelles*. The schematic drawing explains why they are called like this. The flowerlike micelles consist of a *core* of hydrophobic tails surrounded by a *corona* of looped, hydrophilic middle blocks, see figure 1.3.

By increasing the flowerlike micelle concentration, these micelles get closer and closer to each other. At a certain threshold concentration, the *gel concentration*, it becomes possible for the telechelic polymers to put their end-groups in different micellar cores. This phenomenon is referred to as *bridging* between micelles. The bridging between the micelles leads to a transient network of interconnected micelles, which causes the viscosity of the solution to increase. Hence, the name associative thickeners. The paint acquires some of the desired flow properties, thanks to the transient network properties. Figure 1.4 visualizes the molecular picture of an aqueous solution of these associative thickeners upon increasing their concentration.

The use of associative thickeners in water-based coatings has greatly improved the overall quality of these coatings. There are, however, still some problems with the water-based coatings available today: i) Associative thickeners are thought to be related to a stability problem in these paints, known as the 'clear liquid separation'.[5] ii) The onset of thickening is poorly controlled, and cannot be switched on or off. iii) The degree of thickening can hardly be controlled once the associative thickeners are dissolved in the formulation. iv) If different transient network properties are desired, a completely new (mix of) associative thickener(s) has to be prepared. v) Solvent-based coatings are still superior in terms of performance, durability and finish. To try to close the gap between solvent-based and water-based coatings, and to solve the other issues related to the use of associative thickeners, researchers continuously look for new opportunities to prepare weak physical gels. One new possibility is described in this Thesis, where we investigate if we can prepare transient networks based on *electrostatic interactions*, instead of the hydrophobic interactions that are currently used.

1.3 Polyelectrolytes and complex coacervation

1.3.1 Polyelectrolytes

We need charges if we want to use electrostatic interactions as driving force for transient network formation. It is possible to prepare charged polymers, which are called *polyelectrolytes*. A polyelectrolyte can either be strong or weak, analogous to strong and weak acids and bases. Upon dissolving a strong polyelectrolyte in water, all chargeable groups become charged. Upon dissolving a weak polyelectrolyte in water, a dissociation equilibrium is established. The charge of a weak polyelectrolyte in aqueous solution is therefore dependent on the solution pH. This has the advantage that the charge on the polyelectrolyte can be controlled. However, the disadvantage is that the charge on the polyelectrolyte is not exactly known. Note that polyelectrolytes are always surrounded by clouds of small ions, the so-called *counterions*, compensating the charges on the polyelectrolyte.

1.3.2 Complex Coacervation

Intuitively, one expects two objects of opposite sign to attract each other. This also happens with polyelectrolytes of opposite charge. When two polyelectrolyte chains of opposite charge collide, they will stick together for one, and sometimes two, reasons:[8] i) since the charges on the polyelectrolytes compensate each other after the two oppositely charged polyelectrolytes stick together, the counterions are not needed anymore. These counterions are therefore 'freed' from their polyelectrolytes, and they can diffuse to anywhere in the solution. This leads to a gain in entropy. ii) The opposite polymeric charges might get closer to each other after the two polyelectrolytes stick together, compared to the average distance of the oppositely charged ions in the ion-cloud. If this is the case, then this leads to a favourable change in energy.

Because oppositely charged polyelectrolytes stick together, they can phase separate from solution. Such an associative phase separation leads to two macroscopic phases; one phase dense in the two oppositely charged polyelectrolytes and one phase mainly consisting of solvent and counterions, see figure 1.5. When this phase separation is a liquid-liquid phase separation, the polymer-rich phase is called the *complex coacervate* phase. A liquid-liquid phase separation caused by two oppositely charged polyelectrolytes was first described by Tiebackx at the beginning of the twentieth century.[9] However, Bungenberg de Jong and Kruyt were the first to investigate complex coacervation systematically, and were the ones who came up with the name 'complex coacervation'.[10,11] The name 'complex' coacervation was

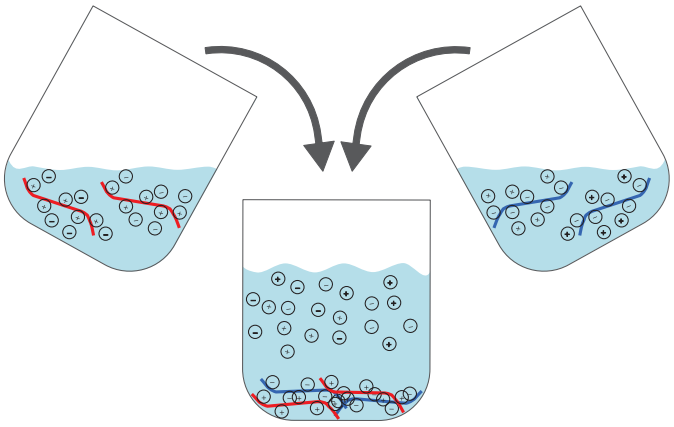

Figure 1.5: Schematic drawing of the liquid-liquid phase separation caused by two oppositely charged polyelectrolytes. The polyelectrolyte rich phase (lower phase) is called the complex coacervate phase.

introduced to discriminate between a two-component liquid-liquid phase separation and a liquid-liquid phase separation caused by one type of polymers, which is known as 'simple' coacervation.[12,13]

Mixing two oppositely charged polyelectrolytes will not always lead to a liquid-liquid phase separation. Often the two polyelectrolytes will stick together to form a solid-like phase, a precipitate.[13] Such a precipitate is also called an 'InterPolyElectrolyte Complex' (IPEC).[14] IPEC's have the tendency to become insoluble, when the two polyelectrolytes are mixed at approximately stoichiometric charge ratio. The resulting complexes are electroneutral and thus precipitate out of aqueous solution. An excess of one of the two polyelectrolytes will lead to a net charge on the complexes, which makes them, in general, water soluble.[14]

1.4 Polyelectrolyte complex micelles

We cannot make transient networks by mixing two oppositely charged polyelectrolytes. To be able to do so, we first have to prevent the macroscopic phase separation described in the previous section. A macroscopic phase separation can be restricted to the microscopic, or colloidal, domain through the stabilization of one phase in the other phase. In aqueous solutions, the stabilizing agent must be hydrophilic, dissolving the otherwise unstable phase. This is exactly what happens in the case of the flowerlike micelles. The hydrophobic core is stabilized by the hydrophilic middle-blocks, see figure 1.3.

If we now combine the block copolymer design, the phenomenon of complex co-

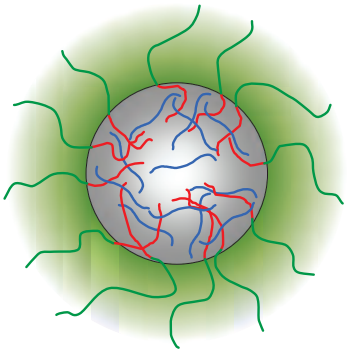

Figure 1.6: Schematic drawing of a polyelectrolyte complex micelle in aqueous solution. The oppositely charged polyelectrolytes are the core of the micelle, while the micelle is stabilized by a corona of neutral hydrophilic polymers.

acervation and the knowledge that we can restrict phase separation to the colloidal domain, we can envision the concept of a microscopic complex coacervate phase separation stabilized by hydrophilic parts of a block copolymer. This is exactly what Harada and Kataoka achieved in the mid 1990's. They mixed two diblock copolymers, each containing one hydrophilic poly(ethylene glycol) block and either a polycation block or a polyanion block, in water at 1:1 charge ratio. Stable micelles were obtained, which were named 'PolyIon Complex' (PIC) micelles.[15] The suggested structure of such a micelle is a spherical core containing the two oppositely charged polyelectrolytes, stabilized by a spherical corona of hydrophilic polymer blocks.

One year later, Kabanov *et al.* showed that stable micelles can be formed from a diblock copolymer, consisting of a hydrophilic poly(ethylene oxide) block and a negatively charged block, and a positively charged homopolymer, mixed at stoichiometric charge ratio.[14] These micelles were named 'Block Ionomer Complexes' by these authors.[14]

Another two years later, Cohen Stuart *et al.* showed that the formation of stable micelles is possible by using a diblock copolymer, consisting of a hydrophilic block and a positively charged block, and a negatively charged homopolymer.[16] The authors stress the fact that both polymers are completely water soluble, and hence electrostatic attraction and counterion release are the only driving forces for association. During the experiments a phase rearrangement from a macroscopic phase separation to a microscopic phase separation was witnessed.[16] Such a rearrangement can only happen when the polymeric phase is mobile, *i.e.* liquid-like. This inspired the authors to call these micelles Complex Coacervate Core Micelles (C_3M's), see figure 1.6. In real life it is very hard to determine whether or not

the core of a complex coacervate core micelle is actually liquid-like. Therefore we prefer to name this class of micelles *polyelectrolyte complex micelles* throughout this Thesis.

There exists quite some variety in charged block copolymers. This implies an even greater variety in possibilities of micelle formation based on diblock-diblock or diblock-homopolymer combinations. Since the formation of polyelectrolyte complex micelles always requires two different polymers, one positively charged and one negatively charged, we speak of electrostatically driven *co-assembly*. This differs from self-assembly in the case of the associative thickeners, because these require only one component. A rather extensive review on the electrostatically driven co-assembly of (partly) polyelectrolytes was recently written by Voets and coworkers, which is advised for further reading on this subject.[17]

1.5 Physical Gels based on Charge-Driven Co-Assembly

From polyelectrolyte complex micelles it is only one more step to reach the 'core' of this PhD project: to make transient networks based on electrostatically driven co-assembly. We can achieve this by combining the associative thickener design with the design of polyelectrolyte complex micelles. In other words, if we can synthesize triblock copolymers with charged end-blocks and a neutral water-soluble middle-block, and mix these triblock copolymers in water with homopolymer of opposite charge, then the polymers should be able to co-assemble into flowerlike polyelectrolyte complex micelles. At higher concentrations, the triblock copolymers should be able to bridge between two micellar cores, leading to a charge-driven transient network of interconnected polyelectrolyte complex micelles. Since the result will be a thickening of the water, we can speak of a new class of associative thickeners. The thickeners based on hydrophobic interactions shall therefore be referred to as *classical* associative thickeners. An illustration of the proposed mechanism for charge-driven transient network formation is given in figure 1.7.

So why would a physical gel based on charge-driven co-assembly potentially solve some of the problems that are related to the use of the classical associative thickeners in the coatings industry? Well, to start with, it is a two component thickener in which both components are water soluble. There is no driving force for transient network formation unless both components are present in solution. This means that one of the two components can already be dissolved during the formulation process, without inducing a large viscosity increase. The advantage is that a lower viscosity fluid reduces the costs and environmental impact of the produc-

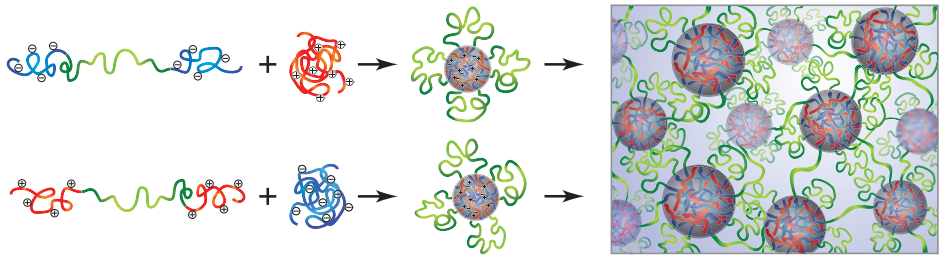

Figure 1.7: Artists impression of the principle of charge-driven transient network formation. Triblock copolymer with charged end-blocks can co-assemble with oppositely charged homopolymer to form flowerlike polyelectrolyte complex micelles. At high concentrations triblock copolymers can stick each end-block in a different micellar core, thereby bridging between two micelles. If enough micelles are bridged we obtain an aqueous physical gel based on interconnected polyelectrolyte complex micelles.

tion process, because pumping and mixing low viscosity fluids requires considerable less energy than pumping and mixing viscous fluids. The second component can be added at the end of the formulation process, to obtain the desired rheological properties. Other potential advantages are related to the versatility of a two component charge-driven physical gel. As long as one of both components is a triblock copolymer, transient networks should be able to develop in concentrated solutions. As mentioned before, there are many types of polyelectrolytes. Research in the past has shown that the interaction strength between the two oppositely charged moieties is greatly dependent on the specific combination of polyelectrolytes.[8,17] The interaction strength will have a major influence on the relaxation time of the micelles, as discussed above, and therefore on the flow properties. Network formation might also be influenced by the charge ratio in which the two components are mixed. Other options are to mix two triblock copolymers with oppositely charged end-blocks,[18] or replace the homopolymer in figure 1.7 by a charged nanoparticle. The length of all components can be varied, which allows for additional tuning of the interaction strength. Long end-blocks will be more difficult to remove from an oppositely charged environment than small end-blocks. The middle-block length can also be varied, which will influence the amount of polymer needed to be able to form a network, *i.e.* the longer the middle-block is, the longer are the distances that can be bridged. Besides properties of the polymers themselves, the interaction strength can be tuned by external variables. Obvious variables are concentration and temperature. However, the electrostatic driving force allows to tune the interaction between the oppositely charged moieties more precisely. Small ions can screen the electrostatic interactions between two polyelectrolytes, thereby weaken-

ing the associative strength. Salt concentration will thus have a major influence on the gel properties. In case weak polyelectrolytes are used, the charge density on the polymers can be controlled by the pH of the solution, giving another parameter to tune the interaction between the polymers. It is safe to say that charge-driven physical are truly *multi-responsive*.

What should be clear by now is that the microstructure of a material, *i.e.* the type of molecules used and how they arrange and interact, determines how a material behaves on a much larger scale. In other words, the microstructure determines the macroscopic properties. Almost all the work in this Thesis is aimed at clarifying why a certain experimentally determined microstructure leads to certain experimentally determined properties. To find out, we combine experimental techniques probing the nano-scale, such as (dynamic) light scattering ((D)LS), small-angle X-ray scattering (SAXS) and (cryogenic) scanning electron microscopy ((cryo-)SEM), with macroscopic experimental techniques, such as rheometry. This combination has proven to be rather powerful in clarifying the structure-property relationship of soft condensed matter.

1.5.1 Synthesis

The only thing we need to get started are triblock copolymers with charged end-blocks. Because such triblock copolymers cannot be bought commercially we have to synthesize these triblock copolymers ourselves. The detailed synthetic protocols are given in Chapter 2 and 3, but here we will discuss and display the mechanisms that are used to obtain the two triblock copolymers that we have used in this Thesis.

The synthesis of the triblock copolymers with charged end-blocks is a two step process. First we have to prepare the middle-block for polymerization. Next, we have to grow the end-blocks piece by piece to obtain the desired triblock copolymers.

Macro-initiator synthesis

In case the initiator in a polymerization reaction is already a polymer itself, the initiator is referred to as a *macro-initiator*. Macro-initiators are often used to synthesize graft or block copolymers. Poly(ethylene oxide), also called poly(ethylene glycol) (PEG), is cheap, readily available, water soluble and relatively monodisperse. For these reasons, PEG has been used already many years to synthesize polymers with different functional moieties.[19] The hydroxyl end-groups can be the starting point of many reactions to change the properties of the PEG, including

polymerization. In these polymerization reactions, di-functional PEG will lead to triblock copolymers, but, using the same chemistry, mono-functional PEG can be used to synthesize diblock copolymers.

To prepare the macro-initiator that we need, we have to replace the hydroxyl end-groups by bromo-esters. This is done in a reaction with either 2-bromopropionyl chloride/bromide[20,21] or 2-bromoisobutyryl bromide.[22,23] We have used the latter in our macro-initiator synthesis, which is displayed in figure 1.8.

The structural analysis of the reaction given in figure 1.8 is rather easy. The hydroxyl end-groups in PEG molecules give a base-line separated ^{1}H-NMR-peak in deuterated dimethyl sulfoxide (DMSO-d_6) at 4.56 ppm.[19] The degree of substitution can be determined by comparing the ratio of the hydroxyl group integral with the integral typical for the substituted end-group. If all hydroxyl groups are substituted, the typical hydroxyl peak vanishes.[24]

Triblock copolymer synthesis

The triblock copolymer was synthesized by *Atom Transfer Radical Polymerization* (ATRP). ATRP was derived from living cationic polymerization,[26] and was first described as Living Radical Polymerization by Kato and coworkers.[27] The ATRP reaction mechanism was more thoroughly described in the same year by Wang and Matyjaszewski,[28] who were the first to actually come up with the name 'Atom Transfer Radical Polymerization'. ATRP is an example of a controlled radical polymerization (CRP), characterized by an equilibrium between active and inactive chain-ends. The idea behind the reaction is that the chains remain in a dormant state most of the time. Once the chain-ends are activated, one monomer is added to the chain-end, after which the active chain-end is quickly put back in its dormant state. In this way, all chains start to grow at approximately the same time, the chains grow at the same rate and termination reactions are suppressed.[29] This yields relatively monodisperse block copolymers. A general ATRP reaction scheme is given in figure 1.9.[25]

The triblock copolymers that we have synthesized are based on literature descriptions of diblock copolymers. As stated before, mono-functional macro-initiator will lead to diblock copolymers, while bifunctional macro-initiators will lead to triblock copolymers. The reaction mechanism is completely similar in both cases.

In 2003 Li *et al.* described the synthesis of a positively charged diblock copolymer.[30] The main point of the synthesis was the ATRP of positively charged [(TriMethylAmino)Ethyl] MethAcrylate monomers (TMAEMA), instead of the polymerization of DMAEMA and subsequent quaternization in a separate reaction.

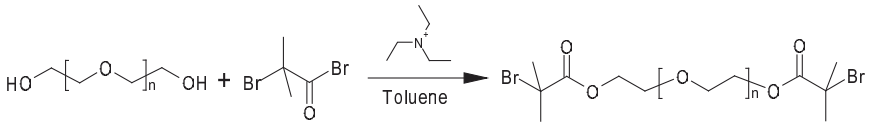

Figure 1.8: A typical reaction to prepare an ATRP macro-initiator. The bromide-containing compound used in this reaction is 2-bromoisobutyryl bromide.

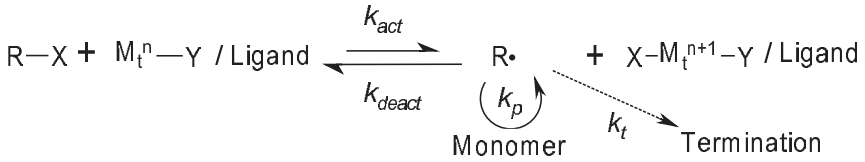

Figure 1.9: A general scheme of an ATRP reaction. Scheme redrawn from Matyjaszewski and Xia.[25] R—X is the initiator and/or dormant species, X is a (pseudo)halogen atom, M_t^n—Y / Ligand is the transition metal complex, in which Y can be another ligand or a counterion, and R· is the radical that can react with monomers to form the growing chain.

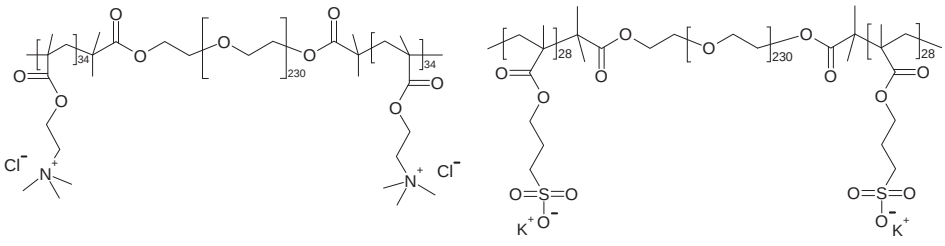

(a) **(b)**

Figure 1.10: Chemical structures of the synthesized triblock copolymers. **(a)** Triblock copolymer with positively charged end-blocks. **(b)** Triblock copolymer with negatively charged end-blocks.

The study showed that a water/2-propanol (1:1) solvent mixture was most robust with respect to degree of polymerization (DP) and polydispersity. Adding a Cu(II) salt to the catalyst mixture improved control of the reaction, as expected on the basis of work of Perrier *et al.*.[31] The resulting triblock copolymer that we synthesized based on this protocol is depicted in figure 1.10a.

Approximately half a year later Masci *et al.* were able to synthesize diblock copolymers with negatively charged blocks.[32] A sulfonated methacrylate (potassium 3-sulfopropyl methacrylate) was used for ATRP polymerization. Polymerization was performed in water/dimethylformamide (DMF) (1:1) solvent mixture, which eliminated side reactions. A [Cu(II)]/[Cu(I)] = 2 ratio gave first order linear kinetics up to temperatures of 60 °C. The triblock copolymer that we synthesized based on this protocol is depicted in figure 1.10b.

Both reactions discussed above show that it is possible to synthesize block copolymers with polyelectrolyte end-blocks, while keeping the synthesis relatively simple.

1.6 Outline of this Thesis

Finally we have discussed all the necessary terms and mechanisms which are at the basis of the next Chapters in this Thesis. In Chapter 2 we will show that we have succeeded in preparing charge-driven transient networks. We show a strong viscosity increase, while SAXS measurements show ordered spherical objects: the flowerlike micelles. Furthermore, we show that the gels are responsive to concentration, temperature, charge composition, salt concentration and pH.

The effect of charge composition is studied in more detail in Chapter 3. Charge composition is an obvious but rarely studied parameter in charge-driven co-assembly. Because we can produce relatively large quantities of our polymers, we can study the influence of charge composition in detail. We find an asymmetry in microscopic structure of the co-assembled objects. However, this asymmetry is not reflected in the macroscopic properties of gels formed under non-stoichiometric conditions.

In Chapter 4 we have a closer look on the influence of polymer concentration and salt concentration on the topology of the transient network. Addition of polymers leads to more micelles, which become more ordered as they get more densely packed. Adding salt to the physical gels leads to smaller micelles, but also more micelles. It also leads to micelles that are more easily disrupted. However, it does not lead to a weakening of the network, because the elastic modulus is little influenced by an increase in salt concentration.

We get somewhat closer to water-based paints in Chapter 5, where we show that it is possible to prepare charge-driven physical gels by mixing triblock copolymers with charged end-blocks with oppositely charged nanoparticles. Since such gels have never been prepared before, we named this new class of physical gels 'complex composite gels'. We show that the nanoparticles in the gels are not irreversibly aggregated and that the transient network is truly charge-driven. By varying the amount of each component we can draw a diagram of states, indicating whether complex composite gel formation is possible and what the appearance of the gel will be. The resulting physical gels are characterized by low elastic moduli, but long relaxation times. We also show that the gels can dry to form a clear complex composite coating, in which the nanoparticles are 'glued' together in the polymeric matrix.

Chapter 6 is the final Chapter of this Thesis. In this Chapter we will try to reflect on the previous Chapters, considering the Thesis as a whole. We will also point to potentially interesting directions for future research. Finally, we will reflect on the application-driven motivation of this PhD Thesis and discuss whether charge-driven thickeners can really solve some of the problems of classical associative thickeners and if they could really be applied in water-based coating formulations.

References

[1] Wikipedia, *keyword: gel.*

[2] Wikipedia, *keyword: gel (disambiguation).*

[3] Mythbusters, *How to make ballistics gel: http://youtu.be/023Ho–XPts.*

[4] Wikipedia, *http://en.wikipedia.org/wiki/Water_Gel_Explosives.*

[5] J. Sprakel, *PhD Thesis*, 2009.

[6] A. J. Reuvers, *Progress in Organic Coatings*, 1999, **35**, 171–181.

[7] F. Lo Verso and C. N. Likos, *Polymer*, 2008, **49**, 1425–1434.

[8] J. van der Gucht, E. Spruijt, M. Lemmers and M. A. Cohen Stuart, *Journal of Colloid and Interface Science*, 2011, **361**, 407–422.

[9] F. Tiebackx, *Zeitschrift für Chemie und Industrie der Kolloide*, 1911, **8**, 198–201.

[10] H. Bungenberg de Jong and H. Kruyt, *Proceedings of the Koninklijke Nederlandse Akademie van Wetenschappen*, 1929, **32**, 849–856.

[11] H. Bungenberg de Jong, *Crystallisation Coacervation Flocculation*, Elsevier, Amsterdam, 1949, vol. II, Chapter X.

[12] IUPAC, *IUPAC Compendium of Chemical Terminology*, International Union of Pure and Applied Chemistry, 2007.

[13] I. K. Voets, *PhD Thesis*, 2008.

[14] A. V. Kabanov, T. K. Bronich, V. A. Kabanov, K. Yu and A. Eisenberg, *Macromolecules*, 1996, **29**, 6797–6802.

[15] A. Harada and K. Kataoka, *Macromolecules*, 1995, **28**, 5294–5299.

[16] M. A. Cohen Stuart, N. A. M. Besseling and R. G. Fokkink, *Langmuir*, 1998, **14**, 6846–6849.

[17] I. K. Voets, A. de Keizer and M. A. Cohen Stuart, *Advances in Colloid and Interface Science*, 2009, **147-48**, 300–318.

[18] J. N. Hunt, K. E. Feldman, N. A. Lynd, J. Deek, L. M. Campos, J. M. Spruell, B. M. Hernandez, E. J. Kramer and C. J. Hawker, *Advanced Materials*, 2011, **23**, 2327–2331.

[19] J. M. Dust, Z. H. Fang and J. M. Harris, *Macromolecules*, 1990, **23**, 3742–3746.

[20] K. Jankova, X. Y. Chen, J. Kops and W. Batsberg, *Macromolecules*, 1998, **31**, 538–541.

[21] M. Bednarek, T. Biedron and P. Kubisa, *Macromolecular Rapid Communications*, 1999, **20**, 59–65.

[22] M. Ranger, M. C. Jones, M. A. Yessine and J. C. Leroux, *Journal of Polymer Science Part A - Polymer Chemistry*, 2001, **39**, 3861–3874.

[23] K. L. Robinson, J. V. M. Weaver, S. P. Armes, E. D. Marti and F. C. Meldrum, *Journal of Materials Chemistry*, 2002, **12**, 890–896.

[24] K. Jankova and J. Kops, *Journal of Applied Polymer Science*, 1994, **54**, 1027–1032.

[25] K. Matyjaszewski and J. H. Xia, *Chemical Reviews*, 2001, **101**, 2921–2990.

[26] T. Higashimura, M. Kamigaito, M. Kato, T. Hasebe and M. Sawamoto, *Macromolecules*, 1993, **26**, 2670–2673.

[27] M. Kato, M. Kamigaito, M. Sawamoto and T. Higashimura, *Macromolecules*, 1995, **28**, 1721–1723.

[28] J. S. Wang and K. Matyjaszewski, *Macromolecules*, 1995, **28**, 7901–7910.

[29] A. Goto and T. Fukuda, *Progress in Polymer Science*, 2004, **29**, 329–385.

[30] Y. T. Li, S. P. Armes, X. P. Jin and S. P. Zhu, *Macromolecules*, 2003, **36**, 8268–8275.

[31] S. Perrier, S. P. Armes, X. S. Wang, F. Malet and D. M. Haddleton, *Journal of Polymer Science Part A - Polymer Chemistry*, 2001, **39**, 1696–1707.

[32] G. Masci, D. Bontempo, N. Tiso, M. Diociaiuti, L. Mannina, D. Capitani and V. Crescenzi, *Macromolecules*, 2004, **37**, 4464–4473.

Chapter 2

Multi-Responsive Reversible Gels based on Charge-Driven Assembly

In this Chapter we show that we are able to prepare physical gels based on the co-assembly of an ABA triblock copolymer with charged end-blocks and an oppositely charged polyelectrolyte. Flowerlike micelles are formed at low concentration. Above the gel concentration, triblock copolymers are able to bridge micelles, thereby forming a sample-spanning transient network of interconnected micelles. These physical gels are responsive to changes in concentration, temperature, ionic strength, pH and charge composition.

This chapter is published as communication with supporting information:
M. Lemmers, J. Sprakel, I.K. Voets, J. van der Gucht, M.A. Cohen Stuart, *Angewandte Chemie International Edition*, **2010**, *49*, 708-711.

2.1 Introduction

Multi-responsive materials are interesting for a wide range of applications, as their properties can be tuned with external triggers. A promising class of responsive materials is that of physically cross-linked polymer networks. These transient networks are typically assembled from telechelic polymers[1–5] or linear triblock copolymers,[6–9] although other architectures have been investigated as well.[10–14] Most widely studied are ABA triblock copolymers with hydrophobic end-groups and a hydrophilic middle-block. These so-called 'associative thickeners' have the ability to change rheological properties of solvents at relatively low concentrations. For this reason, they are widely used as rheology modifiers in industry. However, the hydrophobic interaction on which the gelation of these 'classical' associative thickeners is based, can be tuned only by changing the temperature or solvent, or by synthesizing a new molecule. In order to have more control over the gel properties, reversible gels based on an entirely different driving force are needed.

In this paper we present a novel class of multi-responsive reversible gels, based on the co-assembly of a triblock copolymer having two charged end-blocks with an oppositely charged homopolymer. These reversible gels respond not only to changes in temperature and concentration, but also to ionic strength, cationic/anionic composition and, in case weak polyelectrolytes are used, pH.

Mixing two aqueous solutions of oppositely charged polyelectrolytes generally leads to phase separation.[15–17] Addition of a neutral solvophilic block to the polyelectrolyte chain can prevent macroscopic phase separation. Instead, a microscopic phase separation occurs, leading to micelles consisting of a core containing polyelectrolyte complex, stabilized by a corona of neutral solvophilic blocks.[18–22]

When using triblock copolymers with two charged end-blocks instead of diblock copolymers, flowerlike micelles can be formed, see figure 2.1a. These micelles are stabilized by a corona of looped solvophilic chains. At polymer concentrations above a critical gel concentration (C_{gel}), the triblock copolymer will bridge between two different micellar cores. The micelles thus become connected with each other, leading to a reversible gel, see figure 2.1b.

2.2 Experimental

2.2.1 Triblock copolymer synthesis

A bifunctional macro-initiator was prepared by dissolving 150 g of poly(ethylene glycol) (PEG) with $M_n = 10.000$ g mol^{-1} (Fluka) in 1.5 L toluene (Sigma Aldrich).

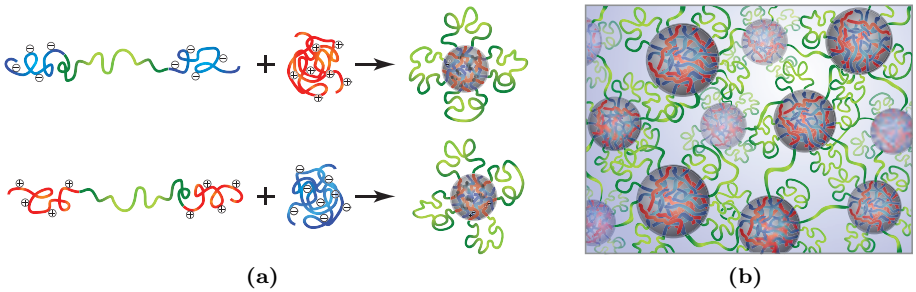

(a) (b)

Figure 2.1: Schematic representation of the formation of reversible gels based on charge-driven assembly. **(a)** Monomers associate into flowerlike micelles in dilute solution. **(b)** The neutral middle-block bridges between the micellar cores to form a transient network.

After azeotropic distillation of 500 mL toluene, a ten-times molar excess, with respect to the amount of PEG, of triethylamine (Sigma Aldrich) was added, which corresponds to 3 mL triethylamine. Subsequently, a ten-times molar excess, with respect to the amount of PEG, of 2-bromoisobutyryl bromide (Sigma Aldrich) was added dropwise, which corresponds to 2.74 mL of 2-bromoisobutyrylbromide. The reaction mixture was stirred for five days at 30 °C.[23]

Purification of the bifunctional macro-initiator was started by treatment of the reaction mixture with decolourising charcoal at 40 °C for 30 min. Subsequently, the solids were removed by Büchner filtration. The solvent was partly removed by evaporation at reduced pressure before precipitation of the product in a ten-fold excess of petroleum ether. After filtration, the product was redissolved in 0.5 L THF before precipitation in a ten-fold excess of petroleum ether (twice). The product was obtained by filtration and dried under vacuum overnight. Yield was determined to be 88%. The degree of esterification was determined by ^{1}H NMR to be 100%.[24,25]

The triblock copolymer was prepared by degassing the solid mixture of 40 g of bifunctional macro-initiator and 56.3 g of 3-sulfopropylmethacrylate potassium salt (KSPMA) (Sigma Aldrich), which is a 59-fold excess of reactive monomer, aiming for an average degree of polymerization of 60. The solid mixture was dissolved in 80 mL of a degassed mixture of water/DMF (1:1) at 60 °C. The reaction mixture was kept under argon flow until completion. An ATRP catalyst mixture was prepared by dissolving an equal molar amount, with respect to the amount of bifunctional macro-initiator, of Cu(I)Cl (Sigma Aldrich), a double molar amount, with respect to the amount of bifunctional macro-initiator, of Cu(II)Cl (Sigma Aldrich) and a 7.5-times molar excess, with respect to the amount of bifunctional

macro-initiator, of 2,2-bipyridine (Sigma Aldrich) in 40 mL of a water/DMF mixture (1:1). The actual amounts used are 0.29 g Cu(I)Cl, 0.77 g Cu(II)Cl and 3.34 g 2,2-bipyridine. The ATRP catalyst mixture was added to the bifunctional macro-initiator/KSPMA solution to start the polymerization. The reaction was quenched after three hours by bubbling oxygen through the sample.[26–28]

Purification of the product was achieved by diluting the polymer solution with water followed by dialysis against 1 M KCl solution at p$H \approx 3$. EDTA salts were added to the dialysis bath up to a concentration of 10 mM to bind the copper ions in the polymer solution. Next dialysis step was against 0.1 M KCl at p$H \approx 3$ and 10 mM of EDTA. Final purification step was extensive dialysis against pure water. The triblock copolymer was obtained by freeze-drying overnight. Yield was determined to be 16%, caused by an unfortunate massive loss of product during dialysis.

2.2.2 Triblock copolymer characterization

Size exclusion chromatography

Size exclusion chromatography (SEC) was performed to determine the relative molecular weight of the triblock copolymer and to detect if there was any unreacted macro-initiator present in the triblock copolymer product. The results are shown in figure 2.2. SEC was carried out in a $NaNO_3$ aqueous solution (0.1 M), with a Waters 600 liquid chromatograph equipped with a 2414 refractive index detector and four Waters Ultrahydrogel columns (Ultrahydrogel 1000, 500, 250 and 120). A flow rate of 0.8 mL min^{-1} was used. Poly(ethylene oxide) standards were used for calibration.

From figure 2.2 it is clear that the triblock copolymer (trace number 3) does not contain any unreacted macro-initiator (trace number 2), and that the average molecular weight of the triblock copolymer has increased significantly compared to the molecular weight of the macro-initiator. The polydispersity index for the triblock copolymer was determined to be 1.1.

^{1}H-NMR

The triblock copolymer product was dissolved in D_2O to determine the structure by ^{1}H-NMR on a Bruker Avance III 400 MHz NMR spectrometer. The triblock copolymer structure and its relation to the ^{1}H-NMR spectrum is indicated in figure 2.3. The degree of polymerization (DP) was determined using the ratio of the integrals of peak **e** and the peak of PEO. Taking into account the amount of

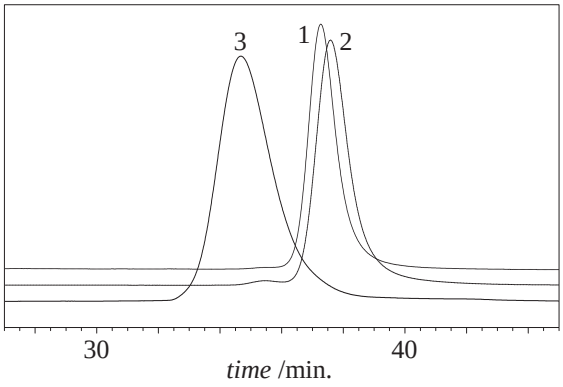

Figure 2.2: Size exclusion chromatogram of PEG_{230} starting material (peak 1, dotted line), bifunctional macro-initiator (peak 2, dashed line) and triblock copolymer $PSPMA_{28}$—PEO_{230}—$PSPMA_{28}$ (peak 3, full line).

protons in a PEO monomer and group **e** of the triblock copolymer, the DP was determined by $\mathrm{DP} = \frac{4I_e}{2I_{\mathrm{PEO}}} \cdot N_{\mathrm{PEO}}$ with I_e the integral of peak **e**, I_{PEO} the integral of the PEO peak and $N_{\mathrm{PEO}} = 230$, which is the average amount of PEO groups in the starting PEO, based on SEC against PEO standards. From this calculation it follows that the average degree of polymerization is 55.

2.2.3 Sample preparation

Poly(allylamine hydrochlorid) (PAH) (Sigma Aldrich) of $M_n = 16$ kg mol^{-1} was used as oppositely charged homopolymer, see figure 2.3a.

Gels were prepared by mixing two separate polyelectrolyte solutions containing either the triblock copolymer or the oppositely charged homopolymer. All gels were prepared at charge stoichiometric ratio: $f^+ = 0.5$, see section 2.3. To determine and control the ionic strength of the samples, complete counterion release upon co-assembly of the two oppositely charged moieties was assumed.

2.2.4 Dynamic light scattering titrations

Dynamic light scattering titrations were performed on an ALV light scattering instrument equipped with an ALV-5000/60X0 external digital correlator and a 300 mW solid state laser (Cobolt Samba-300 DPSS laser) operated at a wavelength of 532 nm. Angle of detection was always 90°. A refractive index matching bath of filtered cis-decalin surrounded the cylindrical scattering cell, and the temperature was controlled at 20±0.1 °C using a Haake F8-C35 thermostat. Titration steps were automated using a Schott-Geräte TR 250 computer-controlled titration setup

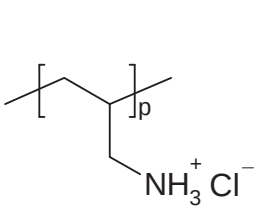

(a) p ≈ 160.

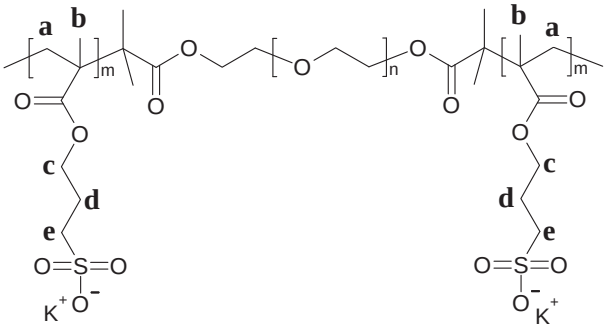

(b) n ≈ 230; m ≈ 28.

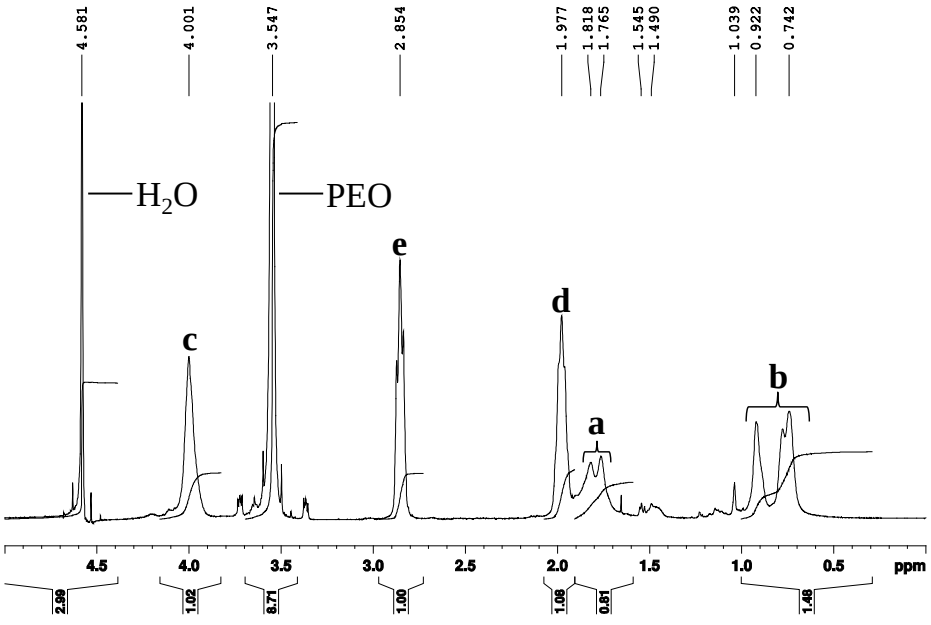

(c)

Figure 2.3: (a) Molecular structure of the positively charged homopolymer PAH_{160}. **(b)** Molecular structure of the negatively charged triblock copolymer $PSPMA_{28}$—PEO_{230}—$PSPMA_{28}$. Labels correspond to the peaks in the ^{1}H-NMR spectrum, figure 2.3c. **(c)** ^{1}H-NMR spectrum of the triblock copolymer.

for sequential addition of titrant and cell stirring. After each DLS measurement, the pH was measured and the sample was stirred for one minute before addition of the titrant, followed by a period of stirring for eight minutes and a one minute rest period, before starting DLS measurements again.

Light scattering intensity was measured in 40 separate measurements of 12 s each after each titration step. Each separate measurement generates an average scattered light intensity over the measured 12 s. The values presented in the main text for the average light scattering intensity $\langle I \rangle$ are the averages over these 40 separate measurements.

The pH DLS titration data were obtained using a more sophisticated script, which evaluates the stability of the scattered light intensity during the measurement. The user can determine for how many DLS measurements the intensity should be within a certain range (depending on the intensity) to assume equilibrium. The duration of each measurement is automatically adjusted to the measured scattered light intensity. We decided that 15 runs stable is equilibrium, with a minimum duration of a measurement of 12 s.

The average scattered light intensity was normalized by the total polymer concentration ($\frac{\langle I \rangle}{C_p}$) in the measuring cell, assuming $I \propto C_p$, which was checked to be correct in the concentration regime investigated in this paper. The hydrodynamic radii (R_h) were determined by averaging the values of each separate DLS measurement, as given by the standard ALV software, which is based on the cumulants method.[29]

2.2.5 Small-angle X-ray scattering

Small-angle X-ray scattering (SAXS) measurements were performed at the Adolphe Merkle Institute. The SAXSess lab system from Anton Paar (Graz, Austria) comprises an X-ray generator (PANalytical, PW 3830) operating at 40 kV and 50 mA with a sealed-tube Cu anode (Philips 2773/00 long fine focus). A Göbel mirror (AXO Dresden, C40-0641) and a Kratky block collimation system were used to convert the divergent polychromatic X-ray beam into a focused line-shaped beam of Cu-K radiation ($\lambda = 0.1542$ nm). The samples were filled at room temperature into the sample holder (1 mm quartz capillary in a metal block, temperature controlled by a Peltier element, 20±0.1 °C. The 2D scattering pattern was recorded by a CCD camera from Princeton Instruments (Trenton, NJ, USA). The 2D image was radially integrated to obtain $I(q)$ using SAXSQuant software (Anton Paar, Graz, Austria) in the range $0.08 < q < 2$ nm^{-1}.

The measured scattering curves were corrected for solvent scattering, put on

absolute scale by measuring the scattering intensity of water, and desmeared using the SAXSQuant software. Interactions were modelled using a hard sphere structure factor, yielding an *effective* volume fraction and radius, because the micelles are not real hard spheres. Model fitting was done using the SASfit program,[30] employing a form factor for polydisperse (Gaussian distribution) homogeneous spheres. The data has also been analysed using generalized indirect Fourier transformation as described in detail elsewhere.[31–33] (G)IFT analysis of SAXS data for samples between 2 and 160 g L^{-1} yielded pair distance distribution functions (p(r)) with a very symmetrical shape, typical for spherical particles, with $R_g = 8.1 \pm 0.4$ nm.

2.2.6 Rheological measurements

Rheological measurements were performed on either an Anton Paar MCR 301 or Anton Paar MCR 501 rheometer, both in strain controlled mode. Cone-plate geometry was used for both oscillatory and rotational measurements. A cone with a diameter of 50 mm and a tilt angle of 1° was used for most experiments. Occasionally, a cone with a diameter of 25 mm and a tilt angle of 1° was used. The zero-shear viscosity (η_0) of low viscosity samples was measured separately using a Couette geometry with a diameter of 10 mm and a gap width of 0.841 mm. Temperature was controlled by a Peltier element in the plate or Couette measuring cell. Measurements started one hour after sample loading, to assure complete relaxation of the gel samples before starting measurements. A solvent trap was used to minimize the effect of evaporation. At least two different samples were measured for each concentration and ionic strength of the gels.

Frequency sweeps with an angular frequency (ω) between 0.01-628 rad s^{-1}, were performed at a strain of 5%. It was checked that the applied strain of 5% corresponded to the linear visco-elastic regime for all applied frequencies, by performing amplitude sweeps at multiple frequencies.

Rotational measurements were performed with shear rates ($\dot{\gamma}$) between 0.001-1 s^{-1}. Values for η_0 were obtained by the low shear rate viscosity plateau values, assuming Newtonian behaviour at shear rates approaching zero.

The values given for the viscosity in the main text were measured as the low-frequency complex viscosity (η^*), or, assuming Newtonian behaviour for low shear rates, zero-shear viscosity (η_0). It was experimentally checked that these two viscosities coincide for the applied frequencies and shear rates.

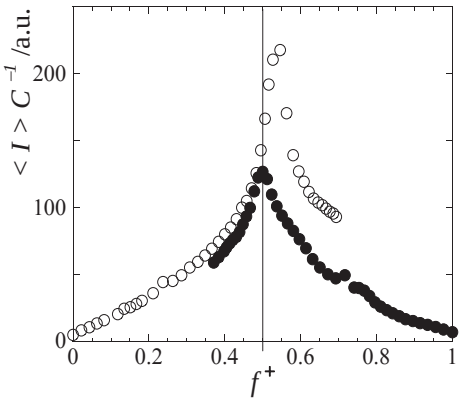

Figure 2.4: The average scattered light intensity, normalized by the total polymer weight concentration, as a function of the composition variable f^+. Titrations were started either with only triblock copolymer in solution (○), or only homopolymer in solution (●). The titrations are performed at low concentration ($\approx$ 1 g L^{-1}) and at [KCl]= 0.2 M. The driving force for complex coacervation is strongest at charge stoichiometry, $f^+ = 0.5$. The difference in scattering between the two measurements is probably due to non-equilibrium structures.

2.3 Results & Discussion

To investigate the co-assembly of $PSPMA_{28}$—PEO_{230}—$PSPMA_{28}$ with PAH_{160} in dilute solution, dynamic light scattering (DLS) titrations were used. We define a charge composition variable:[22]

$$f^+ = \frac{[+]}{[+] + [-]} \tag{2.1}$$

which is the concentration of positively chargeable groups, [+], divided by the total amount of chargeable groups, [+] + [−]. Upon titrating either of the two components to the other, complexes are formed, as indicated by an increase in scattered light intensity. The scattered light intensity increases up to the point of charge stoichiometry, after which it decreases again, see figure 2.4. The complexes that are formed in these dilute solutions are flowerlike micelles with a hydrodynamic radius of approximately 20 nm.

When $PSPMA_{28}$—PEO_{230}—$PSPMA_{28}$ and PAH_{160} are mixed at higher concentrations, a highly viscous and transparent reversible gel is formed spontaneously. This indicates that an interconnected micellar network is indeed formed.

To further investigate the shape of, and interactions between, the micelles, small-angle X-ray scattering measurements were performed. Excellent agreement between experimental SAXS data and fits can be achieved by using a form factor

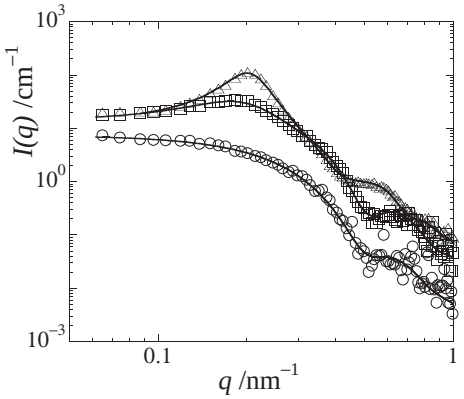

Figure 2.5: Small-angle X-ray scattering curves for three different polymer concentrations at fixed salt concentration of 0.4 M KCl; 1%(w/w)(○); 8%(w/w)(□) and 16%(w/w)(△).

for polydisperse (Gaussian) homogeneous spheres, in combination with an effective structure factor for the higher concentrations, see figure 2.5. Generalized indirect Fourier transform[31–33] analysis indicates that the scattering objects, the micellar cores, have a spherical shape with a radius of gyration $R_g = 8.1 \pm 0.4$ nm. For samples above 4%(w/w), the structure factor becomes more pronounced, exhibiting a peak for the gel samples at $q \approx 0.21$ nm^{-1}. This corresponds to an inter-micellar distance of approximately 30 nm.

The viscosity (η) of the reversible gels as a function of concentration (C) was investigated with rheometry. A surprisingly strong dependence is found: η increases by more than six orders of magnitude over a fourfold increase in concentration, see figure 2.6. The C_{gel} is approximated to be 4%(w/w), by extrapolating the data points to the viscosity of a 5 °C PEG_{230} solution. The gels are responsive to temperature, since the viscosity decreases roughly by an order of magnitude upon an increase in temperature by 25 degrees.

Charge-driven assemblies are responsive to ionic strength. The scattered light intensity decreases with increasing [KCl], indicating that the driving force for micelle formation is weakened with increasing salt concentration, see figure 2.7a. From this figure, a critical KCl concentration $I_{cr} = 1.7$ M KCl can be determined. The light scattering data are in agreement with the rheological data. The viscosity decreases strongly as a function of salt concentration, see figure 2.7b. As I_{cr} is approached, η approaches the value of a 16%(w/w) PEG_{230} solution, because of complete disintegration of the micelles. Hence, an almost solid-like gel can be transformed into a water-like fluid, simply by adding salt.

Since the homopolymer used in this particular system is a weak polyelectrolyte,

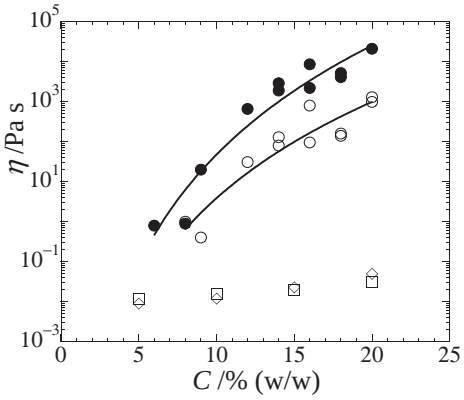

Figure 2.6: Viscosity as a function of the total polymer concentration at a fixed salt concentration of 0.4 M KCl. The viscosity of the reversible gel is given for two different temperatures: 5 °C (•) and 30 °C (○). The lines are drawn to guide the eye. Also shown are the viscosities of PEG_{230} (◇) and PAH_{160} (□) solutions in water at 5 °C and 0.4 M KCl.

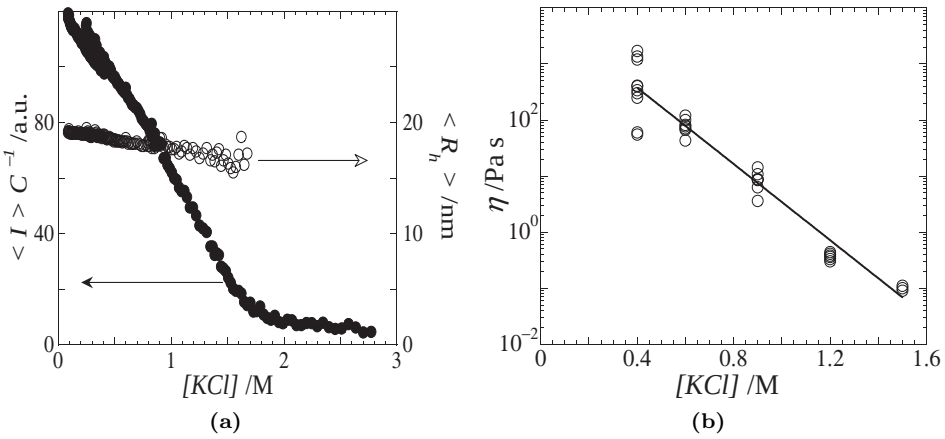

Figure 2.7: Influence of ionic strength in dilute solutions **(a)**, and concentrated solutions **(b)**. **(a)** Effect of ionic strength on the formation of flowerlike micelles. The average scattered light intensity normalized by the total polymer weight concentration, ($\langle I \rangle C^{-1}$, •, left axis) and average hydrodynamic radius ($\langle R_h \rangle$, ○, right axis), as a function of [KCl]. **(b)** Viscosity of a 16%(w/w) gel at 20 °C as a function of [KCl]. The line is an exponential fit through the data points.

the system also responds to pH. Upon increasing the pH of a dilute solution of micelles, the amount of micelles in solution slowly decreases, as indicated by a decrease in scattered light intensity, see figure 2.8a. This is due to discharging of the homopolymer PAH_{160} at p$H \geq 8$. The decrease in the number of micelles at p$H \geq 8$ is also noticeable in the gels. Addition of KOH to an 18%(w/w) gel

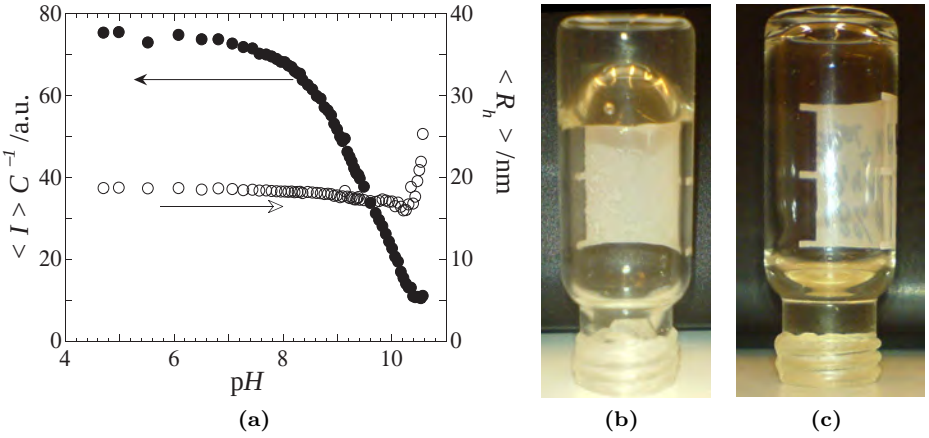

Figure 2.8: Influence of pH on the co-assembly of $PSPMA_{28}$—PEO_{230}—$PSPMA_{28}$ and PAH_{160} at 0.4 M KCl. **(a)** Average scattered light intensity normalized by total polymer weight concentration (•, left axis) and average hydrodynamic radius (○, right axis) as a function of pH. **(b)** The viscosity of a 18%(w/w) gel is high enough to take a picture with the gel sticking at the bottom of the vial. **(c)** Same gel as in (b), but with KOH added, leading to p$H \approx 9$. The viscosity has decreased such that the gel flows directly to the bottom when turning the vial up-side-down.

at 0.4 M KCl and $f^+ = 0.5$, drastically decreases the viscosity of the gel, see figures 2.8b and 2.8c.

2.4 Conclusions & Outlook

Concluding, in this Chapter we have presented a new class of multi-responsive reversible gels based on charge-driven co-assembly of two water soluble components: an ABA triblock copolymer with a neutral and hydrophilic middle-block and polyelectrolyte end-blocks, and an oppositely charged homopolymer. Based on SAXS data we conclude that these reversible gels consist of a network of interconnected polyelectrolyte complex micelles. The properties of this network can be tuned by varying the concentration, temperature, ionic strength, pH and charge composition.

In general, the multi-responsiveness of this new class of reversible gels, combined with the ability to choose both the type and length of each of the individual components, allows for an almost endless variety in gel properties. This makes charge-driven reversible gels interesting candidates for a multitude of possible applications.

References

[1] R. A. Register, M. Foucart, R. Jerome, Y. S. Ding and S. L. Cooper, *Macromolecules*, 1988, **21**, 1009–1015.

[2] R. D. Jenkins, C. A. Silebi and M. S. El-Asser, *Acs Symposium Series*, 1991, **462**, 222–233.

[3] T. Annable, R. Buscall, R. Ettelaie and D. Whittlestone, *Journal of Rheology*, 1993, **37**, 695–726.

[4] P. Kujawa, H. Watanabe, F. Tanaka and F. M. Winnik, *European Physical Journal E*, 2005, **17**, 129–137.

[5] J. Sprakel, E. Spruijt, M. A. Cohen Stuart, N. A. M. Besseling, M. P. Lettinga and J. van der Gucht, *Soft Matter*, 2008, **4**, 1696–1705.

[6] C. Tsitsilianis, I. Iliopoulos and G. Ducouret, *Macromolecules*, 2000, **33**, 2936–2943.

[7] F. Bossard, T. Aubry, G. Gotzamanis and C. Tsitsilianis, *Soft Matter*, 2006, **2**, 510–516.

[8] N. Stavrouli, T. Aubry and C. Tsitsilianis, *Polymer*, 2008, **49**, 1249–1256.

[9] P. J. Skrzeszewska, F. A. de Wolf, M. W. T. Werten, A. Moers, M. A. Cohen Stuart and J. van der Gucht, *Soft Matter*, 2009, **5**, 2057–2062.

[10] V. Tirtaatmadja, K. C. Tam and R. D. Jenkins, *Macromolecules*, 1997, **30**, 3271–3282.

[11] L. E. Bromberg and D. P. Barr, *Macromolecules*, 1999, **32**, 3649–3657.

[12] E. J. Regalado, J. Selb and F. Candau, *Macromolecules*, 1999, **32**, 8580–8588.

[13] A. C. Lara-Ceniceros, C. Rivera-Vallejo and E. J. Jimenez-Regalado, *Polymer Bulletin*, 2007, **58**, 425–433.

[14] C. Tsitsilianis, N. Stavrouli, V. Bocharova, S. Angelopoulos, A. Kiriy, I. Katsampas and M. Stamm, *Polymer*, 2008, **49**, 2996–3006.

[15] F. Tiebackx, *Zeitschrift für Chemie und Industrie der Kolloide*, 1911, **8**, 198–201.

[16] H. Bungenberg de Jong and H. Kruyt, *Proceedings of the Koninklijke Nederlandse Akademie van Wetenschappen*, 1929, **32**, 849–856.

[17] H. Bungenberg de Jong, *Crystallisation Coacervation Flocculation*, Elsevier, Amsterdam, 1949, vol. II, Chapter X.

[18] A. Harada and K. Kataoka, *Macromolecules*, 1995, **28**, 5294–5299.

[19] A. Harada and K. Kataoka, *Science*, 1999, **283**, 65–67.

[20] A. V. Kabanov, T. K. Bronich, V. A. Kabanov, K. Yu and A. Eisenberg, *Macromolecules*, 1996, **29**, 6797–6802.

[21] M. A. Cohen Stuart, N. A. M. Besseling and R. G. Fokkink, *Langmuir*, 1998, **14**, 6846–6849.

[22] S. van der Burgh, A. de Keizer and M. A. Cohen Stuart, *Langmuir*, 2004, **20**, 1073–1084.

[23] K. Jankova, X. Y. Chen, J. Kops and W. Batsberg, *Macromolecules*, 1998, **31**, 538–541.

[24] J. M. Dust, Z. H. Fang and J. M. Harris, *Macromolecules*, 1990, **23**, 3742–3746.

[25] K. Jankova and J. Kops, *Journal of Applied Polymer Science*, 1994, **54**, 1027–1032.

[26] M. Kato, M. Kamigaito, M. Sawamoto and T. Higashimura, *Macromolecules*, 1995, **28**, 1721–1723.

[27] J. S. Wang and K. Matyjaszewski, *Macromolecules*, 1995, **28**, 7901–7910.

[28] G. Masci, D. Bontempo, N. Tiso, M. Diociaiuti, L. Mannina, D. Capitani and V. Crescenzi, *Macromolecules*, 2004, **37**, 4464–4473.

[29] D. E. Koppel, *Journal of Chemical Physics*, 1972, **57**, 4814–&.

[30] J. Kohlbrecher and I. Bressler, *SASfit*, 2010.

[31] O. Glatter, *Journal of Applied Crystallography*, 1977, **10**, 415–421.

[32] B. Weyerich, J. Brunner-Popela and O. Glatter, *Journal of Applied Crystallography*, 1999, **32**, 197–209.

[33] A. Bergmann, G. Fritz and O. Glatter, *Journal of Applied Crystallography*, 2000, **33**, 1212–1216.

Chapter 3

The Influence of Charge Ratio on Transient Networks of Polyelectrolyte Complex Micelles

We study the influence of charge ratio on the transient network formation of bridged polyelectrolyte complex micelles. The polyelectrolyte complex micelles are based on mixing an ABA triblock copolymer in which the A-blocks are positively charged and the B-block is neutral and hydrophilic, and a negatively charged homopolymer. We investigate the microstructure of our samples with (dynamic) light scattering and small-angle X-ray scattering, and the mechanical properties by rheometry. At charge stoichiometric conditions, we obtain flowerlike polyelectrolyte complex micelles. These micelles become interconnected at high concentrations, leading to a sample-spanning transient network. For excess negative charge conditions, we obtain so-called 'soluble complexes' which are small aggregates carrying the excess negative charge on the polyelectrolyte complex parts. For excess positive charge conditions, micelles stay intact, because the triblock copolymers can localize the excess positive charge at the periphery of the micellar corona. This structural asymmetry is not reflected in the mechanical properties, which show a strong decrease in viscosity on either side of the charge stoichiometric point.

This chapter is published as paper with supporting information:
Marc Lemmers, Evan Spruijt, Lennart Beun, Remco Fokkink, Frans Leermakers, Giuseppe Portale, Martien A. Cohen Stuart and Jasper van der Gucht, *Soft Matter*, 2012, **8**, 104-117.

3.1 Introduction

The mechanical properties of liquids can be drastically altered by incorporation of a network forming agent. In physical gels the network consists of non-permanent cross-links that can break and reform continuously, contrary to covalently cross-linked chemical gels. This makes physical gels responsive to external stimuli. It also enables the relaxation of internal stresses, meaning that physical gels are essentially liquid-like.

For environmental reasons, water is the ideal solvent for applications. There are many examples of water-based physical gels, of which the hydrophobically end-capped polyurethane associative thickeners are most extensively studied and applied.[1–6] In these systems, hydrophobic groups on the extremities of a long polymeric spacer cluster together to form the micellar nodes in the transient network. Hydrophobicity of the end-blocks is the driving force in many other examples of water-based transient networks.[7–10] Some of the possibilities for reversible network formation have recently been reviewed.[11]

Of all driving forces for association, electrostatic interaction is possibly the most versatile. There are, however, only a few examples of transient networks in which electrostatic interactions play a key role.[12,13] Recently, we developed a water-based two component physical gel based on electrostatic interactions only. We have achieved this by mixing an aqueous ABA triblock copolymer solution, in which the A blocks are negatively charged and the B block is neutral and hydrophilic, with an aqueous solution of positively charged homopolymer. The two polymeric components interact to form a well defined multi-responsive transient network of interconnected polyelectrolyte complex micelles (see Chapter 2).[14]

Dilute solutions of polyelectrolyte complex micelles have been studied for quite some years,[15–17] and this has led to a basic understanding of the principles governing the properties of polyelectrolyte complex micelles in dilute solutions.[18–20] Understanding the dominant phenomena in charge-driven association was key to the creation of more 'exotic' types of polyelectrolyte complex micelles.[21–23]

A defining property of polyelectrolyte complex micelles is that at least two oppositely charged moieties are needed to create a driving force for association. This implies that charge composition is a new variable: one can mix, or synthesize, the charged moieties in different ratios. Since electrostatic interaction is the driving force for association, it is convenient to express the composition of the charged moieties in terms of charge ratio. The influence of charge ratio on micellar systems has been recognized from the beginning,[15] and it is now well established that the association of the oppositely charged moieties is strongest at a 1:1 charge ratio.[17,24–29]

This is not only valid for polyelectrolyte complex micelles, but is a generic feature of charge-driven association.[20,30–33] On the contrary, it is much less clear what happens to the polyelectrolyte complex micelles away from the charge stoichiometric point. Generally it is assumed that excess charge accumulates in the polyelectrolyte complex, which progressively destabilizes the micelles, making them eventually fall apart into so-called 'soluble complexes',[17,24] a term originally assigned to non-stoichiometric complexes of two oppositely charged homopolymers.[34]

The dependence of the transient network topology on concentration and ionic strength at charge stoichiometric conditions has been described recently (see also Chapter 4).[35] However, what happens to transient networks of interconnected polyelectrolyte complex micelles away from the charge stoichiometric point has never been investigated, despite charge composition being a crucial parameter in charge-driven association. Understanding the role of charge composition is also of industrial interest, for it is another parameter to tune the mechanical properties of this water-based multi-responsive two-component rheology modifier.

Here we present a study on the influence of charge ratio on transient networks of polyelectrolyte complex micelles. We do so by preparing polyelectrolyte complex micelles and their transient networks in an analogous manner as in previous studies (Chapters 2 and 4),[14,35] with the difference that in this Chapter we use a triblock copolymer with positively charged end-blocks and a negatively charged homopolymer. We vary the charge composition, while keeping the total polymer concentration constant. Scattering techniques in combination with rheometry clarify the microstructure at non-stoichiometric conditions. We find a remarkable asymmetry in the microstructure at the two different sides of the stoichiometric composition, which is not reflected in the mechanical behaviour of our gels.

3.2 Experimental

3.2.1 Triblock copolymer synthesis

The triblock copolymer was synthesized in two steps. First, a bifunctional macroinitiator was synthesized based on the method by Jankova and coworkers.[36] The detailed synthetic protocol has been described elsewhere (Chapter 2).[14] In brief, poly(ethylene glycol) of M_n = 10 kg mol^{-1} (Fluka, PDI = 1.04) was dissolved in toluene. After addition of triethylamine and 2-bromoisobutyryl bromide, the reaction mixture was stirred for five days at 30 °C. Purification was performed by treatment with charcoal, filtration, precipitation in petroleum ether, filtration, redissolving in THF and precipitation in petroleum ether (twice), filtration and

drying overnight under vacuum. The degree of esterification was 100% as determined by ^{1}H-NMR.[37,38]

The bifunctional macro-initiator was used to synthesize the triblock copolymer by atom transfer radical polymerization,[39,40] based on the method described by Li and coworkers.[41] In detail, 11.8 g of the bifunctional macro-initiator was mixed with 21.2 g [2-(methacryloyoxy)ethyl] trimethylammonium chloride (Sigma Aldrich, 78wt% in water), 0.9 g bipyridyl (Acros Organics, 99+ %), 2-propanol and deionized water. The solvent ratio was 1:1 (v/v). The mixture was stirred and placed in an oil bath at 40 °C, while removing oxygen by bubbling argon for 45 minutes. Subsequently, 1.1 mmol Cu(I)Cl and 1.1 mmol Cu(II)Cl_2 were added to the mixture to start the reaction. After two hours, additional degassed solvent was added to facilitate stirring. The reaction was quenched after a total of five hours by bubbling oxygen through the mixture. The product was purified by dialysis against deionized water for three days, refreshing the dialysis bath every day. After the partial removal of water by evaporation at reduced pressure, the product was obtained by freeze-drying overnight. The yield by weight was 73% (20 g). On average 68 monomers were attached per macro-initiator molecule, as determined by ^{1}H-NMR, see appendix.

3.2.2 Homopolymer synthesis

Preparation of the negatively charged homopolymer was based on the work of Masci and coworkers.[42] 15.2 g of 3-sulfopropylmethacrylate potassium salt (KSPMA) (62 mmol) was dissolved in approximately 25 ml DI-water/DMF (volume 1:1). The mixture was continuously stirred at approximately 45 °C while removing oxygen by bubbling argon for approximately one hour. Then 167 mg bipyridyl, 28.5 mg Cu(II)Cl_2 followed by 20.8 mg Cu(I)Cl were added to the mixture. To start the polymerization, 45.3 mg (0.23 mmol) of 2-EBiB was added, aiming for a degree of polymerization of approximately 260. The reaction mixture was left for 22 hours to react.

The reaction was quenched by bubbling oxygen through the reaction mixture, and addition of DI-water. The product was purified by dialysis against 1.0 M KCl (3×), to remove the copper catalyst, and DI-water (3×). After filtration of the solution over a 0.2 μm syringe filter and removal of excess water by evaporation at reduced pressure, the product was obtained by freeze-drying overnight. The yield was determined to be 71% by weight (10.8 g).

^{1}H-NMR could not be used to determine the degree of polymerization, since the signal from the protons in the initiator is too weak to be accurately compared with

the signal from the SPMA monomers. Size exclusion chromatography indicated an average degree of polymerization of 173 with a PDI of 1.8, based on poly(styrene sulfonate) standards at identical conditions.

3.2.3 Sample preparation

All samples were prepared on weight basis and in 1 g quantities. Samples were prepared by diluting from stock solutions. In this work we use the total polymeric weight percentage as concentration unit. For example, when we prepare a 20wt% solution, this means that the total weight of both polymers is 0.2 g in 1 g total sample weight. The concentrations investigated are 0.5wt% (dilute), 5wt%, 10wt%, 15wt% and 20wt% (concentrated). All samples were prepared at 0.35 M KCl, including the released counterions of all matched polyelectrolyte ion-pairs. Samples were vortexed for 1 min to mix all the components. More vigorous manual stirring was applied for high viscosity samples. 1 g of sample was enough to do both SAXS and rheometry, in case of the concentrated samples, or SAXS and light scattering, in case of the dilute samples.

In this work we study the influence of charge ratio. The components in this study do not have a similar number of charges per gram of polymer. The number average molecular weight of the triblock copolymer is 24.4 kg mol^{-1} with 68 positive charges (34 on each end-block), and the number average molecular weight of the homopolymer is 42.6 kg mol^{-1} with 173 negative charges. The charge ratio fixes the relative amount of each component. To keep the total polymer concentration constant, we therefore need to change the absolute amount of each component for each charge ratio. Note that the fraction of triblock copolymer per total polymeric weight, and the fraction of homopolymer per total polymeric weight, for each charge composition, is the same for all concentrations. For example, of the total weight of polymeric material in all 1:1 charge ratio samples, 60% of the weight is triblock copolymer and 40% of the weight is homopolymer. Table 3.1 gives an example of the preparation of the 20wt% samples, and the fractions of each component per charge ratio. The last two columns in table 3.1 give the relative fraction and the weight concentration of neutralized units respectively, as explained in the results section.

3.2.4 Light scattering

Dynamic light scattering experiments were performed on an ALV-125 goniometer, combined with a 300 mW Cobolt Samba-300 DPSS laser operating at a wavelength of 532 nm, an ALV optical fiber with a diameter of 50 μm, an ALV/SO Single

Table 3.1: Example of the contents of a 20wt% sample of 1 g total weight. TB means triblock copolymer, HP means homopolymer. Also given are the fractions of each component needed for that charge ratio. The last two columns express the relative and the real weight concentration of neutralized units present in solution, as defined in the text.

f^+	TB	HP	total polymer	solvent	TB	HP	$\frac{C_{nu}(f^+)}{C_{nu}(0.5)}$	C_{nu}
-	g	g	g	g	fraction	fraction	-	wt%
0.0	0.000	0.200	0.20	0.80	0.00	1.00	-	-
0.1	0.028	0.172	0.20	0.80	0.14	0.86	0.24	4.8
0.3	0.078	0.122	0.20	0.80	0.39	0.61	0.65	13.0
0.4	0.098	0.102	0.20	0.80	0.49	0.51	0.83	16.6
0.5	0.120	0.080	0.20	0.80	0.60	0.40	1.00	20.0
0.6	0.138	0.062	0.20	0.80	0.69	0.31	0.76	15.2
0.7	0.154	0.046	0.20	0.80	0.77	0.23	0.55	11.0
0.9	0.186	0.014	0.20	0.80	0.93	0.07	0.18	3.6
1.0	0.200	0.000	0.20	0.80	1.00	0.00	-	-

Photon Detector and an ALV5000/60X0 External Correlator. Temperature was controlled using a Haake F8-C35 thermostatic bath. Angle of detection was varied between 40-130°. The hydrodynamic radius was found to be independent of the angle, see appendix. The values reported in the main text are detected at an angle of 90°, corresponding to a wave vector of $q = 0.022$ nm^{-1}. Examples of correlation functions for various charge ratios are presented in the appendix.

The part of the solutions not used for SAXS measurements was put into glass measuring cells for light scattering measurements.

3.2.5 Small-angle X-ray scattering

SAXS experiments were performed at the Dutch-Belgian Beamline (DUBBLE, BM26B) at the European Synchrotron Radiation Facility (ESRF) in Grenoble, France.[43] SAXS data were recorded on a two-dimensional position-sensitive wire chamber detector. A 10 keV X-ray energy was used with a sample-to-detector distance of about 7 m. The scattering vector range covered was $0.05 < q < 1$ nm^{-1}. The magnitude of the scattering vector is $q = (4\pi/\lambda)\ sin(\theta/2)$, where θ is the scattering angle. The two-dimensional images were radially averaged around the center of the primary beam in order to obtain the isotropic SAXS intensity profiles. The peak positions from a standard specimen of wet rat tail tendon collagen were used to calibrate the scattering vector scale of the scattering curves. A matlab/Fit2D based macro available at DUBBLE has been used to perform the radial integrations. The data were normalized to the intensity of the incident beam, to correct for primary beam intensity fluctuations, and were corrected for absorption and

background scattering. Water and high density polyethylene (ELTEX) were used as secondary standards in order to calibrate the scattered intensity on absolute scale. Samples were loaded into 2 mm quartz capillaries (Hilgenberg, Germany) using syringes and needles. The filled capillaries were loaded into a home-made multi-capillary holder, enabling fast sample exchange during SAXS measurements. Samples were measured for different times, depending on the concentration, varying from 5 minutes for the most concentrated samples, to 20 minutes for the dilute samples (0.5wt%). We have used the Scatter program (v. 2.4) to fit our SAXS data.[44–46]

3.2.6 Rheometry

Rheological measurements were performed using an Anton Paar Physica MCR301 stress-controlled rheometer, operating in strain-controlled mode. Cone and plate geometries were used, with a cone diameter of either 50 mm or 25 mm. The angle of the cone was 1° for both geometries. The solvent blocker setup was used to minimize the effect of evaporation. Temperature was controlled at 20 °C by Peltier elements in both the plate and the hood. Samples were poured onto the plate if possible. Care was taken to minimize the forces on the sample while bringing the cone into measuring position. Waiting time before the start of the measurement was at least 0.5 h. All data were obtained without a time limit (no time setting) and are therefore considered to be steady-state values.

Frequency sweeps were performed at 2% strain, which was checked to be in the linear visco-elastic regime, by performing amplitude sweeps at multiple frequencies. Flow curves were measured for shear rates of 0.01-1000 s^{-1}, going from low to high shear rate.

Exactly the same samples were used as the ones used for the SAXS experiments, except for the 20wt% $f^+ = 0.5$ sample, which did not contain enough fluid anymore. In that case a fresh gel was prepared and measured a week after preparation.

3.3 Results and Discussion

3.3.1 Scattering of individual objects

We use light scattering and small-angle X-ray scattering to obtain insight in the shape and size of the scattering objects as a function of charge ratio. To express

the ratio of positive to negative charges, we define a charge composition variable:[24]

$$f^+ = \frac{[+]}{[+]+[-]} \tag{3.1}$$

which is the ratio between the concentration of positively chargeable groups on the polymers, [+], and the total concentration of chargeable groups on the polymers, [+] + [−]. f^+ is easily computed from the polymer characterization of groups, since we are dealing here with two strongly charged polyelectrolyte moieties. In this study we investigate the influence of charge ratio for several concentrations; dilute samples at 0.5wt%, and more concentrated samples at 5, 10, 15 and 20wt%. The charge ratio f^+ was varied, while keeping the total polymer weight concentration fixed. This means that the concentrations of both components change when changing f^+. An example for the 20wt% sample is given in table 3.1.

The scattered light intensity is used to compute the excess Rayleigh ratio at a scattering angle of 90°, ΔR_{90}, using equation 3.2.[47,48]

$$\Delta R_{90}(f^+) = \left(\frac{I_{90}(f^+) - I_{bg}(f^+)}{I_{\text{tol}}}\right)\frac{n^2}{n_{\text{tol}}^2}R_{\text{tol}} \tag{3.2}$$

where I_{90} is the scattered light intensity of the sample at a scattering angle of 90°, I_{bg} is the background scattering including solvent scattering and monomer scattering, I_{tol} is the reference scattering intensity of toluene at 90°, $n = 1.3365$ is the refractive index of the solvent,[49] $n_{\text{tol}} = 1.4961$ is the refractive index of toluene[49] and $R_{\text{tol}} = 2.1 \cdot 10^{-3}$ m^{-1} is the Rayleigh ratio of toluene at 90° for $\lambda = 532$ nm.[50] The value for $I_{bg}(f^+)$ for each charge ratio is obtained by a linear interpolation of the scattered light intensities between the two extremes of the charge ratio, *i.e.* $f^+ = 0.0$ and $f^+ = 1.0$, see appendix. This means that we subtract the maximum possible level of scattering not originating from aggregates, which is an overestimation of the real situation. However, this error is small, because the background scattering is much lower than the scattering of the sample, for most charge compositions. Hence, the reported values for the excess Rayleigh ratio originate from co-assembled structures only.

The excess Rayleigh ratio and average hydrodynamic radius for 0.5wt% solutions are displayed in figure 3.1. In the direction of increasing f^+, we initially see a modest increase of the excess Rayleigh ratio as well as the hydrodynamic radius, indicative of the formation of small scattering objects. Such objects have been named 'soluble complexes' in the past.[17,24,34] Upon approaching charge stoichiometry, we see a steep increase in the excess Rayleigh ratio and in the hydrodynamic radius. This increase can be attributed to the formation of 'free' micelles. These micelles

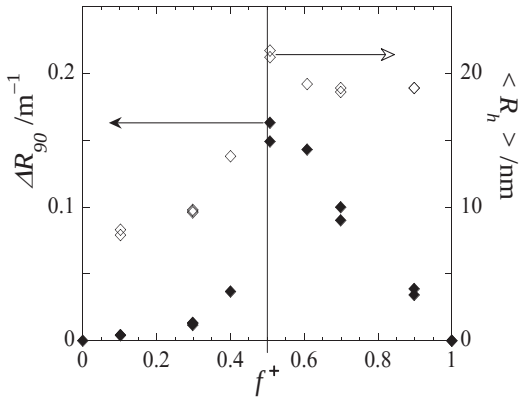

Figure 3.1: Excess Rayleigh ratio (ΔR_{90}, ♦, left axis) and hydrodynamic radius (R_h, ◇, right axis), as a function of charge stoichiometry, f^+. Samples are prepared by direct mixing, and have been given time to equilibrate. Total polymer concentrations are 0.5wt% for all samples.

have a polyelectrolyte complex core, consisting of the charged end-blocks of the triblock copolymer and the oppositely charged homopolymer. The polyelectrolyte complex core is stabilized by a corona of looped middle-blocks, since bridge formation is unlikely at these low concentrations. The micelles at charge stoichiometric conditions are named flowerlike polyelectrolyte complex micelles, since the looped middle-blocks represent the petals of a flower in a two dimensional representation of the micelles, see figure 3.9.[14,35] For the excess positive charge side of figure 3.1, $f^+ > 0.5$, the excess Rayleigh ratio decreases, but the drop is not as strong as on the excess negative charge side. The hydrodynamic radius of the scattering objects decreases somewhat compared to the 1:1 charge ratio, but the objects maintain a hydrodynamic radius that is in the micellar range of 15-25 nm. Clearly, the light scattering results show asymmetry as a function of charge ratio.

Such pronounced asymmetry has been observed only once for polyelectrolyte complex micelles based on diblock copolymers.[51] On the contrary, there are many reports showing more symmetric profiles.[17,24–29] A similar trend in the hydrodynamic radius as in figure 3.1 was observed in a previous study with other triblock copolymers (Chapter 4).[35] Both results indicate that in the case of an excess of the triblock copolymer, objects of micellar size can be tolerated in solution.

To further investigate the light scattering results, we have to make some assumptions about the origin of the scattering. The excess Rayleigh ratio is related to the weight concentration (C), the composition dependent mass ($M(f^+)$) and

shape of the scattering objects, and the interaction between the scattering objects:

$$\Delta R_{90}(q, f^+) = KCM(f^+)P(q)S(q) \tag{3.3}$$

where $P(q)$ is the particle form factor, $S(q)$ is the structure factor and K is the optical constant defined as:

$$K = \frac{4\pi^2 n^2}{N_A \lambda^4} \left(\frac{\mathrm{d}n}{\mathrm{d}C}\right)^2 \tag{3.4}$$

where $n = 1.3365$ is the refractive index of the solvent,[49] N_A is Avogadro's number, $\lambda = 532$ nm is the wavelength of the light and $\left(\frac{\mathrm{d}n}{\mathrm{d}C}\right) = 1.39$ is the estimated refractive index increment, see appendix. If we assume that the refractive index increment is independent of the overall stoichiometry,[52] we find a value for the optical constant of $K = 8.97 \cdot 10^{-6}$ m^2 mol kg^{-2}. We furthermore assume that $P(q) \approx 1$ (since $qR_h \leq 0.5$) and that the 0.5wt% solutions are dilute enough so that $S(q) \approx 1$. The values for the excess Rayleigh ratio given in figure 3.1 are therefore proportional to the product of the weight concentration and the mass of the scattering objects.

We can now consider two extreme cases for the composition of the scattering objects: A) All polymers in solution are present in aggregates and thus contribute to the excess scattering. Since the overall concentration is equal in all samples, we can attribute the increase and decrease of the excess Rayleigh ratio to an increase and decrease in the mass of the aggregates. A consequence of this hypothesis is that all the excess charge is present on the aggregates themselves. B) The aggregates are electroneutral and the excess charge is present as free polymers in solution. In this case the increase and decrease in excess Rayleigh ratio originate from changes in weight concentration as well as changes in mass of the aggregates.

The real situation is probably somewhere in between these two extreme cases. However, we argue that the second case is closer to reality than the first, for four reasons: i) From a systematic study on polyelectrolyte-protein complexes, it has been shown that the charge ratio inside such a complex is close to stoichiometric, independent of the overall mixing ratio.[30] This implies that the excess charge is present in solution as free polymers. ii) For case A, the decrease in scattered light intensity observed for $f^+ > 0.5$ in figure 3.1 must be caused by a decrease in the mass of the scattering objects. This is in disagreement with our observations shown in the same figure that the size of the scattering objects remains approximately constant for $f^+ \geq 0.5$. iii) In case A all the polymers are present in aggregates, which means sacrificing a lot of translational entropy of the poly-

mers. iv) Aggregates with excess charge are unfavourable because of electrostatic repulsion. The electrostatic energy needed to incorporate one extra charge is $e\Psi_d$ with Ψ_d the surface potential of the micellar core. This should not be much larger than the thermal energy kT, so that Ψ_d cannot be much more than 25 mV. From this we estimate the maximum surface charge $\sigma \approx \epsilon\kappa\Psi_d \approx 0.05$ C m^{-2}, with κ the inverse Debye screening length. Taking the surface area of the micellar core as a few hundred nm^2, this means that at most 1-5 extra triblock copolymers, or 1-2 extra homopolymers, can be incorporated per polyelectrolyte complex. As we will see below, this number is small compared to the overall aggregation number, so that the relative deviation from stoichiometry is small. Larger deviations from stoichiometry would require the incorporation of counterions into the polyelectrolyte complex core to compensate the excess charge, which would lead to a large loss of counterion entropy.

More detailed theoretical calculations by Shklovskii *et al.* and Rubinstein *et al.* substantiate our arguments in favour of case B, showing that a coexistence of neutral polyelectrolyte complexes and charged aggregates is more favourable than distributing all charges evenly over all complexes.[53,54]

Based on these arguments, we propose that the relative deviations from the stoichiometric ratio in the polyelectrolyte complex core are small, and that most of the excess polymeric charge resides as free polymers in the solution. This means that for the calculation of the mass of the scattering objects it is reasonable to assume that all charges in the polyelectrolyte complex core are compensated, so that it can be considered as composed of neutral units. To proceed, we define the smallest possible charge neutral unit that can be present in an aggregate, which is one triblock copolymer exactly neutralized by oppositely charged homopolymer. Such a single neutralized unit is merely a convenient calculation aid; it does not really exist in our system, because there is a significant mismatch between the number of charges in one triblock copolymer and one homopolymer. Hence, we only use it for estimating the mass of our aggregates, where we assume that the charge mismatch averages out in the polyelectrolyte complex. The corresponding molar mass of such a neutralized unit is $M_{nu} \approx 41.1$ kg mol^{-1}. The weight concentration of neutralized units present in solution varies per charge ratio and can be calculated taking into account the charge concentration of the minority species, thereby assuming that all of the minority species ends up in aggregates. The weight concentration of neutralized units, relative to the maximum weight concentration of neutralized units at charge stoichiometry, can be found in table 3.1 and is shown graphically in the appendix.

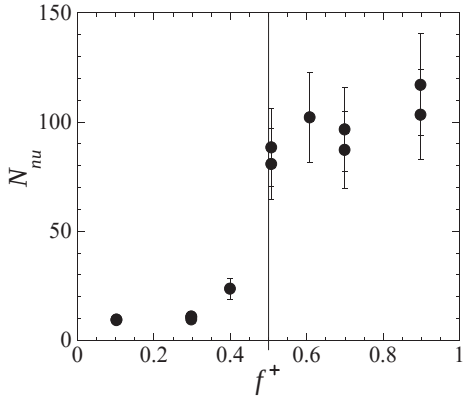

Figure 3.2: Estimate of the average number of neutralized units per aggregate, N_{nu}, as a function of charge ratio f^+. The error bars indicate the estimated degree of accuracy of ±20%.

We can now rewrite equation 3.3 to:

$$\Delta R_{90}(f^+) \approx KC_{nu}(f^+)M_{nu}N_{nu}(f^+) \tag{3.5}$$

where $C_{nu}(f^+)$ is the known weight concentration of neutralized units and $N_{nu}(f^+)$ is the average number of neutralized units per aggregate. Since all other values are known, we can easily estimate the number of neutralized units as a function of charge ratio from equation 3.5. The results are shown in figure 3.2. Taking only C_{nu} as the weight concentration of aggregates may be an underestimation, because it does not include the possible excess polymers in the core. Therefore the values shown in figure 3.2 are an upper limit. The real number of neutralized units will be slightly lower, especially far way from $f^+ = 0.5$. We estimate the uncertainties in the calculated values to be in the order of 20%.

Figure 3.2 shows that for values of $f^+ < 0.5$, the average number of neutralized units per scattering object is rather low, which is in agreement with the dynamic light scattering results showing objects of relatively small hydrodynamic radius. Upon approaching the charge stoichiometric ratio, there is a sudden increase in the number of neutralized units per aggregate, indicative of the formation of flowerlike micelles at $f^+ = 0.5$. The steep increase of the excess Rayleigh ratio for $0.3 \leq f^+ \leq 0.5$ in figure 3.1, can thus be explained by an increase in both the mass per scattering object and the weight concentration of scattering objects. For values of $f^+ \geq 0.5$, the weight concentration of scattering objects decreases, because C_{nu} decreases, but at the same time the mass per scattering object increases, see figure 3.2. This increase in mass per scattering object is the origin of the

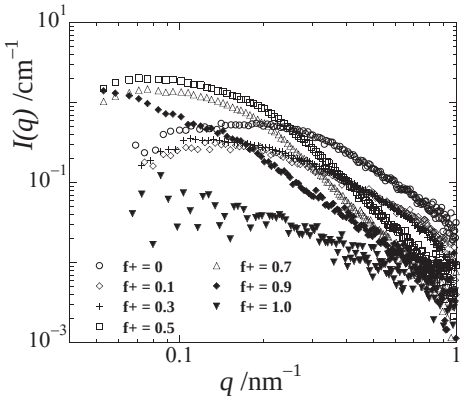

Figure 3.3: SAXS curves for 0.5wt% total polymer concentration. Only 30% of the data points are shown. Symbols correspond to charge ratios as indicated in the graph.

asymmetric shape of the excess Rayleigh ratio in figure 3.1.

Apparently the micelles can become more massive at excess positive charge conditions. One possible way by which this happens is by the detachment of charged blocks from the core and concomitant unfolding of loops in the corona, and the subsequent replacement of the detached blocks by new triblock copolymers to maintain charge neutrality in the core. In this way, the polyelectrolyte complex core composition does not change, while at the same time the mass of the micelle increases, see figure 3.9. This exchange mechanism, where one looped triblock copolymer is exchanged for two triblock copolymers having one end in the polyelectrolyte core and one end free in solution, is plausible for the following reasons: i) the triblock copolymer end-block is hydrophilic; ii) the polyelectrolyte complex core can stay close to electroneutral; iii) the excess charge that accumulates in the corona can be spread over periphery of the corona, because the chains are still mobile, to minimize the charge density in the corona; iv) the relatively high salt concentration used in this study causes only short ranged electrostatic repulsion, in the order of 1 nm, and facilitates the exchange of polyelectrolyte end-blocks.

We performed small-angle X-ray scattering measurements to further investigate the shape of the scattering objects and their interactions. Equation 3.3 also holds for X-ray scattering, provided that we take into account the different contrast for X-rays and the different magnitudes of the wave vectors q. The scattered intensity is now expressed as $I(q, f^+)$ instead of the excess Rayleigh ratio in the case of light scattering. The scattering curves for charge compositions of $f^+ = 0.0$ to $f^+ = 1.0$ are shown in figure 3.3.

In this figure we have also included 0.5wt% polymer solutions of both pure components, namely homopolymer only ($f^+ = 0$) and triblock copolymer only ($f^+ = 1$). We can now see the difference between the X-ray contrast of the two polymers. Clearly, the homopolymer has a higher scattering contrast than the triblock copolymer, which is probably due to the presence of the sulfur atom in the sulfonate moiety.

Rather strikingly, we see that almost all curves in figure 3.3 show a weak maximum at lower q-values. Only the $f^+ = 0.9$ and $f^+ = 1.0$ curves do not show a maximum. The curve of the $f^+ = 0.9$ sample has a somewhat peculiar shape, without a 'plateau' at low q. This shape would be difficult to explain and may be an experimental artefact. The weak maxima are indicative for interactions between the scattering objects. Apparently, a concentration of 0.5wt% is not dilute enough to rule out interactions. Even the homopolymer solution shows signs of a repulsive interaction. The interaction must be predominantly of steric origin, since the electrostatic interactions are only short ranged at a salt concentration of 0.35 M.

Considering the formation of complexes, we can see that the curves for $f^+ = 0.1$ and $f^+ = 0.3$ nearly overlap, indicating that a similar number of scattering objects of similar shape and size are present in solution. The curves of $f^+ = 0.5$ and $f^+ = 0.7$ can be clearly distinguished from the other curves, having a relatively high scattered intensity at low-q values, and a stronger q-dependence at higher q values. The shape of both curves is rather similar, the main difference being that the scattering of the $f^+ = 0.7$ curve is somewhat lower than for the 1:1 charge ratio, indicating that there are fewer scattering objects in solution.

None of the curves in figure 3.3 show form-factor minima, suggesting that the scattering objects are relatively polydisperse, even at 1:1 charge ratio. From previous reports it is known that salt concentration has a profound influence on the polydispersity of polyelectrolyte complex micelles.[17,35,55,56] However, lowering the salt concentration to a minimum of 10 mM KCl, does not change the SAXS curve significantly, see appendix. As shown by Spruijt and coworkers, we should not consider the absolute salt concentration as measure for the driving force for complex formation, but rather consider how close we are to the critical salt concentration.[57] The latter is defined as the salt concentration where the driving force to form a complex between two oppositely charged homopolymers of equal length vanishes. The critical salt concentration for the currently investigated combination of polyelectrolytes is a factor of three lower than for the combination studied in previous papers (Chapters 2 and 4).[14,20,35] A lower driving force for complex formation leads to less well-defined objects, which explains the polydisperse nature of the complexes studied in this Chapter.

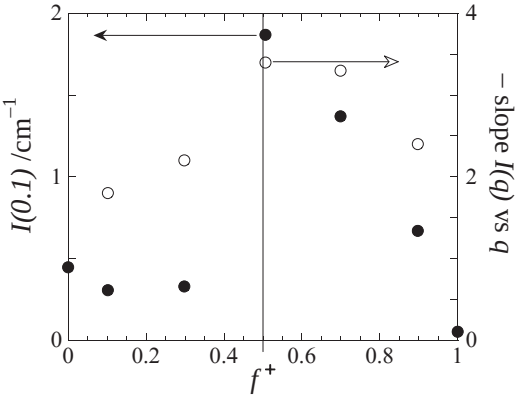

Figure 3.4: Values for $I(0.1)$ from the scattering curves (•, left axis), and minus the slope of the SAXS curves at high-q (∘, right axis), as a function of charge ratio f^+, for the 0.5wt% sample.

To see if the asymmetry in the excess Rayleigh ratio is also present in the X-ray scattering, we plot the values for $I(0.1)$ as function of charge ratio in figure 3.4. We assume here that this low-q scattering depends only on the weight concentration of scattering objects and the mass per scattering object. The shape of the $I(0.1)$ graph is very similar to the one in figure 3.1, both showing asymmetry as a function of charge composition. Note that the difference in $I(0.1)$ between $f^+ = 0.5$ and $f^+ = 0.7$ is relatively small, considering the relatively big difference in concentration of neutralized units in solution, see table 3.1. This means that the scattering at $f^+ = 0.7$ is higher than expected based on the weight concentration of scattering objects. This can only be explained by an increase in mass per scattering object at $f^+ = 0.7$, which is in agreement with the results of figure 3.2.

Also the slopes of the SAXS curves at high q in figure 3.3 change as a function of charge stoichiometry. We have analysed the slopes for $q \geq 0.3$ nm^{-1} for the different charge ratios, and the result can be found in figure 3.4. Again we see an asymmetric shape, with a maximum at 1:1 charge ratio. The higher the slope, the sharper is the interface of the scattering object. In other words, the scattering objects are the least 'fluffy' at 1:1 charge ratio.

3.3.2 Scattering of concentrated solutions

We have measured SAXS patterns also for more concentrated samples of 5wt%, 10wt%, 15wt% and 20wt%, to investigate how the scattering objects interact with each other. Figure 3.5 shows the result of the 20wt% samples. The scattering curves of 5wt%, 10wt% and 15wt% can be found in the appendix.

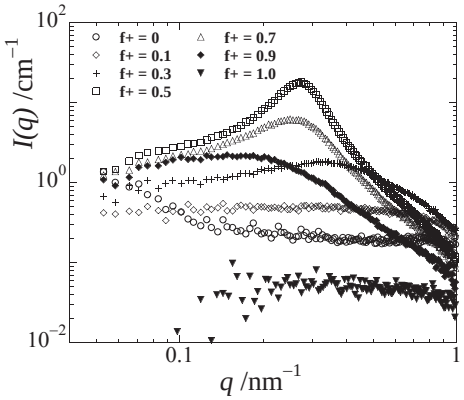

Figure 3.5: SAXS curves for 20wt% total polymer concentration samples. Only 30% of the data points are shown. Symbols correspond to charge compositions as indicated in the graph.

The scattering curves of both the homopolymer only and triblock copolymer only solutions are independent of q, indicating that the solutions are above the overlap concentration and that the typical length scale is beyond the limit of our explored q-range. The scattering of the $f^+ = 0.1$ sample is somewhat higher than the $f^+ = 0$ sample, caused by the formation of small objects; we can just see the influence of the form factor for the highest q-values. Apparently the volume fraction of these small scattering objects is low, since there is no sign of interactions in the curve. All other investigated samples do show a structure peak. This peak is most pronounced in the 1:1 charge ratio sample.

In general, the position of the maximum in the scattered intensity corresponds to a typical length scale, meaning that the centers of the scattering objects are frequently found at a distance of $D = \frac{2\pi}{q_{\text{peak}}}$ apart from each other. A true peak in the scattered intensity can be seen in the curves around charge stoichiometry, *i.e.* for the values of $f^+ = 0.3$, $f^+ = 0.5$ and $f^+ = 0.7$. We have computed the values for D for these three charge compositions and for the four different concentrations investigated, see figure 3.6a. The distance between the centers of the scattering objects decreases with increasing concentration, as expected. D decreases approximately with the cubic root of the concentration for $f^+ = 0.5$ and $f^+ = 0.7$, meaning that the volume fraction of the scatterers increases linearly with concentration. Note that the values at 5wt% are less accurate than the other values, since no clear maximum can be seen in the scattering curves, see appendix. Extrapolating the $f^+ = 0.7$ data fit to a concentration of 0.5wt% yields a typical length scale of $D \approx 75$ nm, corresponding to a $q_{\text{peak}} \approx 0.08$ nm^{-1}. This is indeed the value where we start to see interactions between the scattering objects, in the

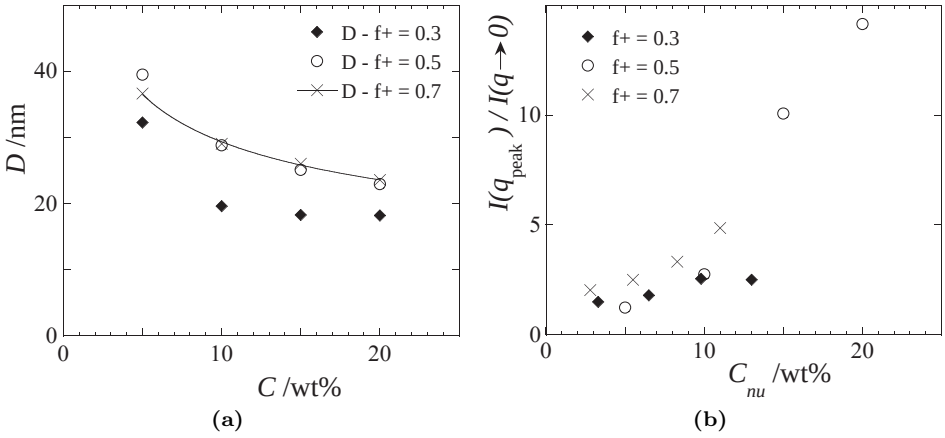

Figure 3.6: Qualitative measures for the degree of order in the different samples. **(a)** Typical distance between the centers of the scattering objects. The line is a power-law fit to the $f^+ = 0.7$ data, and scales as $C^{-0.3}$. **(b)** $\frac{I(q_{\text{peak}})}{I(q \to 0)}$, as a function of weight concentration of neutralized units, C_{nu}, for $f^+ = 0.3$ (♦), $f^+ = 0.5$ (○) and $f^+ = 0.7$ (×).

form of a weak maximum, for the dilute $f^+ = 0.7$ samples, see figure 3.3.

Comparing the results for different charge compositions, we see again that the samples of $f^+ = 0.5$ and $f^+ = 0.7$ are almost similar. D is lower for the $f^+ = 0.3$ sample, in agreement with the previous findings that the scattering objects at this charge ratio are considerably smaller.

A different qualitative measure for the degree of ordering in the sample is the ratio of the scattered intensity maximum and the scattered intensity at low q-values, $\frac{I(q_{\text{peak}})}{I(q \to 0)}$. These values have been computed for the three different charge compositions and are plotted as a function of the concentration of neutralized units (see appendix) in figure 3.6b.

The order in the samples increases with increasing concentration of neutralized units for the $f^+ = 0.5$ and the $f^+ = 0.7$ samples. For low concentrations, the ordering for the $f^+ = 0.7$ samples seems to be consistently higher than for the other samples. In other words, with the same amount of aggregated material the ordering is stronger in the $f^+ = 0.7$ samples. This may be caused by a longer ranged repulsion in these samples, or by an increased volume fraction with the same amount of aggregates. The latter implies that the density of the total aggregates is somewhat lower for $f^+ > 0.5$ conditions.

For higher concentrations of neutralized units, we see a pronounced increase in structure formation for the $f^+ = 0.5$ samples. This strong increase is caused by the combination of the attractive bridging interactions and the repulsion between

the micellar coronas, which keeps the micelles at a preferred distance from each other.[14,35] The $f^+ = 0.7$ samples show a similar upturn in structure formation. Unfortunately, we cannot determine whether this would keep increasing, as C_{nu} does not become higher than 11wt% in the $f^+ = 0.7$ samples. The ordering is least in the $f^+ = 0.3$ samples. Apparently, the volume fraction of these smaller aggregates is too low to induce pronounced ordering, which would mean that the density of these aggregates is higher than for $f^+ \geq 0.5$ conditions. Another possible explanation for the lack of ordering in this sample is that the particles are softer.

3.3.3 SAXS data fitting

Although there are no form- and structure factors available describing the shape and interactions of non-stoichiometric polyelectrolyte complex micelles, we assume that a core-shell model does reasonably well to get an idea of the size of the scattering objects. Interactions between particles may be described by the hard-sphere model, as a first approximation. We use these simple models, which were shown to work well for flowerlike micelles of stoichiometric charge ratio,[14,35] to get an idea of the relevant sizes and the range of interactions. The resulting fits and fitting parameters can be found in the appendix, as well as the fitted values for $I(0)$ for both 0.5wt% and 20wt%, which show similar asymmetry as figures 3.1 and 3.4. Here we show the results for the fitted radii R_{core}, R_{shell} and total aggregate radius $R_{\text{agg}} = R_{\text{core}} + R_{\text{shell}}$, the effective hard sphere radius, R_{HS}, and the effective volume fraction of hard spheres, ϕ.

Figure 3.7 shows the results for the several radii obtained by model fitting the SAXS data in dilute (0.5wt%, figure 3.7a) and concentrated (20wt%, figure 3.7b) samples. Note that the 0.5wt% SAXS curves could be satisfactorily fitted by applying a form factor fit only, see appendix. From figure 3.7a we can see that, in the dilute samples, $R_{\text{shell}} > R_{\text{core}}$ for all charge compositions. The shell thickness increases with increasing f^+, whereas the core radius seems to have a maximum around $f^+ = 0.5$. There is a steep increase in shell radius from $f^+ = 0.7$ to $f^+ = 0.9$, which fits the hypothesis that the loops in the corona unfold, sticking one charged end-block into the solution. Overall, the SAXS fitting results are in agreement with the dynamic light scattering data of figure 3.1. For excess negative charge we have smaller scattering objects of approximately 10 nm, and for excess positive charge we have bigger scattering objects of 15-20 nm. However, the hydrodynamic radius from figure 3.1 seems to be more or less constant for excess positive charge, and does not display this 'jump' for $f^+ = 0.9$.

Model fitting of the 20wt% samples results in smaller micelles than in the diluted

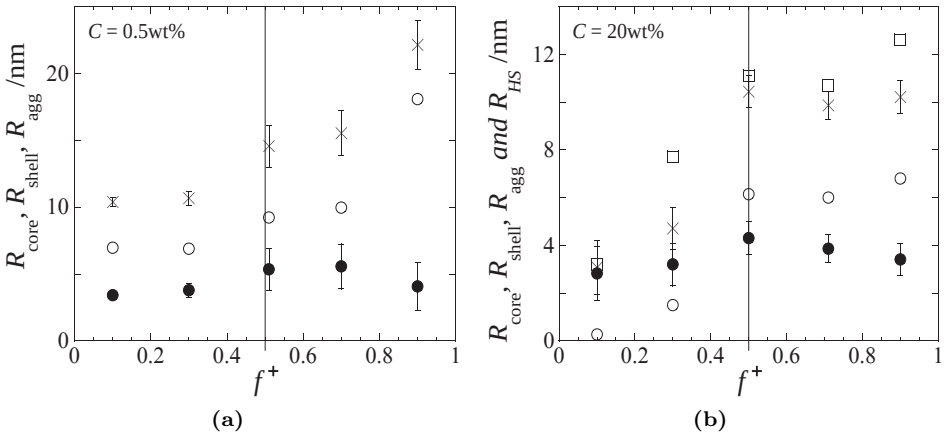

Figure 3.7: Graphs show the different radii as obtained from model fitting the SAXS data. Symbols indicate different radii: R_{core} (•), R_{shell} (○), R_{agg} (×) and R_{HS} (□). Error bars correspond to the relative standard deviation of R_{core}, as obtained by the fit. **(a)** Radii from fitting the 0.5wt% data. **(b)** Radii from fitting the 20wt% data.

samples, see figure 3.7b. The core radius seems to exhibit again a maximum around $f^+ = 0.5$. The shell seems to be almost absent in the $f^+ = 0.1$ sample, after which its thickness increases towards a constant value for values $f^+ \geq 0.5$. The hard-sphere radius R_{HS} is always slightly bigger than the total aggregate radius R_{agg}, and corresponds quite well to half of the average center-to-center distance D, as shown in figure 3.6a.

From the structure factor fit we obtain the hard-sphere radius and the effective volume fraction of hard-spheres. The fitted effective volume fraction values are displayed in figure 3.8 and show asymmetry, similar to the experimental results of figures 3.1 and 3.4. That the volume fraction exhibits a maximum at 1:1 charge ratio is obvious, since at this point C_{nu} is highest. Since ϕ is approximately linear with concentration, we can correct for the concentration by dividing the volume fraction by the relative amount of neutralized units from table 3.1. What we obtain is a measure for the average volume per neutralized unit, see figure 3.8. The increase observed in this figure must mean that the average density of the scattering objects decreases for excess positive charge, as compared to the $f^+ = 0.5$ sample. This is in agreement with the results in figure 3.6b for the $f^+ = 0.7$ samples.

3.3.4 Structural summary

Overseeing all the results from the scattering experiments, the following picture emerges, which is summarized in figure 3.9. For dilute solutions at charge stoi-

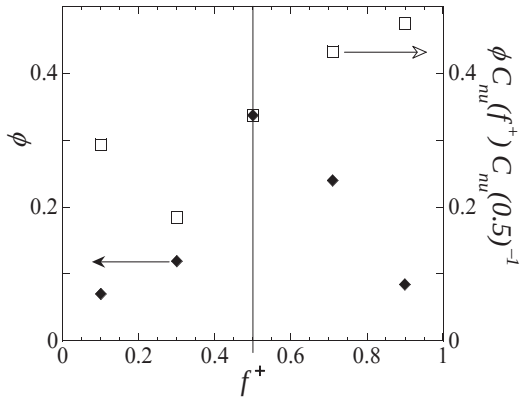

Figure 3.8: Effective volume fraction of hard-spheres as a function of charge ratio (♦, left axis) and the volume fraction corrected for the relative amount of neutralized units in solution (□, right axis).

chiometric conditions, $f^+ = 0.5$, we obtain relatively polydisperse spherical flower-like micelles of radius 15-20 nm. The core is at the maximum of its size and density at these conditions.

For dilute solutions with excess negative charge, $f^+ < 0.5$, we assume that all triblock copolymers bind to the negatively charged homopolymer. Since there is an excess of homopolymer, it is likely that smaller aggregates are formed, composed of a few neutralized units, see the upper-left part of figure 3.9. These aggregates must carry some excess negative charge that prevents them from further aggregation into bigger clusters. As discussed above, even a relatively small excess of the negatively charged homopolymer in terms of mass could already lead to large surface potential. Such small aggregates are typically called 'soluble complexes'.[17,24] Probably most excess negative charge is present in solution in the form of unbound homopolymer. Upon approaching the charge stoichiometric point, the soluble complexes grow in size, thereby decreasing the excess charge in the complex, until we have a maximum amount of aggregated material in the form of neutral flowerlike micelles.

The situation is somewhat different for the excess positive side of the composition diagram, where $f^+ > 0.5$. All data suggest that we still have objects of micellar size, probably with even higher aggregation numbers per object than in the 1:1 charge ratio situation. Such behaviour has not been observed before for polyelectrolyte complex micelles prepared from (combinations of) diblock copolymers. Therefore this behaviour must be explained by the properties of the triblock copolymer. For excess positive charge conditions, triblock copolymers have the choice to put both end-blocks in the polyelectrolyte complex core, or to put only one end-block in the core and leave the other end-block free in solution. The latter

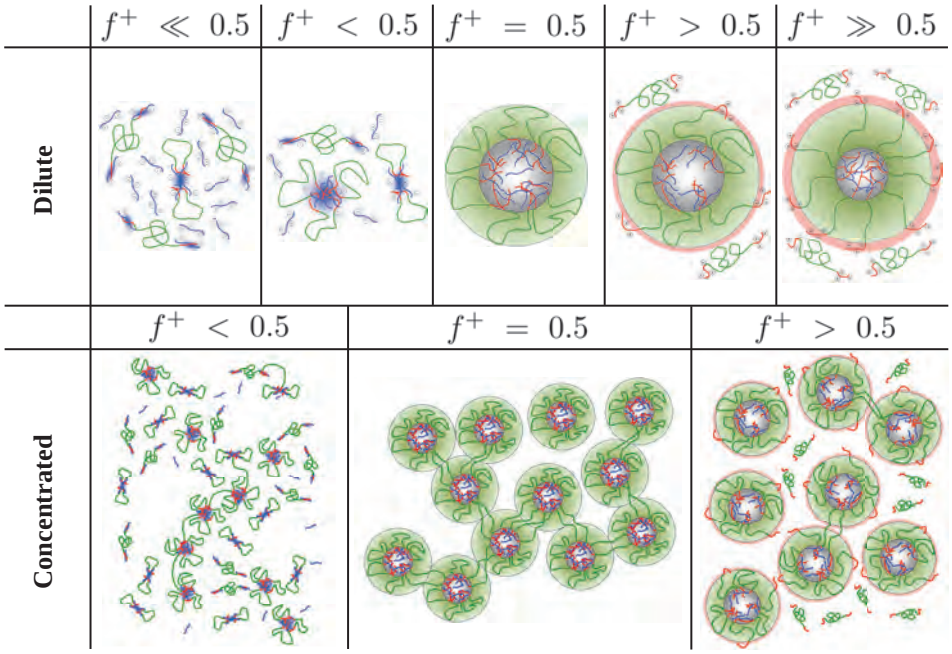

Figure 3.9: Several illustrations showing the different situations for excess negative charge, charge stoichiometry and excess positive charge, for two concentration regimes, dilute and concentrated.

option is a convenient way of dealing with the excess positive charge; the polyelectrolyte complex core can stay close to electroneutral, while the excess charge is spread out over the periphery of the corona. With increasing f^+, the amount of loops will decrease and the amount of free end-blocks will increase, see the upper-right part of figure 3.9. The strong increase of the shell radius for $f^+ = 0.9$ might be caused by the enhanced stretching of the corona chains, either because of crowding or to minimize the charge density at the exterior of the corona. The more stretched the coronas become, the softer and less well defined the micelles become. If all triblock copolymers have adapted a stretched conformation, instead of the looped conformation at $f^+ = 0.5$, while keeping the total amount of charges in the core equal, the aggregation number has to increase by approximately a factor of 1.5. This is in good agreement with figures 3.2 and 3.8.

For the concentrated samples at charge stoichiometry the flowerlike micelles become somewhat smaller. With increasing concentration, the flowerlike micelles get closer and closer to each other, until the average distance between the micelles approaches the value of twice the hard-sphere radius.

Concentrated solutions of excess negative charge lead to significantly smaller

soluble complexes as compared to the dilute conditions. The volume fraction of soluble complexes in the investigated samples is too low to cause strong ordering. However, we do see a relatively big difference between the aggregate radius and the hard-sphere radius at $f^+ = 0.3$. It is not likely that this is caused by a long ranged electrostatic repulsion between the negatively charged complexes, because the Debeye screening length is in the order of 1 nm at 0.35 M KCl.

Concentrated solutions of excess positive charge also show a decrease in micellar size as compared to the dilute situation. However, the radius of the aggregates is approximately constant for excess positive charge conditions and high concentrations, contrary to the increase in radius for these conditions in the dilute samples, see figure 3.7. Apparently, the presence of the other micelles limits the corona's ability to stretch. The ordering in these samples might be even more pronounced than in the 1:1 charge ratio samples, for equal weight concentrations of neutralized units. This is because the aggregates take up more volume for equal concentrations of neutralized units at excess positive charge conditions. The latter implies that the average density of the aggregates decreases with increasing f^+.

3.3.5 Rheometry of concentrated solutions

Since our triblock copolymers have two 'sticky' end-blocks, it is possible for a triblock copolymer to stick both end-blocks in a different micellar core, forming a bridge. The average number of bridges per micelle depends predominantly on the average distance between the micelles, which is in turn determined by the concentration of neutralized units. If the concentration of micelles is high enough, a percolating path of interconnected micelles can be formed, leading to physical gel formation. For triblock copolymers with a PEO(10k) middle-block, the concentration of neutralized units where a percolating network can be formed is between 4wt% and 8wt%.[14,35] The microstructure is reflected in the mechanical properties of a gel, which can be probed experimentally by measuring the elastic modulus, G. The elastic modulus of a polymeric network is related to the microstructure by:

$$G \simeq \nu kT \tag{3.6}$$

where ν is the number density of elastically active chains, k is Boltzmann's constant and T is the absolute temperature. Hence, the higher the number density of elastically active chains, the higher the elastic modulus. The elastic modulus can be obtained from a rheological frequency sweep experiment, if one can measure a high-frequency plateau of the storage modulus, where $G'(\omega) =$ constant. The stor-

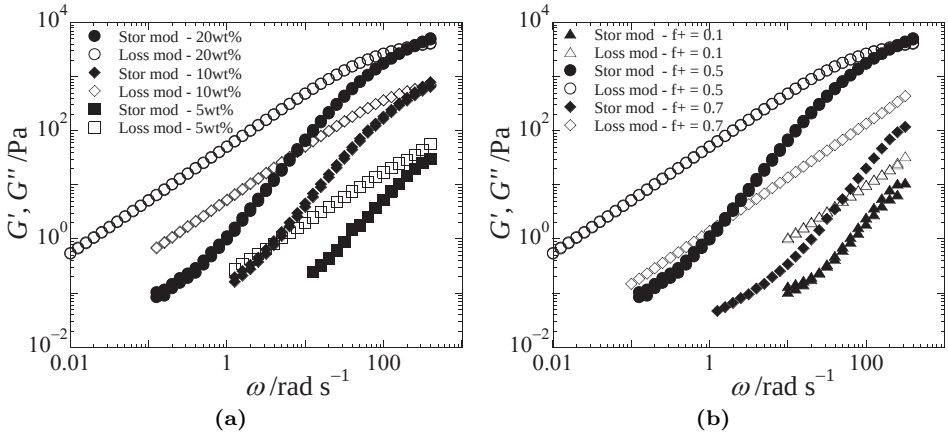

Figure 3.10: Results of frequency sweep measurements. **(a)** Frequency sweeps for fixed charge ratio of $f^+ = 0.5$, for different total polymer concentrations. **(b)** Frequency sweeps for fixed total polymer concentration of 20wt%, for different charge compositions. Storage moduli, G', are indicated as filled symbols, loss moduli, G'', are indicated as open symbols. The meaning of the symbols is explained in the graphs.

age modulus can only be measured if the bridges in the material can be regarded as 'frozen' on the time scale of the applied deformation, *i.e.* when $\omega^{-1} < \tau$, where τ is the mechanical relaxation time of the sample. The relaxation time can be approximated as the inverse of the cross-over frequency, where $G' = G''$. Hence, whether a plateau modulus can be measured depends on the relaxation time of the sample, and the dynamic range of the rheometer.

Figure 3.10 shows the results of frequency sweep measurements in which we varied either the concentration or the charge ratio. From figure 3.10a we can see that the cross-over frequency, and thus the relaxation time, is a weak function of concentration. Between the 10wt% and 20wt% the cross-over frequency shifts from 400 rad s^{-1} to 250 rad s^{-1}, corresponding to a relaxation time in the order of a few milliseconds. The shift in relaxation time from 5wt% to 10wt% is caused by further development of the network, which is very open at 5wt%. In open networks, the probability to form so-called 'super-chains' is higher than in more dense networks. According to Annable and coworkers, super-chains can relax stresses more rapidly than single bridges, which possibly explains the concentration dependence of the relaxation time for concentrations close to the gel concentration.[2] Figure 3.10b shows that the relaxation time for the off-stoichiometric charge compositions is even shorter, making the relaxation time and plateau modulus impossible to assess with a conventional rheometer. Note that the values for the loss moduli in figure 3.10

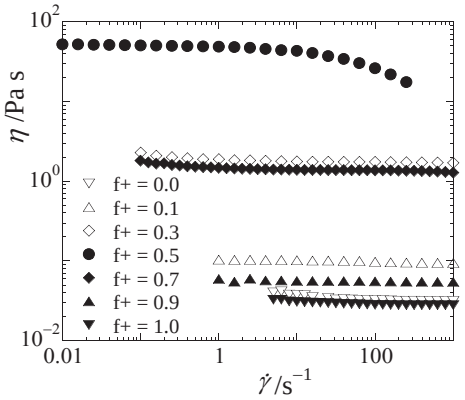

Figure 3.11: Flow curve for the 20wt% samples for different charge compositions as indicated in the graph.

are parallel, scaling as $G'' \propto \omega^1$, which indicates Newtonian liquid-like behaviour over the measured frequency domain.

Since it is not possible to measure the plateau modulus for these systems, we investigate the shear viscosity. The viscosity reflects both the number of bridges in the sample and their relaxation dynamics. For a single relaxation time Maxwell liquid:

$$\eta \simeq G\tau \tag{3.7}$$

The viscosity of the 20wt% samples is shown in figure 3.11, as a function of shear rate. There is a Newtonian plateau in the shear viscosity for low enough shear rates, in accordance with the frequency sweep experiments. The low-shear plateau value of the viscosity is referred to as the zero-shear viscosity, η_0. The 1:1 charge ratio sample shows the onset of shear thinning behaviour at shear rates between 10-100 s^{-1}, which is at somewhat lower shear rates than expected, given the mechanical relaxation time of a few milliseconds obtained by frequency sweep measurements.

In figure 3.12 we have plotted the values for η_0 as a function of charge ratio, and for different polymer concentrations, both on a linear scale (figure 3.12a) and on a logarithmic scale (figure 3.12b). In figure 3.12a we can see that for the 10-20wt% samples there is a very pronounced peak in the zero-shear viscosity for charge stoichiometric conditions. The difference in zero-shear viscosity going from 10wt% to 20wt% is almost exclusively caused by an increase in the number density of elastically active chains in the transient network, because there is little difference in relaxation time for the 1:1 charge ratio samples of 10-20wt%, see figure 3.10a.

On the logarithmic y-axis in figure 3.12b, we can see that the one-component

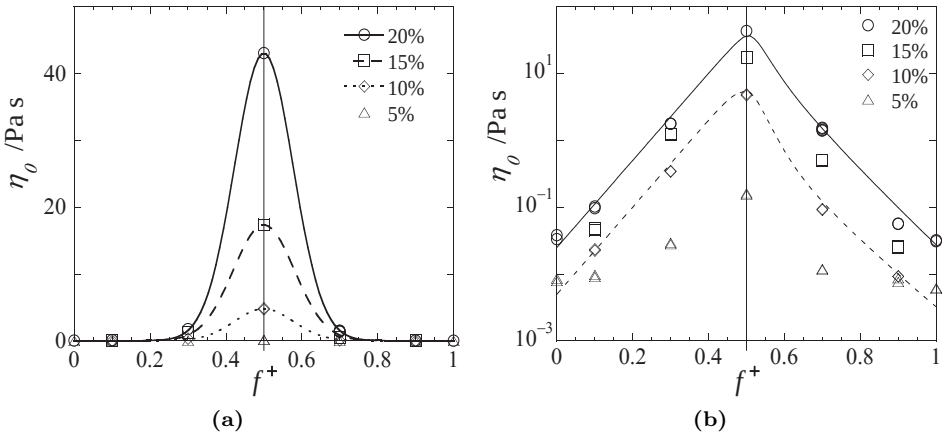

Figure 3.12: Zero-shear viscosity as a function of charge ratio, for different concentrations. Symbols correspond to concentrations as displayed in the legend. The lines in **(a)** and **(b)** are fits to the data, and are meant to guide the eye.

polymer solutions show the lowest viscosity, approximately 10-30 times the viscosity of water. We can also see that the effect of charge ratio on the zero-shear viscosity is stronger in the 10-20wt% samples than in the 5wt% samples. In the case of the more concentrated solutions, we see that the zero-shear viscosity increases almost exponentially with decreasing excess charge, reaching the maximum value at $f^+ = 0.5$.

A close inspection of figure 3.12b shows that the viscosity as function of charge ratio is not precisely symmetric. The viscosities of solutions with excess negative charge are higher than solutions with the same excess positive charge. Even though the effect is not very pronounced, it is consistent for all concentrations. This asymmetry can be explained by the relative weight concentration of neutralized units in the samples. As can be seen in table 3.1, the excess negative side has relatively more neutralized units than the excess positive side, for equal distance from the charge stoichiometric point. More neutralized units allows for more structure formation in the samples which leads to a higher viscosity.

Can we deduce from the data presented whether transient network formation is possible also at off-stoichiometric conditions? To answer this question it is convenient to replot the data in figure 3.12, as a function of the concentration of neutralized units. This is done in figure 3.13, both on a linear scale (figure 3.13a) and on a logarithmic scale (figure 3.13b). Again we can see the dramatic increase in viscosity for the 1:1 charge ratio samples in figure 3.13a. This strong increase

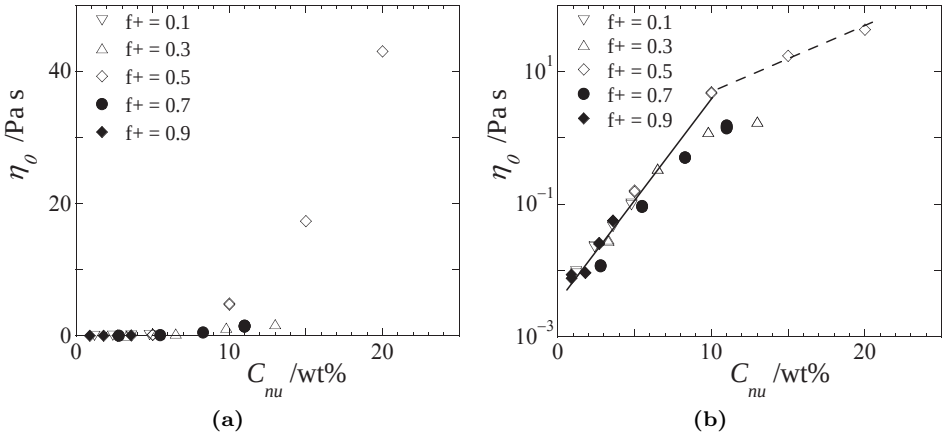

Figure 3.13: Zero-shear viscosity as a function of weight concentration of neutralized units, for different charge compositions. Symbols correspond to charge compositions, as displayed in the legend. The lines in figure **(b)** are guides to the eye.

is characteristic for the build-up of a percolating network beyond the percolation threshold of $C_{\text{gel}} \approx 8$wt%. This value is approximately two times the overlap concentration of the middle-block PEO(10k). The strong increase in viscosity is related to the strong increase in structural order, as presented in figure 3.6b. It is however remarkable that the structural order is almost similar for the $f^+ = 0.5$ and $f^+ = 0.7$ samples, see figure 3.6b, whereas the viscosity in the $f^+ = 0.7$ samples is clearly lower than in the $f^+ = 0.5$ samples, for $C_{nu} \geq 8$wt%. This means that it is not the structural order in the sample, but the bridge formation between the micelles that causes the increase in viscosity for the 1:1 charge ratio samples.

Figure 3.13b displays the increase in zero-shear viscosity as a function of concentration of neutralized units on a logarithmic scale. Somewhat to our surprise, all data points below C_{gel} collapse onto a master-curve, showing an exponential increase of the zero-shear viscosity with the concentration of neutralized units. The higher the concentration of neutralized units is, the more difficult it is for the aggregates to slide past each other and, hence, the higher is the resistance to flow. The size, or excess charge of the aggregates seems to be of little influence to the viscosity.

An exponential increase of the viscosity has been reported in rheological experiments on other soft colloidal systems such as emulsions[58] and polymer solutions.[59,60] It has also been predicted by Semenov *et al.*, who showed that the relaxation time, and thus the viscosity, of a transient network of triblock copolymers should increase exponentially with concentration, in a concentration regime

just above the overlap concentration.[61] This may well be the concentration regime we are investigating here.

For higher concentrations we see that the viscosity keeps increasing for the samples of $f^+ = 0.3$, $f^+ = 0.5$ and $f^+ = 0.7$. The increase is most clearly observed for the $f^+ = 0.5$ sample, where we see a change in slope for the increase of the viscosity at $C_{nu} \approx 10$wt%. Since the relaxation time is approximately constant in this concentration regime, the increase in viscosity for this sample is mainly caused by the increase in the number of bridges between the micelles. More details about the gel properties at charge stoichiometry can be found elsewhere (Chapters 2 and 4).[14,35] The viscosities of the $f^+ = 0.3$ and $f^+ = 0.7$ samples are approximately an order of magnitude lower than the $f^+ = 0.5$ samples, and the change in slope seems to be present at somewhat lower concentrations of neutralized units. The decreased viscosity, as compared to the $f^+ = 0.5$ sample, can be caused either by suppressed bridge formation or by a lower relaxation time.

It is likely that bridge formation is suppressed in the excess positive charge samples. In this case the polyelectrolyte complex cores of the micelles remain close to electroneutral. Hence, there is no driving force for association of the free end-blocks. For entropic reasons, these chain-ends want to stay 'free' in solution and thus the free end-blocks act as network stoppers, see bottom-right part of figure 3.9. The situation might be different for the soluble complexes at excess negative charge conditions. The soluble complexes should still be able to function as nodes in a network, given that $C_{nu} \geq 8$wt%. However, the soluble complexes might be too small and/or too dense and therefore too dilute to come close enough to each other to enable bridge formation. Indeed the size of a soluble complex is relatively small compared to the distance between the micelles, see figures 3.6a and 3.7b. Another possibility is that transient network formation is possible, but that the dynamics of a negatively overcharged network are much faster than at charge stoichiometric conditions. One can imagine that a polyelectrolyte complex carrying excess charges is more likely to break up than a neutral polyelectrolyte complex. Probably suppressed bridge formation and enhanced dynamics are both of importance, but based on the current data we cannot be conclusive about what happens on the molecular level of concentrated solutions of soluble complexes. The bottom-left part of figure 3.9 gives an illustration of this situation.

3.4 Conclusions

We have studied the influence of charge composition on the formation of polyelectrolyte complex networks consisting of a negatively charged homopolymer and an ABA triblock copolymer, in which the A blocks carry positive charges. Scattering studies were performed on dilute as well as concentrated samples, rheological studies were performed on the concentrated samples only. Based on the experimental results, the following picture emerges.

For excess negative charge conditions, the triblock copolymer and homopolymer associate into small aggregates of radius 5-10 nm, called soluble complexes. These soluble complexes carry excess negative charge on the polyelectrolyte complex itself, combined with free homopolymer in solution. In concentrated solutions of these soluble complexes, the viscosity is significantly lower than in the charge stoichiometric situation. The lower viscosity is caused either by enhanced dynamics of the charged polyelectrolyte complex aggregates, or by the lack of network formation due the relatively larger distance between the soluble complexes, making bridge formation unlikely.

At charge stoichiometry, neutral flowerlike micelles of radius 15-20 nm are present in solution. The flowerlike micelles are best defined at this 1:1 charge ratio. At sufficiently high concentrations these flowerlike micelles become interconnected, leading to a transient network.

Excess positive charge conditions lead again to a different situation. Objects of micellar size are present in solution. This is a unique feature of our triblock copolymer system, and does not occur in diblock copolymer systems. Polyelectrolyte complex micelles carrying excess positive charge can be tolerated in solution, because the triblock copolymers can localize the excess positive charge on the periphery of the micellar corona, rather than in the micellar core. This enables the existence of a neutral polyelectrolyte complex core, even for excess positive charge conditions. The larger the excess charge in the system, the more free end-blocks protrude into solution. This also leads to the stretching of the triblock copolymer chains in the corona. In concentrated solutions, the micelles shrink considerably leading to a somewhat denser corona. The free end-blocks act as network stoppers, since there is no driving force for these free end-blocks to associate with a neutral polyelectrolyte complex core. Bridge formation between the micelles is therefore suppressed, leading to significantly lower viscosities as compared to charge stoichiometric conditions. Figure 3.9 summarizes the various states of the system in pictorial form.

An inverse description should hold for the inverse system, *i.e.* a positively charged homopolymer combined with a triblock copolymer carrying negatively charged end-blocks. Whether similar behaviour can be seen in other systems, will predominantly depend on the association strength of the used polyelectrolyte pair and the salt concentration in solution. We believe that with the right combination of parameters, similar behaviour must show up in experiments with alike systems. The possibility to vary the charge ratio is a unique feature of two-component polyelectrolyte systems. The influence of this parameter on the transient network formation has now been studied for the first time. Changing the charge ratio to off-stoichiometric conditions creates opportunities for further fine-tuning of the transient network properties, and therewith the mechanical properties of this two-component rheology modifier.

References

[1] S. T. Milner and T. A. Witten, *Macromolecules*, 1992, **25**, 5495–5503.

[2] T. Annable, R. Buscall, R. Ettelaie and D. Whittlestone, *Journal of Rheology*, 1993, **37**, 695–726.

[3] R. D. Jenkins, D. R. Bassett, C. A. Silebi and M. S. Elaasser, *Journal of Applied Polymer Science*, 1995, **58**, 209–230.

[4] X. X. Meng and W. B. Russel, *Journal of Rheology*, 2006, **50**, 189–205.

[5] J. Sprakel, N. A. M. Besseling, M. A. Cohen Stuart and F. A. M. Leermakers, *European Physical Journal E*, 2008, **25**, 163–173.

[6] J. Sprakel, E. Spruijt, M. A. Cohen Stuart, N. A. M. Besseling, M. P. Lettinga and J. van der Gucht, *Soft Matter*, 2008, **4**, 1696–1705.

[7] J. F. Berret, D. Calvet, A. Collet and M. Viguier, *Current Opinion in Colloid & Interface Science*, 2003, **8**, 296–306.

[8] P. Kujawa, H. Watanabe, F. Tanaka and F. M. Winnik, *European Physical Journal E*, 2005, **17**, 129–137.

[9] D. Mistry, T. Annable, X. F. Yuan and C. Booth, *Langmuir*, 2006, **22**, 2986–2992.

[10] R. Obeid, E. Maltseva, A. F. Thunemann, F. Tanaka and F. M. Winnik, *Macromolecules*, 2009, **42**, 2204–2214.

[11] C. Tsitsilianis, *Soft Matter*, 2010, **6**, 2372–2388.

[12] R. C. W. Liu, Y. Morishima and F. M. Winnik, *Polymer Journal*, 2002, **34**, 340–346.

[13] F. Bossard, V. Sfika and C. Tsitsilianis, *Macromolecules*, 2004, **37**, 3899–3904.

[14] M. Lemmers, J. Sprakel, I. K. Voets, J. van der Gucht and M. A. Cohen Stuart, *Angewandte Chemie-International Edition*, 2010, **49**, 708–711.

[15] A. Harada and K. Kataoka, *Macromolecules*, 1995, **28**, 5294–5299.

[16] A. V. Kabanov, T. K. Bronich, V. A. Kabanov, K. Yu and A. Eisenberg, *Macromolecules*, 1996, **29**, 6797–6802.

[17] M. A. Cohen Stuart, N. A. M. Besseling and R. G. Fokkink, *Langmuir*, 1998, **14**, 6846–6849.

[18] M. A. Cohen Stuart, B. Hofs, I. K. Voets and A. de Keizer, *Current Opinion in Colloid & Interface Science*, 2005, **10**, 30–36.

[19] I. K. Voets, R. de Vries, R. Fokkink, J. Sprakel, R. P. May, A. de Keizer and M. A. Cohen Stuart, *European Physical Journal E*, 2009, **30**, 351–359.

[20] J. van der Gucht, E. Spruijt, M. Lemmers and M. A. Cohen Stuart, *Journal of Colloid and Interface Science*, 2011, **361**, 407–422.

[21] I. K. Voets, A. de Keizer, P. de Waard, P. M. Frederik, P. H. H. Bomans, H. Schmalz, A. Walther, S. M. King, F. A. M. Leermakers and M. A. Cohen Stuart, *Angewandte Chemie-International Edition*, 2006, **45**, 6673–6676.

[22] Y. Yan, N. A. M. Besseling, A. de Keizer, A. T. M. Marcelis, M. Drechsler and M. A. Cohen Stuart, *Angewandte Chemie-International Edition*, 2007, **46**, 1807–1809.

[23] S. Lindhoud, R. de Vries, W. Norde and M. A. Cohen Stuart, *Biomacromolecules*, 2007, **8**, 2219–2227.

[24] S. van der Burgh, A. de Keizer and M. A. Cohen Stuart, *Langmuir*, 2004, **20**, 1073–1084.

[25] B. Hofs, I. K. Voets, A. de Keizer and M. A. Cohen Stuart, *Physical Chemistry Chemical Physics*, 2006, **8**, 4242–4251.

[26] B. Hofs, A. de Keizer and M. A. Cohen Stuart, *Journal of Physical Chemistry B*, 2007, **111**, 5621–5627.

[27] I. K. Voets, A. de Keizer, M. A. Cohen Stuart, J. Justynska and H. Schlaad, *Macromolecules*, 2007, **40**, 2158–2164.

[28] I. K. Voets, R. Fokkink, T. Hellweg, S. M. King, P. de Waard, A. de Keizer and M. A. Cohen Stuart, *Soft Matter*, 2009, **5**, 999–1005.

[29] S. Lindhoud, W. Norde and M. A. Cohen Stuart, *Journal of Physical Chemistry B*, 2009, **113**, 5431–5439.

[30] J. Gummel, F. Boue, B. Deme and F. Cousin, *Journal of Physical Chemistry B*, 2006, **110**, 24837–24846.

[31] H. V. Saether, H. K. Holme, G. Maurstald, O. Smidsrod and B. T. Stokke, *Carbohydrate Polymers*, 2008, **74**, 813–821.

[32] M. Antonov, M. Mazzawi and P. L. Dubin, *Biomacromolecules*, 2010, **11**, 51–59.

[33] R. Chollakup, W. Smitthipong, C. D. Eisenbach and M. Tirrell, *Macromolecules*, 2010, **43**, 2518–2528.

[34] V. A. Kabanov and A. B. Zezin, *Die Makromolekulare Chemie*, 1984, **6**, 259–276.

[35] M. Lemmers, I. K. Voets, M. A. Cohen Stuart and J. van der Gucht, *Soft Matter*, 2011, **7**, 1378–1389.

[36] K. Jankova, X. Y. Chen, J. Kops and W. Batsberg, *Macromolecules*, 1998, **31**, 538–541.

[37] J. M. Dust, Z. H. Fang and J. M. Harris, *Macromolecules*, 1990, **23**, 3742–3746.

[38] K. Jankova and J. Kops, *Journal of Applied Polymer Science*, 1994, **54**, 1027–1032.

[39] M. Kato, M. Kamigaito, M. Sawamoto and T. Higashimura, *Macromolecules*, 1995, **28**, 1721–1723.

[40] J. S. Wang and K. Matyjaszewski, *Macromolecules*, 1995, **28**, 7901–7910.

[41] Y. T. Li, S. P. Armes, X. P. Jin and S. P. Zhu, *Macromolecules*, 2003, **36**, 8268–8275.

[42] G. Masci, D. Bontempo, N. Tiso, M. Diociaiuti, L. Mannina, D. Capitani and V. Crescenzi, *Macromolecules*, 2004, **37**, 4464–4473.

[43] W. Bras, I. P. Dolbnya, D. Detollenaere, R. van Tol, M. Malfois, G. N. Greaves, A. J. Ryan and E. Heeley, *Journal of Applied Crystallography*, 2003, **36**, 791–794.

[44] S. Forster and C. Burger, *Macromolecules*, 1998, **31**, 879–891.

[45] S. Forster, A. Timmann, M. Konrad, C. Schellbach, A. Meyer, S. S. Funari, P. Mulvaney and R. Knott, *Journal of Physical Chemistry B*, 2005, **109**, 1347–1360.

[46] S. Forster, L. Apostol and W. Bras, *Journal of Applied Crystallography*, 2010, **43**, 639–646.

[47] G. Deželić, *Pure and Applied Chemistry*, 1970, **23**, 327–354.

[48] H. Lindner and O. Glatter, *Particle & Particle Systems Characterization*, 2000, **17**, 89–95.

[49] D. R. Lide, *CRC Handbook of Chemistry and Physics*, CRC Press, Boca Raton, FL, 2005.

[50] H. Wu, *Chemical Physics*, 2010, **367**, 44–47.

[51] J. F. Gohy, S. K. Varshney, S. Antoun and R. Jerome, *Macromolecules*, 2000, **33**, 9298–9305.

[52] I. K. Voets, *PhD Thesis*, 2008.

[53] R. Zhang and B. T. Shklovskii, *Physica A - Statistical Mechanics and Its Applications*, 2005, **352**, 216–238.

[54] N. P. Shusharina, E. B. Zhulina, A. V. Dobrynin and M. Rubinstein, *Macromolecules*, 2005, **38**, 8870–8881.

[55] Y. Yan, A. de Keizer, M. A. Cohen Stuart, M. Drechsler and N. A. M. Besseling, *Journal of Physical Chemistry B*, 2008, **112**, 10908–10914.

[56] J. Wang, A. de Keizer, R. Fokkink, Y. Yan, M. A. Cohen Stuart and J. van der Gucht, *The Journal of Physical Chemistry B*, 2010, **114**, 8313–8319.

[57] E. Spruijt, J. Sprakel, M. A. Cohen Stuart and J. van der Gucht, *Soft Matter*, 2010, **6**, 172–178.

[58] C. G. Quintero, C. Noik, C. Dalmazzone and J. L. Grossiord, *Rheologica Acta*, 2008, **47**, 417–424.

[59] R. E. Whittier, D. W. Xu, J. H. van Zanten, D. J. Kiserow and G. W. Roberts, *Journal of Applied Polymer Science*, 2006, **99**, 540–549.

[60] E. Choppe, F. Puaud, T. Nicolai and L. Benyahia, *Carbohydrate Polymers*, 2010, **82**, 1228–1235.

[61] A. N. Semenov, J. F. Joanny and A. R. Khokhlov, *Macromolecules*, 1995, **28**, 1066–1075.

[62] S. W. Provencher, *Computer Physics Communications*, 1982, **27**, 213–227.

[63] S. W. Provencher, *Computer Physics Communications*, 1982, **27**, 229–242.

[64] W. F. Polik and W. Burchard, *Macromolecules*, 1983, **16**, 978–982.

[65] M. Mertoglu, A. Laschewsky, K. Skrabania and C. Wieland, *Macromolecules*, 2005, **38**, 3601–3614.

[66] A. Naderi, J. Iruthayaraj, A. Vareikis, R. Makuska and P. M. Claesson, *Langmuir*, 2007, **23**, 12222–12232.

[67] V. M. M. Soto and J. C. Galin, *Polymer*, 1984, **25**, 254–262.

[68] P. Starck, W. K. J. Mosse, N. J. Nicholas, M. Spiniello, J. Tyrrell, A. Nelson, G. G. Qiao and W. A. Ducker, *Langmuir*, 2007, **23**, 7587–7593.

Appendix

Polymer characterization

NMR spectrum of the triblock copolymer

^{1}H-NMR of the triblock copolymer was performed in D_2O on a Bruker Advance III 400MHz NMR spectrometer. 64 Scans were performed, with a relaxation time between two subsequent pulses of 60 s to allow full relaxation of the protons in the PEO middle-block. The average number of charged groups on the triblock copolymers was determined by comparing the integral values of the peak corresponding to the protons in the PEO middle-block ($\delta \approx 3.6$ ppm) and the peak of the protons of the trimethylamino group ($\delta \approx 3.2$ ppm), taking into account the relative amount of protons per group. We obtain an average value of 68 monomers per PEO middle-block, corresponding to an average of 34 charged monomers per A block. The ^{1}H-NMR spectrum of the triblock copolymer is shown in figure 3.14. The origin of each peak is indicated in the graph.

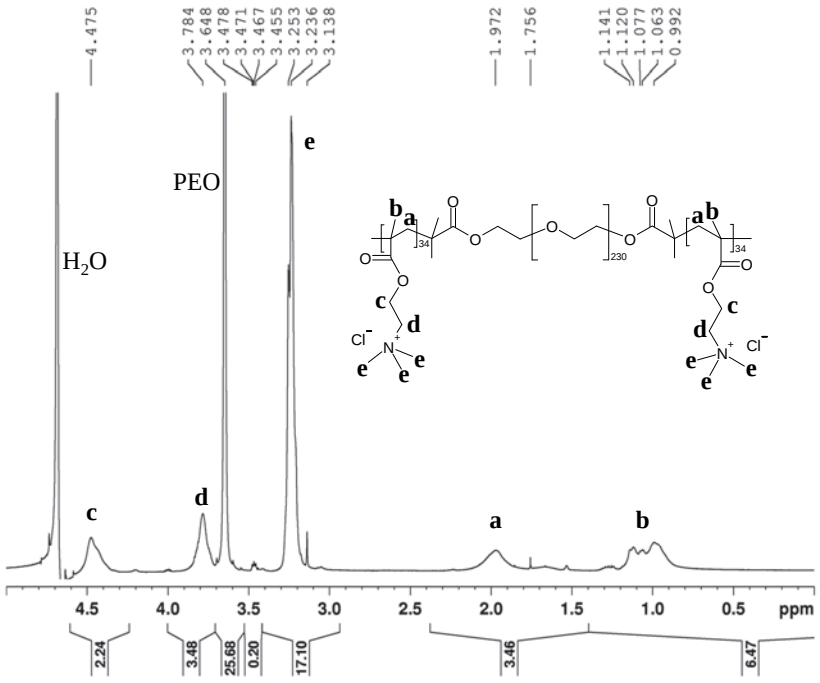

Figure 3.14: ^{1}H-NMR spectrum of the ABA triblock copolymer as synthesized according to the procedure indicated in the experimental section.

NMR spectrum of the PSPMA homopolymer

Figure 3.15 shows the ^{1}H-NMR spectrum of the PSPMA homopolymer. The spectrum was recorded in D_2O on a Bruker Advance III 400MHz NMR spectrometer. 166 Scans were performed, with a relaxation time between two subsequent pulses of 60 s. The origin of each peak is indicated in the graph.

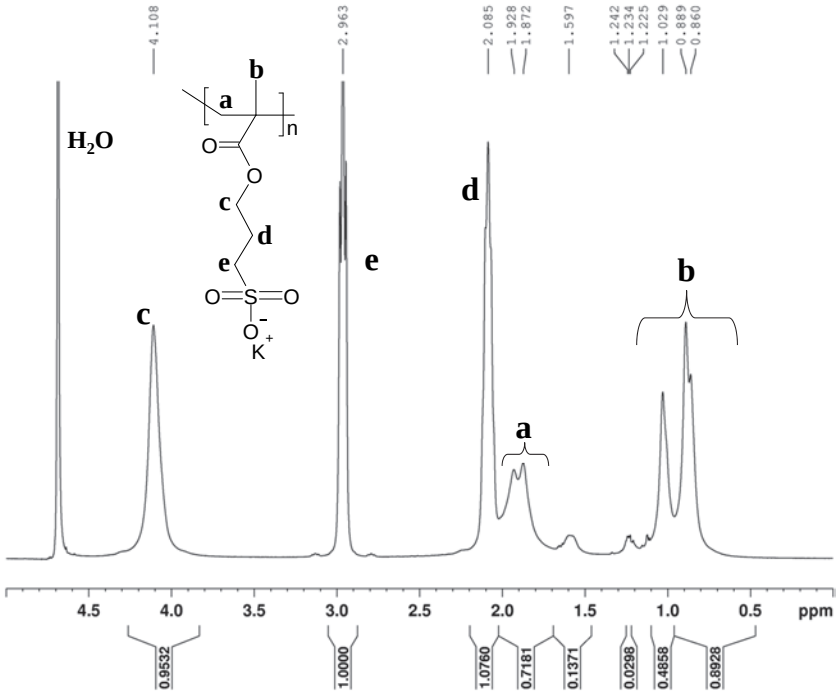

Figure 3.15: ^{1}H-NMR spectrum of the PSPMA homopolymer as synthesized according to the procedure indicated in the experimental section.

Sample preparation

Relative concentration of neutralized units

Figure 3.16 displays the relative amount of neutralized units present in solution, and is the graphical presentation of the numbers in table 3.1 in the main text. Basically the numbers mean that for a 20wt% sample at 1:1 charge ratio, we have 20wt% of neutralized units. However, for a 20wt% sample at $f^+ = 0.1$ it means that we have $0.24 \times 20 = 4.8$wt% of neutralized units in solution. All concentrations of neutralized units have been calculated and are shown in table 3.2.

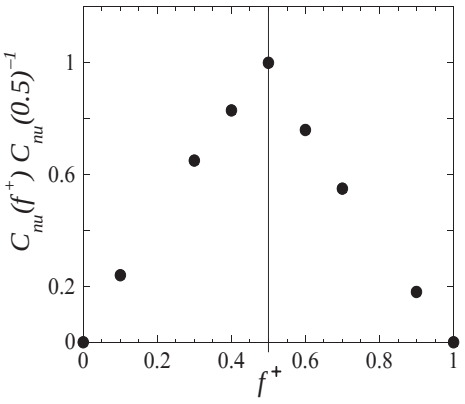

Figure 3.16: Relative ratio of neutralized units in solution, as defined in the main text.

Table 3.2: Table with the values for the weight concentration of neutralized units, per charge ratio.

f^+	$\frac{C_{nu}(f^+)}{C_{nu}(0.5)}$	20 wt%	15 wt%	10 wt%	5 wt%
0.1	0.24	4.8	3.6	2.4	1.2
0.3	0.65	13.0	9.8	6.5	3.3
0.5	1.00	20.0	15.0	10.0	5.0
0.7	0.55	11.0	8.3	5.5	2.8
0.9	0.18	3.6	2.7	1.8	0.9

Dynamic Light Scattering

Additional graphs

Figure 3.17a shows the dependence of the diffusion coefficient on the scattering vector. Diffusion coefficients are obtained from CONTIN[62,63] fits of the correlation functions, see also figure 3.18. There is no dependence of the diffusion coefficient on the scattering vector, except for small q-values. The lowering of the diffusion coefficient might be caused be a small fraction of larger aggregates present in the sample. Figure 3.17b shows the hydrodynamic radius, based on the same CONTIN[62,63] fits as in figure 3.17a, as a function of scattering angle θ. For $\theta > 50°$, there is no dependence of the hydrodynamic radius of the aggregates. At lower scattering angles an upturn can be caused by the presence of a small fraction of larger aggregates.

Typical intensity correlation functions and fits for 0.5wt% samples for three charge compositions are shown in figure 3.18. The curves are shifted in correlation

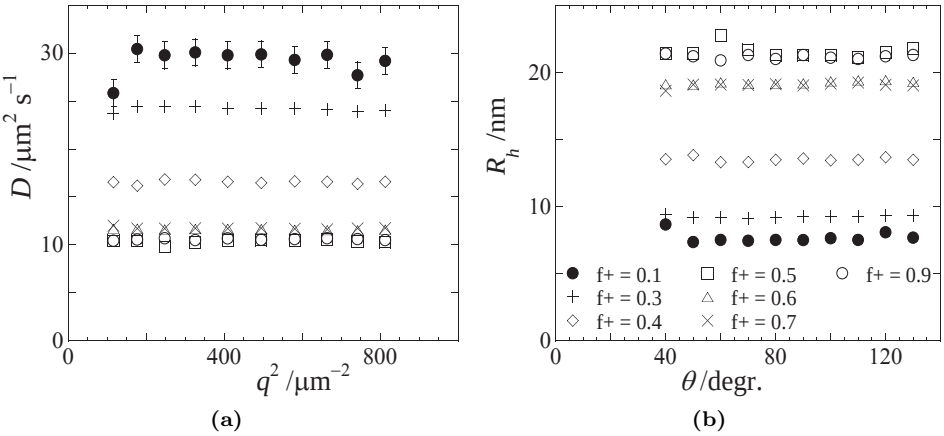

Figure 3.17: **(a)** Values for the diffusion coefficients as a function of q^2. The symbols for the different charge compositions are similar as displayed in **(b)**. Standard deviations are in the order of the size of the symbols, except for $f^+ = 0.1$, where they are displayed in the graph. **(b)** Values for the measured hydrodynamic radius as a function of scattering angle θ. The symbols for the different charge compositions are indicated in the graph. Standard deviations are in the order of the size of the symbols.

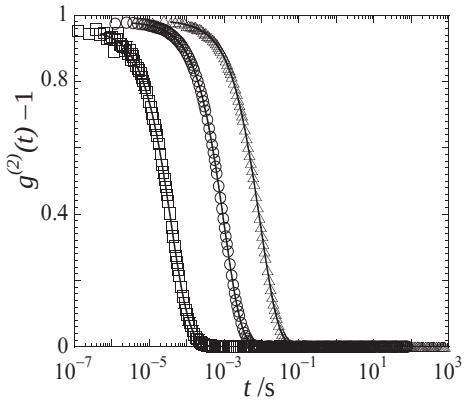

Figure 3.18: Intensity correlation as a function of correlation time for samples of 0.5wt% at three charge compositions; $f^+ = 0.1$ (□), $f^+ = 0.5$ (◯) and $f^+ = 0.9$ (△). The correlation functions are shifted by a factor of 10 in correlation time for reasons of clarity. Lines are fits to the data.

time by a factor of ten from each other, to prevent overlap. Fits to the data are displayed as lines through the data points.

Table 3.3: Values used to estimate the refractive index increment of a neutralized unit.

Component	Mass kg mol^{-1}	Mass fraction	$\left(\frac{dn}{dC}\right)$ ml g^{-1}	Contribution to $\left(\frac{dn}{dC}\right)$ ml g^{-1}
PEO	10.3	0.250	0.135[64]	0.034
PTMAEMA	14.1	0.342	0.158[66]	0.054
PSPMA	16.7	0.407	0.125[65]	0.051
Neutralized unit	41.1	1	-	0.139

Refractive index increment

Here we derive an estimate for the value of the refractive index increment of the neutralized units. A neutralized unit is defined as a triblock copolymer exactly neutralized with oppositely charged homopolymer. The mass of such a neutralized unit is 41.1 kg mol^{-1}, of which 25.0wt% is PEO, 34.2wt% is TMAEMA and 40.8wt% is PSPMA. The refractive index increment of each individual component is known.[64–66] If we assume that the refractive index increment is weakly dependent on the wavelength of the light, and if we assume that each component contributes proportional to its mass fraction in a neutralized unit, we estimate the refractive index increment of a neutralized unit to be $1.39 \cdot 10^{-4}$ m^3 kg^{-1}. This value is close to the value obtained for polymers with zwitter-ionic side chains that contain both the TMAEMA and the SPMA moiety in one chain.[67,68] The actual values and references are given in table 3.3.

Estimation of I_{bg}

We estimate the background scattering over the whole charge ratio domain by interpolating between the two points at the extremities. Hence, we subtract the maximum possible amount of background scattering, which would be the scattered light intensity in case no aggregates are formed at all. Since the weight concentration of all samples is equal, we overestimate the contribution of the background scattering at charge compositions where polymers end-up in aggregates. The values for the two extremities are: $< I > (0.0) = 18.5$ and $< I > (1.0) = 11.4$. Linear interpolation yields the relation between the hypothetical background and charge ratio: $I_{bg} = 18.5 - 7.1 \cdot f^+$. This relation was used to obtain a value for I_{bg} at all charge compositions.

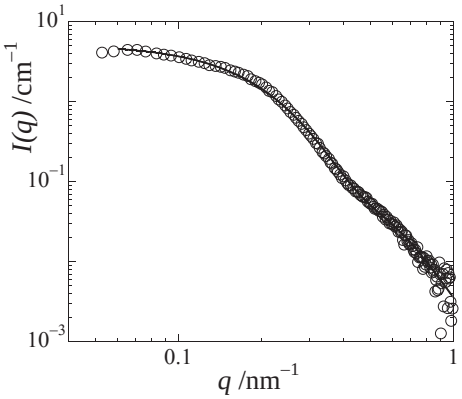

Figure 3.19: Data and fit of the 0.5wt% $f^+ = 0.5$ sample at a KCl concentration of 10 mM.

Small Angle X-ray Scattering

Additional graphs

The $f^+ = 0.5$ low salt concentration sample (10 mM KCl) shows somewhat more features in the SAXS curve than the 0.35 M KCl samples. However, still no clear form factor minimum can be seen, see figure 3.19. The curve could be fitted by a model employing a polydisperse homogeneous core and homogeneous shell. Fitting parameters can be found in table 3.4.

SAXS curves and model fitting results of 0.5wt% samples for different charge stoichiometries are given in figure 3.20a. The curves are similar as in figure 3.3, but now shifted for reasons of clarity. Lines indicate the results of model fitting. The data was fitted with a model comprising a polydisperse homogeneous core and homogeneous shell. The fitting parameters are given in table 3.5.

SAXS curves and model fitting results of 20wt% samples for different charge stoichiometries are given in figure 3.20b. The curves are similar as in figure 3.5, but now shifted for reasons of clarity. Lines indicate the results of model fitting. The data were fitted with a model consisting of a polydisperse homogeneous core and homogeneous shell, combined with a Percus-Yevick closure for the modelled hard-sphere interactions. The fitting parameters are given in table 3.6.

Figure 3.21 shows the fitted $I(0)$ values for both 0.5wt% and 20wt% fits. The figure is in agreement with the light scattering results.

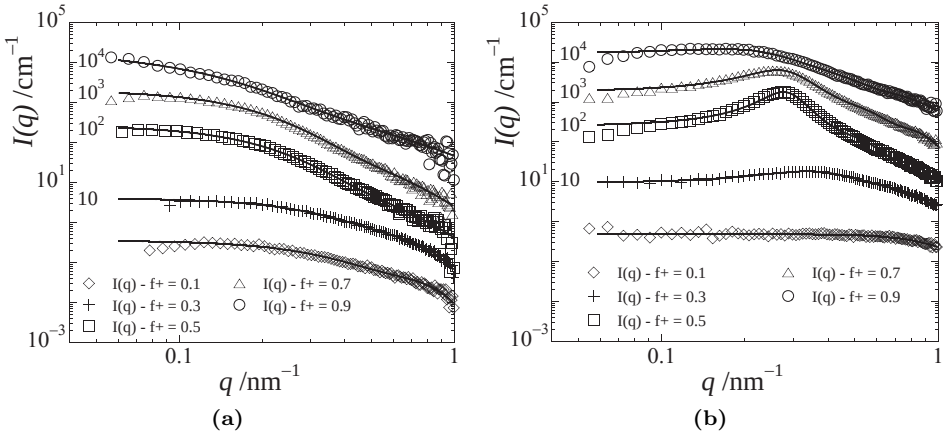

Figure 3.20: Data(symbols) and fits (lines) of the **(a)** 0.5wt% samples and **(b)** 20wt% samples, for different charge compositions, as shown in the legend, and fixed KCl concentration of 0.35 M. Curves are shifted with respect to each other by shift factors as indicated in the graph. Only 20% of the data points are shown for reasons of clarity.

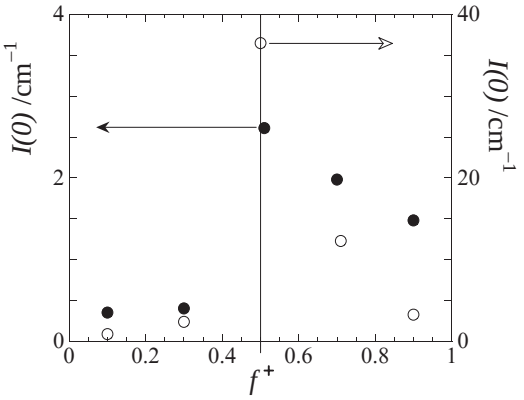

Figure 3.21: Fitted $I(0)$ values as a function of charge ratio for 0.5wt% (•, left axis) and 20wt% (∘, right axis) SAXS data fits.

Figures 3.22, 3.23 and 3.24 show the SAXS curves for the 5wt%, 10wt% and 15wt% samples, respectively.

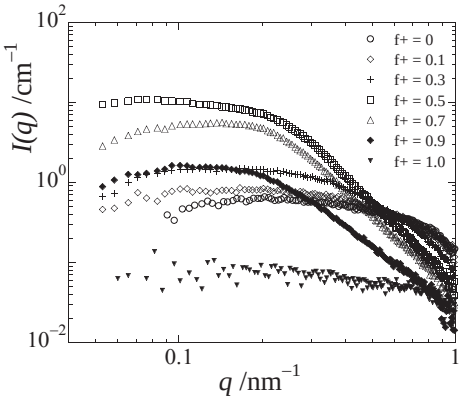

Figure 3.22: SAXS curves for 5wt% total polymer concentration. 30% of the data points are shown. Symbols correspond to charge compositions as indicated in the graph.

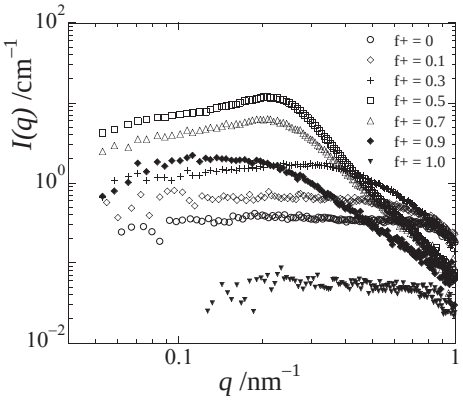

Figure 3.23: SAXS curves for 10wt% total polymer concentration. 30% of the data points are shown. Symbols correspond to charge compositions as indicated in the graph.

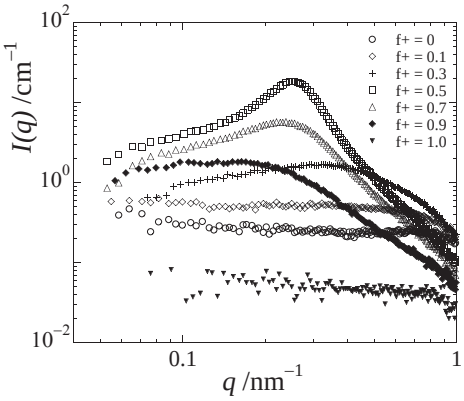

Figure 3.24: SAXS curves for 15wt% total polymer concentration. 30% of the data points are shown. Symbols correspond to charge compositions as indicated in the graph.

Fitting parameters

Table 3.4: Table with model fitting parameters for the 0.5wt% SAXS curves at 10 mM KCl.

f^+	$I(0)$ cm^{-1}	R_{core} nm	R_{shell} nm	R_{agg} nm	density shell/core
0.51	5.36	5.9 ±1.3	8.9	14.8 ±1.3	0.14

Table 3.5: Table with model fitting parameters for the 0.5wt% SAXS curves at 0.35 M KCl.

f^+	$I(0)$ cm^{-1}	R_{core} nm	R_{shell} nm	R_{agg} nm	density shell/core
0.10	0.35	3.4 ±0.3	7.0	10.4 ±0.3	0.02
0.30	0.40	3.8 ±0.5	6.9	10.7 ±0.5	0.03
0.51	2.61	5.4 ±1.6	9.2	14.6 ±1.6	0.12
0.70	1.98	5.6 ±1.7	10.0	15.5 ±1.7	0.12
0.90	1.48	4.1 ±1.8	18.1	22.1 ±1.8	0.04

Table 3.6: Table with model fitting parameters for the 20wt% SAXS curves at 0.35 M KCl.

f^+	$I(0)$ cm^{-1}	R_{core} nm	R_{shell} nm	R_{agg} nm	density shell/core	R_{HS} nm	ϕ
0.10	0.86	2.8 ±1.1	0.3	3.1 ±1.1	0.06	3.2	0.07
0.30	2.38	3.2 ±0.9	1.5	4.7 ±0.9	0.11	7.7	0.12
0.50	36.5	4.3 ±0.7	6.1	10.4 ±0.7	0.12	11.1	0.34
0.71	12.3	3.9 ±0.6	6.0	9.9 ±0.6	0.08	10.7	0.24
0.90	3.25	3.4 ±0.7	6.8	10.2 ±0.7	0.05	12.6	0.08

Chapter 4

Transient Network Topology of Interconnected Polyelectrolyte Complex Micelles

In this Chapter we study transient networks formed by co-assembly of an ABA triblock copolymer with charged A blocks and a neutral water-soluble B block, and an oppositely charged homopolymer. Above the CMC, the polymers associate into flowerlike micelles consisting of a polyelectrolyte complex core and a neutral corona consisting of looped middle blocks. At higher concentrations, the micelles become interconnected, leading to a physical network with visco-elastic properties. We use a combination of (dynamic) light scattering, small-angle X-ray scattering and rheometry, to characterize how the transient network structure changes with polymer concentration and ionic strength, and how these changes affect the macroscopic elastic properties of the network. We find that an increase in ionic strength leads to a decrease in aggregation number and size of the individual micelles, which simultaneously leads to an increase in the number density of micelles. These two effects compensate each other such that the probability of bridge formation is equal at all salt concentrations, meaning that the elastic modulus of the gels is independent of salt concentration.

This chapter is published as paper with supporting information:
Marc Lemmers, Ilja K. Voets, Martien A. Cohen Stuart and Jasper van der Gucht, *Soft Matter*, 2011, **7**, 1378-1389.

4.1 Introduction

Soft matter scientists try to understand how the microstructure of a material influences its macroscopic properties. New or improved (combinations of) experimental techniques give us the opportunity to study this micro-macro relation in more detail then ever before. An interesting class of materials to study, in this respect, are physical gels. In physical gels, the flow of solvent is restricted by a sample-spanning transient network of a 'thickening' polymer. Typically, thickening polymers have some kind of sticky end-groups that can cluster together to form the nodes of the network. Such thickening polymers are effective at relatively low volume fractions due to their ability to overcome large distances. The nodes in the network are dynamic, meaning that nodes are broken and reformed all the time by thermal energy. The ability to break existing nodes and reform them some time later allows these gels to relax applied stresses or strains. Physical gels are therefore also called reversible gels and have the industrially interesting property that they are self-healing.

Well known transient network formers are the hydrophobically end-capped poly(urethane)s or HEUR associative thickeners.[1–7] In aqueous solution, the hydrophobic end-groups spontaneously self-assemble into micellar domains, which are stabilized by loops of the solvophilic middle block, leading to flowerlike micelles. At higher concentrations, a fraction of the telechelic polymers will stick each end-group in a different micellar core, thus connecting the micelles and forming a transient network. These associative thickeners are applied in paint formulations, cosmetics and oil recovery. Other telechelic polymers,[8–12] triblock copolymers[13,14] or other molecular architectures[15–21] are based on the same mechanism and driving force. Some of this work is summarized in a recent review by Tsitsilianis.[22]

The rheological properties of hydrophobically modified thickeners can be tuned by concentration and temperature, or by designing and synthesizing a new type of molecule. To have more sophisticated control of the gel properties, we need to prepare physical gels based on different driving forces.

Electrostatic interaction is, of all driving forces for association that one can think of, perhaps the most versatile, and is therefore an interesting candidate for physical gel formation. However, surprisingly little research is done on transient networks based on electrostatic interaction as driving force for association. Telechelic polymers with one single negatively charged end-group neutralized by multi-valent metal salts in organic solvent were studied by Register and coworkers in the late 1980's.[23–25] One other interesting case of charge-driven self-assembly was presented by Bossard, who describes a physical gel based on intermolecular bonds

between ABA triblock copolymers with oppositely charged A and B blocks.[26]

In a recent paper we have introduced an aqueous two component physical gel based on electrostatic interaction as driving force (Chapter 2).[27] The association is based on the co-assembly between an ABA triblock copolymer, in which the A blocks are charged and the B block is neutral and hydrophilic, and an oppositely charged homopolymer. The transient network formation is based on the association of the two oppositely charged polyelectrolyte moieties. In the case of mixing two oppositely charged homopolymers in water, the solution phase separates,[28–32] driven by ion pair formation and release of counterions in solution.[33–35] Adding a neutral hydrophilic block to one or both of the polyelectrolyte chains, prevents macroscopic phase separation, and leads to the formation of polyelectrolyte complex micelles.[35–39] These micelles have a polyelectrolyte complex core, stabilized by the hydrophilic corona. In case the polyelectrolyte complex core is liquid-like, one speaks of complex coacervate core micelles (C_3M's).[29,38] When one of the components is a triblock copolymer, flowerlike micelles are formed. At sufficiently high concentration, the triblock copolymer can bridge between two micelles, sticking either end-block in a different micellar core, leading to a sample-spanning transient network, see figure 4.1. Because electrostatic interaction is the driving force for association, the gel properties can be (reversibly) tuned by concentration, temperature, charge ratio, salt concentration and pH.[27] The multi-responsiveness and enhanced control of gelation, make these reversible gels promising candidates for future applications in responsive materials.

To understand the mechanical properties of physical gels, one has to obtain a detailed understanding of the microstructure of the transient network, *i.e.* the network topology. Small-angle scattering is the best available option to study the network structure of concentrated samples of associative polymers. Again, only a few studies are available in which small-angle scattering is used to probe the network structure of concentrated solutions of associative polymers based on solvophobic interactions.[40,41]

Although there are many similarities between these 'classical' associative thickeners and our charge-driven gels, there are also differences because of the different driving force for network formation. In this paper, we investigate how the transient network topology responds to changes in polymer concentration and ionic strength by combining (dynamic) light scattering, small-angle X-ray scattering and rheometry. In this way we obtain insight in the relevant length scales, aggregation numbers and number of bridges in the network, and how these microscopic changes translate to the macroscopic behaviour. To our surprise, we find that the storage modulus of the network is independent of ionic strength.

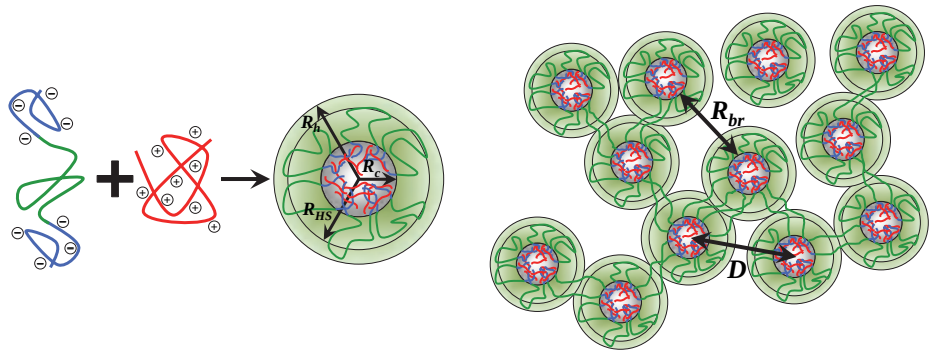

Figure 4.1: Artistic impression of charge-driven transient network formation. **(a)** Triblock copolymers and oppositely charged homopolymers associate into flowerlike micelles above the CMC. **(b)** At higher concentration the triblock copolymers are able to bridge between the micelles, leading to a transient network of interconnected micelles. Indicated with arrows are the different length scales that are described in the text.

4

4.2 Experimental

4.2.1 Materials

As positively charged homopolymer poly(allylamine hydrochlorid) (PAH) (95% pur.) with a molar mass of 16 kg mol^{-1} was used, corresponding to, on average, 170 monomers per homopolymer, see figure 4.2a.

4.2.2 Synthesis

A detailed synthetic protocol is provided as supporting information in Lemmers *et al.* (appendix Chapter 2),[27] but is briefly described here. ABA triblock copolymers with negatively charged end-blocks and a water soluble neutral middle-block were synthesized in two steps. An ATRP bifunctional macro-initiator was synthesized based on the method by Jankova and coworkers.[42] The bifunctional macro-initiator was prepared by dissolving poly(ethylene glycol) (PEG) with M_n = 10 kg mol^{-1} in toluene. After azeotropic distillation of the toluene, triethylamine was added. Subsequently, a ten-fold molar excess of 2-bromoisobutyryl bromide was added dropwise. The reaction mixture was stirred for five days at 30 °C. Purification was started by treatment of the reaction mixture with decolourising charcoal at 40 °C. The solids were removed by Büchner filtration, followed by precipitation of the product in a ten-fold excess of petroleum ether. After filtration of the product, it was redissolved in THF before precipitation in a ten-fold excess of petroleum ether

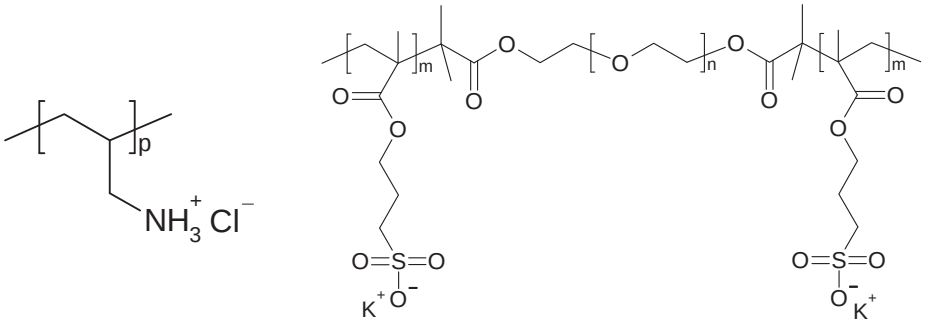

(a) p ≈ 170 **(b)** n ≈ 230; m ≈ 28

Figure 4.2: Molecular structures of **(a)** the positively charged homopolymer PAH_{170} and **(b)** the negatively charged triblock copolymer $PSPMA_{28}$—PEO_{230}—$PSPMA_{28}$.

(twice). The bifunctional macro-initiator was obtained by filtration and dried under vacuum overnight. The degree of esterification was determined by ^{1}H-NMR to be 100%.[43,44]

The triblock copolymer with negatively charged end-blocks was prepared by an atom transfer radical polymerization (ATRP) reaction,[45,46] based on a method described by Masci and coworkers.[47] The triblock copolymer was prepared by degassing the solid mixture of bifunctional macro-initiator and 3-sulfopropylmethacrylate potassium salt (KSPMA), aiming for an average degree of polymerization of 60. The solid mixture was dissolved in water/DMF (1:1) at 60 °C. The ATRP catalyst mixture based on $Cu^{I}Cl$, $Cu^{II}Cl_2$ and 2,2-bipyridine in a water/DMF mixture (1:1) was added to the bifunctional macro-initiator/KSPMA solution to start the polymerization. The reaction mixture was kept under argon flow until completion. The reaction was quenched after three hours by bubbling oxygen through the sample. Purification of the product was achieved by dialysis. The triblock copolymer was obtained by freeze-drying overnight. The degree of polymerization was determined by ^{1}H-NMR to be 55. Size exclusion chromatography showed that there was no macro-initiator left in the final product. The PDI of the triblock copolymer was determined to be 1.1.[27] The molecular structure of the triblock copolymer is given in figure 4.2b.

4.2.3 Characterization techniques

Light scattering titrations

Light scattering titrations were performed on an ALV light scattering instrument equipped with an ALV-5000/60X0 external digital correlator and a 300 mW solid

state laser (Cobolt Samba-300 DPSS laser) operated at a wavelength of 532 nm. The angle of detection was 90°, corresponding to a wave vector of $q = 0.022$ nm^{-1}. A refractive index matching bath of filtered cis-decalin surrounded the cylindrical scattering cell, and the temperature was controlled at 20±0.1 °C using a Haake F8-C35 thermostat. Titration steps were automated using a Schott-Geräte TR 250 computer-controlled titration setup for sequential addition of titrant and cell stirring. After each measurement, the pH was measured and the sample was stirred for one minute before addition of the titrant, followed by a period of stirring for eight minutes and a one minute rest period, before starting the next measurement.

The light scattering data were obtained using a script which evaluates the value of the average scattered light intensity during a set of measurements. We decided that 15 consecutive measurements with a deviation in average scattered light intensity less than 1% can be regarded as a system in equilibrium. The duration of each measurement depends on the scattered light intensity of that particular measurement, and is automatically adjusted to give reliable output, with 12 s being the minimum duration for a measurement.

The average scattered light intensity was normalized by the total polymer concentration $\langle I \rangle / C$ in the measuring cell, assuming $I \propto C$, which was checked to be correct in the concentration regime investigated in this paper. The hydrodynamic radii (R_h) were determined by averaging the values of each separate DLS measurement, as given by the standard ALV software, which is based on the cumulants method.[48]

Small-angle X-ray scattering

Small-angle X-ray scattering (SAXS) was performed at the Adolphe Merkle Institute on a pinhole SAXS camera from Rigaku Innovative Technologies equipped with a microfocus X-ray source ($\lambda = 1.5405$ Å). Low concentration samples were filled at room temperature into the sample holder: 1 and 2 mm quartz capillaries in a metal block, temperature controlled by a Peltier element to 20 ± 0.1 °C. Gelled samples at concentrations above 12%(w/w) were fluidized in a short preheating step to facilitate sample transfer into the capillaries. The 2D scattering pattern was recorded on a Triton 2-dimensional multi-wire proportional counter from Rigaku Innovative Technologies. The 2D image was radially integrated to obtain $I(q)$ using SAXSGui software (Rigaku Innovative Technologies). The measured scattering curves were corrected for solvent scattering and put on absolute scale by measuring the scattered intensity of water using the SAXSQuant software (Anton Paar, Graz, Austria). Model fitting was done using the SASfit program

developed by Kohlbrecher and coworkers at the Paul Scherrer Institute (PSI).[49] SAXS data were fitted using a form factor for polydisperse (Gaussian distribution) core-shell spheres and a hard-sphere structure factor for concentrations in excess of 1%(w/w), yielding an effective volume fraction and hard-sphere radius. A table with fitting parameters can be found in the appendix.

Rheometry

Rheological measurements were performed on Anton Paar MCR 301 or 501 stress-controlled rheometers. A cone-and-plate geometry was used to obtain the data, using a cone with a diameter of either 50 mm or 25 mm, both with an angle of 1°. The rheometer was operated in strain-controlled mode at a strain of $\gamma = 2\%$, which was checked to be in the linear viscoelastic regime. The measuring protocol was programmed such that only steady-state data were obtained (no time setting). Either a solvent trap, or a solvent blocker was used to minimize the effect of evaporation. Unless stated otherwise, all data are recorded at 20 °C.

4.3 Results and discussion

4.3.1 Flowerlike micelle formation

The co-assembly of $PSPMA_{28}$—PEO_{230}—$PSPMA_{28}$ with PAH_{170} in dilute solutions was investigated using (dynamic) light scattering. In previous work it was shown that the co-assembly of polyelectrolyte micelles depends on the overall charge composition.[27,35,50] By stepwise addition of one component to the other in a (dynamic) light scattering titration, the co-assembly as a function of charge composition can be investigated. The charge composition is expressed as:[35]

$$f^+ = \frac{[+]}{[+] + [-]} \tag{4.1}$$

which is the concentration of positively chargeable groups, [+], divided by the total amount of chargeable groups, $[+] + [-]$. The scattered light intensity usually exhibits a maximum close to the charge stoichiometric point, $f^+ = 0.5$, because the driving force for co-assembly is highest at charge stoichiometry.[35,50–52] Figure 4.3 shows the results of two charge composition titrations, one starting from $f^+ = 0$ and the other starting from $f^+ = 1$, for $PSPMA_{28}$—PEO_{230}—$PSPMA_{28}$ with PAH_{170} at a fixed ionic strength of 1.0 M KCl. It can be seen that the $\langle I \rangle / C$ values in both titrations are approximately equal, indicating that there is little hysteresis. Moreover, the average hydrodynamic radius is approximately constant

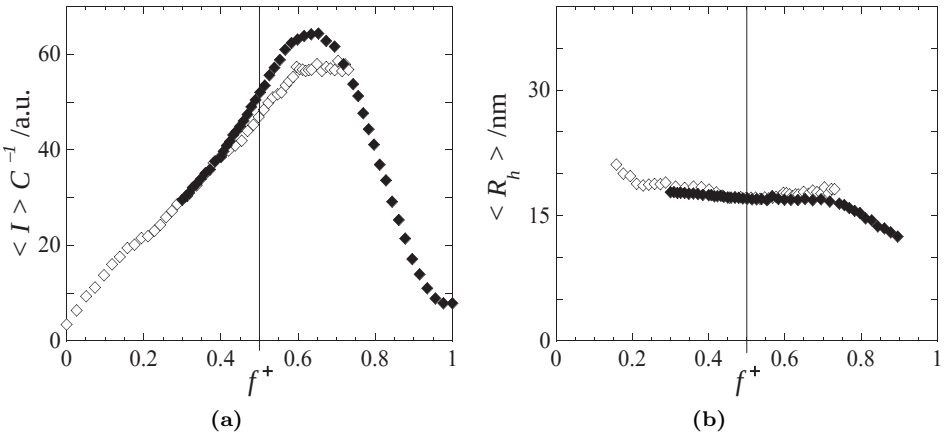

Figure 4.3: **(a)** The average scattered light intensity, normalized by the total polymer weight concentration, as a function of the charge composition variable f^+. **(b)** The average hydrodynamic radius, $\langle R_h \rangle$, as a function of f^+. The titrations were performed at concentrations of approximately 1 g l^{-1}. Titration of a solution of PAH_{170} to a solution of $PSPMA_{28}$—PEO_{230}—$PSPMA_{28}$ is indicated by open symbols; the reverse experiment is indicated by filled symbols.

4

at $\langle R_h \rangle \approx 18$ nm in the composition domain of $0.3 \leq f^+ \leq 0.7$, independent of sample history. The micelles in solution can therefore be regarded as equilibrium structures.

Figure 4.3a shows that the maximum in scattered light intensity is not exactly at charge stoichiometry in this particular case. Deviations of this kind have been observed before.[53] In part, they can be explained by proton transfer effects, *i.e.* weak polyelectrolytes, such as PAH, may be partly charged at the conditions investigated here. However, f^+ is based on the amount of *chargeable* groups. The shift of the peak to the positive side of the charge composition diagram means that more PAH_{170} had to be titrated to the solution than expected from the amount of chargeable groups in solution. This suggests that not all amino groups contribute to ion pairing. Another possible reason for the maximum occurring at $f^+ \approx 0.6$, is the experimental inaccuracy in the estimated number of negative charges. This number is determined from the ratio of the peak integrals in the ^{1}H-NMR spectrum of the triblock copolymer, which can be slightly off due to the relatively big difference in integral value of the middle-block compared to the integral value of the methyl group in the end-blocks.

The ionic strength in solution is an important parameter in our study, because the co-assembly of our triblock copolymers with oppositely charged homopolymer is

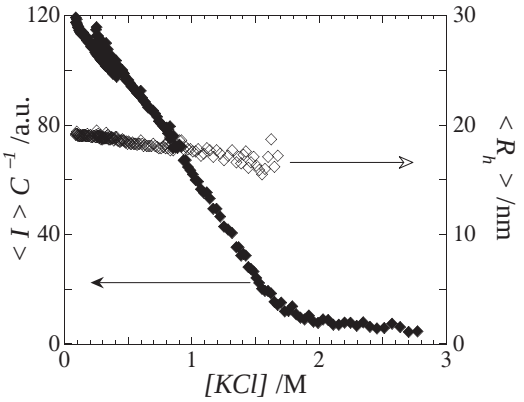

Figure 4.4: The average scattered light intensity, normalized by the total polymer concentration, on the left axis (♦) and the average hydrodynamic radius on the right axis (◊), as a function of [KCl]. Three experiments were performed by addition of water to a polymer/salt solution, thereby changing two parameters at the same time; the salt concentration and the polymer concentration.

driven by electrostatics. Salt ions can screen the electrostatic interactions between oppositely charged polyelectrolyte moieties, thereby decreasing the driving force for co-assembly. Figure 4.4 shows the influence of [KCl] on the co-assembly between $PSPMA_{28}$—PEO_{230}—$PSPMA_{28}$ and PAH_{170} in dilute solution.[27] It can be seen that an increase in ionic strength leads to a decrease in average scattered light intensity, as well as a slight decrease in the hydrodynamic radius of the micelles, R_h. Since $qR_h \approx 0.4$ and the concentration of polymers is low so inter-particle interactions can be neglected, the form and structure factor can be taken equal to unity. The scattered light intensity is therefore proportional to:

$$I \propto \left(\frac{\mathrm{d}n}{\mathrm{d}C}\right)^2 (C - CMC) N_{\mathrm{agg}} M_{bb} \tag{4.2}$$

where $\frac{\mathrm{d}n}{\mathrm{d}C}$ is the refractive index increment, C is the weight concentration of polymer, CMC is the critical micelle concentration, N_{agg} is the average number of building blocks in the micelle and M_{bb} is the average molecular weight of a building block. A building block is defined here as one triblock copolymer molecule plus the amount of oppositely charged homopolymer needed to exactly neutralize it. In our case $M_{bb} \approx 29$ kg mol^{-1}. Assuming $\frac{\mathrm{d}n}{\mathrm{d}C}$ to be independent of [KCl], the change of $\langle I \rangle / C$ in figure 4.4 can only be caused by changes of the CMC and/or N_{agg} with [KCl]. It is known that both the CMC and the aggregation number are dependent on the ionic strength in polyelectrolyte complex micelles.[54,55] The CMC increases with increasing salt concentration, the aggregation number decreases with increas-

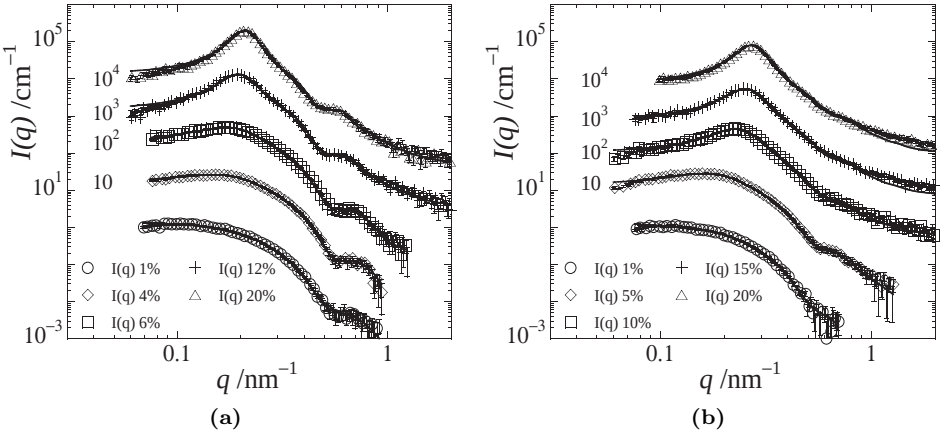

Figure 4.5: SAXS data for gels at concentrations of 1%–20%, for **(a)** 0.4 M KCl and **(b)** 1.0 M KCl, at 20 °C. Concentrations increase from bottom to top, as indicated by the legend in the graphs. Only 30% of the data points is shown. Lines are fits trough the data points, as described in the text. The curves are shifted for reasons of clarity, shift factors are indicated in the graphs.

ing salt concentration. Both effects lead to a decrease of $\langle I \rangle / C$ with increasing salt concentration. In figure 4.4 we see that $\langle I \rangle / C$ levels off for [KCl]$\geq$ 1.7 M. Since $C \approx 1$ g l^{-1} at that point, we infer that the CMC at a salt concentration of 1.7 M KCl equals approximately 1 g l^{-1}.

4.3.2 Shape, structure and interactions

Small-angle X-ray scattering measurements were performed to obtain insight into the shape and size of the micelles, the interactions between the micelles, and the structure of the transient network that forms at higher concentrations. The SAXS results are shown in figure 4.5, for various polymer concentrations and at two salt concentrations of 0.4 M KCl (4.5a) and 1.0 M KCl (4.5b), respectively. The curves are shifted with respect to each other by a shift factor as indicated in the graph.

For both salt concentrations it is assumed that the lowest weight concentration of 1%(w/w) is low enough to neglect the contribution of interactions between the flowerlike micelles, *i.e.* we assume that the q-dependence of the data is caused by the form-factor only. Since the critical micelle concentration is far below 1%(w/w), the contribution of free polymer to the scattered intensity can be safely neglected.

Fitting the data with polydisperse homogeneous spheres yields scatterers with an average radius of 8 nm. The hydrodynamic radius of the micelles in this study is $R_h \approx 18$ nm, see figures 4.3 and 4.4. This value is approximately twice as large

as the radius obtained from fitting the SAXS data, suggesting that the scattering predominantly originates from the micellar core.[50,56]

The core of a complex coacervate core micelle is, however, not homogeneous. Depending on the conditions, the interface between the core and corona might not be so well defined. To correct for the inhomogeneity of the complex coacervate core, we employ a model that improves the data fitting considerably, see appendix. We use a homogeneous sphere of radius R_{sphere} and a fixed relative contrast, on top of which we model a polydisperse 'interface' with variable thickness, R_{int}, and variable relative contrast, depending on the polymer concentration and salt concentration. We assume that the radius of the homogeneous sphere plus the thickness of the 'interface' together determine the radius of the micellar core R_c,[50,56] so that $R_c = R_{\text{sphere}} + R_{\text{int}}$. The micellar corona is invisible in the SAXS experiments.

The value of R_c that we find does not depend on our choice for R_{sphere}, and is the same as found by fitting the data with a form factor for homogeneous spheres, see appendix. The best fit for the 1%(w/w) SAXS data was obtained by a sphere of radius $R_{\text{sphere}} = 6.7$ nm for 0.4 M KCl and $R_{\text{sphere}} = 4.8$ nm for 1.0 M KCl, together with a Gaussian distribution of interface radii (R_{int}). The average value for the core radius was determined to be $R_c = R_{\text{sphere}} + R_{\text{int}} = 8.3 \pm 1.7$ nm for both salt concentrations, which is in agreement with values found in a previous study (Chapter 2).[27]

With increasing concentration, the micelles in the sample get more and more ordered, as can be seen from the development of a structure peak in figure 4.5. With increasing concentration the peak becomes more pronounced and shifts to higher q-values. For concentrations of 4%(w/w) and above, the SAXS data were fitted using both the form factor we described above, and an effective hard-sphere structure factor. The low-q data is determined mainly by the structure factor, while at high q the form factor dominates. We adjusted the thickness of the polydisperse interface and relative interfacial contrast in the form factor if this contributed to a better fit of the data. Note that the flowerlike micelles are equilibrium structures that can adapt their composition and size depending on the conditions. The resulting fits are in good agreement with the data.

The core size R_c is plotted as a function of concentration in figure 4.6. The core radius is approximately constant for the 0.4 M KCl gels, while it seems to decrease slightly with increasing concentration in the 1.0 M KCl samples. The origin of this decrease is not clear.

The hard-sphere structure factor contains two parameters, the effective hard-sphere radius, R_{HS}, and the volume fraction of hard spheres, ϕ. Both R_{HS} and

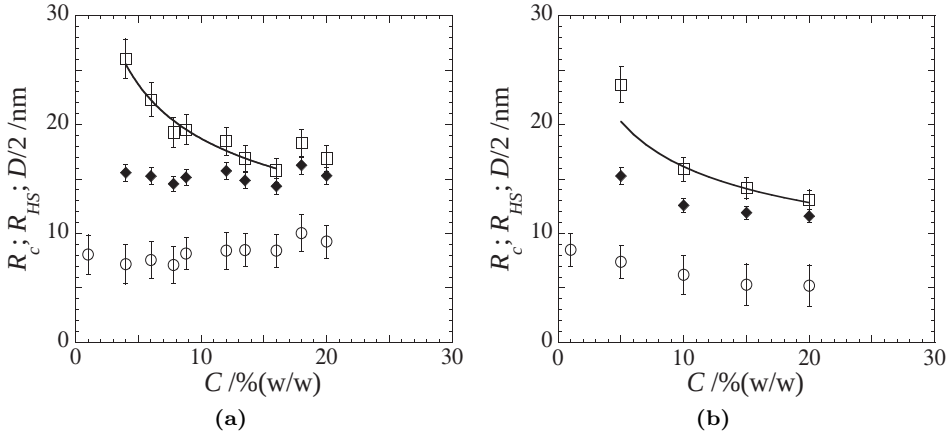

Figure 4.6: Overview of different radii as a function of total polymer concentration, as obtained by model-fitting the SAXS data of 0.4 M KCl **(a)** and 1.0 M KCl **(b)** gels. The symbols correspond to R_c (○), R_{HS} (♦), and $\frac{D}{2}$ (□). The lines display $D \propto C^{-1/3}$, as discussed in the text.

ϕ can be obtained within 5% accuracy of the fits, as the position and the shape of the structure peak are rather sensitive to these parameters. The effective hard-sphere radius as a function of polymer concentration is plotted in figure 4.6. It is approximately constant in the 0.4 M KCl samples, $R_{HS} \simeq 15$ nm, and is slightly below the hydrodynamic radius of the micelles of $R_h \simeq 18$ nm in dilute solution, as determined by DLS, see figure 4.4. The hard-sphere radius of the 1.0 M KCl samples is somewhat lower than in the 0.4 M KCl samples, as expected based on the lower value of R_c and the slightly lower hydrodynamic radius from DLS measurements. Also in the 1.0 M KCl samples, the hard sphere radius is smaller than the hydrodynamic radius as determined in the dilute regime. It seems to decrease with increasing concentration, in line with the decrease in core radius.

The change of the volume fraction of hard spheres, *i.e.* the volume fraction of micelles, as a function of polymer concentration is depicted in figure 4.7. For both salt concentrations the volume fraction of micelles increases approximately linearly with polymer concentration, up to a concentration of 10–15%(w/w). At polymer concentrations above 15%, the increase in volume fraction seems to level off, indicating that the density of the micelles is somewhat increased.

The inset in figure 4.7 shows the number density of micelles, $n = \phi / \left(\frac{4}{3}\pi R_{HS}^3\right)$, as a function of polymer concentration. It shows that the number density of micelles is higher in the 1.0 M KCl solution than in the 0.4 M KCl solution. For equal polymer concentration and $C \gg CMC$, an increase in number density can only be

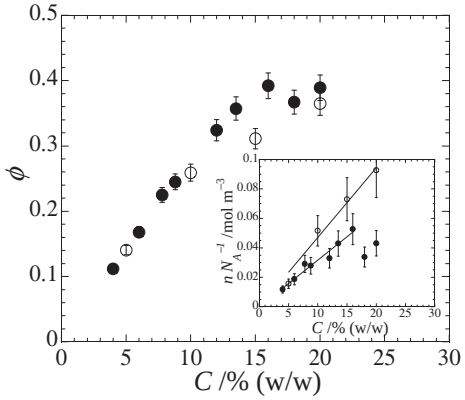

Figure 4.7: Volume fraction of hard-spheres, and number density of micelles (inset), based on fitting of the SAXS data, as a function of polymer weight concentration. The symbols represent data for two different salt concentrations; 0.4 M KCl (•) and 1.0 M KCl (○). The lines in the inset are linear fits through the data points.

accompanied by a decrease in aggregation number, because

$$C = \frac{nN_{\text{agg}}M_{bb}}{N_A} \tag{4.3}$$

where N_{agg} is the aggregation number, N_A is Avogadro's number and M_{bb} is the molar mass of an electroneutral building block, $M_{bb} \approx 29$ kg mol^{-1}. In other words, for equal polymer concentrations the polymers are distributed over more but smaller micelles in higher salt concentration samples, compared to lower salt concentration samples. The number density increases linearly with polymer concentration up to 15% to 20%, for 0.4 M KCl and 1.0 M KCl respectively. The levelling off of n at high polymer concentrations for 0.4 M KCl can be caused by an increase in aggregation number,[40] leading to more dense and slightly bigger micelles.

From the number density of micelles, we immediately obtain the average center-to-center distance between the micelles, $D = n^{-1/3}$. This distance is plotted in figure 4.6 as $D/2$ so that these values can be compared with the hard-sphere radius. Obviously, the average center-to-center distance decreases with increasing polymer concentration. In the region where the number density of micelles increases linearly with concentration, the average center-to-center distance decreases as $D \propto C^{-1/3}$, which corresponds to the lines in figure 4.6.

The aggregation number of the micelles can be estimated from equation 4.3. The aggregation number obtained in this way is plotted in figure 4.8a, as a function of polymer concentration for both salt concentrations. Note that the aggregation

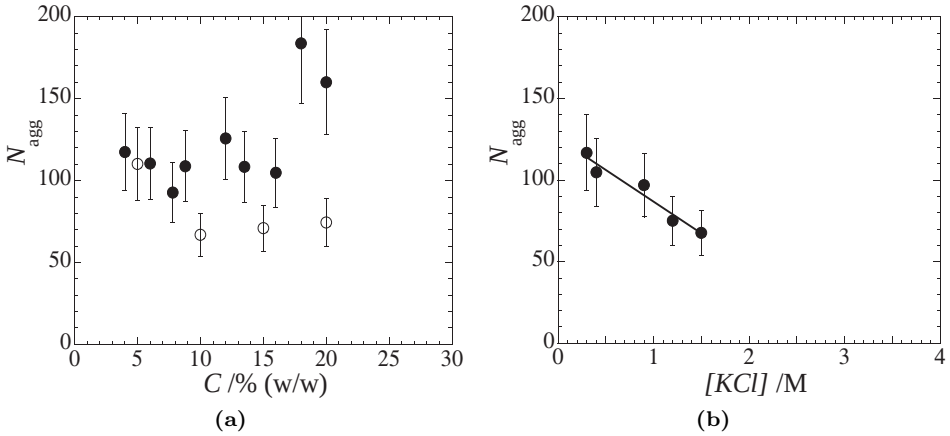

Figure 4.8: **(a)** Number of building blocks N_{agg} per micelle as a function of polymer weight concentration, for two different salt concentrations: 0.4 M KCl (•) and 1.0 M KCl (○). **(b)** Number of building blocks per micelle as a function of salt concentration at fixed polymer concentration of 16%(w/w). The line is a linear fit through the data points.

number is expressed as the average number of neutralized triblock copolymers per micelle and that the actual number of triblock copolymers participating in a micelle depends on the polymer concentration. That is, at low concentration there are more loops and hence less triblock copolymers participating compared to higher concentrations, where there are more bridges between the micelles and hence more triblock copolymers participating.

Despite the scatter on the data, it is clear that the number of building blocks in the 0.4 M KCl gels, approximately 110, is higher than that of the 1.0 M KCl gels, approximately 70. These numbers are comparable to values recently found by Wang and coworkers on complex coacervate core micelles with iron-based coordination polymers stabilized by a PEO corona block of approximately equal length as used in this study.[55] Other studies report somewhat lower aggregation numbers for polyelectrolyte complex micelles prepared from different combinations of diblock copolymers with homopolymer.[50,56]

To investigate the effect of salt on the aggregation number in more detail, we performed additional SAXS measurements on samples with the same polymer concentration (16%(w/w)), but different KCl concentrations. The scattering curves can be found in the appendix of this Chapter. The resulting aggregation numbers are shown in figure 4.8b, as a function of salt concentration. From this graph it is clear that N_{agg} decreases with increasing [KCl]. The decrease is almost linear with increasing [KCl], in agreement with the results of Wang and coworkers.[55] These

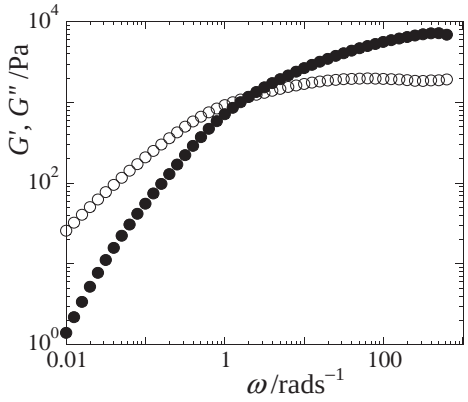

Figure 4.9: Storage modulus, G' (•), and loss modulus, G'' (○), as a function of angular frequency (ω), for a 20%(w/w) gel at 0.4 M KCl and 20 °C.

authors explained this nearly linear decrease in aggregation number by combining a scaling argument for micellization[57] with the mean-field theory for complex coacervation of Voorn and Overbeek,[33,58] leading to an almost linear dependence of the aggregation number on salt concentration:

$$N_{\text{agg}} \propto (c_{cr} - c_s)^{6/5} \tag{4.4}$$

where c_s is the salt concentration and c_{cr} is the critical salt concentration above which no complex coacervation occurs between homopolyelectrolytes of similar length as used in this study. Extrapolating the linear fit to $N_{\text{agg}} \approx 0$ results in a critical salt concentration of approximately 3.5 M KCl for this polymer concentration. This high value is not unreasonable, since equally high salt concentrations are needed to disintegrate polyelectrolyte multi-layers of PAH and poly(styrene sulfonate); the latter polymer carries a negatively charged sulfonate group similar to the triblock copolymer used in this study.[59,60]

4.3.3 Mechanical properties

To probe the mechanical properties of the networks, we performed dynamic rheological measurements. Figure 4.9 shows an example of a frequency sweep for a 20%(w/w) gel at 0.4 M KCl and at 20 °C. The frequency sweep shows the viscoelastic properties of the charge-driven gels. At low frequencies the gels behave liquid-like, *i.e.* $G' < G''$, while at high frequencies the gels behave solid-like, *i.e.* $G' > G''$. For high enough frequencies, the storage modulus (G') reaches a plateau, as can be seen in figure 4.9.

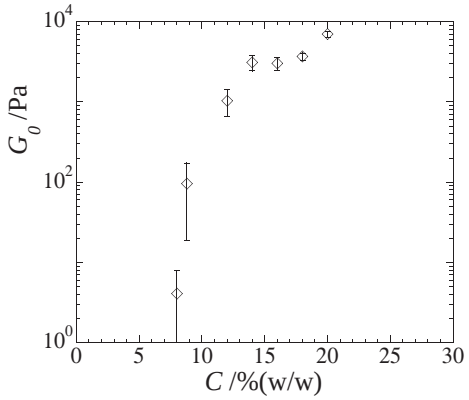

Figure 4.10: G_0 as a function of polymer weight concentration C at 0.4 M KCl. Shown are average values over multiple measurements. Error bars indicate plus or minus the standard deviation of the measurement series.

Based on multiple series of frequency sweeps, the plateau value of the storage modulus, G_0, is plotted as a function of polymer concentration in figure 4.10. For concentrations below the gel concentration, $C_{\text{gel}} \approx 8\%$(w/w), the plateau modulus was too small to be detected. Between 8% and 10%(w/w) G_0 increases strongly. The increase in plateau modulus, or viscosity,[27] is unlikely to be caused by jamming of the micelles, since the effective volume fraction of micelles is approximately 0.2–0.4, for polymer concentrations between 8%–20%(w/w), see figure 4.7. In concentrated systems of soft colloids that are unable to form bridges, only a small increase of viscosity and or modulus is reported for similar or even higher effective volume fractions.[61–65] We therefore conclude that the increase of the plateau modulus with concentration results from the formation of more and more bridges between the micelles.

According to the classical theory of entropic polymer networks, each elastically active chain contributes kT to the elastic modulus:[66]

$$G_0 = \nu kT \tag{4.5}$$

where ν is the number density of elastically active chains, *i.e.* elastically active bridges between the micelles in the network. At low polymer concentrations, bridge formation is unlikely, because of the large average separation distance between the micelles. With increasing concentration, the average intermicellar distance decreases, so that bridge formation becomes more probable and the modulus of the gel increases.

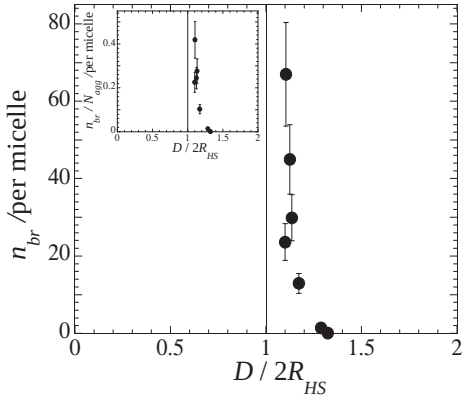

Figure 4.11: Number of elastically active chains per micelle as a function of the normalized distance between the micelles, for the 0.4 M KCl gels. The inset shows the bridging fraction ($\frac{n_{br}}{N_{\mathrm{agg}}}$) as a function of the normalized distance.

By combining the scattering data with rheological data, we can obtain an estimate for the average number of bridges per micelle:

$$n_{br} \simeq \frac{G_0 D^3}{kT} \tag{4.6}$$

In figure 4.11 the value of n_{br} is shown as a function of the average distance between the micelles, normalized by the hard-sphere diameter. As expected, the number of bridges per micelle is a strong function of the average distance between the micelles.[67–71] The number of elastically active chains per micelle increases drastically as the coronas of the micelles get close to each other, *i.e.* when the intermicellar distance is approximately twice the hydrodynamic radius. A comparison with the aggregation number of the micelles (figure 4.8a) shows that at high concentrations (where $D \approx 2R_{HS}$), a bit less than half of the triblock copolymers forms a bridge. This is in line with theoretical calculations, which predict limiting values of either $1/3$[68,70] or $1/2$.[67,69,72] However, the actual number of bridges per micelle might deviate from the values in figure 4.11, because we compute only the bridges that contribute to the elasticity of the network. However, there might be bridges present in the gel in the form of dangling ends or superchains,[2] which would mean that the numbers in figure 4.11 are underestimated. On the other hand, there may be contributions to the modulus from entanglements, which would overestimate the number of bridges per micelle as presented in figure 4.11.

For salt concentrations of [KCl] $\geq$ 1.0 M, no plateau could be observed in G' in the accessible range of frequencies. To overcome this difficulty, we applied

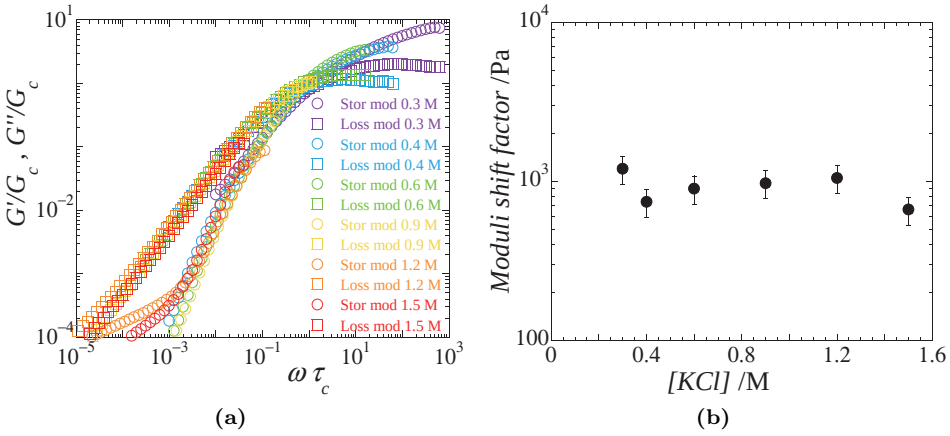

Figure 4.12: **(a)** Rescaled frequency sweeps measured at different salt concentrations to obtain the mastercurve. The rescaled modulus G/G_c is plotted as a function of rescaled frequency $\omega\tau_c$, where the shift factors G_c and τ_c are chosen such that all curves superimpose. The polymer concentration and temperature are constant at 16%(w/w) and 20 °C, respectively. Storage moduli are in circles (○), loss moduli in squares (□). Salt concentrations are given in different colours, as indicated in the figure. **(b)** Moduli shift factors used to obtain the master curve applying time-salt superposition. Shift factors are chosen such that the point where $G' = G''$ is approximately unity.

4

'Time-Salt Superposition', a technique described in a recent paper.[73] We found that frequency sweeps, measured at different salt concentrations, could be superimposed by shifting them along the frequency axis, see figure 4.12a. By doing so, we assume that the addition of salt affects all relaxation processes in the system, in the accessible range of frequencies, in the same way. There was almost no need for a vertical shift along the moduli axis, *i.e.* the shift factors are approximately equal, see figure 4.12b. From this we conclude that the plateau modulus is hardly affected by the salt concentration.

To understand why the elastic modulus does not dependent significantly on salt concentration, we consider the average distance between the interfaces of two neighbouring micellar cores, $R_{br} = D - 2R_c$. This is the average distance over which the middle-block of a triblock copolymer has to stretch to form a bridge. This distance is plotted as a function of polymer concentration in figure 4.13 for both 0.4 M KCl and 1.0 M KCl salt.

As expected, the average bridging distance decreases with increasing concentration, approximately as a power-law with an exponent of -0.6. Moreover, figure 4.13 shows that the average bridging distance is independent of salt concentration, even though the size and number density of the micelles is rather different for the two

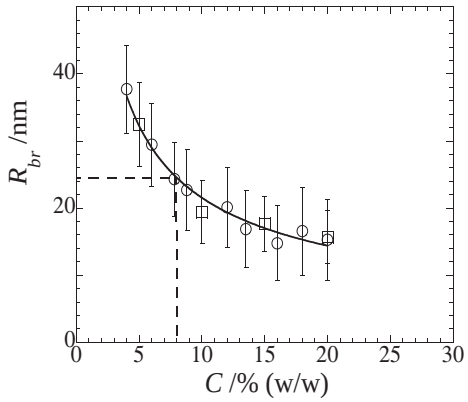

Figure 4.13: R_{br} as a function of weight concentration of polymer for the two different salt concentrations; 0.4 M KCl (○) and 1.0 M KCl (□). The full line is a power-law fit with an exponent of -0.6. The dashed line indicates the point of percolation, and the average distance the middle-block has to stretch at this point to connect two micelles. Error bars indicate minimum and maximum possible values for R_{br}, taking into account the errors in D and R_c.

salt concentrations, see figures 4.6 and 4.7. With increasing salt concentration the aggregation number decreases, leading to a decrease in R_c. This is accompanied by an increase in the number density of micelles, see equation 4.3, leading to a decrease in D. Apparently these two effects exactly compensate each other, so that R_{br} is independent of salt concentration. Since the average number of bridges per micelle is determined by the average bridging distance, it is clear that if the bridging distance is independent of salt concentration, the elastic modulus is also independent of salt concentration. In other words, it is the total amount of triblock copolymers in the system that determines the number density of elastically active chains. How the triblock copolymers are distributed throughout the system, in more smaller micelles or in fewer bigger micelles, is not important. Note that this contrasts with numerical calculations[68] and Monte-Carlo simulations[70] on bridge formation between micelles. Both studies showed an increase of the number of bridges for smaller cores at the same value for R_{br}. Possibly the effect of salt on the size of our micelles is too small to see this effect.

Simulations on bridging by telechelic polymers between spherical particles show that the interaction potential between two micelles is characterized by a short-ranged steric repulsion, followed by an attractive minimum due to bridging.[70] The range of this attraction is on the order of three times the radius of gyration of the free polymer. In our case, with a PEO middle-block that has an $R_g \approx 5$ nm,[74,75]

this means that bridges should start to form only when the bridging distance is on the order of 14 nm. Since the thickness of the corona of our micelles ($R_{HS} - R_c$) is approximately 6–7.5 nm, this means that the coronas must be nearly touching when two micelles connect to each other.

The dashed line in figure 4.13 indicates the concentration at which a modulus can be measured and thus a percolated network is formed, see figure 4.10. The corresponding average bridging distance between two micellar cores is approximately 24 nm. This means that on average the PEO_{230} middle-block has to stretch approximately five times its radius of gyration in water to bridge two micelles.[74,75] This is rather unlikely, for reasons mentioned above. The transient network is thus very open and inhomogeneous at the point of percolation. The number of micelles that become elastically active, increases with polymer concentration. For concentrations of 20%(w/w) and above, where the average center-to-center distance approaches the value of two times the effective hard-sphere radius, or where $R_{br} \approx 3R_g$(PEO), almost all micelles can act as an elastically active node in a (homogeneous) transient network.

4.3.4 Phase diagram

Based on the experimental results in this and previous work[27] (Chapter 2), we propose a 'phase diagram' for the class of charge-driven micellar systems, see figure 4.14. To clarify the phase diagram, the different phases are illustrated within the diagram. The phase diagram shows the total polymer concentration on the x-axis and the salt concentration, or driving force for association, on the y-axis. Below the CMC, the triblock copolymers and homopolymers are free in solution. The CMC shifts to higher values with increasing salt concentration.[54,55] Above the CMC, flowerlike micelles are formed. The number density of micelles and the aggregation number vary with salt concentration. For $C \gg CMC$, the aggregation number decreases and the number density of micelles increases, with increasing salt concentration. With increasing polymer concentration the micelles are packed more closely, enabling the formation of bridges between micelles. In the gel phase, the micelles maintain their shape and size. The connectivity of the network increases drastically when the average distance between the micelles becomes close to twice their hydrodynamic radius. Note that the phase boundaries might shift depending on the chemistry of the polyelectrolytes, the length of the blocks, the types of counterions and charge ratio. Still, we are convinced that the characteristics of this phase diagram are universal for charge-driven micellar networks at charge stoichiometric conditions.

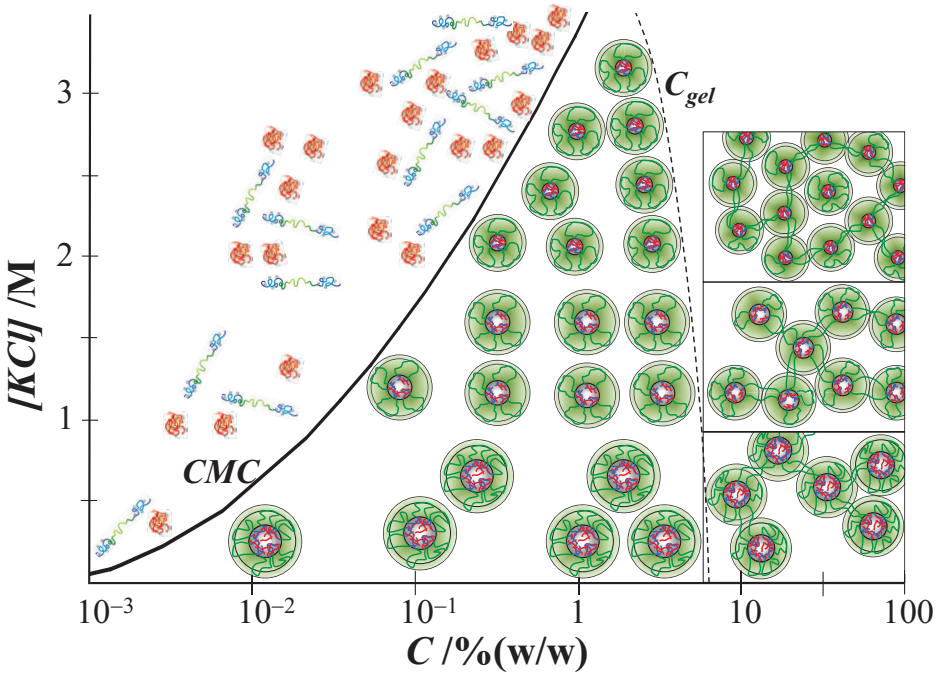

Figure 4.14: Schematic 'phase diagram' for charge-driven micelle formation and gelation. The size of the micelles decreases with decreasing driving force for association, while the number of micelles increases with decreasing driving force for association. Below the, salt dependent, CMC only unimers exist. Above the gel concentration a sample-spanning transient network is formed.

4.4 Conclusion

We have shown that an ABA triblock copolymer co-assembles with an oppositely charged homopolymer to form flowerlike micelles in aqueous solution. At high concentrations, the triblock copolymers form bridges between the micelles, leading to a transient network of polyelectrolyte complex micelles with visco-elastic properties. The flowerlike micelles in our gels can be modelled by a core-shell form factor, combined with an effective hard-sphere structure factor. The influence of concentration and ionic strength on the modulus of the gels was explained by calculating the distance that a middle-block has to overcome to form a bridge between two micelles. We showed that the modulus of the gels is independent of salt concentration, because the bridging distance is independent of salt concentration. This paper is a good example of the power of combining microscopic techniques (DLS, SAXS) with a macroscopic technique (rheometry). We believe that this combination is essential for obtaining a fundamental understanding of soft matter.

References

[1] R. D. Jenkins, C. A. Silebi and M. S. El-Asser, *Acs Symposium Series*, 1991, **462**, 222–233.

[2] T. Annable, R. Buscall, R. Ettelaie and D. Whittlestone, *Journal of Rheology*, 1993, **37**, 695–726.

[3] R. D. Jenkins, D. R. Bassett, C. A. Silebi and M. S. Elaasser, *Journal of Applied Polymer Science*, 1995, **58**, 209–230.

[4] T. Annable, R. Buscall and R. Ettelaie, *Colloids and Surfaces a-Physicochemical and Engineering Aspects*, 1996, **112**, 97–116.

[5] J. F. Le Meins and J. F. Tassin, *Colloid and Polymer Science*, 2003, **281**, 283–287.

[6] L. A. Hough and H. D. Ou-Yang, *Physical Review E*, 2006, **73**, year.

[7] J. Sprakel, E. Spruijt, M. A. Cohen Stuart, N. A. M. Besseling, M. P. Lettinga and J. van der Gucht, *Soft Matter*, 2008, **4**, 1696–1705.

[8] C. Tsitsilianis, I. Iliopoulos and G. Ducouret, *Macromolecules*, 2000, **33**, 2936–2943.

[9] P. Kujawa, H. Watanabe, F. Tanaka and F. M. Winnik, *European Physical Journal E*, 2005, **17**, 129–137.

[10] D. Mistry, T. Annable, X. F. Yuan and C. Booth, *Langmuir*, 2006, **22**, 2986–2992.

[11] F. C. Giacomelli, I. C. Riegel, C. L. Petzhold, N. P. da Silveira and P. Stepanek, *Langmuir*, 2009, **25**, 731–738.

[12] R. Obeid, E. Maltseva, A. F. Thunemann, F. Tanaka and F. M. Winnik, *Macromolecules*, 2009, **42**, 2204–2214.

[13] G. T. Gotzamanis, C. Tsitsilianis, S. C. Hadjiyannakou, C. S. Patrickios, R. Lupitskyy and S. Minko, *Macromolecules*, 2006, **39**, 678–683.

[14] F. Bossard, T. Aubry, G. Gotzamanis and C. Tsitsilianis, *Soft Matter*, 2006, **2**, 510–516.

[15] V. Tirtaatmadja, K. C. Tam and R. D. Jenkins, *Macromolecules*, 1997, **30**, 3271–3282.

[16] L. Bromberg, *Macromolecules*, 1998, **31**, 6148–6156.

[17] E. J. Regalado, J. Selb and F. Candau, *Macromolecules*, 1999, **32**, 8580–8588.

[18] K. C. Tam, W. K. Ng and R. D. Jenkins, *Journal of Applied Polymer Science*, 2006, **102**, 5166–5173.

[19] A. C. Lara-Ceniceros, C. Rivera-Vallejo and E. J. Jimenez-Regalado, *Polymer Bulletin*, 2007, **58**, 425–433.

[20] C. Rufier, A. Collet, M. Viguier, J. Oberdisse and S. Mora, *Macromolecules*, 2008, **41**, 5854–5862.

[21] C. Tsitsilianis, N. Stavrouli, V. Bocharova, S. Angelopoulos, A. Kiriy, I. Katsampas and M. Stamm, *Polymer*, 2008, **49**, 2996–3006.

[22] C. Tsitsilianis, *Soft Matter*, 2010, **6**, 2372–2388.

[23] R. A. Register, M. Foucart, R. Jerome, Y. S. Ding and S. L. Cooper, *Macromolecules*, 1988, **21**, 1009–1015.

[24] Y. S. Ding, S. R. Hubbard, K. O. Hodgson, R. A. Register and S. L. Cooper, *Macromolecules*, 1988, **21**, 1698–1703.

[25] R. A. Register, G. Pruckmayr and S. L. Cooper, *Macromolecules*, 1990, **23**, 3023–3026.

[26] F. Bossard, V. Sfika and C. Tsitsilianis, *Macromolecules*, 2004, **37**, 3899–3904.

[27] M. Lemmers, J. Sprakel, I. K. Voets, J. van der Gucht and M. A. Cohen Stuart, *Angewandte Chemie-International Edition*, 2010, **49**, 708–711.

[28] F. Tiebackx, *Zeitschrift für Chemie und Industrie der Kolloide*, 1911, **8**, 198–201.

[29] H. Bungenberg de Jong and H. Kruyt, *Proceedings of the Koninklijke Nederlandse Akademie van Wetenschappen*, 1929, **32**, 849–856.

[30] H. Bungenberg de Jong, *Crystallisation Coacervation Flocculation*, Elsevier, Amsterdam, 1949, vol. II, Chapter X.

[31] R. Chollakup, W. Smitthipong, C. D. Eisenbach and M. Tirrell, *Macromolecules*, 2010, **43**, 2518–2528.

[32] E. Spruijt, A. H. Westphal, J. W. Borst, M. A. Cohen Stuart and J. van der Gucht, *Macromolecules*, 2010.

[33] J. Overbeek and M. Voorn, *Journal of Cellular and Comparative Physiology*, 1957, **49**, 7–26.

[34] J. Kriz, J. Dybal and H. Dautzenberg, *Journal of Physical Chemistry A*, 2001, **105**, 7486–7493.

[35] S. van der Burgh, A. de Keizer and M. A. Cohen Stuart, *Langmuir*, 2004, **20**, 1073–1084.

[36] A. Harada and K. Kataoka, *Macromolecules*, 1995, **28**, 5294–5299.

[37] A. V. Kabanov, T. K. Bronich, V. A. Kabanov, K. Yu and A. Eisenberg, *Macromolecules*, 1996, **29**, 6797–6802.

[38] M. A. Cohen Stuart, N. A. M. Besseling and R. G. Fokkink, *Langmuir*, 1998, **14**, 6846–6849.

[39] J. F. Gohy, S. K. Varshney, S. Antoun and R. Jerome, *Macromolecules*, 2000, **33**, 9298–9305.

[40] M. E. Seitz, W. R. Burghardt, K. T. Faber and K. R. Shull, *Macromolecules*, 2007, **40**, 1218–1226.

[41] T. Koga, F. Tanaka, R. Motokawa, S. Koizumi and F. M. Winnik, *Macromolecules*, 2008, **41**, 9413–9422.

[42] K. Jankova, X. Y. Chen, J. Kops and W. Batsberg, *Macromolecules*, 1998, **31**, 538–541.

[43] J. M. Dust, Z. H. Fang and J. M. Harris, *Macromolecules*, 1990, **23**, 3742–3746.

[44] K. Jankova and J. Kops, *Journal of Applied Polymer Science*, 1994, **54**, 1027–1032.

[45] M. Kato, M. Kamigaito, M. Sawamoto and T. Higashimura, *Macromolecules*, 1995, **28**, 1721–1723.

[46] J. S. Wang and K. Matyjaszewski, *Macromolecules*, 1995, **28**, 7901–7910.

[47] G. Masci, D. Bontempo, N. Tiso, M. Diociaiuti, L. Mannina, D. Capitani and V. Crescenzi, *Macromolecules*, 2004, **37**, 4464–4473.

[48] D. E. Koppel, *Journal of Chemical Physics*, 1972, **57**, 4814–&.

[49] J. Kohlbrecher and I. Bressler, *SASfit*, 2010, version 0.92.3.

[50] I. K. Voets, S. van der Burgh, B. Farago, R. Fokkink, D. Kovacevic, T. Hellweg, A. de Keizer and M. A. Cohen Stuart, *Macromolecules*, 2007, **40**, 8476–8482.

[51] I. K. Voets, A. de Keizer, M. A. Cohen Stuart, J. Justynska and H. Schlaad, *Macromolecules*, 2007, **40**, 2158–2164.

[52] I. K. Voets, R. Fokkink, T. Hellweg, S. M. King, P. de Waard, A. de Keizer and M. A. Cohen Stuart, *Soft Matter*, 2009, **5**, 999–1005.

[53] I. K. Voets, A. de Keizer, F. A. M. Leermakers, A. Debuigne, R. Jerome, C. Detrembleur and M. A. Cohen Stuart, *European Polymer Journal*, 2009, **45**, 2913–2925.

[54] Y. Yan, A. de Keizer, M. A. Cohen Stuart, M. Drechsler and N. A. M. Besseling, *Journal of Physical Chemistry B*, 2008, **112**, 10908–10914.

[55] J. Wang, A. de Keizer, R. Fokkink, Y. Yan, M. A. Cohen Stuart and J. van der Gucht, *The Journal of Physical Chemistry B*, 2010, **114**, 8313–8319.

[56] I. K. Voets, R. de Vries, R. Fokkink, J. Sprakel, R. P. May, A. de Keizer and M. A. Cohen Stuart, *European Physical Journal E*, 2009, **30**, 351–359.

[57] E. Y. Kramarenko, A. R. Khokhlov and P. Reineker, *Journal of Chemical Physics*, 2006, **125**, year.

[58] E. Spruijt, J. Sprakel, M. A. Cohen Stuart and J. van der Gucht, *Soft Matter*, 2010, **6**, 172–178.

[59] O. V. Lebedeva, B. S. Kim, K. Vasilev and O. I. Vinogradova, *Journal of Colloid and Interface Science*, 2005, **284**, 455–462.

[60] M. Cornelsen, C. A. Helm and S. Block, *Macromolecules*, 2010, **43**, 4300–4309.

[61] J. Roovers, *Macromolecules*, 1994, **27**, 5359–5364.

[62] V. Castelletto and I. W. Hamley, *Langmuir*, 2003, **19**, 3229–3235.

[63] T. Nicolai, F. Lafleche and A. Gibaud, *Macromolecules*, 2004, **37**, 8066–8071.

[64] A. V. Korobko, W. Jesse, A. Lapp, S. U. Egelhaaf and J. R. C. van der Maarel, *Journal of Chemical Physics*, 2005, **122**, year.

[65] L. Dahbi, M. Alexander, V. Trappe, J. K. G. Dhont and P. Schurtenberger, *Journal of Colloid and Interface Science*, 2010, **342**, 564–570.

[66] R. Larson, *The Structure and Rheology of Complex Fluids*, Oxford University Press, Inc., New York, 1999, p. 663.

[67] S. T. Milner and T. A. Witten, *Macromolecules*, 1992, **25**, 5495–5503.

[68] S. R. Bhatia and W. B. Russel, *Macromolecules*, 2000, **33**, 5713–5720.

[69] X. X. Meng and W. B. Russel, *Macromolecules*, 2003, **36**, 10112–10119.

[70] V. Testard, J. Oberdisse and C. Ligoure, *Macromolecules*, 2008, **41**, 7219–7226.

[71] J. Sprakel, E. Spruijt, J. van der Gucht, J. T. Padding and W. J. Briels, *Soft Matter*, 2009, **5**, 4748–4756.

[72] J. Sprakel, N. A. M. Besseling, M. A. Cohen Stuart and F. A. M. Leermakers, *European Physical Journal E*, 2008, **25**, 163–173.

[73] E. Spruijt, J. Sprakel, M. Lemmers, M. A. Cohen Stuart and J. van der Gucht, *Physical Review Letters*, 2010, **105**, 208301.

[74] K. Devanand and J. C. Selser, *Macromolecules*, 1991, **24**, 5943–5947.

[75] K. L. Linegar, A. E. Adeniran, A. F. Kostko and M. A. Anisimov, *Colloid Journal*, 2010, **72**, 279–281.

Appendix

Multiple form factor fits

We employed several models for the form factor to model the polyelectrolyte complex core micelles. Some examples are shown in figure 4.15. The simplest model is a Gaussian distribution of homogeneous spheres. This fit yields homogeneous spheres with an average radius of 8.2 nm. However, the fit does not describe the data very well for $q > 0.5$ nm^{-1}, see fit 1 in figure 4.15. The mismatch is probably caused by the inhomogeneity of the core of a polyelectrolyte complex core micelle, as explained in the main text. To correct for the inhomogeneity of the core, we apply a model containing two contributions: i) a monodisperse sphere of radius R_{sphere} with fixed relative contrast; ii) a polydisperse (Gaussian) 'interface' of radius R_{int} surrounding the monodisperse sphere, with an adjustable thickness and relative contrast. The fitting quality increases considerably using this model, see fits 2–5 in figure 4.15. As shown in table 4.15, the total radius $R_c = R_{\text{sphere}} + R_{\text{int}}$ is approximately the same for all fits.

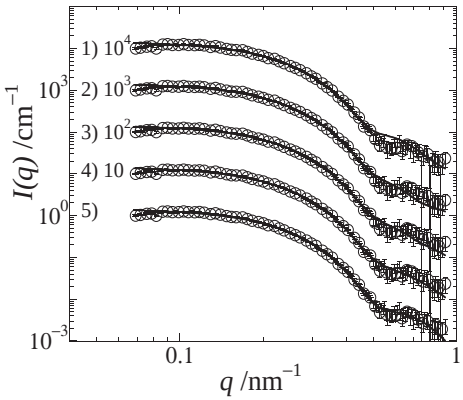

Figure 4.15: SAXS intensity as a function of q for polymer concentration of 1%(w/w) and salt concentration of 0.4 M KCl. Shown are different form factor fits to the data: 1) Homogeneous sphere of radius 8.2 nm; 2) Sphere-interface model with $R_{\text{sphere}} = 4$ nm; 3) Sphere-interface model with $R_{\text{sphere}} = 5$ nm; 4) Sphere-interface model with $R_{\text{sphere}} = 6$ nm; 5) Sphere-interface model with $R_{\text{sphere}} = 6.7$ nm as is shown in the main text. Shift factors are indicated in the graph.

Table of fitting parameters

Table 4.1 describes the parameters used to fit the SAXS data of the 1% 0.4 M KCl sample, as displayed in figure 4.15. The standard deviation of the Gaussian distribution of the interface thickness is taken as error value for the total core radius.

Table 4.1: Table with fitting parameters for the different fits of the 1%(w/w) 0.4 M KCl SAXS data.

Fit number	R_{sphere} nm	R_{int} nm	η_{int} 10^{-6} cm^{-2}	R_c nm
1	8.2 ±1.7	0	-	8.2 ±1.7
2	4.0	4.5 ±1.6	0.74 ±0.03	8.5 ±1.6
3	5.0	3.5 ±1.6	0.80 ±0.025	8.5 ±1.6
4	6.0	2.3 ±1.7	0.84 ±0.025	8.3 ±1.7
5	6.7	1.4 ±1.8	0.85 ±0.03	8.1 ±1.8

The relative scattering length density difference between the sphere and the solvent is equal in all fits: $\eta_{\text{sphere}} = 10^{-6}$ cm^{-2}. The relative scattering length density difference between the interface and the solvent is indicated by η_{int}.

SAXS curves 16%(w/w) [KCl] series

Figure 4.16 displays the SAXS data of a series of samples with constant polymer concentration 16%(w/w) and varying KCl concentration. Note that the features of the curve become less and less pronounced as the [KCl] increases. This is mainly caused by an increase in polydispersity of the scatterers. For the 1.5 M KCl sample in particular, the form factor is not well defined. However, the structure factor contribution is still well defined. To compute the aggregation number of the scatterers we use only the structure factor information, see main text. In the high salt concentration samples, the fits cannot describe the scattering at high q. This implies that the form factor that we use is not fully compatible with the real flowerlike micelles at these salt concentrations. Differences can also be caused by errors in background subtraction, additional to the errors on the data itself.

Table of fitting parameters

Table 4.2 describes the parameters used to fit the SAXS data of the 16%(w/w) [KCl] series. The standard deviation of the Gaussian distribution of the interface thickness is taken as error value for the total core radius. Errors in the R_{HS} and ϕ are estimated to be within 5%. The relative scattering length density difference between the sphere and the solvent is equal in all fits: $\eta_{\text{sphere}} = 10^{-6}$ cm^{-2}. The relative scattering length density difference between the interface and the solvent is indicated by η_{int}. An additional background contribution was sometimes used to indicate the limit of $I(q)$ for high q-values.

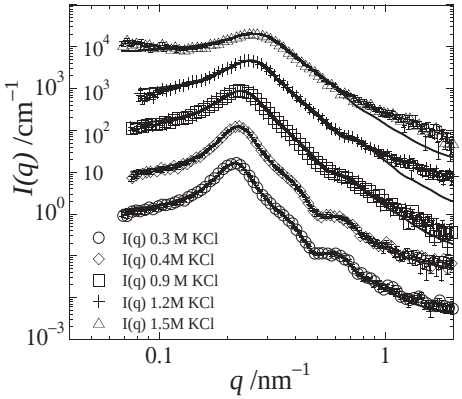

Figure 4.16: SAXS intensity as a function of q for multiple KCl concentrations and fixed polymer concentration of 16%(w/w). Lines are fits to the data. Symbols and corresponding KCl concentrations are indicated in the graph. Curves are shifted with respect to each other for graphical reasons. Shift factors are indicated in the graph.

Table 4.2: Table with fitting parameters for the 16%(w/w) [KCl] series.

[KCl] M	R_{sphere} nm	R_{int} nm	η_{int} 10^{-6} cm^{-2}	R_c nm	R_{HS} nm	ϕ -	background cm^{-1}
0.3	6.7	2.4 ±1.4	1.0	9.1 ±1.4	15.0	0.40	0.0035
0.4	6.7	1.7 ±1.5	1.0	8.4 ±1.5	14.3	0.39	0.0045
0.9	4.8	2.3 ±1.9	1.2	7.1 ±1.9	13.2	0.33	0.001
1.2	4.0	1.1 ±2.0	1.4	5.1 ±2.0	11.8	0.30	0.001
1.5	2.0	1.0 ±2.4	1.6	3.0 ±2.4	10.3	0.23	0.0015

Fitting parameters of the scattering curves in the main text

The following tables describe the parameters used to fit the SAXS data of the two concentration series, as shown in the main text. The standard deviation of the Gaussian distribution of the interface thickness is taken as error value for the total core radius. Errors in the R_{HS} and ϕ are estimated to be within 5%. The relative scattering length density difference between the sphere and the solvent is equal in all fits: $\eta_{\text{sphere}} = 10^{-6}$ cm^{-2}. The relative scattering length density difference between the interface and the solvent is indicated by η_{int}. An additional background contribution was sometimes used to indicate the limit of $I(q)$ for high q-values.

0.4 M KCl polymer concentration series

Table 4.3: Table with fitting parameters for the polymer concentration series at 0.4 M KCl.

Concentration %(w/w)	R_{sphere} nm	R_{int} nm	η_{int} 10^{-6} cm^{-2}	R_c nm	R_{HS} nm	ϕ -	background cm^{-1}
1	6.7	1.4 ±1.8	0.85	8.1 ±1.8	-	0	-
4	6.7	0.5 ±1.8	0.81	7.2 ±1.8	15.6	0.11	-
6	6.7	0.9 ±1.7	0.93	7.6 ±1.7	15.3	0.17	-
8	6.7	0.4 ±1.7	1.0	7.1 ±1.7	14.5	0.23	-
9	6.7	1.5 ±1.5	0.91	8.2 ±1.5	15.2	0.24	-
12	6.7	1.7 ±1.7	1.0	8.4 ±1.7	15.8	0.32	0.004
14	6.7	1.8 ±1.5	1.0	8.5 ±1.5	14.9	0.36	0.001
16	6.7	1.7 ±1.5	1.0	8.4 ±1.5	14.3	0.39	0.005
18	6.7	3.3 ±1.7	1.0	10.0 ±1.7	16.3	0.37	0.007
20	6.7	2.6 ±1.5	1.0	9.3 ±1.5	15.3	0.39	0.005

1.0 M KCl polymer concentration series

Table 4.4: Table with fitting parameters for the polymer concentration series at 1.0 M KCl.

Concentration %(w/w)	R_{sphere} nm	R_{int} nm	η_{int} 10^{-6} cm^{-2}	R_c nm	R_{HS} nm	ϕ -	background cm^{-1}
1	4.8	3.7 ±1.5	0.66	8.5 ±1.5	-	0	-
5	4.8	2.6 ±1.5	1.07	7.4 ±1.5	15.3	0.14	-
10	4.8	1.4 ±1.8	1.23	6.2 ±1.8	12.6	0.26	0.006
15	4.8	0.5 ±1.9	1.33	5.3 ±1.9	11.9	0.31	0.007
20	4.8	0.4 ±1.9	1.33	5.2 ±1.9	11.6	0.37	0.0095

Chapter 5

Charge-Driven Complex Composite Gels

In this Chapter we show that we can prepare aqueous physical gels consisting of negatively charged silica nanoparticles bridged by ABA triblock copolymers, in which the A blocks are positively charged and the B block is neutral and water soluble. Irreversible aggregation of the silica nanoparticles is prevented by precoating the nanoparticles with a neutral hydrophilic polymer. We show that electrostatic interactions are the driving force for the association between the end-blocks and the silica particles, and that the bridging of particles is reversible on timescales of minutes to hours. The versatility of the electrostatic driving force and straightforward synthesis of the triblock copolymer makes charge-driven bridging of particles by triblock copolymers a promising strategy for thickening of aqueous particle containing materials, such as water-based coatings.

This chapter is submitted as paper with supporting information

5.1 Introduction

Polymers are commonly used as rheology modifiers for solvents, because they can enhance the solvent viscosity at relatively low volume fractions by forming entanglements. By incorporating 'active' groups in the polymers these effects become more pronounced, especially when the groups interact to form a physical gel. In contrast to chemical gels, physical gels consist of a network with non-permanent cross-links. This transient network entraps the solvent, thereby restricting its flow. Moreover, an internal network can tolerate a certain level of stress, giving the material stiffness and elasticity. Because the network has the ability to rearrange, the material can relax applied stresses or strains. Physical gels are therefore viscoelastic, self-healing materials, while mainly consisting of solvent.

The most abundant and environmentally friendly solvent is water. Water-based physical gels are of great interest to academia as well as industry, where they are applied as rheology modifiers in foods, cosmetics, enhanced oil recovery fluids and water-based coatings. It is therefore not surprising that there is an ongoing, and perhaps even increasing, effort to understand water-based physical gels, to enhance their properties, and to invent new ways of preparing them.

One way to enhance the mechanical properties of materials is to incorporate inorganic particles as fillers. It is well known from chemically cross-linked materials and polymer melts that incorporating inorganic nano-sized particles can lead to further enhancement of the material properties.[1–5] Inorganic particles can also be used as cross-linking points in chemical gels.[6–8]

Incorporating high amounts of particles in a physical gel, while stabilizing these particles at the same time, is, however, a real challenge. Often, particle suspensions are unstable when mixed with polymers, caused by irreversible aggregation of the particles in a process known as flocculation.[9–11] Learning how to avoid flocculation of particles in physical gels will be of great benefit to, for example, the coatings industry.

There are several examples of water-based physical gels in which inorganic particles are introduced within an existing physical network, leading to 'composite' or 'hybrid' gels. The inorganic particles, often clay or silica, then act as additional physical cross-linking points in the network, resulting in higher values for the elastic modulus.[12–17] Special cases are the 'shake gels', that show gelation upon shearing.[10,18]

A strategy to avoid particle flocculation in physical gels is to use the particles as the nodes in the transient network. There are, however, very few reports on physical gels in which inorganic nanoparticles are used exclusively as nodes in

the transient network. Petit and coworkers have prepared hybrid gels of graft copolymers mixed with silica particles, in which the grafts physically adsorb onto the silica particle surface.[19] Another example is the study by Xu and coworkers, where they describe a gel based on graphene sheets bridged by ssDNA.[20] In both cases, the binding interactions are non-covalent, but they are so strong that they are essentially irreversible at room temperature. A reversible gel comes from Wang and coworkers.[21] These authors describe a water-based physical gel, presumably based on the electrostatic interaction between a positively charged dendritic end-group and the negatively charged surface of clay particles. Whereas the clay particles are cheap, the dendritic binder is expensive, because the synthesis of the dendritic end-groups is rather labour intensive, involving multiple reaction steps, which inevitably leads to relatively low amounts of product.[21]

Here, we describe the combination of cheap and easy to synthesize ABA triblock copolymers and silica nanoparticles to prepare, for the first time, a charge-driven water-based composite physical gel, existing of precoated silica nanoparticles bridged by the ABA triblock copolymers. The ABA triblock copolymer consists of A blocks that are positively charged, and a B block which is neutral and water soluble. The precoated silica particles are negatively charged in water at neutral pH. Mixing these two oppositely charged components together leads to transient network formation, in which the silica particles are the nodes in the network, see figure 5.1. As we will show, the binding between the triblock copolymers and silica particles is reversible on timescales of minutes to hours, the particles do not suffer from irreversible aggregation and the resulting 'complex composite' gels are stable for at least a month. Moreover, the interaction strength and thus the rheological properties are highly tunable by means of, *e.g.*, composition, concentration, block lengths and salt concentration.

5.2 Experimental

5.2.1 Triblock copolymer synthesis

The triblock copolymer was synthesized in two steps. First, poly(ethylene glycol) of $M_n = 10$ kg mol^{-1} was used to synthesize a bifunctional macro-initiator based on the method by Jankova and coworkers.[22] The detailed synthetic protocol has been described elsewhere (appendix Chapter 2).[23] The degree of esterification was 100% as determined by ^{1}H-NMR.[24,25]

The bifunctional macro-initiator was used to synthesize the triblock copolymer by atom transfer radical polymerization,[26,27] based on the method described by Li

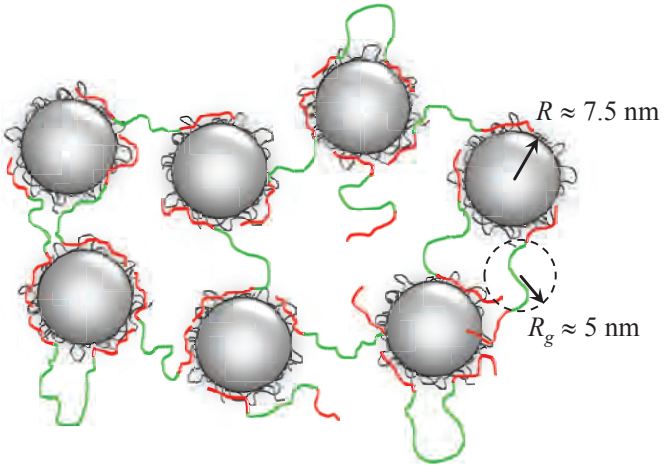

Figure 5.1: A schematic drawing of silica nanoparticles connected by triblock copolymers, thereby forming a transient network. The PEO middle-block is drawn in green, the positively charged end-blocks are drawn in red and the physisorbed PVP is drawn in gray.

and coworkers.[28] A detailed synthetic protocol has recently been described elsewhere (Chapter 3).[29] In brief, bifunctional macro-initiator, [2-(methacryloyoxy) ethyl] trimethylammonium chloride and bipyridyl were mixed with 2-propanol and deionized water (1:1 v/v). The mixture was stirred at 40 °C while degassing by bubbling argon for 45 minutes. Subsequently, equal molar amounts of Cu(I)Cl and Cu(II)Cl were added to start the reaction. After five hours, the reaction was quenched by bubbling oxygen through the mixture. The product was purified by dialysis against deionized water. The product was obtained by freeze-drying overnight. The yield by weight was 73% (20 g). On average 68 monomers were attached per macro-initiator molecule, as determined by ^{1}H-NMR, see appendix.

5.2.2 Composite gel preparation

To prepare the coated silica nanoparticles, Ludox LS 30 (Sigma Aldrich, 30% (w/w) in 10 mM salt solution in water) colloidal silica particles, with a particle radius of approximately 7.5 nm, were mixed with a 10 mM salt solution of poly(vinylpyrrolidone) K25 (PVP) (Fluka, $M_w = 40$ kg mol^{-1}). The amount of PVP in solution was twice the amount that is expected to physically adsorb, based on reflectometry measurements (see appendix). The soaking of particles in the PVP solution was done at least one day before further use of the coated particles, to saturate the silica surface with PVP. As solvent in all samples we used the composition of the Ludox solvent, which is 0.002% (w/w) of chloride as NaCl and 0.010% (w/w) of sulfate as Na_2SO_4.

The pH of the solvent was adjusted to p$H = 7.0 \pm 0.2$ to minimize the chance of hydrolysis of the ester bonds in the end-blocks of the triblock copolymers.

The PVP-coated silica particles were subsequently added to a 10 mM salt triblock copolymer solution. The sample was shortly vortexed directly after addition of the silica particles. The samples were left to rest for one day before starting rheological measurements. Note that there is no resting period for the samples measured with DLS, for this is a non-invasive technique and one can study the relaxation behaviour directly after mixing.

5.2.3 High resolution and cryogenic scanning electron microscopy

HRSEM and cryo-SEM experiments were performed at the Wageningen Electron Microscopy Center. For cryo-SEM, small droplets of the samples were placed in two aluminum platelets with a depth of 0.3 mm each (Wohlwend, Sennwald, Switzerland). The two platelets were put on top of each other, creating a 'sandwich'. This sandwich was high-pressure frozen in a HPM 10 (BalTec, Liechtenstein). The frozen samples were stored in liquid nitrogen before further preparation for cryo-SEM analysis.

The frozen samples were placed in a clamping holder under liquid nitrogen. The samples were transferred to a non-dedicated cryo-preparation system (MED 020/VCT 100, Leica, Vienna, Austria) onto a sample stage at -95 °C in high vacuum ($1.3 \cdot 10^{-6}$ mbar). In this cryo-preparation system the samples were freeze-fractured by removing half of the 'sandwich' followed immediately by sputter-coating the exposed surface with approximately 2 nm Tungsten. The samples were cryo-shielded in high vacuum and transferred into the field emission scanning microscope (Magellan 400, FEI, Eindhoven, The Netherlands). The sample stage was maintained at -120 °C in vacuum ($4 \cdot 10^{-7}$ mbar). The analysis was performed at a working distance of 4 mm with TLD SE detection at 2 kV and 13 pA. All images were recorded digitally.

Ambient HRSEM imaging was performed on dried gels. Small flat droplets of gels were put on a hydrophilic surface (plasma cleaned) of circular cover slips of 8 mm (Menzel, Brauschweig, Germany). These gels were air dried, post dried in vacuum and sputter coated with 2 nm Tungsten. HRSEM analyses was done at 2 kV, 6.3 pA.

5.2.4 Rheometry

Rheological measurements were performed on an Anton Paar Physica MCR 301 stress controlled rheometer. A cone and plate geometry was used with either a

cone-diameter of 50 mm or 25 mm. Both geometries have an angle of 1°. The effect of solvent evaporation was minimized by utilizing the solvent blocker system, which ensures a completely sealed sample environment. Temperatures of both the plate and the hood were Peltier controlled at 20 °C. Oscillatory measurements were performed at 0.05% strain, which was checked to be in the linear viscoelastic regime for the entire time window studied. Creep tests were performed at a shear stress of 0.1 Pa. Sample loading was performed with caution; a limiting normal force of 0.5 N was set. Rheological measurements were started two hours after sample loading, to allow the sample to relax the loading stresses. A 5 ml gel sample was kept in a closed container, out of which small aliquots were taken to investigate the development of the storage modulus of the gel in time.

5.2.5 Dynamic light scattering

Dynamic light scattering is a relatively fast and non-invasive microscopic technique to study relaxation behaviour, and data can be obtained directly after mixing of the components. DLS experiments were performed on an ALV-125 goniometer, combined with a Cobolt Samba-300 DPSS laser (300 mW) operating at a wavelength of 532 nm, an ALV optical fiber with a diameter of 50 μm, an ALV/SO Single Photon Detector and an ALV5000/60X0 External Correlator. Temperature was controlled at 20 °C using a Haake F8-C35 thermostatic bath. The angle of detection was 90°. Due to the high scattering intensity, an optical density filter of 10% was used to ensure linearity of the detector. A total sample volume of 1 ml was measured at different moments in time. Intensity correlation functions were recorded for different time intervals, corrected for the specific measurement setup and shifted if necessary to obtain a intermediate scattering function that starts to decay at unity for the smallest correlation times.

From a dynamic light scattering experiment we obtain the intensity correlation function, $g^{(2)}(t)$, from which we compute the intermediate scattering function $g^{(1)}(t)$ by applying equation 5.1:[30]

$$g^{(1)}(t) = \sqrt{\frac{(g^{(2)}(t) - 1)}{A}} \tag{5.1}$$

where A is an experimental parameter close to unity in our case. The decay of the intermediate scattering function is a measure for the relaxation processes in the gel: at short times the positional correlations are close to unity, while at longer timescales the intermediate scattering function goes to zero, because all positional correlations on length scales of q^{-1} are lost.

5.2.6 Small-angle X-ray scattering

Small-angle X-ray scattering (SAXS) experiments were carried out at the Adolphe Merkle Institute on a pinhole camera (S-Max 3000) from Rigaku Innovative Technologies equipped with a microfocus X-ray source operating at wavelength $\lambda = 1.5405$ Å (Cu-K_α emission) and a Triton 2-dimensional multi-wire gas detector. The sample was loaded into a reusable 2 mm quartz capillary cell and subsequently placed into a sample holder thermostatted to 20 °C by an external Julabo CF 30 circulator. The data is radially averaged and corrected for transmission, background scattering, detector efficiency, and converted into absolute scattering cross sections using water as a calibration standard. The SASfit program developed by Kohlbrecher and coworkers at the Paul Scherrer Institute (PSI) is used for data analysis.[31]

5.3 Results and Discussion

5.3.1 Sample preparation

To avoid irreversible aggregation of the particles, we first coated the silica nanoparticles with a layer of poly(vinylpyrrolidone) (PVP), a neutral hydrophilic polymer. Coating of the particles was achieved by physical adsorption of PVP, which is known to be essentially irreversible on silica surfaces.[32] The PVP coating also prevents physical adsorption of the poly(ethylene oxide) (PEO) middle-block, because the adsorption energy of PEO is much lower than that of PVP.[32–34] The adsorbed amount of PVP on the silica surface is approximately 0.5 mg m^{-2}, see appendix.

To physically bind the negatively charged silica nanoparticles in a transient network, we utilize an ABA triblock copolymer consisting of a PEO middle-block, and two strongly charged poly(trimethylaminoethyl methacrylate) (PTMAEMA) end-blocks. To obtain such a triblock copolymer, TMAEMA monomers were polymerized from a PEO-based bifunctional macro-initiator by aqueous ATRP,[26–28] as described in more detail in the experimental section. The end-product was characterized by ^{1}H-NMR as $PTMAEMA_{34}$—PEO_{230}—$PTMAEMA_{34}$, see appendix. Mixing this triblock copolymer with a solution of precoated silica nanoparticles can lead to transient network formation, as illustrated in figure 5.1.

The silica particle concentration and the triblock copolymer concentration are the two major factors that influence transient network formation. We have investigated the effect of varying these two parameters by making samples of different composition. To prepare a sample-spanning transient network, the concentration

of potential nodes must be high enough to facilitate a percolating structure. We have found that the silica particle concentration should be above approximately 10%(w/w) to cause any noticeable increase in viscosity. As expected, the viscosity of the gels increased with increasing silica particle concentration, because more particles leads to more nodes in the transient network. The viscosity decreased with increasing triblock copolymer concentration. This decrease can be caused by an increase in the formation of loops and dangling ends of the triblock copolymer, thereby reducing the number of bridges between the particles. Another possibility is that the particles themselves become repulsive when we overcharge the particles with positive charges.

From earlier work on polyelectrolyte complexes, it is well known that the driving force for charge-driven association is strongest at a 1:1 charge ratio.[23,35–37] In this case we found that we needed to overdose the system with positive charge at least three times to obtain reasonably transparent gels, indicative of relatively small-scale density fluctuations.[38] Less triblock copolymer led to more turbid samples, meaning that the density fluctuations are larger in these samples. The turbidity decreases with increasing silica particle concentration, but this effect is subtle. The diagram of states in figure 5.2 summarizes the influence of silica concentration and triblock copolymer concentration on the physical appearance of the gels.

We further tested the mechanical properties and time evolution of these gels using a 13%(w/w) silica nanoparticles and 3.4%(w/w) triblock copolymer gel, indicated by the big circle in figure 5.2a. When we mix the coated silica nanoparticles with an aqueous solution of the ABA triblock copolymer at this composition, we initially obtain a turbid gel, a sign of large-scale density fluctuations in the sample. Within half an hour the gel becomes almost transparent, indicating that the large-scale density fluctuations evolve spontaneously into smaller ones. Photographs of the different states can be found in the appendix.

We assume that upon the physical binding of a TMAEMA group with an oppositely charged group on the silica surface, counterions from both components are released into the solution. The entropy gain related to this counterion release is an important part of the driving force in charge-driven association.[39] As a result of this counterion release, the salt concentration in the gel rises, to approximately 0.1 M for this specific case.

5.3.2 Gel structure and properties

We performed rheological studies to prove that the material under study is truly a physical gel. A frequency sweep applied to an approximately 1000 hours (43 days)

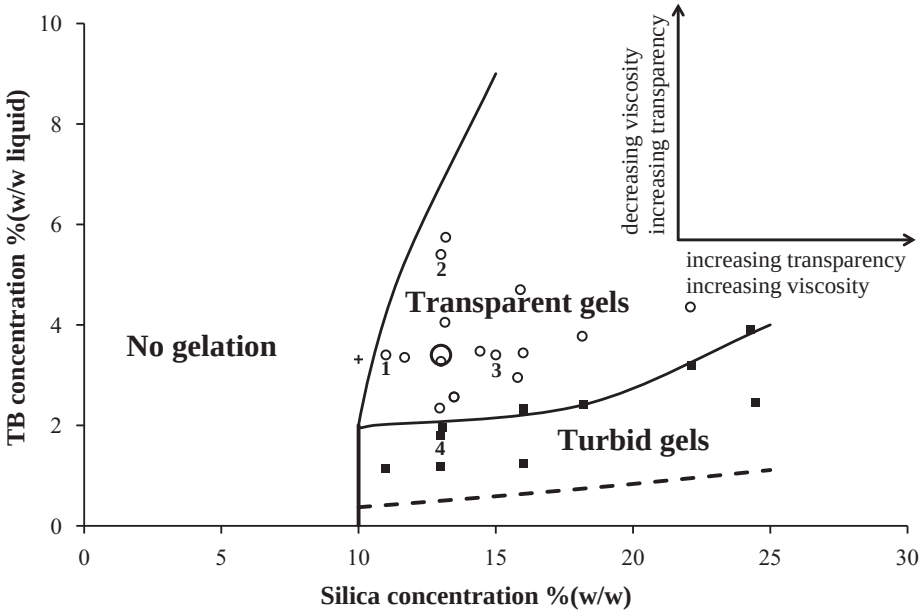

(a)

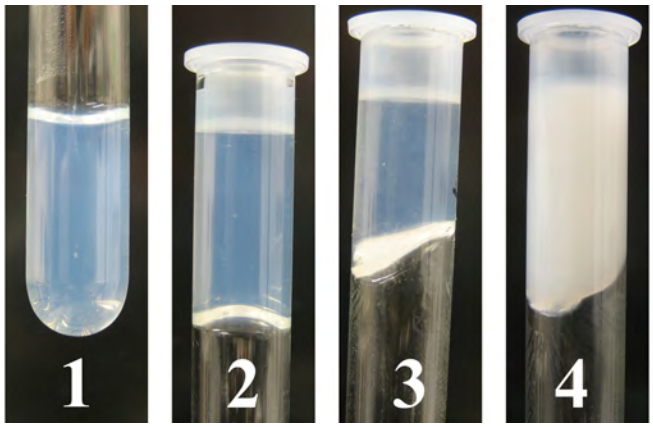

(b)

Figure 5.2: **(a)** Phase diagram sketching the phase boundaries (solid lines) between samples that appear as liquids (+), turbid gels (■) and transparent gels (○). The calculated dashed line indicates charge stoichiometry between the silica particles and the triblock copolymers. The big circle indicates the sample used for further studies. The inset shows the observed direction of increased transparency and increased or decreased viscosity. The numbers in the phase diagram belong to the data points directly above the numbers and correspond to the photographs of the samples as shown in figure 5.2b. **(b)** Photographs of samples to show the differences in appearance of the samples. The numbers correspond to the numbers in the phase diagram.

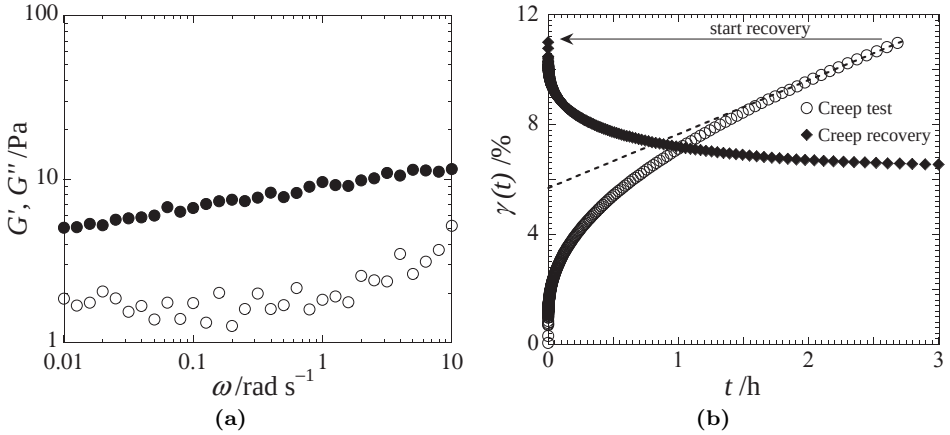

Figure 5.3: **(a)** Frequency sweep of a complex composite gel, approximately 1000 h (43 days) after preparation. G' (•) $>$ G'' (○), over the measured frequency domain. **(b)** Creep curve of the same complex composite gel, at fixed shear stress of 0.1 Pa. Shown is the strain in time, for both the creep test (○) and the creep recovery (♦), after cessation of the shear stress. The graph displays only 10% of the data points.

old complex composite gel is shown in figure 5.3a. We find that $G' > G''$ over the measured frequency domain, indicating that the material behaves solid-like on the investigated timescales. In other words, the relaxation time associated with the mechanical response must be longer than 100 s. In polymeric gels, the value of the storage modulus is related to the number of elastically active chains in the transient network.[40] In our samples, the value for the storage modulus is relatively low. If every triblock copolymer would act as an elastically active bridge, G' would reach several kPa. What we measure is orders of magnitude lower, meaning that the amount of elastically active bridges is in the order of a few percent of the maximum possible amount. This is not surprising, since at this concentration of particles in the gel, the average particle center-to-center distance would be approximately 33 nm, if the particles were homogeneously dispersed. This means that to connect two particles, the triblock copolymers would have to bridge approximately 18 nm between the surfaces of two particles. The radius of gyration of the middle-block is approximately 4-5 nm,[41,42] so that strong stretching is needed to bridge 18 nm, which is very unfavourable. The fact that we do have a physical gel, must therefore mean that the network has a very open structure.

To probe the material at longer time-scales we performed a creep test. We applied a constant shear stress of $\sigma = 0.1$ Pa to the sample and measured the strain of the sample as a function of time, $\gamma(t)$. Figure 5.3b shows a creep curve

for the same sample as studied in figure 5.3a. There is an almost instantaneous response of the material to the applied stress, which is associated with the elasticity of the gel. After the initial response, the gel continues to deform under the applied stress, *i.e.* the gel starts to flow. This indicates that the bonds between the triblock copolymer end-blocks and the coated silica particles are able to break and reform in time.

In figure 5.3b we see that it takes approximately two hours to reach a regime of constant slope, *i.e.* a constant shear rate. The inverse of the slope is related to the shear viscosity. With a value of approximately 11 kPa s this is a relatively viscous system. Since the modulus is relatively low, the relaxation processes must be very slow. This is consistent with the results from the frequency sweep measurement in figure 5.3a.

Relaxation processes in our complex composite gels must involve the desorption of the polyelectrolyte blocks from the silica surface. Due to the strong electrostatically driven adsorption, this is unfavourable and therefore expected to be a slow process.[43] The gradual change in slope of the creep test in figure 5.3b indicates that there is a wide spectrum of relaxation times, which may reflect a wide distribution of adsorbed conformations of the end-blocks.

An estimate for the stored energy in the gel can be found by extrapolating backward from the region of constant slope to the y-axis, see dashed line in figure 5.3b. In this example we obtain a value of approximately 2 Pa as an estimate for the stored energy, which is approximately 0.02 kT per particle. Several Pascal's is in agreement with the value for the storage modulus measured in the frequency sweep experiment. Extrapolating even further backwards to the crossing with the x-axis yields an estimate for the longest relaxation time, which is in this case approximately three hours, or 11,000 s.

Our observation that there are many processes involved in the relaxation of stress in these gels is confirmed by measuring the strain recovery immediately after cessation of the applied shear stress. In figure 5.3b we can see an initial fast relaxation, followed by a slow relaxation of the strain in time. After two hours the strain becomes constant, indicating that the gel has relaxed almost all the remaining shear stress. Two hours is also the time after which the creep curve becomes linear. Note that the gel does not recover completely, which is typical for a viscoelastic liquid.

To visualize the structure of our gels, we performed freeze-fracture cryogenic scanning electron microscopy. Typical cryo-SEM images of such a gel, at different magnifications, are shown in figure 5.4. The silica particles can clearly be seen as

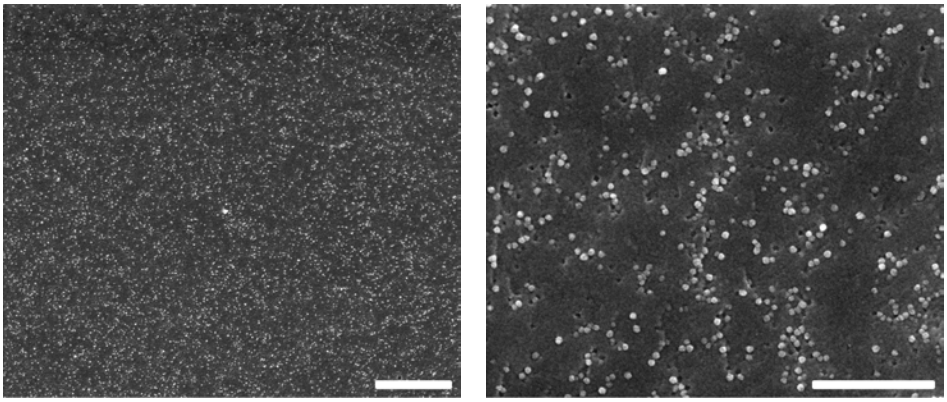

(a) Scale bar represents 1 μm **(b)** Scale bar represents 400 nm

Figure 5.4: Cryogenic scanning electron microscopy images of a 72 days old complex composite gel at two different magnifications. Scale bars are indicated at the bottom of the pictures and represent 1 μm in **(a)** and 400 nm in **(b)**.

bright spots. Perhaps more difficult to see are the black holes in the background, caused by silica particles that popped out of the matrix during the fracturing step. From figure 5.4 it can be seen that it is a matter of scale whether or not the particles appear to be homogeneously distributed. The more you zoom in, the clearer it becomes that there are areas denser in particles than others. These small-scale density fluctuations are causing the slightly opaque appearance of the gels.

Upon closer inspection of figure 5.4b, one can see that some particles are isolated, but most particles seem to be in the vicinity of other particles. We can identify short 'strings' of particles, suggesting that these particles are connected. The particles are not actually touching each other: there is a few nanometers of space in between two neighbouring particles. A few nanometers is the appropriate spacing for our triblock copolymers to fit in, since the radius of gyration of the middle-block is 4-5 nm.[41,42] The cryo-SEM images therefore suggest that the silica nanoparticles can be bridged by our triblock copolymers. Structural analysis based on figure 5.4b can be found in the appendix.

To confirm the internal structure of the complex composite gels, we performed small-angle X-ray scattering (SAXS) measurements. The results are given in figure 5.5. The scattering curve shows the characteristics of a spherical form factor combined with a small contribution of a structure factor ($S(q)$) at low q-values. Hence, the particles are not irreversibly aggregated or flocculated into a fractal

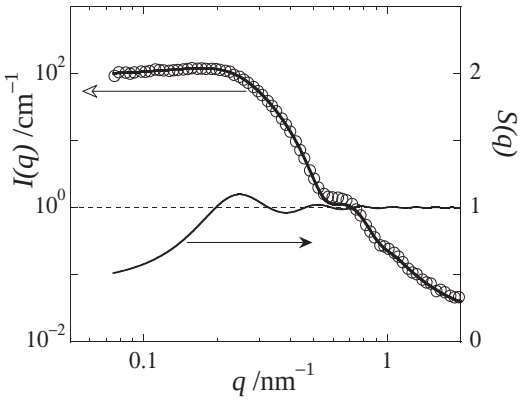

Figure 5.5: The left axis shows the small-angle X-ray scattering curve of a complex composite gel containing 13%(w/w) silica nanoparticles and 3.4%(w/w) triblock copolymer, 40 days after preparation. Error bars on the data are not shown, as they are considerably smaller than the size of the symbols. The thick line is a fit to the data obtained by the SASfit program. The right axis shows the effective structure factor $S(q)$ (thin line) as a function of q. The dashed line indicates unity.

structure, in agreement with the cryo-SEM results. The scattering curve was successfully fitted with a form factor for polydisperse (Gaussian) spheres of radius $R = 7.6 \pm 1.2$ nm and an effective hard-sphere structure factor.[31] The effective hard-sphere radius is $R_{HS} = 11.9$ nm, meaning that the polymer layer around the particles is approximately 3-6 nm thick. The effective volume fraction is $\phi = 0.11$, which is approximately twice the volume fraction of bare silica particles.

The effective structure factor, $S(q)$, is displayed on the right axis of figure 5.5. The structure factor has a maximum around $q = 0.25$ nm^{-1}, which corresponds to a particle center-to-center distance of approximately 25 nm. This suggests that the spacing between two particle surfaces is approximately 10 nm, which is somewhat more than what we see in the cryo-SEM images. This difference can be explained by the difficult estimation of distances in a planar representation of a three dimensional structure. What it does show is that the particles are certainly not irreversibly aggregated, or flocculated, as is often the case when polymers are mixed with particles.

5.3.3 Temporal evolution of the gel

We already mentioned that the gel visually evolves with time, as shown by photographs in the appendix. We noticed that the gel not only evolved visually, but also we noticed a strong increase in viscosity the first days after sample preparation. An increase in viscosity can either be caused by an increase in the number of

bridges or by an increase in relaxation times. To investigate the structural evolution of the complex composite gels in more detail, we followed the evolution of the storage modulus, G', in time. The values for the storage modulus were measured by frequency sweep experiments performed two hours after sample loading. Since the storage modulus is relatively low, it is difficult to measure accurately, and we estimate the uncertainty to be $\pm 25\%$. The displayed values are the values for the storage modulus at a frequency of 1 rad s^{-1}, $G'(1)$. The results are shown in figure 5.6a.

From figure 5.6a we see that the storage modulus increases in the first 200 hours, before reaching a constant value of approximately 8 Pa. The increase in storage modulus means that the number of elastically active chains in the network increases during the first 200 hours. The value of the storage modulus is still relatively low, which means that the network maintains its open structure over a long period of time.

The structural development was also investigated with cryo-SEM. However, the cryo-SEM images of a 24 hours old complex composite gel do not show a visibly different structure than the structure of the 1000 hours old gel described above, see appendix.

The other contribution to the increase in viscosity can be an increase in relaxation time. As mentioned above, relaxation times are difficult to obtain by rheometry. As an alternative, we have used dynamic light scattering (DLS) to study the relaxation behaviour of our gels. It is especially useful for the complex composite gels, because these already contain scattering silica nanoparticles. We therefore do not need to add extra particles to probe the dynamics of the network.

The intermediate scattering functions of a complex composite gel at 0.1 M salt, for different times after preparation, are shown in figure 5.6b. Two reference samples are also shown; 1%(w/w) PVP coated silica particles and 13%(w/w) PVP coated silica particles. The first shows a single exponential decay, originating from the diffusive motion of the particles at this concentration. The obtained hydrodynamic radius is 13 nm, slightly larger than the effective hard-sphere radius obtained by SAXS. At 13%(w/w) of PVP coated silica particles, the intermediate scattering function does not decay as a single exponential function anymore, meaning that the particles interact with each other.

The complex composite gel shows again different behaviour. We can distinguish three regimes in the intermediate scattering function. First an initial exponential decay. We then have a second regime in which the intermediate scattering function

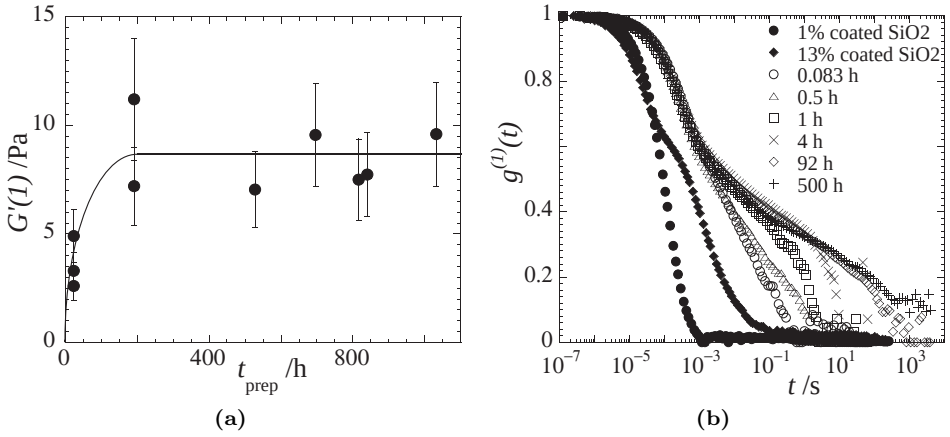

Figure 5.6: Temporal evolution of the complex composite gel. **(a)** Development of the storage modulus at 1 rad s^{-1} as a function of time after sample preparation. The error bars are ±25%. The line is a guide to the eye. **(b)** Intermediate scattering functions of reference samples containing 1%(w/w) PVP coated silica particles (●) or 13%(w/w) PVP coated silica particles (◆), and a 0.1 M complex composite gel sample at 0.083 hours (○), 0.5 h (△), 1 hour (□), 4 hours (×), 92 hours (◇) and 500 hours (+) after preparation. Only 50% of the data points are shown. The intensity correlation functions at 0.083 h, 0.5 h, 1 h and 4 h after preparation, have been recorded for 5 minutes. The other intensity correlation functions were recorded for 4 hours. Reference samples were recorded for 0.33 h.

decays gradually. This is followed by a third regime, a final exponential decay. The initial decay in the complex composite gel, which must be related to the short-time diffusion of the particles while bound to the network, is much slower than for the reference samples. This indicates that the short-time motion of the particles is restricted by the presence of the triblock copolymers. The associated relaxation time scales with q^{-2}, which proves that this initial relaxation is a diffusion-driven process, see appendix. The intermediate decay is related to various internal relaxation processes or network reorganization processes.[44–48] Reorganization of the network requires the breaking and reforming of bonds between the particles and triblock copolymers. The gradual decay of the intermediate scattering function means that there is a wide distribution of relaxation times associated with the reorganization of the network, which is in agreement with the rheological measurements. The final exponential decay is associated with the longest relaxation time, after which the positional correlations on length scales of q^{-1} are lost. While the initial decay is independent of time after preparation, the longest relaxation time increases strongly with time after preparation, see figure 5.6b. A more detailed analysis of the relaxation curves can be found in the appendix.

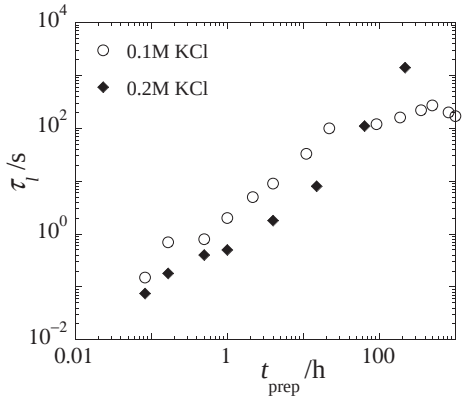

Figure 5.7: The values for the longest relaxation time, τ_l, as a function of time after sample preparation, t_{prep}. Shown are the values for the 0.1 M KCl gel (○) and the 0.2 M KCl gel (◆).

In figure 5.7 we plot the development of the longest relaxation time, τ_l, as a function of time after preparation. From this figure we can see that the longest relaxation time increases in the first 24 hours after initial mixing of the components. After 24 hours, the longest relaxation time hardly changes anymore. Since the structural changes end after approximately 200 hours, see figure 5.6a, we conclude that this gel reaches a steady state 200 hours after the initial mixing of the components. Note that the values for the longest relaxation time as found by rheometry and DLS cannot be directly compared.[49]

Based on these experimental results we propose the following mechanism to explain the temporal evolution of the gels. The PVP stabilizes the silica nanoparticles, preventing irreversible aggregation upon addition of the triblock copolymer. Immediately after mixing, the end-blocks of the triblock copolymers stick to the particles, leading to large-scale fluctuations in the particle density throughout the sample and causing the white appearance. The bond between the triblock copolymer end-blocks and the silica particles is initially relatively weak due to the intervening PVP layer. This enables the redistribution of the particles, leading to density fluctuations of smaller size and consequently a decrease in turbidity, while the transient network of interconnected particles builds up. In time, the number of physical bonds between the particles and the polymers increases, thereby slowing down the dynamics of the particles in the gel. PVP might be slowly displaced from the silica surface in this process.

We assume that electrostatic interactions between the triblock copolymer and the silica particles are responsible for binding the particles in the transient network.

Small ions can screen the electrostatic interactions between the triblock copolymer and the silica nanoparticles. Therefore we expect that addition of extra salt enhances the dynamics of the bonds between the oppositely charged components, as has been shown before for electrostatically assembled systems.[37,50] To test this hypothesis, we prepared a complex composite gel with the same ratio of components, except that we doubled the salt concentration to 0.2 M. We noticed that the addition of extra salt decreased the time needed to reach the almost transparent appearance, proving that electrostatic interactions are indeed important in our complex composite gels.

The shape of the intermediate scattering functions for the 0.2 M salt gel are basically the same as for the 0.1 M salt gel, see appendix. The values for the longest relaxation time are also displayed in figure 5.7. Here we can see that the longest relaxation time is lower in the 0.2 M salt sample, up to a time after preparation of approximately 70 hours. The dynamics of the particles, and thus the relaxation of the network, is faster at higher salt concentrations. This confirms that the association of the triblock copolymers with the particles is of electrostatic origin.[50]

For longer times after preparation, the longest relaxation time of the 0.2 M salt gel keeps increasing. We also observe that the scattered light intensity increases over time as well as the intensity fluctuations, see appendix. Based on these observations we conclude that the particles at this salt concentration are aggregating irreversibly extremely slowly. This is confirmed by the slowing down of the fast mode as the gel ages, see appendix.

5.3.4 Towards applications

One could think of our triblock copolymers as a thickening agent for particle suspensions, for example in water-based coating formulations. However, a thickening agent should not influence the appearance of the coating. The gel that we have described is not completely transparent, see appendix. To test whether the gel maintains its turbidity when applied as a coating, we performed a simple drying test. The results are shown in figure 5.8.

Upon drying, the lump of gel shrinks, through the evaporation of water. This shrinking causes a flattening of the drop, which then becomes a thin layer of gel. Due to the decrease in volume, the components in the gel are concentrated, leading to a more or less homogeneous distribution of the particles in the gel. This in turn decreases the scattering of the drying gel, which becomes fully transparent after two hours of drying. The resulting microstructure of the dried gel is shown in figure 5.8e. The particles are indeed much closer together in the dried state,

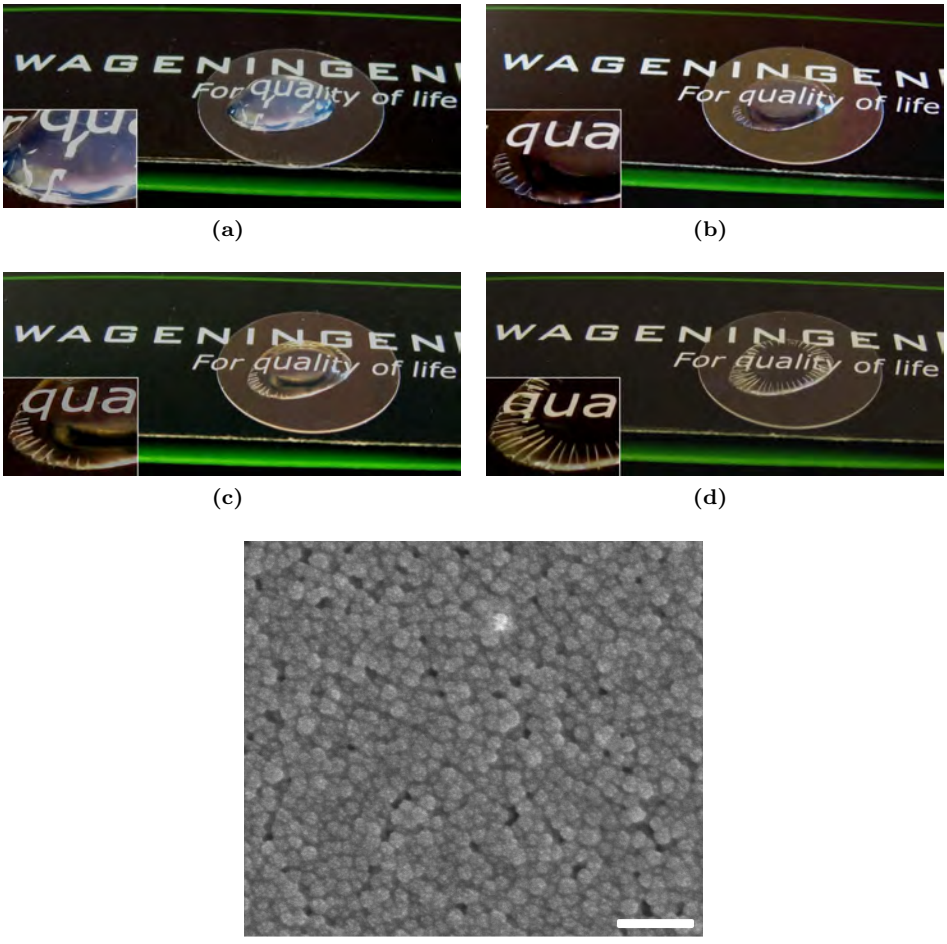

Figure 5.8: Photographs of a drying complex composite gel, deposited on a glass disc, showing that while drying the gel restructures to form a transparent coating. **(a)** initial deposition of the gel; **(b)** 105 minutes after deposition; **(c)** 125 minutes after deposition; **(d)** 195 minutes after deposition. The insets show a magnification of the drying gel. **(e)** Scanning electron microscopy image of the dried gel, revealing the microstructure of the complex composite. The scale bar represents 100 nm.

leaving tiny pores every now and then. Still, the particles do not touch each other, but rather seem to be 'glued' together. This glue must be (a mix of) the polymeric content of the complex composite gels. Since the material is quite brittle, we suggest that the polymeric matrix is in a glassy state.

5.4 Conclusions & Outlook

In this paper we have shown that we have succeeded in preparing an aqueous physical gel, existing of a transient network of precoated inorganic silica nanoparticles and ABA triblock copolymers, without causing irreversible particle aggregation. In this open network, the particle surfaces are frequently found 5-10 nm apart from each other, which is the appropriate spacing for a triblock copolymer to bridge two particles. We have shown that electrostatic interactions are the driving force for the association between the positively charged end-blocks and the negatively charged silica nanoparticles. The physical bonds between the end-blocks and the particles are reversible on time-scales from minutes to hours.

The base materials that we use are cheap and the triblock copolymer can be easily produced on scales of hundreds of grams. This two component system has a large set of parameters that can be tuned individually to reach the desired material properties: concentration of the components, the (charge) ratio between the components, temperature, salt concentration, pH, and finally, the type of monomers and the length of the end-blocks. The spacing between the particles might be controlled by controlling the (responsive) middle-block length. Changing the type, size and shape of the particles, for example with optical, electrical or magnetic properties, will again lead to different complex composite gels. More advanced control of these interactions might lead to the use of analogous systems in many different applications, such as water-based coatings, photonic crystals, enhanced oil recovery, biomineralization, tissue engineering scaffolds and water desalination.

References

[1] B. J. Anderson and C. F. Zukoski, *Macromolecules*, 2009, **42**, 8370–8384.

[2] C. W. Chang, A. van Spreeuwel, C. Zhang and S. Varghese, *Soft Matter*, 2010, **6**, 5157–5164.

[3] W. C. Lin, W. Fan, A. Marcellan, D. Hourdet and C. Creton, *Macromolecules*, 2010, **43**, 2554–2563.

[4] B. I. Dach, H. R. Rengifo, N. J. Turro and J. T. Koberstein, *Macromolecules*, 2010, **43**, 6549–6552.

[5] F. Deng, M. Ito, T. Noguchi, L. F. Wang, H. Ueki, K. Niihara, Y. A. Kim, M. Endo and Q. S. Zheng, *ACS Nano*, 2011, **5**, 3858–3866.

[6] K. Haraguchi and T. Takehisa, *Advanced Materials*, 2002, **14**, 1120–1124.

[7] O. Okay and W. Oppermann, *Macromolecules*, 2007, **40**, 3378–3387.

[8] Y. Liu, X. L. Liu, Y. T. Wu, B. Sun, M. F. Zhu, M. Takafuji and H. Ihara, *Chemical Communications*, 2010, **46**, 430–432.

[9] R. K. Iler, *Journal of Colloid and Interface Science*, 1971, **37**, 364–&.

[10] B. Cabane, K. Wong, P. Lindner and F. Lafuma, *Journal of Rheology*, 1997, **41**, 531–547.

[11] C. P. Whitby, P. J. Scales, F. Grieser, T. W. Healy, G. Kirby, J. A. Lewis and C. F. Zukoski, *Journal of Colloid and Interface Science*, 2003, **262**, 274–281.

[12] S. K. Agrawal, N. Sanabria-DeLong, G. N. Tew and S. R. Bhatia, *Langmuir*, 2008, **24**, 13148–13154.

5

[13] Y. S. Pek, A. C. A. Wan, A. Shekaran, L. Zhuo and J. Y. Ying, *Nature Nanotechnology*, 2008, **3**, 671–675.

[14] N. Puech, S. Mora, G. Porte, T. Phou, I. Grillo and J. Oberdisse, *Brazilian Journal of Physics*, 2009, **39**, 198–204.

[15] F. Song, L. M. Zhang, J. F. Shi and N. N. Li, *Colloids and Surfaces B-Biointerfaces*, 2010, **81**, 486–491.

[16] E. Loizou, L. Porcar, P. Schexnailder, G. Schmidt and P. Butler, *Macromolecules*, 2010, **43**, 1041–1049.

[17] N. Puech, S. Mora, T. Phou, G. Porte, J. Jestin and J. Oberdisse, *Soft Matter*, 2010, **6**, 5605–5614.

[18] J. Zebrowski, V. Prasad, W. Zhang, L. M. Walker and D. A. Weitz, *Colloids and Surfaces A - Physicochemical and Engineering Aspects*, 2003, **213**, 189–197.

[19] L. Petit, L. Bouteiller, A. Brulet, F. Lafuma and D. Hourdet, *Langmuir*, 2007, **23**, 147–158.

[20] Y. X. Xu, Q. O. Wu, Y. Q. Sun, H. Bai and G. Q. Shi, *ACS Nano*, 2010, **4**, 7358–7362.

[21] Q. Wang, J. L. Mynar, M. Yoshida, E. Lee, M. Lee, K. Okuro, K. Kinbara and T. Aida, *Nature*, 2010, **463**, 339–343.

[22] K. Jankova, X. Y. Chen, J. Kops and W. Batsberg, *Macromolecules*, 1998, **31**, 538–541.

[23] M. Lemmers, J. Sprakel, I. K. Voets, J. van der Gucht and M. A. Cohen Stuart, *Angewandte Chemie-International Edition*, 2010, **49**, 708–711.

[24] J. M. Dust, Z. H. Fang and J. M. Harris, *Macromolecules*, 1990, **23**, 3742–3746.

[25] K. Jankova and J. Kops, *Journal of Applied Polymer Science*, 1994, **54**, 1027–1032.

[26] M. Kato, M. Kamigaito, M. Sawamoto and T. Higashimura, *Macromolecules*, 1995, **28**, 1721–1723.

[27] J. S. Wang and K. Matyjaszewski, *Macromolecules*, 1995, **28**, 7901–7910.

[28] Y. T. Li, S. P. Armes, X. P. Jin and S. P. Zhu, *Macromolecules*, 2003, **36**, 8268–8275.

[29] M. Lemmers, E. Spruijt, L. Beun, R. Fokkink, F. Leermakers, G. Portale, M. A. Cohen Stuart and J. van der Gucht, *Soft Matter*, 2012, **8**, 104–117.

[30] P. Lindner and T. Zemb, *Neutrons, X-rays and Light: Scattering Methods Applied to Soft Condensed Matter*, Elsevier Science B.V., Amsterdam, 2002.

[31] J. Kohlbrecher and I. Bressler, *SASfit*, 2010.

[32] M. A. Cohen Stuart, G. J. Fleer and J. M. H. M. Scheutjens, *Journal of Colloid and Interface Science*, 1984, **97**, 526–535.

[33] F. Lafuma, K. Wong and B. Cabane, *Journal of Colloid and Interface Science*, 1991, **143**, 9–21.

[34] A. Nelson, K. S. Jack, T. Cosgrove and D. Kozak, *Langmuir*, 2002, **18**, 2750–2755.

[35] M. A. Cohen Stuart, N. A. M. Besseling and R. G. Fokkink, *Langmuir*, 1998, **14**, 6846–6849.

[36] S. van der Burgh, A. de Keizer and M. A. Cohen Stuart, *Langmuir*, 2004, **20**, 1073–1084.

[37] M. Lemmers, I. K. Voets, M. A. Cohen Stuart and J. van der Gucht, *Soft Matter*, 2011, **7**, 1378–1389.

[38] J. F. Cardenas, *Colloids and Surfaces A: Physicochemical and Engineering Aspects*, 2005, **252**, 213–219.

[39] J. van der Gucht, E. Spruijt, M. Lemmers and M. A. Cohen Stuart, *Journal of Colloid and Interface Science*, 2011, **361**, 407–422.

[40] R. Larson, *The Structure and Rheology of Complex Fluids*, Oxford University Press, Inc., New York, 1999.

[41] K. Devanand and J. C. Selser, *Macromolecules*, 1991, **24**, 5943–5947.

[42] K. L. Linegar, A. E. Adeniran, A. F. Kostko and M. A. Anisimov, *Colloid Journal*, 2010, **72**, 279–281.

[43] E. Spruijt, M. A. Cohen Stuart and J. van der Gucht, *Macromolecules*, 2010, **43**, 1543–1550.

[44] J. E. Martin, J. Wilcoxon and J. Odinek, *Physical Review A*, 1991, **43**, 858–872.

[45] D. Adolf and J. E. Martin, *Macromolecules*, 1991, **24**, 6721–6724.

[46] S. Z. Ren, W. F. Shi, W. B. Zhang and C. M. Sorensen, *Physical Review A*, 1992, **45**, 2416–2422.

[47] M. C. Blanco, D. Leisner, C. Vazquez and M. A. Lopez-Quintela, *Langmuir*, 2000, **16**, 8585–8594.

[48] R. G. Liu, X. Gao and W. Oppermann, *Polymer*, 2006, **47**, 8488–8494.

[49] C. H. Wang, *Macromolecules*, 1992, **25**, 1524–1529.

[50] E. Spruijt, J. Sprakel, M. Lemmers, M. A. Cohen Stuart and J. van der Gucht, *Physical Review Letters*, 2010, **105**, 208301.

[51] J. C. Dijt, M. A. Cohen Stuart, J. E. Hofman and G. J. Fleer, *Colloids and Surfaces*, 1990, **51**, 141–158.

Appendix

Nuclear magnetic resonance

^{1}H-NMR of the triblock copolymer was performed in D_2O on a Bruker Advance III 400 MHz NMR spectrometer. 64 Scans were performed, with a relaxation time between two subsequent pulses of 60 s to allow full relaxation of the protons in the PEO middle-block. The average number of charged groups on the triblock copolymers was determined by comparing the integral values of the peak corresponding to the protons in the PEO middle-block ($\delta \approx 3.6$ ppm) and the peak of the protons of the trimethylamino group ($\delta \approx 3.2$ ppm), taking into account the relative amount of protons per group. We obtain an average value of 68 monomers per PEO middle-block, corresponding to an average of 34 charged monomers per A block. The ^{1}H-NMR spectrum of the triblock copolymer is shown in figure 5.9. The origin of each peak is indicated in the graph.

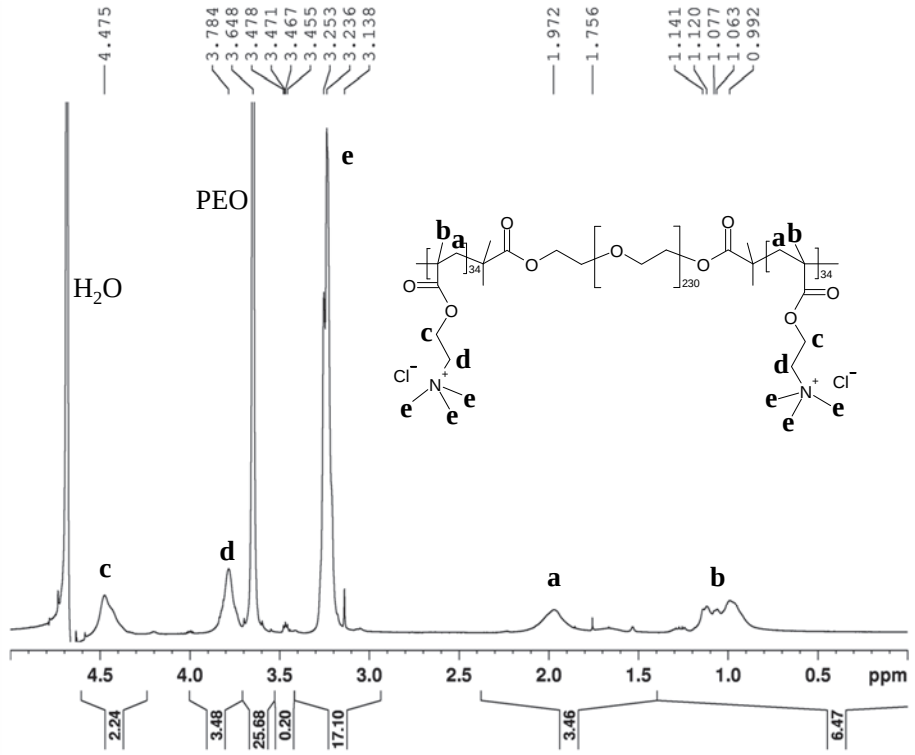

Figure 5.9: ^{1}H-NMR spectrum of the ABA triblock copolymer as synthesized according to the procedure indicated in the experimental section.

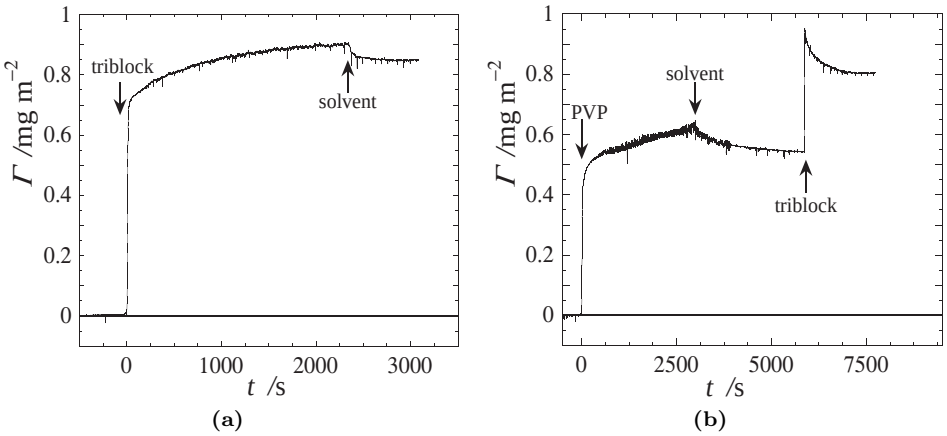

Figure 5.10: Total adsorbed amount as a function of time from reflectometry experiments. **(a)** Adsorption of triblock only. **(b)** Sequential adsorption of PVP and triblock.

Reflectometry

Method

Poly(vinylpyrrolidone) adsorption and triblock copolymer adsorption onto bare silica, as well as sequential adsorption, was studied by reflectometry. A detailed description of the experimental setup has been given by Dijt and coworkers.[51] Silica surfaces were prepared by heating a silicon wafer at 1000°C for two hours. The oxidized wafer had an oxide layer thickness of 77.0 nm. Before use in reflectometry experiments, strips of oxidized wafer were cleaned by rinsing with water and ethanol, and subsequent plasma treatment for two minutes. Polyvinylpyrrolidone K25 (PVP) (M_w = 40 kg mol^{-1}) was obtained from Fluka. As solvent for both PVP solutions and triblock copolymer solution, a 10 mM salt solution (0.002% (w/w) of chloride as NaCl and 0.010% (w/w) of sulfate as Na_2SO_4 in water at pH = 7.0±0.2 was used.

Results

The result of the triblock copolymer adsorption onto a flat silica surface is shown in figure 5.10a, expressed as the adsorbed amount ($\Gamma(t)$) as a function of time. From this figure it can be seen that the triblock copolymer adsorbs up to a saturating value of approximately 0.9 mg m^{-2}. Additional flowing of solvent has hardly any effect on the adsorbed amount. PVP adsorption onto silica is shown in figure 5.10b. PVP-only can adsorb slightly over 0.5 mg m^{-2}, and cannot be washed away with solvent. Subsequent addition of the triblock copolymer leads to an additional

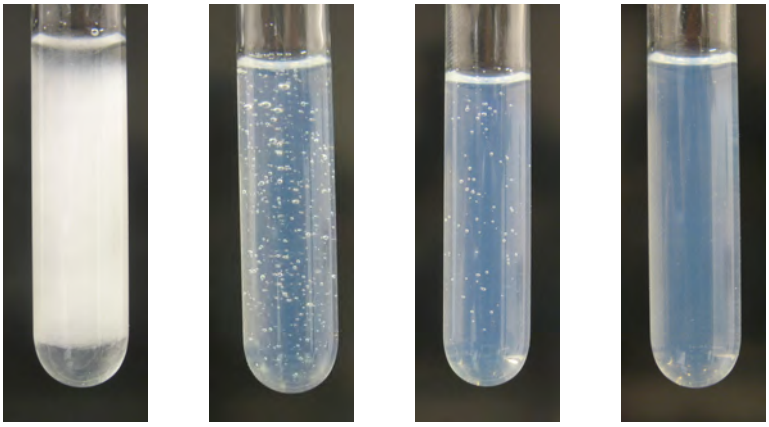

(a) $t = 0$ h **(b)** $t = 0.5$ h **(c)** $t = 24$ h **(d)** $t = 190$ h

Figure 5.11: Photographs showing the visual appearance of the complex composite gels in time: **(a)** immediately after mixing; **(b)** 30 minutes after mixing; **(c)** 24 hours after mixing; **(d)** eight days after mixing.

adsorption with a maximum absorbed amount close to 1 mg m^{-2}. The adsorbed amount decreases in time to reach a plateau value of approximately 0.8 mg m^{-2}. The decrease in time is probably caused by a replacement of PVP with triblock copolymer.

Sample preparation

Photographs showing the changes in visual appearance of the complex composite gels in time are shown in figure 5.11. The turbidity of the gel disappears in time, showing that the large scale density fluctuations spontaneously restructure into smaller ones. Note that after 24 hours the amount of air bubbles that appeared after vortexing has decreased, showing that this gel still has liquid-like properties.

2-Dimensional pair correlation function

Figure 5.12 shows the steps and results of the image analysis. By identifying the relative positions of the centers of the particles in the image one can compute the 2D pair correlation function, or radial distribution function. The centers of all the particles and holes in figure 5.4b are determined manually. A magnification of a part of figure 5.4b is given in figure 5.12a, where the centers of the particles and holes are given by the red pixels. The centers of the particles and holes were filtered

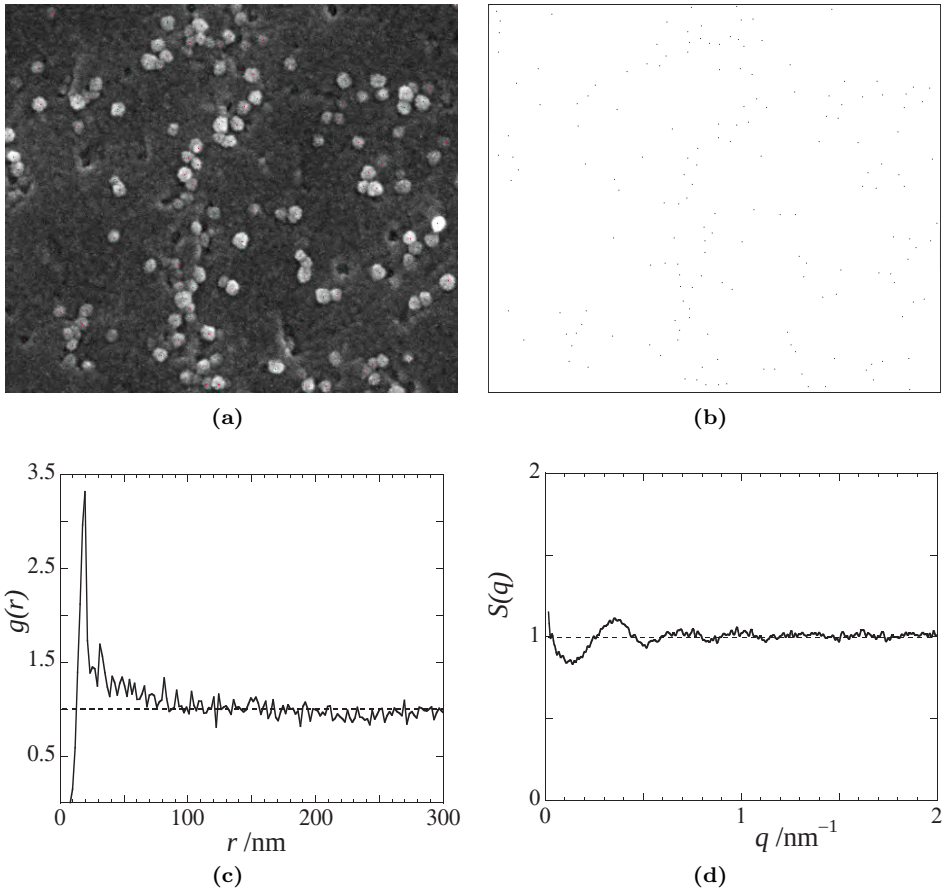

Figure 5.12: Several steps in the computing of the structure factor based on the cryo-SEM image in figure 5.4b. **(a)** Magnification showing the particle selection; **(b)** Filtered image of **(a)**, showing the particle centers; **(c)** Radial distribution function, $g(r)$, computed from **(b)**; **(d)** Structure factor, $S(q)$, based on the RDF in **(c)**.

out using ImageJ, see figure 5.12b. Next, we applied an ImageJ macro to compute the radial distribution function, $g(r)$, from the filtered image, see figure 5.12c. The peak at approximately 20 nm corresponds to the distance between the centers of two adjacent particles. A distance of 20 nm is plausible, taking into account the particle radii, 2×7.5 nm, and a polymer layer of approximately 5 nm.

Figure 5.12c also shows a gradual decrease towards unity for distances smaller than 100 nm. We attribute this gradual decrease to a distribution of 'typical length scales' related to the typical size of the particle density fluctuations.

To compare the image with the SAXS results we need to Fourier transform $g(r)$

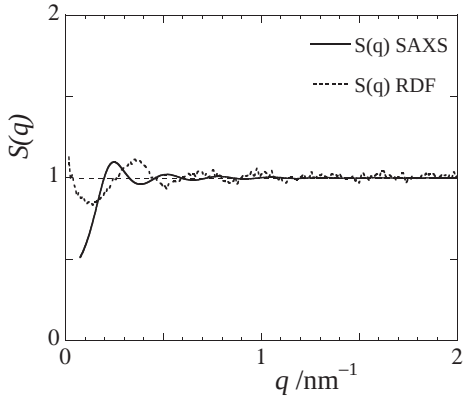

Figure 5.13: Structure factors as obtained by small-angle X-ray scattering and image analysis. The full line is the structure factor based on the SAXS curve fit, the dashed line is the structure factor based on the RDF obtained from image analysis of figure 5.4b.

to obtain the structure factor $S(q)$, see equation 5.2:

$$S(q) = 1 + \rho \int_0^\infty \exp(-iqr)(g(r) - 1)\mathrm{d}r \tag{5.2}$$

where ρ is the particle density. The resulting structure factor is displayed separately in figure 5.12d, and together with the SAXS based structure factor in figure 5.13.

The structure factors obtained by the two methods have similar shapes and amplitudes, however, the graphs do not overlap. Both graphs show clear primary maxima, originating from a 'characteristic length scale', which is the center-to-center distance. Since the volume fraction of particles is relatively low, we see no pronounced secondary or higher order maxima in the graphs. The typical distance that the centers of the particle are apart from each other seems to depend on the applied method. It is clear that the SAXS-based approach is more reliable in this case, since it is based on a scattering volume containing lots of particles, rather than a small 2D image. Moreover, we cannot resolve the real distance between particles in a two-dimensional representation. Particles always appear closer to each other in a planar representation of their spatial positions. The peak of the RDF-based structure factor appears indeed at a higher q-value.

The strong decrease of the RDF-based structure factor at low q-values is related to the second 'typical length scale', the typical size of the particle density fluctuations. Here we have plotted the RDF-based structure factor to the lowest possible q-value, which is of course limited by the size of the investigated image. These density fluctuations should cause an upturn in the SAXS profile at low q-values. However, in the SAXS measurements we cannot reach low enough q-values

to detect this upturn.

Cryo-SEM images 24 hours after preparation

We performed cryo-SEM on gel samples that were frozen-in 24 h after initial mixing. The features of this gel are, at least to the eye, similar as the 1000 hours old gel described in the main text, see figure 5.14. We see again that there are some areas denser in particles, while other areas are depleted with particles. The particles are sometimes alone and sometimes aligned in small strings. Again we can see that the particles are not touching each other, leaving a gap of 4-5 nm in between two adjacent particles.

Light Scattering

Intermediate scattering functions

To obtain a more quantitative understanding of the gel dynamics, we fit the intermediate scattering function of the 0.1 M salt complex composite gel with equation 5.3:[44,48]

$$g^{(1)}(t) = A\exp(t/\tau_f) + B(1 + t/\tau_i)^{\alpha/2} + C\exp(t/\tau_l) \tag{5.3}$$

where τ_f is the fast relaxation time, τ_i is the relaxation time where the power-law regime begins and τ_l is the longest relaxation time. From the fits we obtain estimates for the relaxation times in the gels. The fits to the intermediate scattering function are displayed as lines in figure 5.15.

The behaviour of the longest relaxation time has already been discussed in the main text. Figure 5.16 shows the fitting results of the fast relaxation time, τ_f, the relaxation time where the power-law regime begins, τ_i, and the value for the exponent, α (inset). From this figure we can see that the fast relaxation time is indeed independent of time after preparation, having a value of approximately 0.2 ms. The value for τ_i decreases with time after preparation, as does the value for the exponent α. Both parameters reach an approximately constant value 11 hours after preparation. The decrease in τ_i means that the power-law regime becomes already pronounced at shorter correlation times, although the effect is small relative to the total range of correlation times. The decrease in α means that the slope of the power-law decay decreases, *i.e.* the internal relaxation processes slow down while the network develops. Both results substantiate the results in the main text that the dynamics of the gel reaches a steady state within 24 hours after mixing. All other fitting parameters are approximately constant with time after preparation.

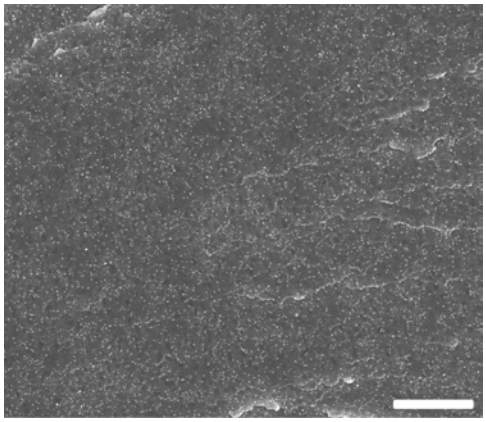

(a) Scale bar represents 1 μm

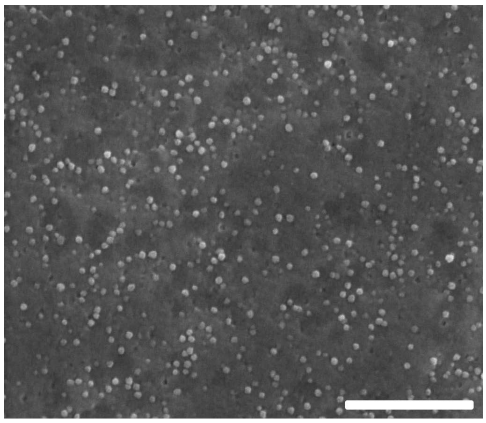

(b) Scale bar represents 400 nm

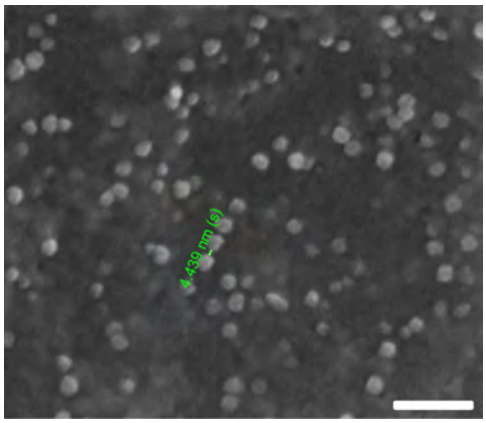

(c) Scale bar represents 100 nm

Figure 5.14: Cryo-SEM images of a complex composite gel 24 h after preparation, shown in different magnifications. The scale bar indicates 1 μm in **(a)**, 400 nm in **(b)** and 100 nm in **(c)**.

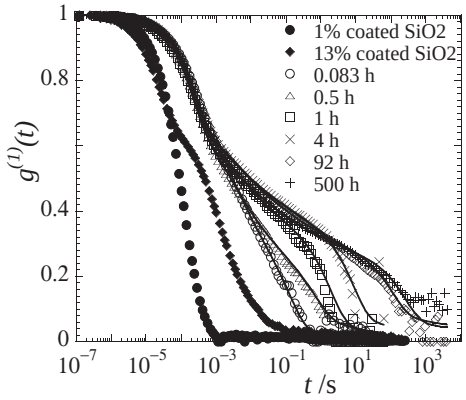

Figure 5.15: Intermediate scattering functions of reference samples containing 1%(w/w) PVP coated silica particles (•) or 13%(w/w) PVP coated silica particles (⧫), and a 0.1 M complex composite gel sample at 0.083 hours (○), 0.5 h (△), 1 hour (□), 4 hours (×), 92 hours (◇) and 500 hours (+) after preparation. Only 50% of the data points are shown. The intensity correlation functions at 0.083 h, 0.5 h, 1 h and 4 h after preparation, have been recorded for 5 minutes. The other intensity correlation functions were recorded for 4 hours. Reference samples were recorded for 0.33 h. The lines represent fits of the data, according to equation 5.3.

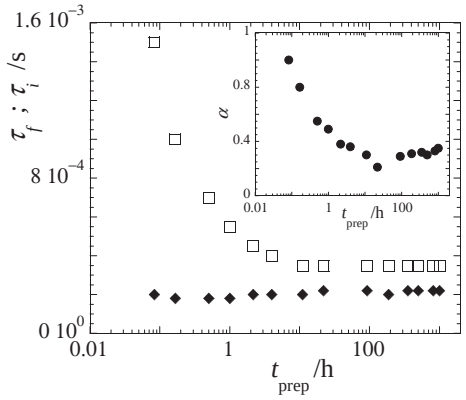

Figure 5.16: The fast relaxation time, τ_f(⧫), and the intermediate relaxation time, τ_i(□) as a function of time after preparation, t_{prep}. The inset shows the dependence of the exponent, α(•) on t_{prep}. The values are based on the fits in figure 5.15.

To prove that the fast relaxation time is associated with the local diffusive motion of the particles in the network, we have investigated the q-dependence of the fast relaxation time. We recorded the intensity correlation function at 20-60°, in steps of 10°. The resulting intermediate scattering function was fitted according to equation 5.3 to obtain estimates for the fast relaxation time. The result is displayed in figure 5.17. It shows that τ_f increases linearly with q^{-2}, meaning that

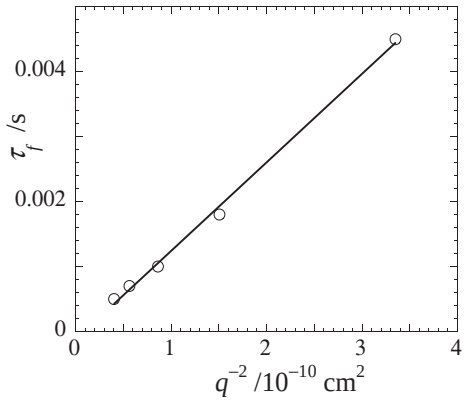

Figure 5.17: Fitted values for the fast relaxation time, τ_f as a function of q^{-2}. The line is a linear fit to the data.

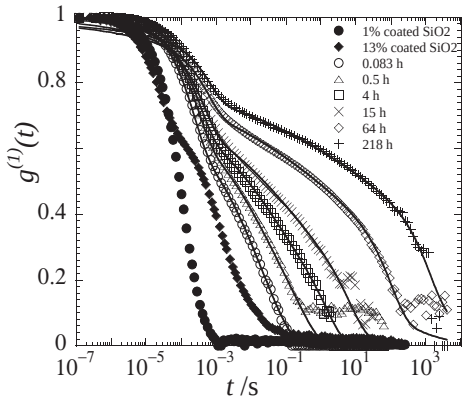

Figure 5.18: Intermediate scattering functions of reference samples containing 1%(w/w) PVP coated silica particles (•) or 13%(w/w) PVP coated silica particles (♦), and a 0.2 M complex composite gel sample at 0.083 hours (○), 0.5 hours (△), 4 hours (□), 15 hours (×), 64 hours (◇) and 218 hours (+) after preparation. The intensity correlation functions at 0.083 h, 0.5 h, 4 h and 15 h after preparation have been recorded for 5 minutes. The other intensity correlation functions were recorded for 4 hours. Reference samples were recorded for 0.33 hours. The lines are fits to the data.

the fast relaxation time is related to a diffusive motion. The longest relaxation time appeared to be q-independent.[47]

The intermediate scattering functions of the 0.2 M salt complex composite gel were fitted with a slightly adjusted version of equation 5.3, inserting a stretched exponential term instead of a power-law term. Doing so, we obtain again estimates for the relaxation times. The fits are shown as lines in figure 5.18.

The slow relaxation time has been discussed in the main text. In figure 5.19 we

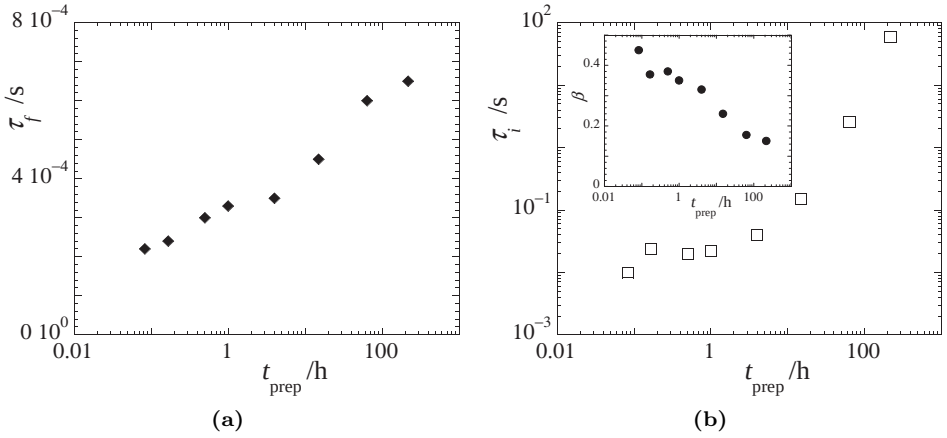

Figure 5.19: **(a)** Fast relaxation time as a function of time after preparation. **(b)** Intermediate relaxation time and the stretching exponent β as a function of time after preparation (inset). The values are based on the fits in figure 5.18

show the dependence of the fast relaxation time, the intermediate relaxation time in the stretched exponential, τ_i, and the stretching exponent, β (inset). Whereas the fast relaxation time is constant in the 0.1 M complex composite gel, we see an increasing value for τ_f in the 0.2 M salt gel. This means that the motion of the particles gradually slows down, as if they would become more massive in time, see figure 5.19a. We interpret this increase in the value for τ_f as a sign of irreversible aggregation/flocculation of the particles, albeit extremely slowly. This interpretation is substantiated by the increase in average scattered light intensity, as well as its fluctuations, see figure 5.20b.

The intermediate relaxation time increases with time after preparation, while the stretching exponent decreases with time after preparation. The increase in τ_i means that the internal relaxations of the network slow down in time, which can also be caused by the slow flocculation of the particles in the gel. The decrease in the value for β indicates that the distribution of relaxation times widens as the gel evolves. Note that the values for τ_i obtained from the stretched exponential fit can not be compared with the values for τ_i obtained from the power-law fit.

Scattered light intensity

In figure 5.20a we show the values for the scattered light intensity as a function of time after preparation, t_{prep}, for both the 0.1 M salt gel, figure 5.20a and the 0.2 M salt gel, figure 5.20b.

There is a difference in the evolution of the scattered light intensity between

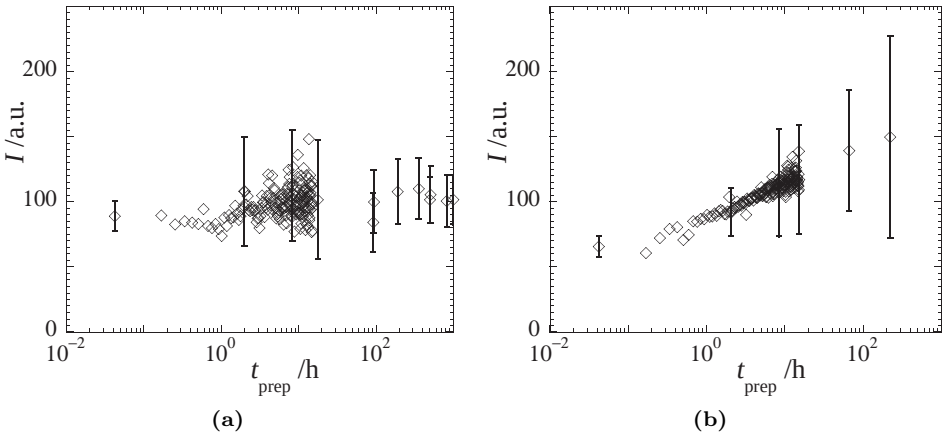

Figure 5.20: The scattered light intensity as a function of time after preparation, t_{prep}. The graphs show the averaged scattered light intensity ($\diamond$). Error bars correspond to the standard deviation of the intensity fluctuations of the raw signal. **(a)** Scattered light intensity for the 0.1 M salt complex composite gel; **(b)** Scattered light intensity for the 0.2 M salt complex composite gel.

the two gels. In the 0.1 M salt gel the fluctuations in scattered light intensity stabilize over time, as well as the value for the averaged scattered light intensity. On the contrary, in the 0.2 M salt gel the fluctuations keep increasing in time, as well as the averaged scattered light intensity. The increase in intensity fluctuations is visualized as an increase in standard deviation of the raw signal. We interpret this as a feature for a slowly flocculating system, in which the mass of the clusters slowly grows in time. This is in agreement with increase of the fast relaxation time, as displayed in figure 5.19a.

5

Chapter 6

Summary & General Discussion

In this Chapter we will summarize the other Chapters in this Thesis. This comprehensive overview allows to more easily locate similarities and differences between the individual Chapters. In the General Discussion section we try to 'bridge' the Chapters to discuss the individual results in the context of the whole Thesis. We revisit the motivation for this PhD project and point to remaining questions and interesting future possibilities for continuation of this line of research.

6.1 Summary

Gels are used in a variety of products ranging from personal care products and food products to explosives. Gels can either be chemical gels, visco-elastic solids, or physical gels, visco-elastic liquids. Chemical gels are generally much stronger than physical gels, but chemical gels can hardly adapt to the environment and they are not self-healing, something that physical gels can do. The origin of this difference lies in the way that the polymers in the gels are connected to each other. These connections are irreversible in the case of chemical gels, whereas they are reversible in the case of physical gels. The network in physical gels is dynamic, and is therefore also referred to as a transient network. Hence, the microscopic structure of a gel determines the macroscopic properties of a gel.

An important area where aqueous physical gels are applied is the water-based coatings industry. Currently, classical associative thickeners are used to form transient networks based on hydrophobic interactions. Although this technology has greatly improved the properties of water-based coatings, there remain some problems related to the use of these classical associative thickeners. Researchers therefore try to find new ways of preparing aqueous physical gels that might improve on any of the current issues related to the use of the classical associative thickeners.

In this Thesis we investigate aqueous physical gels based on interconnected polyelectrolyte complex micelles, as a new two-component associative thickener. The physical gels are prepared from an ABA triblock copolymer, with charged A-blocks and a neutral hydrophilic B-block, mixed with either an oppositely charged homopolymer or nanoparticle. Electrostatic interaction is the driving force for association of the oppositely charged components, leading to transient networks of interconnected flowerlike micelles or particles, depending on the origin of the oppositely charged component. The fact that we deal with a two-component system, as well as a completely different driving force for association, could potentially solve some of the current problems related to the use of the classical associative thickeners.

Throughout this Thesis we have tried to link the microstructure of the gels to the macroscopic properties. We do so by combining microscopic experimental techniques, such as (dynamic) light scattering, small-angle X-ray scattering and (cryo-) scanning electron microscopy with macroscopic experimental techniques such as rheometry. We believe that this combination is very powerful and is at the heart of obtaining a better understanding of all soft condensed matter, including physical gels.

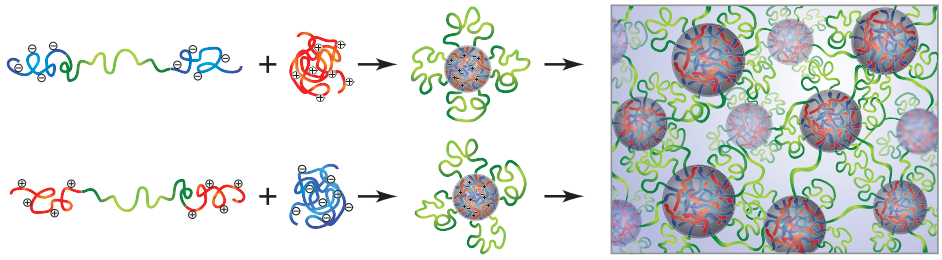

Figure 6.1: Triblock copolymers with charged end-blocks form flowerlike polyelectrolyte complex micelles when mixed with oppositely charged homopolymers. With increasing total polymer concentration, more and more micelles are formed, which eventually become interconnected to form an aqueous physical gel.

In chapter 2 we show that we successfully prepared an aqueous multi-responsive reversible gel based on the bridging of polyelectrolyte complex micelles. We did so by synthesizing ABA triblock copolymers in which the A-blocks are negatively charged, and mixing these triblock copolymers at 1:1 charge ratio with an oppositely charged homopolymer. At low concentrations these two oppositely charged polymers co-assemble spontaneously to form flowerlike polyelectrolyte complex micelles. If two micelles come close enough to each other, the micelles can become connected to each other, because a triblock copolymer can stick both end-blocks in two different micellar cores. This bridging is reversible, meaning that the micelles are continuously connected and disconnected. At high concentrations enough micelles become interconnected to form a percolating path through the sample, hence the solution becomes a physical gel, see figure 6.1.

Due to the electrostatic driving force for the co-assembly of micelles, these gels are truly multi-responsive. We show that the formation of polyelectrolyte complex micelles is strongly dependent on the charge ratio between the two polyelectrolyte blocks, a subject studied in more detail in chapter 3. For charge stoichiometric conditions, we show that the viscosity increases strongly with increasing polymer concentration, and that the viscosity decreases with increasing temperature. Charge-driven assembly allows to tune the electrostatic interactions between the oppositely charged components through changes in the ionic strength of the medium and pH. In dilute solutions, we show that the micelles disappear above a certain salt concentration. This is also reflected in the viscosity, which decreases exponentially with increasing salt concentration. When we increase the pH, to discharge the homopolymer, we show that the micelles disappear above the pK_a value of the homopolymer. Increasing the pH also decreases the viscosity of a concentrated solution to such an extent that it is impossible to make a photograph

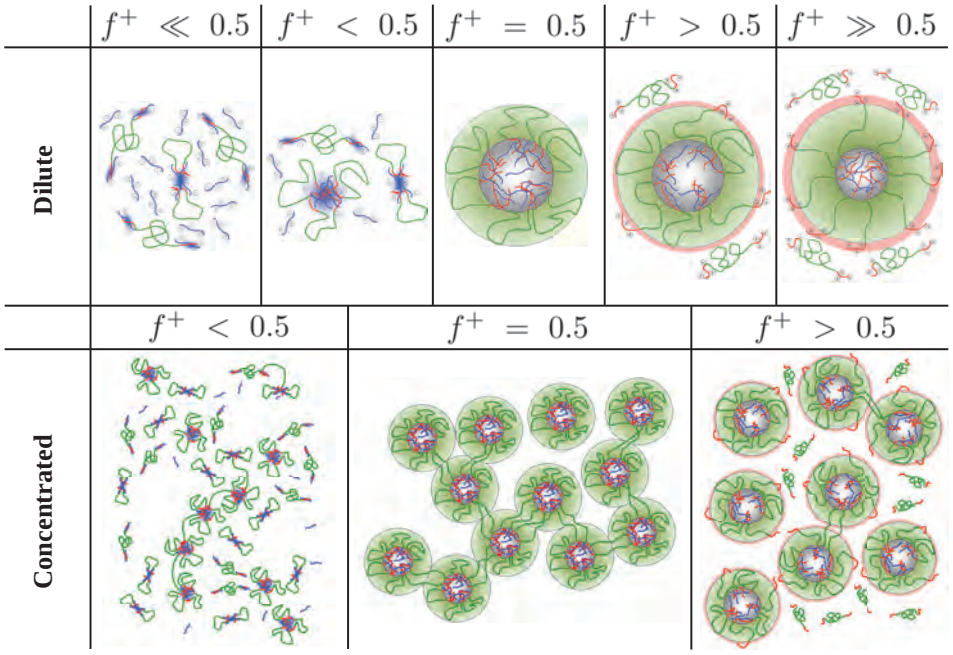

Figure 6.2: Suggested morphologies of the micelles at different charge compositions, for two concentration regimes: dilute solutions (upper half) and concentrated solutions (lower half).

of a vial up-side-down with the solution sticking to the bottom of the vial.

The influence of the charge ratio on the formation of polyelectrolyte complex micelles and their networks is studied in detail in chapter 3. Our measurements suggest an asymmetry, with respect to the charge stoichiometric point, in the shape and size of the co-assembled complexes. This is summarized in figure 6.2.

In case of excess homopolymeric charge, the solution contains so-called 'soluble complexes'. These are small co-assembled structures containing only a few polymers. Most of the excess homopolymeric charge is present as free, uncomplexed homopolymer in solution. However, some excess charge is present on the soluble complexes itself, since there is not enough triblock copolymer available to compensate these charges. The excess charge also stabilizes these soluble complexes, and prevents them from aggregating into bigger structures.

By contrast, in the case of excess triblock copolymeric charge, micelles remain present in solution. We suggest that these micelles have a close-to-electroneutral core, stabilized by a corona of unfolded triblock copolymer chains, see the lower right part of figure 6.2.

The structural asymmetry is not reflected in the macroscopic properties of the concentrated solutions, where we find an almost symmetric dependence of the viscosity on the charge ratio. More importantly, the viscosity decreases strongly as a function of the distance from the charge stoichiometric point. In the case of excess triblock copolymeric charge this can be understood: since the micellar cores can remain close to electroneutral there is no homopolymeric charge available for the free end-blocks to associate with, the free end-blocks have more configurational entropy as compared to an end-block in the micellar core and therefore want to stay 'free', and the charged coronas repel each other. Therefore network formation is likely to be strongly suppressed in the case of excess triblock copolymeric charge, leading to lower viscosities.

For excess homopolymeric charge, network formation should be possible. That we measure a lower viscosity as compared to charge stoichiometric conditions can be caused by a lack of triblock copolymer to form a sample-spanning network with, or by faster relaxation processes in soluble complexes compared to the relaxation processes at charge stoichiometric conditions.

In chapter 4 we take a closer look at the network topology and how this is influenced by total polymer concentration and salt concentration. We show that the volume fraction of micelles increases linearly with total polymer concentration. By combining small-angle X-ray scattering measurements with rheological measurements we can estimate the average number of bridges per micelle. We show that the number of bridges per micelle is a very strong function of the average micellar separation. The latter is again a function of the total polymer concentration. This implies that the elastic modulus of the gel is strongly influenced by the total polymer concentration.

Increasing the salt concentration, at fixed total polymer concentration, leads to smaller flowerlike micelles, because the aggregation number of the micelles decreases. If the total polymer concentration is far above the CMC this implies that the same amount of polymeric material is distributed over more, smaller micelles. Surprisingly, this has almost no effect on the elastic modulus.

In chapter 5 we show that it is possible to use charged inorganic nanoparticles as nodes in a transient network bridged by triblock copolymers with charged end-blocks. Since gels of this kind have never been described before, we named this class of gels *'Complex Composite Gels'*, see figure 6.3.

We use negatively charged silica nanoparticles, because these are cheap and well-studied. To prevent irreversible aggregation of the nanoparticles we precoated the

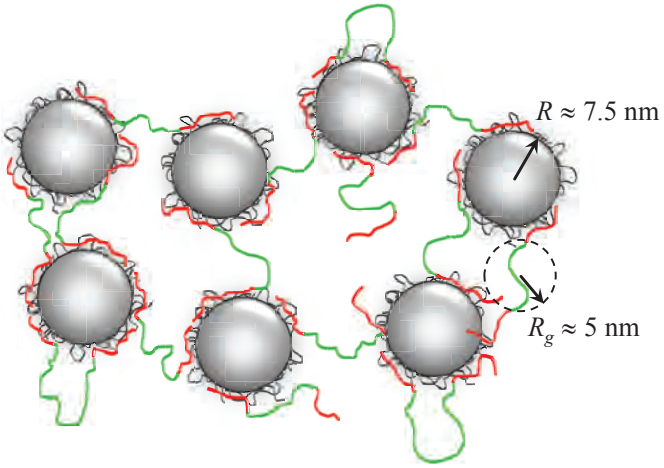

Figure 6.3: Artistic impression of the micro-structure of a complex composite gel. The nanoparticles are stabilized by a layer of poly(vinyl pyrrolidone) (black). Triblock copolymers with neutral middle-block (green) and positively charged end-block (red) bridge the nanoparticles to form a physical gel.

nanoparticles with a neutral layer of physically adsorbed poly(vinyl pyrrolidone). Physical gels form upon mixing triblock copolymer solutions with solutions of the precoated nanoparticles. We investigate several compositions of triblock copolymer to silica nanoparticles from which we draw a diagram of states. We selected a sample of intermediate composition to further investigate the gel properties.

These physical gels have a relatively low modulus, which is in accordance with the open structure observed in cryo-SEM images. These images also show that the particles do not stick together surface-to-surface; there is always a few nanometers of space in between two adjacent particles. This is confirmed by the SAXS measurements showing a relatively monodisperse spherical form factor, weak structuring of the particles and no sign of any fractal structures.

The gels slowly develop in the first few days after mixing. Immediately after mixing the samples turn white, meaning that there are large-scale density fluctuations present in the sample. The white appearance spontaneously disappears within the first couple of minutes and the gels become more transparent. The investigated gels never had a truly transparent appearance, but always remained somewhat opaque. With dynamic light scattering measurements we showed that the longest relaxation time increases in the first 24 hours after mixing, after which it remained constant. The change in the longest relaxation time can be caused by the slow replacement of the stabilizing polymer by the charged blocks, leading to more, or stronger adsorbed end-blocks. We suggest that the longest relaxation

time is associated with the displacement of a charged end-block from the particle surface. Furthermore, we show that the longest relaxation time is responsive to the ionic strength in the medium; the longest relaxation time decreases at higher salt concentrations. This is a strong suggestion that the particle bridging is indeed charge-driven. Besides the dynamical behaviour we show that the modulus increases roughly by a factor of two in the first ten days after mixing.

When we dry a drop of gel on a glass plate, it shrinks through the evaporation of water, thereby concentrating the particles and polymers in the gel. The more homogeneously distributed material causes the opaque appearance of the original gel to disappear, and the *complex composite* ends-up as a transparent coating of the glass. Still, the particles are not aggregated, but rather seemed to be glued together by the polymeric matrix. These complex composite gels might be interesting model systems for research in directions of particle containing materials, such as water based coatings, tissue engineering scaffolds, biomineralization and selective membranes.

6.2 General Discussion

In this Thesis we have made a start investigating the properties of dilute and concentrated solutions of polyelectrolyte complex micelles based on ABA triblock copolymers mixed with homopolymers of opposite charge. Since this was an entirely new concept, the biggest question was, of course, whether it would at all be possible to prepare transient networks analogous to the classical associative thickeners, but now based on electrostatic interactions as driving force. Now, almost four years later, it is safe to say that we indeed can prepare these transient networks, and that we have gained quite some understanding of the properties of these gels. There are, however, questions that remain unanswered, and potentially interesting research paths that remain unexplored. In this section we will touch upon a few of the remaining questions and highlight some of the potentially interesting future directions for possible continuation of this line of research.

6.2.1 Polymer based physical gels

At the heart of charge-driven association is the strength of interaction between the two oppositely charged components. This interaction strength is very much dependent on the specific combination of polyelectrolytes, with sometimes surprising results. For example, mixing PSPMA and PAH leads to very stable polyelectrolyte complexes, see Chapters 2 and 4. Mixing PAH with poly(styrene sulfonate) (PSS),

a polymer containing a similarly charged group as PSPMA, is known to give close-to-indestructible complexes.[1,2] In Chapter 3 we have shown that PTMAEMA leads to moderately stable complexes when mixed with PSPMA homopolymer. Rather strikingly, mixing PTMAEMA with PSS leads to no polyelectrolyte complex formation at all, despite PSS having a charged group that is rather similar to the charged group in PSPMA.[3] Why polyelectrolyte complex formation is so specifically dependent on the combination of polyelectrolytes, is, up to now, not really clear. The current idea is that counterion release always favours polyelectrolyte complex formation, because of the gain in translational entropy of the counterions. The enthalpic contribution to the free energy, predominantly the Coulomb electrostatic attraction, can be favourable or unfavourable.[3] Probably the bulkiness of pendant groups and the linear charge density mismatch between the two polyelectrolytes play an important role here. Other non-electrostatic contributions that might influence the polyelectrolyte complex formation are hydrophobic interactions and the potential loss of conformational entropy of the individual polymer chains.

The very specific interactions between two polyelectrolytes make it very hard to predict the strength of interaction between two oppositely charged polyelectrolyte components on forehand. Up to now, there is no theory that can describe or predict the interaction strength between a given combination of polyelectrolytes.[3] Obviously, this hinders further development of these systems, because finding out by trial and error is laborious and time consuming. The development of a comprehensive theory that describes the interaction processes between two oppositely charged polyelectrolytes will prove to be a major step in the field of polyelectrolyte co-assembly, and would probably also aid in understanding the fundamentals of complicated polymer/protein mixtures, like cells.

The biggest advantage of using electrostatic interactions as driving force for co-assembly, is the tunability of the interaction range and interaction strength by changing different parameters. The gels that we have prepared are therefore multi-responsive, as we have shown in Chapter 2. Obvious variables to change the gel properties are concentration and temperature. The role of concentration was investigated in more detail in Chapter 4. The effect of temperature is only modest, as shown in Chapter 2. The response of the gel to changes in temperature could possibly be enhanced by choosing a different chemistry for the polymers. Some polymers are known to exhibit a sudden change in solubility depending on the temperature of the solvent. Upon passing this 'critical solution temperature', the polymer coil will spontaneously collapse or swell, depending on the specific polymer, solvent and temperature behaviour. Poly(N-isopropylacrylamide) (PNIPAM),

for example, is a frequently used polymer in this respect, because its lower critical solution temperature in water is 32 °C, close to the human body temperature.[4] For medical applications, it would therefore be interesting to try to synthesize triblock copolymers with charged end-blocks, and a PNIPAM middle-block. What would a gel based on this architecture do above 32 °C? Can the polyelectrolyte complex micelles withstand the pulling forces from the middle-blocks that want to collapse? One possibility is that such a system phase separates into a gel phase and a solvent phase. If the polyelectrolyte complex micelles are triggered to fall apart, then temperature could be used as an external trigger to release compounds that otherwise prefer to stay in the polyelectrolyte complex core.

Besides temperature, pH can be used as parameter to tune the interaction strength in case one (or both) of the polyelectrolytes is a weak polyelectrolyte. We have given an example of this in Chapter 2. One problem with the current chemistry of the triblock copolymers is that the ester-bonds that are present in the charged groups, are prone to hydrolyze in basic or acidic conditions. This problem can be solved by changing the chemistry of the charged groups.

Because small ions can screen the electrostatic interactions, the ionic strength of the medium is a key parameter to tune the associative interactions in electrostatically driven systems. We have shown the response to salt concentration in Chapters 2, 4 and 5. For concentrated solutions we have investigated the response to salt concentrations in the regime of 0.3 M KCl to 1.5 M KCl. The lower value is a minimum value set by the polymer concentration, assuming that the counterions are released in the co-assembly process. But what will happen if we lower the salt concentration to a minimum value? In previous papers we have shown that salt has a similar effect on polyelectrolyte complexes as temperature.[3,5,6] In general, decreasing the temperature of common polymer systems leads to an increase in the relaxation times of the polymers, up to a point where the polymers become essentially 'frozen'; the glass transition temperature. In analogy with the temperature effect on common polymer systems, it is expected that the relaxation times of polyelectrolyte complex phases increase dramatically below a minimum salt concentration value; the glass transition salt concentration.[7,8] If we can bring our physical gels below the glass transition salt concentration, we should be able to freeze the dynamics of the micelles. The micelles then become essentially fixed cross-links, meaning that we should be able to mimic chemical gel behaviour with our physical gels.

We prepared, for the first time, a low salt physical gel by dialyzing a 20wt%,

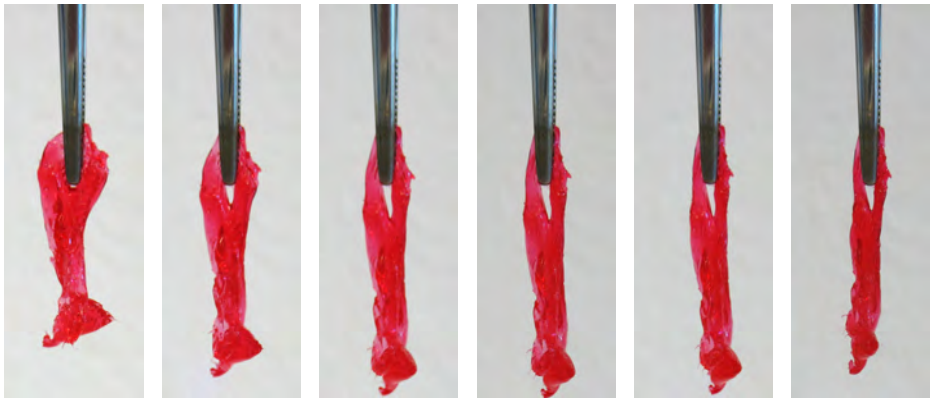

(a) 0 min. **(b)** 9 min. **(c)** 24 min. **(d)** 36 min. **(e)** 60 min. **(f)** 160 min.

Figure 6.4: Appearance of a charge-driven physical gel at minimum salt concentration and estimated concentration of 30wt%-40wt%. The waiting time is given below each photo.

0.3 M KCl gel, based on positively charged $PTMAEMA_{34}$—PEO_{230}—$PTMAEMA_{34}$ triblock copolymer and negatively charged $PSPMA_{175}$ homopolymer at 1:1 charge ratio, against de-ionized water. After dialysis, the gel was left for some hours in the air, so the total polymer concentration is estimated to be 30wt%-40wt%. The resulting gel behaved very solid-like and had to be scraped out of the dialysis cassette. The gel can then be handled with tweezers. To show its solid-like appearance a simple gravity test was performed: a piece of gel, captured with tweezers, was left to relax for some hours, under the influence of gravity. The results are shown in figure 6.4.

Already from the shape of the piece of gel it is clear that this gel is very different from the other gels described in this Thesis. The shape of the gel is not what you would expect for a liquid, because it does not have a smooth surface. In time, we can see that the piece of gel deforms, which is due to both gravity and the relaxation of the polymers after scraping the piece of gel out of the dialysis cassette. After approximately half an hour the gel hardly changes shape, meaning that the polymer dynamics are essentially frozen, and the gel has essentially become a solid, as expected.

Throughout this Thesis we have used 'simple' salts, predominantly KCl and NaCl. It would be interesting to investigate the role of other salts, especially those containing di- or trivalent ions. Multivalent cat- or anions can by themselves bridge two oppositely charged polyelectrolytes together.[9,10] Perhaps it would be possible

to combine homopolymer with a certain fraction of similarly charged multivalent ions to enhance micellar dynamics. The bridging by multivalent ions is probably one of the reasons why it is so difficult to remove the relatively little amounts of Cu^{2+} ions, used in the ATRP reaction, during purification of the triblock copolymer with negatively charged end-blocks.

A variable that is of particular importance in tuning the gel properties is the charge composition. In Chapter 3 we show that transient network formation is suppressed for excess triblock copolymeric charge. What happens at excess homopolymeric charge conditions is somewhat less clear, and therefore the question whether transient network formation is possible at excess homopolymeric charge conditions remains unanswered. It would be of interest to find out by increasing the 'neutralized unit' concentrations to such a level that network formation should be possible.

To verify the conclusions in Chapter 3 it would be good to repeat the measurements in Chapter 3, but now with a fixed weight concentration of triblock copolymers, instead of a fixed weight concentration of total polymeric content. In this way it should be possible to add one component step by step, while keeping the amount of the other component fixed, as in a titration. We should then be able to go through the composition diagram with the same sample, instead of preparing different samples for each composition as is done in Chapter 3. Interestingly, such titrations have been performed in dilute solutions, and the results are shown and discussed in Chapters 2 and 4. So, let us compare the results of the composition titrations shown in Chapters 2 and 4 with the results of Chapter 3.

Because the asymmetry is most clearly represented by the size of the light scattering objects, we show again the data for the hydrodynamic radii of the scattering objects, as discussed in Chapters 2, 4 and 3, in figure 6.5. The hydrodynamic radii values in figure 6.5a are new data, corresponding to the scattered light intensity data reported in Chapter 2. The data in figure 6.5b is also shown in Chapter 4, but here we have added more data points. These points were omitted in Chapter 4, because they were irrelevant for the subject of that Chapter. Note that figures 6.5a and 6.5b originate from exactly the same system, negatively charged PSPMA end-blocks and a positively charged PAH homopolymer, but at different salt concentrations. Figure 6.5c represents a different system, with positively charged PTMAEMA end-blocks and a negatively charged PSPMA homopolymer.

The results of these experiments substantiate the hypothesis put forward in Chapter 3: at excess homopolymeric charge conditions we have small soluble complexes that gradually increase in size, upon approaching the charge stoichiometric

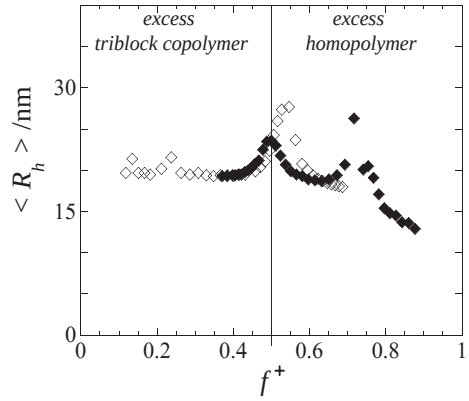

(a) $PSPMA_{28}$—PEO_{230}—$PSPMA_{28}$ and PAH_{160} at 0.20 M KCl.

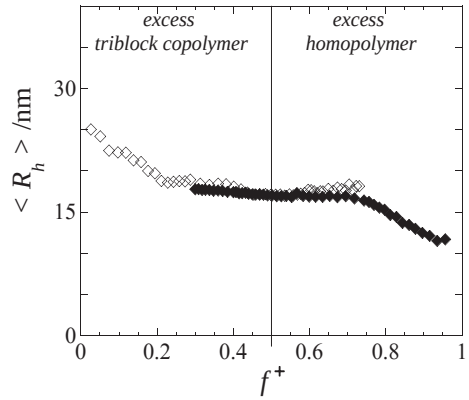

(b) $PSPMA_{28}$—PEO_{230}—$PSPMA_{28}$ and PAH_{160} at 1.0 M KCl.

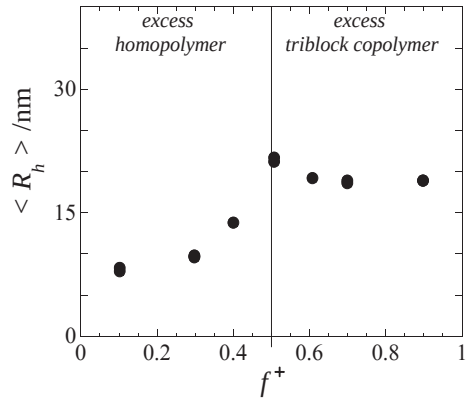

(c) $PTMAEMA_{34}$—PEO_{230}—$PTMAEMA_{34}$ and $PSPMA_{175}$ at 0.35 M KCl

Figure 6.5: Hydrodynamic radii as a function of charge composition.

point. For excess triblock copolymeric charge we have objects of micellar size, which might increase in size upon overdosing the system with triblock copolymeric charge, see figure 6.5b. It is not completely clear why an increase in micellar size is visible in figure 6.5b but not in the other figures, although an increase in size is seen in SAXS results corresponding to figure 6.5c. This discrepancy might be caused by the fact that in DLS experiments one measures a 'diffusion radius', which might be smaller than the actual total radius, because the outer part of the micellar corona is extremely dilute in polymer.

In figure 6.5a we can see a peak in the hydrodynamic radius at the charge stoichiometric point, $f^+ = 0.5$. This increase in radius is probably caused by non-equilibrium structures. The reason that these non-equilibrium structures show up in figure 6.5a and not in figure 6.5b is probably due to the difference in salt concentration. In figure 6.5a the KCl concentration is relatively low for this system, 0.20 M, so that the rearrangements are probably very slow. At 1.0 M KCl, the salt concentration in figure 6.5b, the energy barrier to reach the equilibrium state is much lower, meaning that the new equilibrium state is reached much quicker. It would be interesting to study the development of the hydrodynamic radius over time at the low salt conditions, to see whether it decreases as a function of time or if it is a stable, equilibrium, value. A similar reasoning might hold for the 'second' peak at $f^+ \approx 0.7$ in figure 6.5a. As can be seen in figure 6.5b, this point exactly marks a regime change from real polyelectrolyte complex micelles that can tolerate a certain excess charge to smaller soluble complexes. This rearrangement might take some time, depending on the salt concentration. That is probably why we do not see these peaks in figure 6.5b.

Not only the individual mixing ratio can be varied. One can also think of mixing different components. Instead of mixing triblock copolymers with homopolymers, one can also add a certain fraction of diblock copolymers with a similarly charged block as the triblock copolymers to the system.[11] The diblock copolymers will also be present in the polyelectrolyte complex micelles, and therefore the fraction of triblock copolymers in the micelles will go down. This has the consequence that fewer bridges can be formed between the micelles. Diblock copolymers therefore act as network stoppers.

Another option is to mix the triblock copolymers with a certain fraction of diblock copolymers containing a charged block equal to the homopolymer. This will again lead to different micelles. If two different stabilizing middle-block chemistries are chosen, then it should be possible to extend the work of Voets and coworkers by bridging so-called Janus-micelles together.[12,13] However, this might be a chal-

lenging task.

Yet another option in terms of mixing components is to mix two oppositely charged triblock copolymers together. Inspired by the work in this Thesis, Hunt and coworkers have recently published data on exactly this subject.[14] As expected, transient networks are formed in which polyelectrolyte complex micelles are the nodes.

Besides changing the environmental conditions and mixing different block copolymer architectures to tune the interactions between the oppositely charged polyelectrolytes, the current transient network design also allows to study the influence of block lengths. The middle-block length can be varied to tune the gel concentration. Obviously, the longer the middle-block, the longer are the distances over which the polyelectrolyte complex micelles can be bridged. This lowers the gel concentration. Longer middle-blocks will also lead to smaller micellar cores and lower aggregation numbers, because the pressure in the corona will increase if the middle-block length increases. Drawback is that it becomes progressively more difficult to attach or grow charged blocks onto longer middle-blocks in the synthesis of the triblock copolymers.

Increasing the charged end-block length will lead to stronger association between the two polyelectrolyte components.[3] This means that critical micelle concentrations will be lower, and that the dynamics in the polyelectrolyte complex will be considerably slower.[6] The driving force for polyelectrolyte complex formation should be counterbalanced by a stabilizing force, to stop the polyelectrolyte phase from growing and subsequent phase separating from solution. Therefore the middle-block should have a minimum length with respect to the end-blocks, to make sure that polyelectrolyte micelles are formed.

The homopolyelectrolyte chain length is also of major influence to the microscopic structure of the polyelectrolyte complex micelles. Based on the results in Chapters 3 and 4, we can estimate that there are a few thousand charges present in the core of a polyelectrolyte complex micelle. The longer the homopolymer is, the fewer of them can fit in the core. For relatively small homopolymers this is not an issue, because the system can easily distribute all homopolymers over the micellar cores to obtain the equilibrium number of homopolymers in the core. This process becomes somewhat different for very long polyelectrolytes containing on the order of a thousand charged groups per chain, or more. At some point the system has to choose whether to put one long homopolymer chain into a smaller micellar core or to put two homopolymer chains into a bigger micellar core. The most extreme case is, of course, only one homopolymer per micellar core.

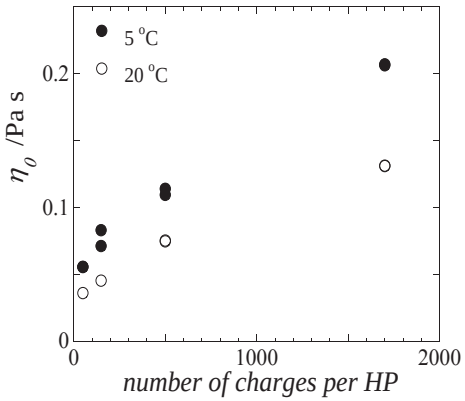

Figure 6.6: Shear viscosity as a function of number of charges per homopolymer, at two different temperatures as indicated in the graph. Salt concentration is 0.2 M KCl and p$H \approx 7$, so all PAA monomers are assumed to be charged. Total polymer concentration is equal in all samples, 15wt% and the polymers are always mixed at charge stoichiometric conditions.

The dynamics of the micelles with fewer longer chains is expected to be slower as compared to the case of more smaller chains. If, for example, one chain has to be exchanged from one micellar core to another, this process can take a relatively long time, since either a relatively big part of the complete micelle has to move with the homopolymer, or all charged groups on the entire homopolymer chain need to be desorbed from compensating groups at exactly the same time. The latter is very unlikely in case of very long chains. In the most extreme case, with only one homopolymer per micellar core, the only way to rearrange the micelles, or to relax stresses, is to physically separate charges and rearrange the triblock copolymers. This process requires a considerable amount of energy, depending on the charged block length of the triblock copolymer, and is therefore also unlikely to occur. Hence, relaxation times in these kind of systems will be relatively high, and dependent on the end-block length of the triblock copolymers. Recent measurements on 15wt% gels of positively charged $PTMAEMA_9$—PEO_{230}—$PTMAEMA_9$ and negatively charged poly(acrylic acid) (PAA) indeed show an increase in shear viscosity with increasing homopolymer chain length, see figure 6.6. The increase in shear viscosity reflects the increase of the relaxation time with increasing homopolymer chain length, assuming that the modulus of the gel is not influenced by the homopolymer chain length.

An opposite case to the situation of one homopolymer per micellar core, in terms of dynamics, is an 'all lengths' homopolymer. This might be achieved by taking a supramolecular polyelectrolyte chain. Polyelectrolyte complex micelles

can be prepared by mixing metal ions, ligands and block copolymers.[15] It should be possible to prepare physical gels of these micelles by using triblock copolymers instead of diblock copolymers. These physical gels might be interesting for imaging applications. The dynamical behaviour of these micelles might be different from the 'standard' polyelectrolyte complex micelles, because there does not have to be a mismatch between the triblock copolymer end-blocks and the supramolecular chain, which can break at any point. In terms of relaxation of the micelles, this means that one triblock copolymer end-block can be displaced from the core, taking an equally long piece of supramolecular chain with it. The extracted piece will be electroneutral, and only the surface tension of the core has to be overcome to extract it. The smaller the electroneutral unit that is extracted, the lower is the increase in surface area, hence, the lower is the energy barrier to do so. This all depends on how easily the supramolecular chain is broken when pulled out with a triblock copolymer end-block from the core.

The possibilities and questions described above are all relatively closely related to the content of this Thesis. However, the principle of physical gels based on charge-driven co-assembly allows to incorporate more advanced functionalities, such as switchable gelling or mechano-optical effects. In switchable gelling we aim to turn the gel state on and off by applying a small stimulus. One possibility to do so is by employing polymers or block copolymers which have LCST or UCST behaviour, as already described above. Another option to achieve this is by employing molecular groups which become charged after excitation at a certain wavelength of light. Some investigations on light induced changes in electrostatically driven systems have recently been reported, and this might be a starting point to further investigate the concept of light induced switchable gelling.[16]

Another challenge is to develop gels which can locally change their appearance, *e.g.* a colour change, as a visual signal when they are locally deformed. One way to achieve this is to choose two weak polyelectrolytes, which titrate each other upon association. By disrupting the electrostatic bonds between the groups by mechanical force, a local change in pH should occur. This local pH change could be picked up, for example, by pH sensitive dyes. Such a system might help in investigating the non-linear rheological behaviour, because it would be possible to see the points or areas of shear localization. In terms of applications such a mechano-optical effect might be very useful as a mechanism to detect defects in network structure before these defects become a macroscopic problem.

Polymer based physical gels can also be applied in areas such as (functional)

foods, cosmetics and pharmaceuticals. In all of these areas biodegradability and biocompatibility are of key importance. Therefore one can think of using biodegradable polymers to prepare physical gels based on charge-driven co-assembly. It should nowadays be possible to prepare block polysaccharides, which can be either positively or negatively charged.[17,18] Even though the electrostatic interactions in low charge density polymers are generally quite weak, this might be a new strategy to find new ways of adding texture and structure to food products or cosmetics, or to incorporate or enhance the uptake of bioactive components.[19–21]

6.2.2 Towards applications

So, after three years and ten months of research, can we answer some of the questions that started this project? As mentioned before, it was unknown whether physical gelation would at all be possible based on interconnected polyelectrolyte complex micelles. After some start-up trouble we succeeded, and in this Thesis we have convincingly shown that transient network formation is indeed possible the way it was hypothesized. This invention even led to the filing of a patent.[22] The coatings industry is one of the co-founders of this project, and in Chapter 1 we have also explained why. It is therefore interesting to speculate whether or not our transient networks might really find application in coating products.

First of all, we have shown that transient network formation is possible based on different combinations of charged groups, including charged nanoparticles. The method of bridging nodes by triblock copolymers with charged end-blocks is thus quite robust. However, is it robust enough to be really applied as new rheology modifier in water-based coating formulations? To answer this question we should consider several generic and some more specific problems.

Water-based coatings are, in general, prepared at relatively high pH values, approximately 10-11. At such basic conditions, the ester-bond in the end-blocks of our triblock copolymers would hydrolyze rather quickly, thereby destroying the triblock copolymer design and thus the transient network. However, it should be possible to solve this problem by synthesizing more stable charged groups as end-groups.

The other general problem is particle destabilization by depletion interactions upon mixing particle suspensions with polymer. However, if the particles are electrostatically stabilized and the used polymers are not too long, *i.e.* $R_g < \kappa^{-1}$, then flocculation by depletion should not be too much of a problem. Particles can also be destabilized as a result of the counterions released by the polymers. The res-

ulting high salt concentration screens the charge of the particles, thereby reducing the electrostatic repulsion between the particles and promoting particles to stick together irreversibly. This so-called primary minimum flocculation can be reduced or avoided by sterically stabilizing the particles with a polymer layer.

Throughout this Thesis we have emphasized the role of salt concentration in the solution. We have also discussed that this is a unique parameter to tune the interaction strength and range of electrostatically driven systems. The problem with regard to applications is, however, that salt is often an unwanted ingredient in coating formulations. One of the reasons is that you do not want to end-up with salt crystals on your coating once the coating has dried. There might be ways to reduce the salt concentration and still use charge-driven association in coating formulations. This can be achieved by using acidic and basic groups as oppositely charged components. In this way water is released instead of counterions. Another possibility is to use ammonium carbonate ($(NH_4)_2CO_3$) as salt.[23] This volatile salt decomposes into ammonia, carbon dioxide and water when exposed to air, thereby reducing the salt concentration in time. Yet another option is to use dialysis to get rid of unwanted salt. However, dialysis is not so easily applied in large-scale industrial processes.

The main components of a water-based coating are: water, latex particles, surfactants, rheology modifier, and pigments.[24] Particles, surfactants and pigments can be charged, and thus might interfere with polymer based charge-driven transient networks as described in this Thesis. Based on these ingredients, two strategies can be developed: 1) Prepare a charge-driven polymeric transient network independent of the particles in the formulation. 2) Use the charged particles to build the transient network, thereby thickening the formulation. The first method requires the use of triblock copolymers with negatively charged end-blocks, because these will not be attracted to the particle and pigment surfaces, assuming that these are also negatively charged. The problem is how to introduce positively charged polymers without causing these polymers to adsorb onto the negatively charged components present in the coatings formulation. This will probably be rather difficult, and therefore this route does not look too promising.

The second method is explored in Chapter 5. Obviously, you would need positively charged triblock copolymers to bind negatively charged particles in a transient network. In Chapter 5 we used silica nanoparticles as nodes in the transient network, instead of micellar cores, to prepare 'complex composite gels'. Being able to bridge nanoparticles in a transient network, opens up a new field of research. As we have seen in Chapter 5, the most important change, compared to polymeric

systems, is that the relaxation times become drastically longer. This is because a nanoparticle cannot deform or split itself in pieces. Relaxation is therefore caused by desorption of triblock copolymer end-blocks, which means separating charges. This is unfavourable and therefore unlikely to occur for the whole end-block simultaneously. Therefore the relaxation times are very high. In some respects the bridging of solid nanoparticles can be compared to the situation of having one oppositely charged homopolymer per micellar core. The slowed down dynamics is enhanced by the fact that the salt concentration in the formulation does not necessarily rise too much. The experiments described in Chapter 5 are done at 100 mM salt, which is approximately the highest salt concentration a water-based coating can contain.

As mentioned before, it is important in the case of mixing particles with polymers to prevent flocculation of particles by depletion interactions and/or the reduced electrostatic repulsion caused by the release of counterions. Steric stabilization of the particles is the option explored in Chapter 5, and this is achieved by physical adsorption of PVP onto the nanoparticle surface. The complex composite gels are very inhomogeneous immediately after mixing, as can be judged from the high turbidity, but become gradually more homogeneous in time until a steady state is reached. The steric stabilization of the particles is necessary to reach the more homogeneous steady state, because without the stabilizing layer the sample will remain turbid. Despite the PVP coating, the particles in our complex composite gel slowly flocculate at somewhat elevated salt concentrations. This is probably due to the slow displacement of the stabilizing PVP in time. It is, however, likely that there are better stabilizers available than the one we applied in Chapter 5.

It would be interesting to investigate whether stabilizers are still needed in case triblock polymers with shorter end-blocks are used to bridge the particles. Shorter end-block lengths will lead to shorter relaxation times, and possibly do not require a stabilizer on the particles to reach the homogeneous steady state. By choosing shorter end-blocks than the ones described in Chapter 5, it should be possible to obtain similar thickening results at even lower salt concentrations, which is advantageous as mentioned before. This effect can be enhanced when longer middle-blocks are used, because less triblock copolymer is needed to form a percolating network in that case.

We have tested the effect of drying on the appearance of the complex composite gel. As shown in Chapter 5, drying a drop of complex composite gel results in a clear transparent coating. In this complex composite coating the particles are concentrated, but they are still not flocculated, meaning that the nanoparticles are

stabilized throughout the drying process.

Something different happens when the complex composite gels are dried at elevated temperatures. By drying a complex composite gel for three weeks at 80 °C, we obtained a yellow-to-orange coloured solid material, very different from the air dried transparent coating described in Chapter 5, see figure 6.7a. Because of this difference in appearance, we analyzed this sample with high resolution scanning electron microscopy to reveal the microstructure. The surface of the 'oven-baked' complex composite is apparently not homogeneous, see figure 6.7b. The background is made up of silica particles with patches of what must be polymer. The particles seem to be irreversibly aggregated, as can be seen in the close-up of the polymer-particle interface in figure 6.7c. Looking at the surface of a freshly cut piece of composite, we can see long threads of polymer, several micrometers in length, which can become entangled in the middle of cracks, see figure 6.7d. A close-up of the threads can be found in figure 6.7e. Here we can see that the pillars have something like a 'foot' on the surface, from which the material seems to be stretched into the thread-like shape. The threads are only visible sticking outwards from the surface. However, their presence deep in the crack, figure 6.7d, suggests that these threads are present throughout the composite. We hypothesize that the following has happened to this material: At high temperatures the particles flocculate and they form the dense network of particles that is visible as the background in the SEM pictures in figure 6.7. The polymer(s), PVP and/or triblock copolymer, desorb from the particles and phase separate into a melt or blend containing the PVP and/or triblock copolymer with associated counterions. Because of the high temperature, the polymeric melt/blend might be fluidized to some extent. Due to the dense particle network, complete phase separation is prevented and what we end-up with are 'channels' of polymer melt in a dense particle matrix. At room temperature the polymer meld/blend is still elastic leading to the thread-like structures upon fracturing of the material. The flat structures on top of the particle network, figure 6.7b, are made of the same polymer melt/blend, but now not stretched or otherwise disturbed.

In figure 6.7f we show a large surface area covered by densely packed threads. It would be interesting to obtain more advanced control of the structures on the surface, because small-scale structures on surfaces might lead to special surface properties. For example, nature applies advanced surface modifications, in the form of nano- and micro-scaled structures, to obtain properties like superhydrophobic leaves or non-reflecting eyes.[25–28]

Practically, it does not really matter which negatively charged compounds are

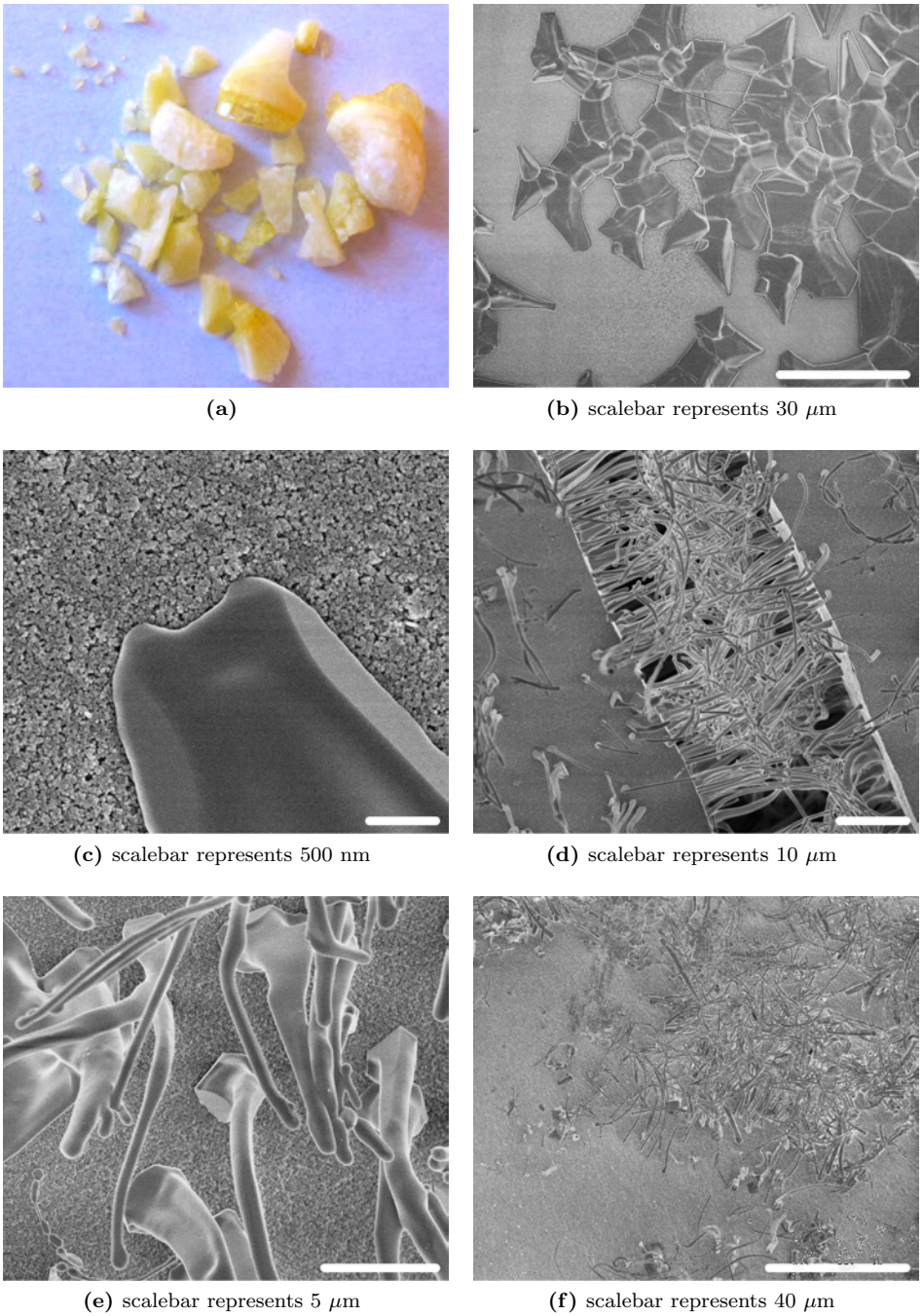

(a)

(b) scalebar represents 30 μm

(c) scalebar represents 500 nm

(d) scalebar represents 10 μm

(e) scalebar represents 5 μm

(f) scalebar represents 40 μm

Figure 6.7: Appearance and microstructure of 'oven-baked' complex composite gels. **(a)** Photograph of some pieces of oven-baked complex composite. **(b)** Surface of a complex composite. **(c)** Interface between polymeric content and particle network. **(d)** Threads protruding into a 20 μm crack. **(e)** Threads protruding outwards of the composite surface. **(f)** Large area of surface containing lots of threads.

held together in the network, as long as a transient network can be maintained in the coating formulation. Utilizing the charge of the particles already present in the coating formulations seems therefore most promising in bringing triblock copolymer gelators to the market.[22]

6.2.3 Particle based physical gels

The use of particles in a reversible network allows new functionalities to be incorporated in physical gels. Besides some of the above mentioned possibilities to change the interaction strength and range between the two charged components, particles can deliver some unique properties to physical gels. The size of particles is an obvious new parameter. Some nanoparticles in the size range of one to a few nanometers have special optical properties and are known as quantum dots. Quantum dots can be coated with covalently attached amine groups, which can be charged at sufficiently low pH.[29] In this way, quantum dots can be used as nodes in a transient network. Alternatively, charged quantum dots could also be incorporated into the micellar cores of a standard polyelectrolyte complex core micelle, because they are very small.

Contrary to small particles, big particles may also interfere with light and if particle spacing upon drying can be controlled, complex composites might interfere with light in a similar fashion as photonic crystals do.

Besides the size, also the shape of particles can be altered. Anisotropic particles are known to interfere with (the polarization of) light.

All these particle designs can be combined with the possibility to prepare particles with more advanced architectures and/or particles that respond to magnetic or electric fields. For example, it is possible to prepare particles that are charged on only one half of their surface,[30] or particles that themselves have an ABA or ABC type of surface.[31] Other options are to incorporate charged magnetic nanoparticles able to associate with oppositely charged polyelectrolyte blocks into the physical gels. These particles produce spherical aggregates without a magnetic field and rod-like aggregates when assembled in the presence of a magnetic field.[32] It is well known that collective alignment of nanoparticles in composite materials improves the strength, of the material at least in one direction. Applying magnetic or electric fields to (co-assembled) rod-like particles in composite materials might improve the mechanical properties of the resulting gels or composites.[33]

6.2.4 For the future

The rather extensive list of possibilities mentioned in this Chapter was made quite long deliberately, to show the reader the versatility of our charge-driven network design, and to show that the possibilities in combining and mixing charged particles/polymer/block copolymers are almost endless. It also implies that a lot is still unknown about these systems. Nevertheless I hope that the work presented in this Thesis provides enough suggestions, information and inspiration to continue research on Physical Gels based on Charge-Driven Co-Assembly, whether it be in academia or in industry.

References

[1] O. V. Lebedeva, B. S. Kim, K. Vasilev and O. I. Vinogradova, *Journal of Colloid and Interface Science*, 2005, **284**, 455–462.

[2] M. Cornelsen, C. A. Helm and S. Block, *Macromolecules*, 2010, **43**, 4300–4309.

[3] J. van der Gucht, E. Spruijt, M. Lemmers and M. A. Cohen Stuart, *Journal of Colloid and Interface Science*, 2011, **361**, 407–422.

[4] H. G. Schild, *Progress in Polymer Science*, 1992, **17**, 163–249.

[5] M. Lemmers, J. Sprakel, I. K. Voets, J. van der Gucht and M. A. Cohen Stuart, *Angewandte Chemie-International Edition*, 2010, **49**, 708–711.

[6] E. Spruijt, J. Sprakel, M. Lemmers, M. A. Cohen Stuart and J. van der Gucht, *Physical Review Letters*, 2010, **105**, 208301.

[7] D. Kovacevic, S. van der Burgh, A. de Keizer and M. A. Cohen Stuart, *Langmuir*, 2002, **18**, 5607–5612.

[8] F. Weinbreck, R. de Vries, P. Schrooyen and C. G. de Kruif, *Biomacromolecules*, 2003, **4**, 293–303.

[9] A. V. Ermoshkin and M. Olvera de la Cruz, *Physical Review Letters*, 2003, **90**, 125504.

[10] N. B. Wyatt and M. W. Liberatore, *Soft Matter*, 2010, **6**, 3346–3352.

[11] Y. R. Sliozberg, K. E. Strawhecker, J. W. Andzelm and J. L. Lenhart, *Soft Matter*, 2011, **7**, 7539–7551.

[12] I. K. Voets, A. de Keizer, P. de Waard, P. M. Frederik, P. H. H. Bomans, H. Schmalz, A. Walther, S. M. King, F. A. M. Leermakers and M. A. Cohen Stuart, *Angewandte Chemie-International Edition*, 2006, **45**, 6673–6676.

[13] I. K. Voets, R. Fokkink, T. Hellweg, S. M. King, P. de Waard, A. de Keizer and M. A. Cohen Stuart, *Soft Matter*, 2009, **5**, 999–1005.

[14] J. N. Hunt, K. E. Feldman, N. A. Lynd, J. Deek, L. M. Campos, J. M. Spruell, B. M. Hernandez, E. J. Kramer and C. J. Hawker, *Advanced Materials*, 2011, **23**, 2327–2331.

[15] Y. Yan, N. A. M. Besseling, A. de Keizer, A. T. M. Marcelis, M. Drechsler and M. A. Cohen Stuart, *Angewandte Chemie-International Edition*, 2007, **46**, 1807–1809.

[16] I. Willerich and F. Grohn, *Macromolecules*, 2011, **44**, 4452–4461.

[17] C. Schatz, S. Louguet, J.-F. LeMeins and S. Lecommandoux, *Angewandte Chemie International Edition*, 2009, **48**, 2572–2575.

[18] C. Schatz and S. Lecommandoux, *Macromolecular Rapid Communications*, 2010, **31**, 1664–1684.

[19] M. E. Gonzalez, B. Alarcon and L. Carrasco, *Antimicrob. Agents Chemother.*, 1987, **31**, 1388–1393.

[20] R. Pearce-Pratt and D. M. Phillips, *Biology of Reproduction*, 1996, **54**, 173–182.

[21] O. Felt, R. Gurny and V. Baeyens, *The AAPS Journal*, 2001, **3**, 87–93.

[22] M. A. Cohen Stuart, F. A. M. Leermakers, M. Lemmers and J. Sprakel, *Triblock copolymer gelators*, 2010.

[23] Wikipedia, *http://en.wikipedia.org/wiki/Ammonium_carbonate*.

[24] J. Sprakel, *PhD Thesis*, 2009.

[25] P. B. Clapham and M. C. Hutley, *Nature*, 1973, **244**, 281–282.

[26] S. J. Wilson and M. C. Hutley, *Optica Acta*, 1982, **29**, 993–1009.

[27] W. Barthlott and C. Neinhuis, *Planta*, 1997, **202**, 1–8.

[28] C. Neinhuis and W. Barthlott, *Annals of Botany*, 1997, **79**, 667–677.

[29] M. Rosso-Vasic, E. Spruijt, Z. Popovic, K. Overgaag, B. van Lagen, B. Grandidier, D. Vanmaekelbergh, D. Dominguez-Gutierrez, L. De Cola and H. Zuilhof, *Journal of Materials Chemistry*, 2009, **19**, 5926–5933.

[30] S. Jiang, Q. Chen, M. Tripathy, E. Luijten, K. S. Schweizer and S. Granick, *Advanced Materials*, 2010, **22**, 1060–1071.

[31] Q. Chen, E. Diesel, J. K. Whitmer, S. C. Bae, E. Luijten and S. Granick, *Journal of the American Chemical Society*, 2011, **133**, 7725–7727.

[32] J. Fresnais, J. F. Berret, B. Frka-Petesic, O. Sandre and R. Perzynski, *Advanced Materials*, 2008, **20**, 3877–3881.

[33] H. N. An, S. J. Picken and E. Mendes, *Soft Matter*, 2010, **6**, 4497–4503.

Samenvatting

In dit proefschrift hebben we onderzocht hoe een nieuwe catagorie van fysische gels (en dus niet gelen[1]) gemaakt kan worden en we hebben een aantal eigenschappen van deze nieuwe gels onderzocht. Om dit werk beter begrijpelijk te maken voor niet-specialisten volgen eerst enkele basisbegrippen, waarna de belangrijkste resultaten van dit proefschrift worden samengevat. Afsluitend is er een korte, maatschappelijke, evaluatie van dit onderzoek.

De basis

Bijna alles op aarde bestaat uit moleculen. Moleculen zijn hele kleine bouwstenen, waaruit grotere objecten zijn opgebouwd. Deze objecten kunnen bestaan uit één enkele soort moleculen, maar veelal betreft het combinaties van verschillende moleculen. Voorbeelden van 'tastbare' objecten opgebouwd uit combinaties van verschillende moleculen zijn lucht, cellen, mensen, bakstenen, auto's, gebouwen, continenten en oceanen. Alles op aarde dus.

Sommige moleculen kunnen met een chemische reactie aan elkaar geklikt worden tot één lang molecuul. De afzonderlijke moleculen worden dan *monomeren* genoemd. De aan elkaar geklikte monomeren vormen samen weer één nieuw groot molecuul: een *polymeer*, zie ook figuur S-1. Polymeren zijn een belangrijk onderdeel van het dagelijkse leven. Zo zijn bijvoorbeeld alle 'plastics' opgebouwd uit (synthetische) polymeren, maar er bestaan ook biologische polymeren, zoals eiwitten of DNA.

Omdat polymeren hele lange moleculen zijn (enkele tientallen nanometers, dat is minder dan één tienduizendste van een millimeter) hebben polymeren bijzondere eigenschappen, vooral als je een heleboel polymeren bij elkaar stopt. Deze eigenschappen komen voort uit het feit dat de polymeren niet door elkaar heen kunnen bewegen en daardoor snel verknoopt raken. Denk aan een bord spaghetti. Het gevolg van deze verknopingen is dat de polymeren een soort 3-dimensionaal visnet of *netwerk* vormen, zie figuur S-2. Het gevolg is dat de polymeren elkaar in de weg zitten als ze zich willen of moeten verplaatsen, bijvoorbeeld wanneer er een kracht uitgeoefend wordt op de polymeren. Een geconcentreerde polymeeroplossing zal daardoor niet zo gemakkelijk vervormen of stromen. De oplossing is stroperig,

ofwel de *viscositeit* is hoog.

Polymeren kunnen opgebouwd zijn uit één soort monomeren, maar meer geavanceerde polymeren bestaan uit meerdere soorten monomeren. Een manier om een polymeer te maken uit verschillende monomeren, is door eerst een polymeer te maken van het ene monomeer, om vervolgens de andere monomeren één voor één vast te knopen aan het eerdere polymeer. Deze strategie is in dit proefschrift gebruikt. Op deze manier onstaat een zogenaamd *blok copolymeer*. Blok, omdat het uit meedere 'blokken' van gelijke monomeren bestaat, en 'copolymeer' omdat het geheel uit verschillende monomeren bestaat, zie ook figuur S-3. Blok copolymeren hebben het voordeel dat ze de eigenschappen van verschillende monomeren combineren in één molecuul.

Gels

Polymeren kunnen gebruikt worden om gels te maken. Gels worden in veel producten toegepast, onder andere in persoonlijke verzorgingsproducten en voedingsmiddelen, maar ook in explosieven.[2–4]

Gels zijn dikker of visceuzer dan vloeistoffen, maar niet zo hard als vaste stoffen. Gels zitten tussen vloeistoffen en vaste stoffen in; gels zijn *visco-elastisch*. Er bestaan twee soorten gels, chemische gels en fysische gels. Het verschil tussen fysische gels en chemische gels is de manier waarop de polymeren met elkaar verknoopt zijn. Bij chemische gels zijn de polymeerketens met een chemische reactie aan elkaar vast geklikt. In dat geval kunnen de polymeerketens alleen nog met bruut geweld van elkaar los worden gemaakt. Gebeurt de chemische reactie terwijl de polymeren opgelost zijn in een vloeistof, bijvoorbeeld water, dan heeft dat tot gevolg dat het water 'vast' wordt. Dat komt doordat de polymeerketens vast zitten aan elkaar in een 3-dimensionaal netwerk, zie figuur S-2, en dus niet meer langs elkaar heen kunnen bewegen. Het water zit dan 'gevangen' in het polymeernetwerk waardoor de oplossing een vaste stof wordt. Chemische gels zijn in essentie een vaste stof.

Bij fysische gels zijn de verbindingen tussen de polymeerketens van een andere aard dan bij chemische gels. Bij fysische gels worden de knooppunten tussen de polymeerketens gevormd op basis van fysische interacties. Bijvoorbeeld electrostatische interacties, waarbij een positief geladen polymeer(deel) en een negatief geladen polymeer(deel) elkaar aantrekken. Fysische bindingen tussen polymeerketens zijn over het algemeen veel zwakker dan chemische bindingen. Het gevolg van de zwakke bindingen is dat deze ook weer los kunnen gaan, spontaan of onder

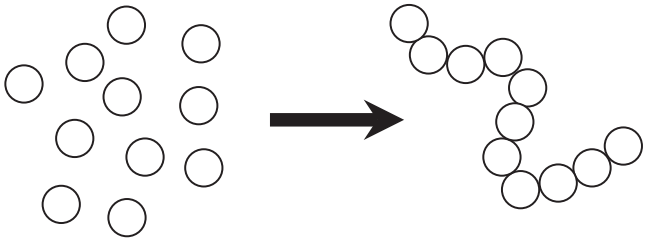

Figuur S-1: Schematische weergave van een polymerisatie reactie. De monomeren (links) worden tijdens de reactie aan elkaar geklikt tot een polymeer (rechts).

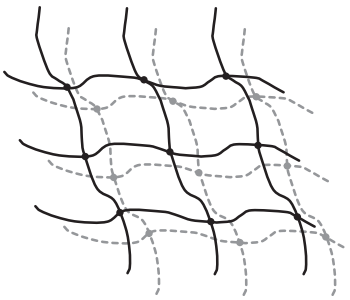

Figuur S-2: Schematische weergave van een 3-dimensionaal verknoopt polymeernetwerk. Doordat de polymeren met elkaar verknoopt zijn kunnen ze moeilijk langs elkaar heen bewegen. Het gevolg is dat geconcentreerde polymeeroplossingen een hoge viscositeit hebben.

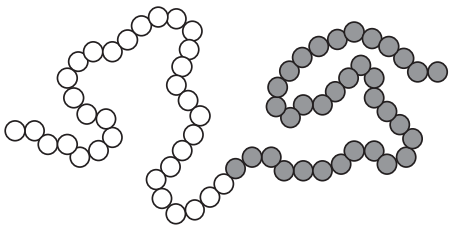

Figuur S-3: Schematische weergave van een blok copolymeer. Het polymeer bestaat uit twee blokken van twee verschillende monomeren, wit en grijs.

invloed van een externe kracht. De knooppunten bestaan dus maar tijdelijk. Een fysische gel kan dus, in tegenstelling tot een chemische gel, wél intern reorganiseren. Fysische gels zijn daarom in essentie vloeistoffen die van vorm kunnen veranderen onder invloed van een externe kracht, bijvoorbeeld de zwaartekracht. Fysische gels zijn ook, zoals alle vloeistoffen, zelf-helend; je kunt twee 'druppels' gels samen laten vloeien tot één geheel. Het wetenschappelijke werk beschreven in dit proefschrift gaat over een nieuwe categorie fysische gels.

Motivatie van het onderzoek

Eén van de producten waarin fysische gels toegepast worden zijn watergedragen verven. Hoewel iedereen bekend is met verf, realiseert niet iedereen zich dat verf een heel complex product is: verf moet dun genoeg zijn om goed te kunnen roeren, maar het moet dik genoeg zijn om niet van de kwast te druppen en aan de muur te kunnen blijven plakken zonder uit te zakken. Toch moet de verf nog wel iets vloeien, om de kwaststrepen kwijt te raken. Het is nog niet zo gemakkelijk om een product te maken dat aan al deze eigenschappen voldoet.

In watergedragen verven zitten naast het oplosmiddel (water) ook nog kleine polymeerballetjes, pigmenten, zeep-achtige moleculen en verdikkers. De verdikkers die in de huidige verven (mede) gebruikt worden, worden ook wel *associatieve verdikkers* genoemd.[5] Deze associatieve verdikkers zijn triblok copolymeren, waarbij de blokken aan de buitenkant niet van water houden, deze zijn hydrofoob, terwijl het veel langere middenblok juist wel van water houdt, dit blok is hydrofiel, zie ook de linkerkant van figuur S-4. Wanneer deze triblok copolymeren in water worden opgelost vouwen ze dubbel en vervolgens zullen de uiteinden van verschillende polymeren bij elkaar plakken in een nanoscopisch 'druppeltje'. Dit gebeurd omdat de uiteinden allemaal niet in het water willen zitten, maar wel bij elkaar. Het nano-druppeltje wordt beschermd door de lussen van de middenblokken en kan daardoor in water bestaan. Eén zo'n gestabiliseerde nano-druppel wordt, in zijn algemeenheid, een *micel* genoemd. In het geval van een oplossing van triblok copolymeren in water onstaan spontaan zogenaamde *bloemachtige micellen*, omdat de micellen lijken op bloemetjes wanneer ze in 2-dimensies worden geschetst, zie het midden van figuur S-4. Op deze manier kunnen alle hydrofobe eindblokken bij elkaar zitten in de *kern*, terwijl de middenblokken in het water steken in de zogenaamde *corona*.

Wanneer je heel veel micellen maakt in water, kunnen de micellen zo dicht bij elkaar in de buurt komen dat het mogelijk wordt voor de triblokken om één

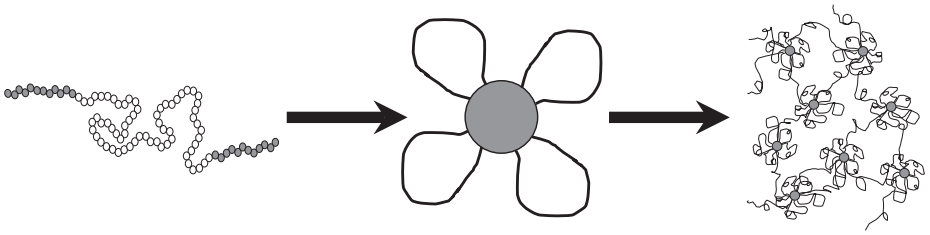

Figuur S-4: Schematische weergave van de werking van associatieve verdikkers in water. De triblok copolymeren (links) plakken in water samen tot bloemachtige micellen (midden). Deze micellen kunnen met elkaar verbonden worden als de concentratie micellen hoog genoeg is. Op deze manier wordt een fysisch netwerk van micellen gevormd. Door de interne weerstand van de micellen om te reorganiseren bestaat er een interne weerstand om te stromen. Dit betekent dat de viscositeit van de oplossing omhoog gaat. Zie ook figuur 1.4

eindblok in de éne micelkern te stoppen en het andere eindblok in een andere micelkern te stoppen. Om ingewikkelde redenen vinden de triblokken dit eigenlijk fijner, en daarom zullen ze dit ook zoveel mogelijk doen als ze er de kans voor krijgen. Wanneer heel veel micellen met elkaar verbonden worden hebben we een 3-dimensionaal netwerk van micellen gecreëerd, waardoor het water wordt ingevangen en we dus een gel hebben gemaakt. Deze fysische gels leveren, in combinatie met andere strategiën, de juiste vloei eigenschappen voor de verven. De verschillende stappen zijn weergegeven in figuur S-4. In tegenstelling tot het chemische netwerk, zijn de knooppunten in het fysische netwerk niet permanent. De micellen vallen ook om de haverklap weer uit elkaar, omdat de kracht die de micellen bij elkaar houdt niet zo heel groot is. Het netwerk verdikt de verf dus wel, maar maakt er niet een vaste stof van.

De toevoeging van associative verdikkers heeft de watergedragen verven een stuk beter gemaakt om mee te werken. Toch zijn de prestaties van watergedragen verven (nog) niet zo goed als traditionele oplosmiddelverven.[6] Zo wordt de houdbaarheid van watergedragen verven mogelijk negatief beïnvloed door de associatieve verdikkers, kan de mate van verdikking moeilijk gecontroleerd worden wanneer de associatieve verdikkers eenmaal zijn opgelost en is het moeilijk om bepaalde resultaten te krijgen wanneer de verf droog is, bijvoorbeeld hoogglans. Om te proberen het gat naar de oplosmiddelverven te dichten, zijn onderzoekers op zoek naar nieuwe strategiën om watergedragen verven te verdikken. Eén nieuwe strategie is beschreven en getest in dit proefschrift.

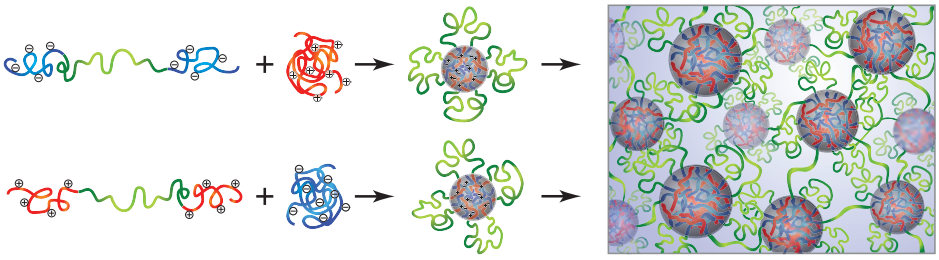

Figuur S-5: Schematische weergave van de vorming van een fysische gel op basis van ladingsgedreven complexatie. Een triblok copolymeer met geladen eindgroepen vormt een bloemachtige polyelectroliet complex micel, wanneer gemengd met een tegengesteld geladen polymeer (links). Wanneer de micellen geconcentreerd worden kunnen bruggen ontstaan tussen de micellen, waardoor een netwerk van verbonden micellen wordt gemaakt, en dus een fysische gel wordt verkregen (rechts).

Nieuwe verdikkingsstrategie

De nieuwe verdikkingsstrategie is gebaseerd op de fysische interactie tussen twee tegengesteld geladen polymeerblokken, aanwezig op twee verschillende polymeren. Het is dus een twee-componenten verdikker, in plaats van de klassieke één- component verdikker. Zoals je intuïtief verwacht, trekken positief geladen polymeren en negatief geladen polymeren elkaar aan. Wanneer we één van de twee componenten ontwerpen op de manier van de klassieke verdikkers, dus als triblok copolymeer, dan kunnen we fysische gels maken op basis van electrostatische interacties.

Het principe is bijna gelijk aan de klassieke verdikkers, alleen nu maken we een triblok copolymeer met geladen groepen aan de uiteinden. Wanneer dit triblok copolymeer in water gemengd wordt met een tegengesteld geladen polymeer, trekken de tegengesteld geladen onderdelen elkaar aan. Het gevolg is dat we wederom een micel krijgen, maar nu met een kern die bestaat uit een zogenaamd *polyelectroliet complex*. Deze kern bevat het geladen polymeer (een polyelectroliet) en de tegengesteld geladen uiteinden van het triblok copolymeer. Het lange middenblok vormt wederom een neutrale corona, gelijk aan de situatie bij de klassieke verdikkers, zie ook de linkerkant van figuur S-5. De resulterende micellen worden *bloemachtige polyelectroliet complex micellen* genoemd. Wanneer deze micellen geconcentreerd worden, kunnen de triblokken de micellen met elkaar verbinden, net zoals in de situatie van de klassieke verdikkers. Op deze manier krijgen we een netwerk van verbonden polyelectroliet complex micellen, en dus een gel, zie de rechterkant van figuur S-5.

De electrostatische interactie is van fysische aard, en veel zwakker dan chemische

verbindingen. De micellen en de verbindingen tussen de micellen zijn dus *reversibel*; de micellen zelf en verbindingen tussen de micellen worden continu gemaakt en weer verbroken. Een maat voor de snelheid waarmee dit gebeurt is de *relaxatietijd*. Een korte relaxatietijd betekent dat de verbindingen tussen de micellen snel verbroken en gevormd kunnen worden. Het netwerk kan zich dan snel aanpassen aan externe krachten en dus is de gel relatief vloeibaar. Het omgekeerde is waar voor lange relaxatietijden. Eén van de potentiële voordelen van de nieuwe verdikkingsstrategie is dat de aantrekkingskracht tussen de tegengesteld geladen componenten beter gecontroleerd kan worden. Dat betekent dat de relaxatietijd beter gecontroleerd kan worden en dus dat de viscositeit van de gels beter gecontroleerd kan worden. Daarnaast zijn er meer parameters om de viscositeit te beïnvloeden; concentratie, temperatuur, mengverhouding, zoutconcentratie en, afhankelijk van de gebruikte polymeren, pH. Deze gels zijn daarom *multi-responsief*.

Uitvoering

Eén van de centrale thema's in dit proefschrift is het leggen van relaties tussen de microscopische, onzichtbare structuur en de macroscopische, zichtbare structuur. In andere woorden, hoe de verdeling van de polymeren en hoe ze met elkaar verbonden zijn, de eigenschappen van de gels op de zichtbare schaal bepalen.

We hebben deze micro-macro afhankelijkheid onderzocht door microscopische technieken, zoals (dynamische) lichtverstrooiing, kleine hoek Röntgen verstrooiing en (cryogene) scanning electronen microscopie, te combineren met macroscopische technieken, zoals reometrie. Deze combinatie van technieken is sterk in het verklaren waarom een materiaal bepaalde mechanische eigenschappen heeft.

De triblok copolymeren die we gebruikt hebben zijn niet te koop, we hebben ze dus zelf moeten maken. Dit hebben we gedaan volgens al beschreven recepten voor diblok copolymeren.[7–10] De uitgangsstof is het middenblok, welke goedkoop in grote hoeveelheden gekocht kan worden. Vervolgens wordt dit middenblok in een eerste reactie geprepareerd voor het maken van een triblok. In deze eerste reactie wordt er een chemisch andere groep geplaatst aan beide uiteinden van het middenblok. Vervolgens worden in een tweede reactie de geladen groepen één voor één aan de uiteinden van het middenblok geklikt. Op deze manier krijg je dus een triblok copolymeer met geladen eindgroepen. De twee types die wij hebben gebruikt in dit proefschrift zijn gegeven in figuur S-6 (voor meer details zie paragraaf 1.5.1).

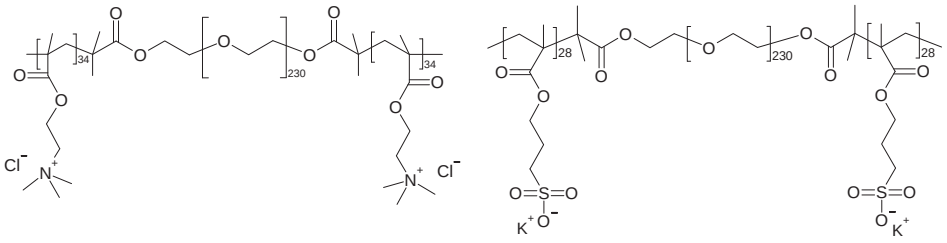

(a) **(b)**

Figuur S-6: Chemische structuren van de gebruikte triblok copolymeren. **(a)** Triblok copolymeer met positief geladen eindblokken. **(b)** Triblok copolymeer met negatief geladen eindblokken.

Resultaten

De nieuwe verdikkingsstrategie zoals hierboven beschreven was aan het begin van dit project een hypothese. Een fysische gel op basis van twee tegengesteld geladen polymeerblokken was door niemand ter wereld ooit gemaakt. In hoofdstuk 2 laten we zien dat het inderdaad mogelijk is om fysische gels te maken op basis van polymeren met tegengestelde ladingen. Daarnaast laten we zien dat deze gels daadwerkelijk multi-responsief zijn: de viscositeit kan beïnvloed worden met temperatuur, concentratie, mengverhouding, zoutconcentratie en pH.

In hoofdstuk 3 laten we zien dat de mengverhouding van de twee componenten grote invloed heeft op de viscositeit van de gels. Alleen wanneer de componenten dichtbij een 1:1 ladingsverhouding gemengd worden, onstaat een gel. Een opmerkelijke bevinding is dat de microstructuur ingrijpend anders is wanneer de ene danwel de andere component in overschot aanwezig is.

In hoofdstuk 4 onderzoeken we de invloed van polymeerconcentratie en zoutconcentratie op de netwerkstructuur. Niet zo verassend is dat de viscositeit van de gels omhoog gaat als je er meer polymeer instopt. Daaruit kunnen we afleiden dat het aantal bruggen tussen de micellen sterk toeneemt wanneer de micellen zo geconcentreerd zijn dat ze ongeveer met de corona's tegen elkaar komen. Met de toevoeging van extra zout in de gels, worden de micellen kleiner, maar komen er tegelijkertijd ook meer micellen. Dit heeft de verassende consequentie dat er eigenlijk niets veranderd aan het totale aantal bruggen in het netwerk. De viscositeit gaat echter wel omlaag, omdat de relaxatietijd omlaag gaat met toenemende zoutconcentratie.

In hoofdstuk 5 onderzoeken we of we positief geladen triblokken kunnen gebruiken om kleine negatief geladen nanodeeltjes aan elkaar te plakken, en of we zo een

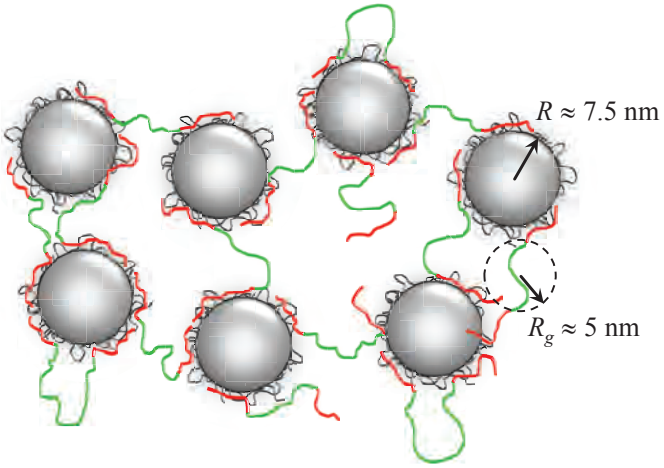

Figuur S-7: Een schematische weergave van silica nanodeeltjes die met elkaar verbonden zijn door triblok copolymeren, om op die manier een netwerk te vormen. Het neutrale middenblok is groen, de positieve eindblokken zijn rood en het extra laagje polymeer is grijs.

netwerk kunnen vormen, zie figuur S-7. Dit is een stap dichter bij toepassingen, omdat in veel coatings ook nanodeeltjes voorkomen. Onder bepaalde condities is dit inderdaad gelukt. De deeltjes moesten eerst voorzien worden van een laagje ander polymeer, om te voorkomen dat het neutrale middenblok zelf op de deeltjes zou plakken. Het gebruikte middenblok is namelijk moleculair gezien nogal plakkerig, zeker in combinatie met het gebruikte deeltjesoppervlak, silica. We bewijzen dat het netwerk daadwerkelijk een tijdelijk karakter heeft, dat wil zeggen dat de deeltjes en triblok copolymeren los kunnen komen van elkaar om vervolgens nieuwe verbindingen aan te gaan. De onderzochte gels worden gekarakteriseerd door een lage graad van verbondenheid, maar een hele hoge relaxatietijd, waardoor de viscositeit van deze 'complex composieten gels' toch erg hoog is.

Verantwoording

In de huidige tijd waarin onderzoek meer en meer toepassingsgedreven is, is het goed om te reflecteren op het werk dat is verricht. Ook is het prettig voor de Nederlandse belastingbetaler, die dit onderzoek financieel mede mogelijk maakte, om te weten of zijn geld nuttig besteed is. Een goede manier om dit te doen is door kort een aantal vragen te beantwoorden:

- ✓ Heeft het onderzoek beschreven in dit proefschrift een bijdrage geleverd aan de wetenschap? — Ja, drie hoofdstukken zijn gepubliceerd in wetenschap-

pelijke tijdschriften en één hoofdstuk wacht nog op goedkeuring voor publicatie.

✓ Is vervolgonderzoek nodig? — Om de hypothese van dit proefschrift te beantwoorden niet. We hebben aangetoond dat fysische gels op basis van ladinggedreven associatie gemaakt kunnen worden. Er zijn wel aanknopingspunten voor het doen van vervolgonderzoek. Met name de combinatie van triblok copolymeren met nanodeeltjes biedt kansen op nieuwe of verbeteringen van bestaande materialen.

✓ Is het uitgevoerde onderzoek innovatief? — Ja, er is zelfs een patent aangevraagd.

✓ Heeft het onderzoek beschreven in dit proefschrift geleid tot een nieuw of verbeterd product? — Nee, wellicht in de toekomst.

✓ Is de kwaliteit van leven voor mensen in de wereld verbeterd door het onderzoek beschreven in dit proefschrift? — Nee, niet direct.

✓ Is het Nederlandse belastinggeld goed besteed? — Ja, er is vooruitgang geboekt op wetenschappelijk gebied. Bovendien is er een Nederlandse kenniswerker opgeleid.

S

Referenties

[1] *Van Dale online woordenboek; trefwoord: gel*, 2010.

[2] Wikipedia, *keyword: gel.*

[3] Wikipedia, *keyword: gel (disambiguation).*

[4] Wikipedia, *http://en.wikipedia.org/wiki/Water_Gel_Explosives.*

[5] A. J. Reuvers, *Progress in Organic Coatings*, 1999, **35**, 171–181.

[6] J. Sprakel, *PhD Thesis*, 2009.

[7] M. Kato, M. Kamigaito, M. Sawamoto and T. Higashimura, *Macromolecules*, 1995, **28**, 1721–1723.

[8] J. S. Wang and K. Matyjaszewski, *Macromolecules*, 1995, **28**, 7901–7910.

[9] Y. T. Li, S. P. Armes, X. P. Jin and S. P. Zhu, *Macromolecules*, 2003, **36**, 8268–8275.

[10] G. Masci, D. Bontempo, N. Tiso, M. Diociaiuti, L. Mannina, D. Capitani and V. Crescenzi, *Macromolecules*, 2004, **37**, 4464–4473.

Dankwoord

Alhoewel het vervaardigen en verdedigen van een proefschrift vooral een test van indiviuele bekwaamheid is, zou ik dit proefschrift nooit hebben kunnen maken zonder hulp en advies van een heel aantal mensen. Hieronder volgen een aantal namen die ik speciaal wil noemen, omdat ze op de een of andere manier een belangrijke bijdrage hebben geleverd aan het afronden van dit project.

Allereerst wil ik al mijn docenten bedanken die mij, gedurende mijn leven, zoveel hebben geleerd. Het verkrijgen van de graad van doctor is een hoogtepunt in de persoonlijke ontwikkeling. Vanaf de kleuterschool spelen docenten een essentiële rol in het begeleiden, stimuleren en uitdagen van kinderen en jong-volwassenen. Beste docenten, bedankt voor jullie tijd, geduld, aandacht en kennis. Zonder jullie had ik deze titel nooit kunnen behalen.

Rienk, als enthousiaste scheikundedocent ben je van groot belang geweest bij mijn studiekeuze. Achteraf kun je zeggen dat jij een sleutelfiguur bent geweest in mijn leven. Ik vind het heel bijzonder dat je mijn paranimf wilt zijn, als symbool van dankbaarheid voor al mijn docenten.

Daarna zou ik het Dutch Polymer Institute (DPI), en daarmee indirect het Nederlandse bedrijfsleven en de Nederlandse belastingbetaler, willen bedanken voor het faciliteren van mijn onderzoek. Zonder geld namelijk geen project. De DPI Review- en Annual Meetings heb ik altijd graag bezocht en beide meetings zijn uitstekende gelegenheden om collega's uit de academische en industriële hoek te ontmoeten. Ook met de mensen van het DPI heb ik altijd prettig samengewerkt. John en Harold, bedankt voor jullie interesse in mijn project en het beantwoorden van allerlei DPI-gerelateerde vragen.

Mijn onderzoek is uitgevoerd onder de verantwoordelijkheid van mijn promotor Martien Cohen Stuart. Martien, ik heb veel bewondering voor je manier van werken. Door je enorme kennis en ervaring weet je snel oplossingen te bedenken voor problemen waar AiO's mee te maken krijgen in hun projecten. Het was prettig om na bijeenkomsten weer een duidelijke focus te hebben, vooral in de laatste anderhalf jaar.

De dagelijkse begeleiding was in handen van Jasper van der Gucht. Jasper, bedankt dat je altijd voor mij klaar stond om vragen te beantwoorden of resultaten te bespreken. Jouw kennis en inzicht is van essentieel belang geweest bij het analyseren en interpreteren van data. Ik heb heel veel van je geleerd. Ook met het corrigeren van manuscripten ben je altijd heel snel geweest, ondanks je drukke agenda. Bedankt!

I would also like to acknowledge the two persons who I have spent most time with in the lab: my roommates Evan and Yuan. It was pleasant to share room 0018 with the same persons for almost four years. Evan, I have great respect for your working discipline and knowledge. Thank you for your time for discussions, for all the questions that you answered, and for the pleasant cooperation. The fact that we have (almost) published four papers together shows how effective working with you is. I am glad to have you by my side as my paranimf. Yuan, thank you for bringing liveliness in 0018. There is always something happening when you are around. Thanks for all discussions about life, China and the Netherlands. I learned a lot from you with respect to cultural differences and how to let other people work for you (◡̈). I wish you all the best in your future career and personal life. Hopefully we will meet each other many times in the future.

De hoofdstukken 2, 4 en 5 zijn tot stand gekomen met behulp van Ilja Voets. Ilja, bedankt voor de prettige samenwerking, vooral in het tweede en derde jaar. Ik heb ontzettend veel van je geleerd op het gebied van verstrooiing. Bedankt voor je geduld en je bereidheid keer op keer uit te leggen wat een harde-bollen structuurfactor nou eigenlijk is.

Joris, jouw bijdrage in de eerste twee jaar van dit project was van groot belang om de fysiche gels op basis van ladingsgedreven associatie te kunnen maken. Bedankt voor het leren van polymeersynthese 'Joris-style': beter veel maken, dan houd je nog wat over als je wat verliest. Bedankt ook dat ik van jouw LaTeX template gebruik mocht maken.

Ton Marcelis, van het Laboratorium voor Organische Chemie, heeft meerdere malen geholpen met het beantwoorden van vragen omtrent de synthese van polymeren. Ton, bedankt voor je bereidheid mee te denken met de synthese vraagstukken. De gesynthetiseerde polymeren werden in eerste instantie gekarakteriseerd door NMR spectroscopie. Dit werd altijd uitgevoerd door Barend van Lagen, van het Laboratorium voor Organische Chemie. Barend, NMR is essentieel geweest bij het vaststellen van de polymeer bloklengtes. Bedankt dat je altijd bereid was om op korte termijn onze samples te meten. The first useable batch of triblock

copolymers was also characterized by aqueous GPC, which was kindly performed by the group of Christophe Detrembleur, Université de Liège, Belgium.

Een andere grote bijdrage aan dit proefschrift is geleverd door tekenaar Gert Buurman. Gert, de tekening die jij voor mij maakte heb ik telkens weer gebruikt op posters en in presentaties. Het vat in één figuur mijn project samen. Ook in dit proefschrift staat jouw tekening maar liefst vier keer afgebeeld. Goede en mooie illustraties zijn ontzettend belangrijk bij het effectief communiceren van wetenschappelijke inhoud. Ik ben er van overtuigd dat jouw tekening er toe heeft bijgedragen dat presentaties en posters op congressen 'gemakkelijk' geregeld konden worden. Ik ben dankbaar dat ik nog van je diensten gebruik heb kunnen maken.

Hoofdstuk 3 is tot stand gekomen als gevolg van een bijzondere team-prestatie. De data voor dit hoofdstuk zijn gemeten bij het European Synchrotron Radiation Facility (ESRF) in Grenoble. Frans, Remco, Lennart en Evan, bedankt voor jullie tijd, inzet en de uitstekende samenwerking tijdens ons verblijf in Grenoble. Hier zou ik ook de mannen van de Ontwikkelwerkplaats AFSG willen bedanken voor het zeer snel vervaardigen van een handige multi-capillairen houder. Dankzij deze houder hebben we ongeveer 180 samples kunnen meten in minder dan 48 uur. Also I would like to thank beam scientist Guiseppe Portale for his time and help in setting-up the beam-line and processing the raw data. Ook wil ik de Nederlandse Organisatie voor Wetenschappelijk Onderzoek (NWO) bedanken voor het faciliteren van de beam-tijd.

Hoofdstuk 5 is voortgekomen uit de MSc Thesis van Sabine Akerboom. Sabine, je hebt aan een heel complex onderwerp gewerkt, om vervolgens als eerste in de wereld 'complex composite gels' te maken. Je hebt het heel goed gedaan. Ik hoop dat ik je iets heb kunnen leren. Ik wens je heel veel succes met je eigen AiO project!

De mooie electronen microscopie plaatjes in hoofdstuk 5 zijn gemaakt bij het Wageningen Electron Microscopy Center (WEMC) onder begeleiding van Adriaan van Aelst. Adriaan, het zichtbaar maken van de nanostructuur in onze deeltjes-gels was een mooi avontuur. Het was iedere keer weer spannend wat we te zien zouden krijgen. Bedankt voor je hulp bij het preparen van de samples en bij het maken van de plaatjes.

Remco, jij hebt me vele malen geholpen met problemen op het gebied van statische en dynamische lichtverstrooiing. Ook met het maken van de video's, die ik vele malen heb laten zien in presentaties, was je de helpende hand. Eigenlijk

ben je het eerste aanspreekpunt voor alle technische vragen met betrekking tot wetenschappelijke apparatuur. Zonder jouw kennis en ervaring zouden vele proefschriften er minder goed van af zijn gekomen. Daarmee ben je goud waard voor de vakgroep. Bedankt voor al je hulp!

Op computer-technisch gebied heb ik veel hulp gehad van Ronald Wegh. Ronald, je hebt me altijd snel en adequaat geholpen met allerlei computerproblemen. Dankzij jou was mijn computer-crash drie maanden voor het einde niet fataal voor het afronden van mijn project, en kon ik snel weer verder. Ook de WUR-ICT dienst en service-desk wil ik graag bedanken voor het draaiende houden van alle netwerk faciliteiten, het beschikbaar stellen van software en voor het oplossen van software problemen.

Er zijn veel mensen die in een meer ondersteunende rol van groot belang zijn geweest voor het afronden van dit proefschrift. Zoals de schoonmaakdames, Rhoda, Anneke en Hannie. Bedankt voor de ochtend-koffie en het leefbaar houden van mijn werkplek, ondanks de chaos op mijn bureau. Mara, bedankt voor je hulp bij allerlei dingetjes en voor je persoonlijke interesse. Anita, bedankt voor je adviezen en hulp met Optare. Bert, bedankt voor het afhandelen van declaraties en je hulp bij verschillende administratieve zaken.

Frans, ondanks dat je niet direct betrokken bent geweest bij dit project wil ik je bedanken voor je interesse, adviezen en ontspannende 'koffie-praatjes'. Jouw enthousiasme voor de wetenschap is aanstekelijk en inspirerend. Hans, bedankt voor de leuke en interessante verhalen over vroeger. Ik mocht altijd graag naar je luisteren. Ik vind het heel bijzonder hoe je je nog elke dag kan motiveren om naar Fysko te komen. Zo'n 'drive' is ongekend. Mara en Herman, volgens mij waren wij het beste Fysko koffie-team van de afgelopen jaren. Paulina and Kathelijne, I think we managed to organize a very effective and balanced PhD study-trip. Low-cost, scientifically interesting and relaxing at the same time. Thank you for your cooperation in realizing this PhD study-trip.

Alle andere mensen die het werken bij Fysko zo prettig maken, bedankt!

Er is (gelukkig) ook nog een leven naast het werkende leven. Voor de nodige sportieve ontspanning kon ik altijd rekenen op Schelto, Maarten en Johan. Bedankt dat jullie me hebben leren fietsen. Ik hoop nog vele kilometers samen met jullie te maken.

Harmen, Bart, Erik, Peter-Paul, Schelto, Maarten, Jelle, Pieter, Rudy en Robert, bedankt voor de onvergetelijk mooie tijd in Roma 2011. Zo'n lang weekend ontspanning kon ik goed gebruiken voordat het echte afronden van mijn proefschrift

begon.

Koen, Pieter, Jelle, Peter-Paul en Harmen, bedankt voor jullie vriendschap en betrokkenheid. Het is fijn mensen om je heen te hebben met wie je werkelijk alles kunt delen. Onze vriendschap betekent heel veel voor mij. Ook onze weekenden zijn terugkerende hoogtepunten van ontspanning, vermaak en creativiteit. Het is een fantastisch vooruitzicht dat we nog vele van deze weekenden samen gaan beleven.

Map, Johan en Jaap, bedankt voor jullie interesse in mijn 'studie'. Map en Johan, bedankt voor jullie bereidheid extra op te passen als ik weer eens voor kortere of langere tijd voor mijn werk van huis moest. Het is prettig te weten dat je kind in vertrouwde handen is.

Manon, Maurice, Arlette en Martijn, bedankt voor de leuke en gezellige momenten tijdens de familiebijeenkomsten, en jullie interesse in mijn werk. Manon en Arlette, het is fijn te weten dat ik altijd op jullie kan vertrouwen. Ik kan niet anders dan blij zijn dat ik twee van zulke lieve zussen heb.

Lieve papa en mama, bedankt voor jullie onvoorwaardelijke liefde, die de basis vormde van mijn ontwikkeling. Zonder die basis had ik nooit zover kunnen komen. Bedankt ook voor jullie harde werken en toewijding. Het was het waard; we zijn allemaal beter af. Bedankt voor jullie steun en begrip voor de keuzes die ik heb gemaakt. Het maakt mij intens gelukkig dat ik deze dag samen met jullie kan beleven en vieren. Ik hoop dat we nog vele jaren van elkaar en de kinderen kunnen genieten.

Lieve Lucie en Timme, bedankt dat jullie er zijn. Jullie hebben ons leven verrijkt op een manier die onbeschrijfelijk is. Ik hoop dat dit proefschrift één van de bouwstenen zal zijn voor een onbezorgde, veilige en liefdevolle toekomst.

Lieve Hendrikje, bedankt voor al je liefde, hulp, steun en advies. Bedankt voor je begrip en je betrokkenheid, vooral bij het afronden van dit boekje. Ook van jou heb ik veel geleerd. Lieve Hendrikje, we hebben zoveel mooie (sleutel)momenten beleefd in de afgelopen 5 jaar! En als ik terugkijk op al die momenten, dan kan ik niet anders dan bevestigen, dat wat we al eerder tegen elkaar zeiden: Come what may, samen kunnen we het aan!

Marc

Levensloop

Marc Lemmers is geboren op 11 januari 1982 in Bennebroek. Hij groeide op als middelste van drie kinderen. Zijn basisschooltijd werd doorgebracht op de protestants-christelijke Willinkschool in Bennebroek. Marc vervolgde zijn schooltijd op het protestants-christelijke atheneum 'Adriaen Pauw' in Heemstede. De laatste twee jaren werden, als gevolg van een fusie, doorgebracht in dezelfde klassen, maar op een andere locatie: het 'Kaj Munk College' in Hoofddorp. Op het atheneum groeide de interesse voor de natuurwetenschappelijke vakken. De studie Moleculaire Wetenschappen aan de Wageningen Universiteit was dan ook een logische vervolgstap. In september van het jaar 2000 begon Marc aan deze studie met als hoogtepunten een afstudeervak bij het Laboratorium voor Fysische Chemie en Kolloïdkunde van de Wageningen Universiteit en een stage bij Unilever Research & Development in Port Sunlight, United Kingdom. Tussen het studeren door werd een jaar ingelast als penningmeester sociëteit van de Katholieke Studenten Vereniging Sint Franciscus Xaverius in Wageningen. Eind juni 2007 behaalde Marc zijn Master Molecular Sciences, *cum laude*, met als specialisatie Fysische Chemie. In november 2007 begon Marc aan een promotieonderzoek naar netwerkvormende polymeren op basis van ladingsinteracties bij het Laboratorium voor Fysische Chemie en Kolloïdkunde van de Wageningen Universiteit, onder begeleiding van prof. dr. Martien Cohen Stuart en dr. ir. Jasper van der Gucht. Het resultaat van dit promotieonderzoek is te lezen in dit boek. Tijdens zijn promotietijd is Marc getrouwd met Hendrikje Schoppink en hebben hij en zijn vrouw twee kinderen gekregen, Lucie en Timme.

About the Author

Marc Lemmers was born on the 11th of Januari 1982 in Bennebroek, The Netherlands. He attended the 'Willink-school' primary school in Bennebroek, after which he continued his school-career at the 'Adriaen Pauw' atheneum in Heemstede. The last two years of the atheneum were spent at a different location, due to merging schools, at the 'Kaj Munk College' in Hoofddorp. His interest in the natural sciences grew over the years, which led to the start of the study Molecular Sciences at the Wageningen University, The Netherlands, in September 2000. He specialized in Physical Chemistry, with a MSc-thesis at the Laboratory of Physical Chemistry and Colloid Science of Wageningen University and an internship at Unilever Research & Development, Port Sunlight, United Kingdom. During his studies, Marc took a year off as a treasurer of the Catholic Student Association Sint Franciscus Xaverius in Wageningen. Marc obtained his Master of Molecular Sciences degree, *cum laude*, in June 2007. In November 2007 he started as a PhD student on network forming polymers based on electrostatic interactions, at the Laboratory of Physical Chemistry and Colloid Science of Wageningen University, under the supervision of prof. dr. Martien Cohen Stuart and dr. ir. Jasper van der Gucht. The results can be found in this Thesis. During his time as a PhD student Marc got married to Hendrikje Schoppink and together they got two children, Lucie and Timme.

List of Publications

This Thesis

- **M. Lemmers**, J. Sprakel, I.K. Voets, J. van der Gucht, M.A. Cohen Stuart: Multiresponsive Reversible Gels based on Charge-Driven Assembly, *Angewandte Chemie International Edition*, **2010**, *49*, 708-711
- **M. Lemmers**, I.K. Voets, M.A. Cohen Stuart and J. van der Gucht: Transient Network Topology of Interconnected Polyelectrolyte Complex Micelles, *Soft Matter*, **2011**, *7*, 1378-1389
- **M. Lemmers**, E. Spruijt, L. Beun, R. Fokkink, F.A.M. Leermakers, G. Portale, M.A. Cohen Stuart and J. van der Gucht: The Influence of Charge Ratio on Transient Networks of Polyelectrolyte Complex Micelles, *Soft Matter*, **2012**, *8*, 104-117
- **M. Lemmers**, E. Spruijt, S. Akerboom, I.K. Voets, A.C. van Aelst, M.A. Cohen Stuart and J. van der Gucht: Charge-Driven Complex Composite Gels, submitted
- M.A. Cohen Stuart, F.A.M. Leermakers, **M. Lemmers**, J.H.B. Sprakel: Triblock Copolymer Gelators, Patent Publication number: WO2010/054800

Other work

- J. van der Gucht, **M. Lemmers**, W. Knoben, N.A.M. Besseling, M.P. Lettinga: Multiple Shear-Banding Transitions in a Supramolecular Polymer Solution, *Phys. Rev. Lett.*, **2006**, *97*, 108301
- E. Spruijt, J. Sprakel, **M. Lemmers**, M.A. Cohen Stuart, J. van der Gucht: Relaxation Dynamics at Different Time Scales in Electrostatic Complexes: Time-Salt Superposition, *Phys. Rev. Lett.*, **2010**, *105*, 208301
- J. van der Gucht, E. Spruijt, **M. Lemmers**, M.A. Cohen Stuart: Polyelectrolyte complexes: Bulk phases and colloidal systems, *J. Colloid Interface Sci.*, **2011**, 361, 407-422

Overview of completed training activities

Courses

· Physical Chemistry Winterschool	Han-sur-Lesse (Belgium)	2008 & 2009
· 12th European School on Rheology	Leuven (Belgium)	2009
· Scattering Methods Applied to Soft Condensed Matter ⋆	Bombannes (France)	2010
· RPK-B: Polymer Physics	Utrecht	2010
· Scientific writing	Wageningen	2008
· Mobilizing your professional network	Wageningen	2009
· Project and time management	Wageningen	2010
· Fire extinction instruction	Wageningen	2010
· Career Orientation	Wageningen	2011

Conferences & Colloquia

· Lab Group meetings and Colloquia	Wageningen	2007 - 2011
· DPI Coating Technology Review Meetings (twice per annum) ⋆ ⊓	Wageningen & Eindhoven	2008 - 2011
· DPI Annual Meeting ⊓	The Netherlands	2008 - 2010
· Caput college	Wageningen	2008
· Dutch Polymer Days ⊓	Lunteren	2008 & 2009
· PhD study Trip ⋆	Switzerland & France	2009
· GRC Supramolecular Assemblies ⊓	Waterville (USA)	2009
· Liquids and Interfaces ⋆	Veldhoven	2010
· Dutch Soft Matter meeting ⋆	Wageningen	2010
· Frontiers of Chemistry ⊓	Paris (France)	2010
· 2nd International Soft Matter Conference ⋆	Granada (Spain)	2010
· Colloids and Materials ⋆	Amsterdam	2011
· DPI Annual Meeting ⋆	Zeist	2011

Other activities

· Organizing PhD Study Trip to Switzerland & France	2008 - 2009

⊓ : Poster presentation

⋆ : Oral presentation

Cover design & drop photography by Marc Lemmers
Photo-optimization by Simon Pessel
Special effects by Pieter van Midwoud

Printed by Wöhrmann Print Service, Zutphen